DISSERTATION

AN ANALYSIS OF CELL CYCLE ALTERATIONS AND APOPTOSIS INDUCED BY ETOPOSIDE AND HYPERTHERMIA

Submitted By
Chang-Uk Lim
Cell and Molecular Biology Program

In Partial Fulfillment of the Requirements
For the Degree of Doctor of Philosophy
Colorado State University
Fort Collins, CO 80523
Spring 2004

Reproduced with permission of the copyright owner. Further reproduction prohibited without permission.

UMI Number: 3131683

INFORMATION TO USERS

The quality of this reproduction is dependent upon the quality of the copy submitted. Broken or indistinct print, colored or poor quality illustrations and photographs, print bleed-through, substandard margins, and improper alignment can adversely affect reproduction.

In the unlikely event that the author did not send a complete manuscript and there are missing pages, these will be noted. Also, if unauthorized copyright material had to be removed, a note will indicate the deletion.

UMI®

UMI Microform 3131683

Copyright 2004 by ProQuest Information and Learning Company.

All rights reserved. This microform edition is protected against unauthorized copying under Title 17, United States Code.

ProQuest Information and Learning Company
300 North Zeeb Road
P.O. Box 1346
Ann Arbor, MI 48106-1346

Reproduced with permission of the copyright owner. Further reproduction prohibited without permission.

COLORADO STATE UNIVERSITY

November 11, 2003

WE HEREBY RECOMMEND THAT THE DISSERTATION PREPARED UNDER OUR SUPERVISION BY CHANG-UK LIM ENTITLED "AN ANALYSIS OF CELL CYCLE ALTERATIONS AND APOPTOSIS INDUCED BY ETOPOSIDE AND HYPERTHERMIA" BE ACCEPTED AS FULFILLING IN PART REQUIREMENTS FOR THE DEGREE OF DOCTOR OF PHILOSOPHY.

Committee on Graduate Work

J S Bedford

David E Johnson

Susan M Sakwe

Michael A. Tait

Advisor

Michael A. Tait

Department Head

Reproduced with permission of the copyright owner. Further reproduction prohibited without permission.

ABSTRACT OF DISSERTATION

AN ANALYSIS OF CELL CYCLE ALTERATIONS AND APOPTOSIS INDUCED BY ETOPOSIDE AND HYPERTHERMIA

Many toxic agents cause cells to undergo apoptosis, but different agents may cause cells to undergo apoptosis in different phases of the cell cycle. In addition, cells may undergo cell cycle delays after treatment with toxic agents. I developed three models to analyze apoptosis and the cell cycle: a cell cycle progression model, a cumulative apoptotic index (CAI) estimation model, and an apoptotic quotient calculation. CAI was calculated by measuring apoptotic index (AI) at multiple time points after a treatment. These models allow for identification of the cell cycle distribution of apoptotic and non-apoptotic cells and to determine whether cells in a particular phase of the cell cycle are preferentially sensitive to apoptosis.

I have tested these models with two different cell lines: HL-60 cells and HCW-2 cells, a mutant cell line derived from HL-60 cells that is resistant to apoptosis. Cells were treated with 6.25 μg/ml etoposide for 3 hr or heated at 45.0 °C for 15 or 30 min and analyzed at various times later. HL-60 cells treated with etoposide were resistant to apoptosis in G_1 and G_2/M phases but were sensitive to apoptosis in S phase. Etoposide-treated HL-60 cells also were delayed in G_1 and G_2/M phases. HCW-2 cells treated with etoposide did not undergo apoptosis but experienced an early S phase arrest, late G_1 phase arrest, continuous G_2/M phase block and increasing T_{pot}. HL-60 cells heated at 45.0 °C for 15 min had four phases of apoptosis and 34.8 % cumulative apoptotic cells while cells heated for 30 min had three phases of apoptosis and 93.6 % cumulative apoptotic cells. When the heat dose was increased from 15 to 30 min, CAI,

Reproduced with permission of the copyright owner. Further reproduction prohibited without permission.

T_w (time-window) and T_i (length of each phase) were also increased. The increase in CAI and T_i with a larger heat dose resulted in the production of more apoptotic cells and an increase in T_w, which means that the substrate for the assay existed longer for a greater heat shock. In conclusion, these techniques can provide a more detailed understanding of the kinetics of apoptosis, cell cycle progression and delays simultaneously from TUNEL histograms.

Chang-Uk Lim
Cell and Molecular Biology Program
Colorado State University
Fort Collins, CO 80523
Spring 2004

Reproduced with permission of the copyright owner. Further reproduction prohibited without permission.

Acknowledgements

I would like to give special thanks to my advisor, Dr. Michael H. Fox for the time, direction, patience, and kindness he has given me as well as the resources necessary to complete this degree. I would also like to thank to my committee members, Dr. Joel S. Bedford, Dr. David E. Fahrney and Dr. Susan M. Larue for their support.

I would like to thank Leslie Armstrong-Lea for her advice. My thanks also go to Norma Bulera for her help and friendship and all office-mates, especially Henri J. Dengah for his technical support in the lab.

Lastly, thanks to my Mom, Dad and all my family members, who give nothing but full and loving support to me in all my endeavors - even those that take me far away from them.

Reproduced with permission of the copyright owner. Further reproduction prohibited without permission.

TABLE OF CONTENTS

Reproduced with permission of the copyright owner. Further reproduction prohibited without permission.

Reproduced with permission of the copyright owner. Further reproduction prohibited without permission.

Reproduced with permission of the copyright owner. Further reproduction prohibited without permission.

CHAPTER 1

LITERATURE REVIEW

1.1 Introduction to Apoptosis

Initial questions about the possible existence, mechanisms, and role of physiological programs of cell death emerged at the end of the 19th century from the study of animal development, but only in recent decades has it been realized that certain cells from all multicellular animals are programmed to self-destruct, and that cell survival depends on the repression of this self-destruction program. Apoptosis, or programmed cell death, has become increasingly important to many areas of biomedical research and plays a central role in reshaping tissue during development and differentiation. Overproduction of cells followed by selective cell death to generate the final organism is a common occurrence in the embryonic development of all organisms. In *Caenorhabditis elegans (C. elegans),* a small nematode in which somatic cell lineage has been completely defined, 131 of the 1090 somatic cells formed during adult development undergo programmed cell death - cells die predictably at a defined time and place in each animal (107). Apoptosis has been shown to occur in response to ionizing radiation (2,8,15,23,39,133,150,159,198), UV irradiation (71,112,184), mild hyperthermia (2,3,44,45,60,63,75,111,132,160,170,171,197), certain chemotherapeutic agents

Reproduced with permission of the copyright owner. Further reproduction prohibited without permission.

(4,23,32,36,46,60,88,118,145,186,193), withdrawal of essential growth factors (86,141,175), treatment with glucocorticoids (1,74,81), and activation of certain receptors (83,130,142,146). Another means of initiating apoptosis is used in the immune system where cytotoxic T lymphocytes attack target cells. Also, the tumor suppressor p53 can trigger apoptosis as an important defense against cancer. Apoptosis is important, therefore, not only in tissue development, but also in the immune system in the development of cancer, and in neurodegenerative diseases.

1.1.1 Features of Apoptosis and methods of analysis

The morphological characteristics of apoptotic cells include condensed chromatin around the nuclear periphery, plasma membrane blebs, and shrunken cytoplasm in which the individual organelles remain intact (19,97,158,196). Because many of these changes are characteristic of apoptosis, they have become markers used to identify this mode of cell death by microscopy or flow cytometry (18,20,84).

Cell dehydration is one of the early events of apoptosis. Loss of intracellular water leads to condensation of the cytoplasm followed by a change in cell shape and size. Another change is condensation of nuclear chromatin. DNA in condensed chromatin exhibits hyperchromasia, staining strongly with fluorescent or light absorbing dyes. During apoptosis, the nuclear envelope disintegrates and lamin proteins undergo proteolytic degradation followed by nuclear fragmentation. The nuclear fragments, together with constituents of the cytoplasm, are then packaged and enveloped by fragments of the plasma membrane. These structures, called apoptotic bodies, are then shed from the dying cell. Analysis of scattered light in a flow cytometer provides

Reproduced with permission of the copyright owner. Further reproduction prohibited without permission.

information about the cell size and structure. The intensity of light scattered in a forward direction correlates with cell size. Cell shrinkage during apoptosis results in a decrease in forward light scatter (18). A transient increase in right angle scatter can be seen during apoptosis in some cells. This may reflect an increased light reflectiveness by condensed chromatin and fragmented nuclei. Using light scatter to detect apoptosis is easy, inexpensive, and fast. The light scatter changes, however, are not specific to apoptosis. Mechanically broken cells, isolated cell nuclei, and necrotic cells also have diminished ability to scatter light. This method should be accompanied by another, more specific assay.

Another characteristic event of apoptosis is the degradation of genomic DNA into discrete oligonucleosome fragments by the action of a Ca^{2+}/Mg^{2+}-dependent endonuclease. Gel electrophoresis of an apoptotic cell's nuclear material produces a characteristic "ladder pattern" corresponding to various multiples of 200-base pair (bp) DNA fragments derived from cleaving the DNA between nucleosomes (18,20). Also, enzymatic techniques using DNA polymerase (nick translation) or terminal transferase (tailing) have been developed to detect apoptosis at the cellular level (7,56,58,61,100). The 3' OH termini in DNA breaks are detected by attaching biotin or digoxygenin conjugated nucleotides or fluorescent labeled nucleotides to them using terminal deoxynucleotidyl transferase (TdT). This TUNEL assay (TdT-mediated dUTP-biotin nick end-labeling or terminal dUTP nick-end labeling) appears to be the most specific in terms of positive identification of apoptotic cells. Combining a DNA dye with this method allows one to analyze apoptosis through the cell cycle. A simple method for measuring apoptosis relies on the loss of cleaved DNA from the nucleus resulting in a

Reproduced with permission of the copyright owner. Further reproduction prohibited without permission.

smaller amount of DNA in the cell. After staining the cells with a DNA stain such as propidium iodide (PI) and analyzing them by flow cytometry, a sub-diploid peak is obtained, representing apoptotic cells which have lost some of their DNA.

Another characteristic of apoptosis is the preservation of the structural integrity and function of the plasma membrane, at least during the initial phase of cell death. Other membrane-bound cellular organelles, including mitochondria and lysosomes, also remain preserved during apoptosis. However, the function of mitochondria is impaired during apoptosis. The loss of mitochondrial inner transmembrane potential is associated with the early stages of apoptosis (11,18,20,42). Mitochondrial permeability transition pores (PT pores) play a major role in the collapse of this potential by allowing passage of ions and small molecules. The loss of membrane potential triggers a decoupling of the respiratory chain and the release of cytochrome C into the cytosol.

Mitochondrial function plays a critical role in apoptosis and can be analyzed using flow cytometry. Rhodamine 123 (Rh123) is a green fluorescent cationic dye that accumulates in active mitochondria with high membrane potential (18,20,47,123). Incubating cells with both Rh123 and propidium iodide (PI) labels live cells green (Rh123) and dead cells red (PI). Decreases in mitochondrial transmembrane potential reflect a loss of the cell's ability to accumulate Rh123 or cyanine dyes (e.g., JC-1) (9,90) in mitochondria. This event is associated with an increased production of superoxide anions (reactive oxygen species, ROS) and increased content of the reduced form of cellular glutathione (12,50,55,113). The product of the *bcl-2* gene appears to play a critical role in preventing the loss of the mitochondrial transmembrane potential during

Reproduced with permission of the copyright owner. Further reproduction prohibited without permission.

apoptosis (11). A cartoon of the mitochondrial involvement in apoptosis is shown in Fig. 1.1.

Another organelle that can be probed by flow cytometry is lysosomes. Incubation of cells in the presence of 1-2 μg/ml of the metachromatic fluorochrome acridine orange (AO) results in the uptake of this dye by lysosomes of live cells, which fluoresce red. The uptake is the result of an active proton pump in lysosomes. The high proton concentration (low pH) causes AO, which can enter the lysosome in an uncharged form, to become protonated and thus trapped in the organelle. Dead cells exhibit weak green and minimal red fluorescence at that low AO concentration. This assay is useful for cells that have numerous active lysosomes, such as monocytes and macrophages (19). Anther feature of cells undergoing apoptosis is the loss of asymmetry of the phospholipids on the plasma membrane leading to exposure of phosphatidylserine (PS) on the outer surface (16,26,43,94,178). The human vascular anticoagulant, annexin V, is a 35-36 kDa Ca^{2+}-dependent phospholipid-binding protein that has a high affinity for PS. The presence of PS on the outer membrane leaflet can be measured by binding fluorescent-labeled annexin V to the PS in the presence of calcium ions (178,179). When combined with PI, this can distinguish between early apoptotic and late apoptotic or necrotic cells. Flow cytometry, with its capabilities for multiparameter analysis using methods described above, is the easiest and most rapid technology for studying apoptosis. It offers all the advantages of rapid, multiparameter analysis of large populations of individual cells to investigate the biological processes associated with cell death (19).

Reproduced with permission of the copyright owner. Further reproduction prohibited without permission.

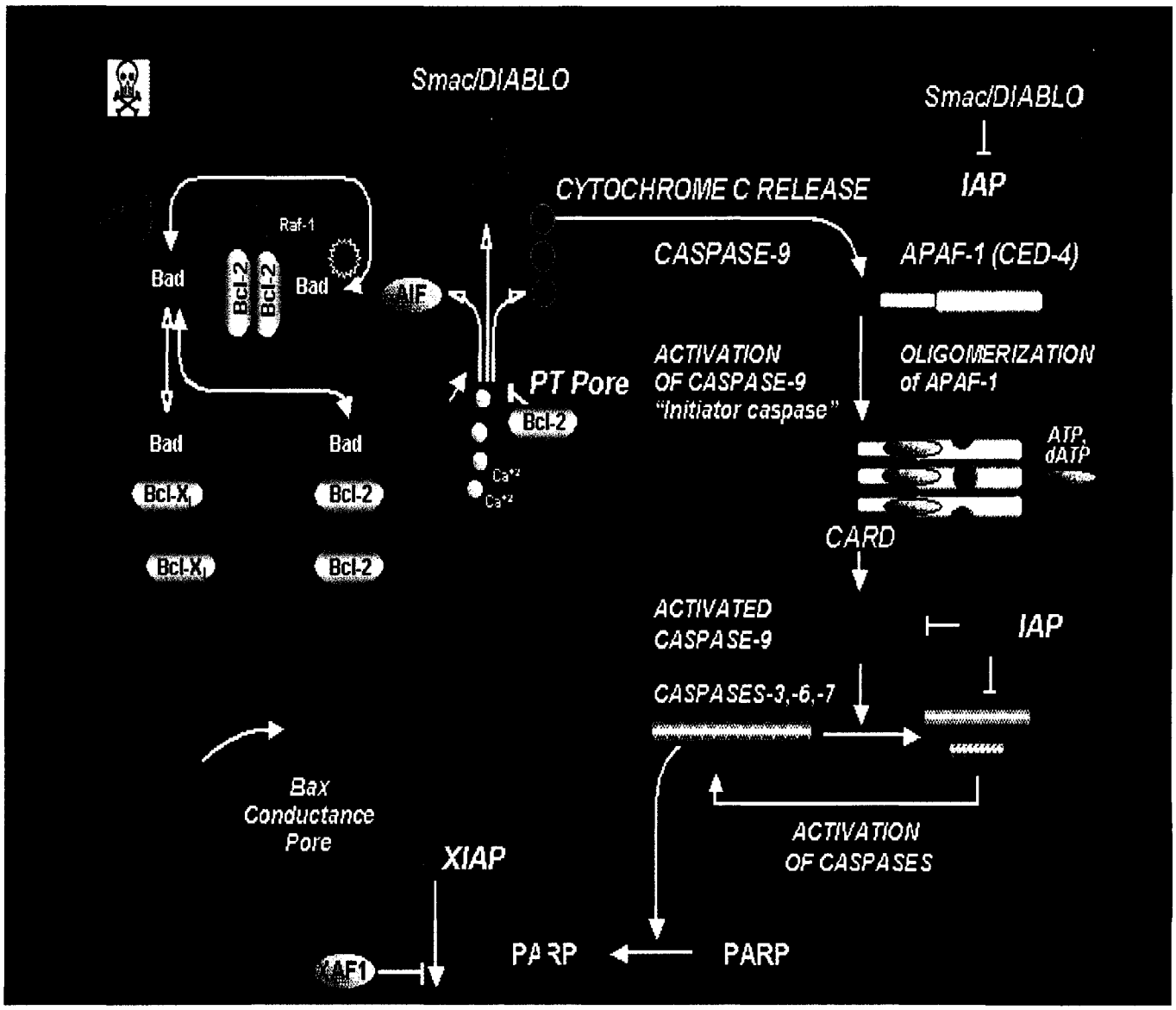

Figure 1.1. The intrinsic mitochondrial apoptotic pathway.

Abbreviation (alphabetical order): AIF (apoptosis-inducing factor), Apaf-1 (apoptotic protease activating factor), CARD (caspase-recruitment domain), Ced-4 (cell death abnormal), DIABLO (direct IAP binding protein with low pI), IAP (inhibitors of apoptosis proteins), PARP (poly [ADP-ribose] polymerase), PT pore (permeability transition pore), Smac (second mitochondria-derived activator of caspases), XAF1 (X-linked inhibitor of apoptosis-associated factor-1), XIAP (X-linked inhibitor-of-apoptosis protein) (courtesy of Dr. Darzynkiewicz, Z.)

Reproduced with permission of the copyright owner. Further reproduction prohibited without permission.

The activation of aspartic acid-specific cysteine proteases (caspases) is another critical feature of apoptosis. An enzyme cascade of caspases results in cellular disassembly. The products cleaved by activated caspases, such as poly [ADP-ribose] polymerase (PARP) (Fig. 1.1), DNA-dependent protein kinase and actin (147,148), are detected electrophoretically by western blot detection with specific antibodies. The second method for detection of active caspase is the use of fluorogenic (or chromogenic) substrates of caspases. Peptide substrates have been developed that are colorless or non-fluorescent but upon caspase cleavage generate colored or fluorescent products (62,87,114). The recognition site is composed of three to four amino acids followed by an aspartic acid residue, with the cleavage occurring after the aspartate. Another method utilizes fluorochrome-labeled inhibitors of caspases (FLICA) for the detection of the activation of caspases. Different caspases can be detected by using different peptide targets of these inhibitors, which are specific for each caspase as described later. FLICA could be used to arrest cells in apoptosis, thereby preventing their disintegration and passage or exit from the time-window for the assay (6,164,165,166). This method allows for the analysis of the apoptotic index (AI) and also the cumulative apoptotic index (CAI). AI represents the fraction of apoptotic cells in a population at a given time point whereas CAI represents the cumulative fraction of apoptotic cells from the beginning of treatment to the collection time point.

Several additional cytosolic features of apoptosis can be measured. Changes of intracellular ion concentration, pH and level of ROS in the cytosol occur during apoptosis. Indo-1 (33,69,183,189) and Fluo-3 (101,154) can be used to measure intracellular, cytosolic free Ca^{2+} concentration, BCECF (2, 7-biscarboxyethyl-5(6)-

Reproduced with permission of the copyright owner. Further reproduction prohibited without permission.

carboxyfluorescein) (21,30,128) and SNARF-1 (5,180,190) can be used to measure pH, and H_2DCFDA (2', 7'-dichlorodihydrofluorescein diacetate or DCFH-DA) (12,96) can be used to measure ROS.

1.1.2 Apoptosis vs. Necrosis

Apoptosis differs from necrosis in several molecular, biochemical and morphological features (Table 1.1) (53,57,64,100,103,105,139,140,158,176). While apoptosis is characterized by active participation of the affected cell in its own demise, necrosis is a passive, catabolic, and degenerative process. Necrosis generally represents the last cellular response to gross injury and can be induced by an overdose of cytotoxic agents.

Early events of necrosis are mitochondrial swelling followed by rupture of the plasma membrane and release of cytoplasmic constituents, which include proteolytic enzymes. DNA degradation is not so extensive during necrosis as in the case of apoptosis, and the products of degradation are heterogeneous in size, failing to form discrete bands on electrophoretic gels.

Apoptotic cells die quietly - they do not cause inflammation, and phagocytes that engulf the apoptotic bodies are not activated. Necrosis, however, stimulates an inflammatory immune response; phagocytes that engulf necrotic cells are activated, and they secrete cytokines that recruit other immune system cells to the area.

Reproduced with permission of the copyright owner. Further reproduction prohibited without permission.

Table 1.1. Morphological criteria for identification of apoptosis or necrosis (19,29,53,105,139,140,158,176)

APOPTOSIS	NECROSIS
Reduced cell size, convoluted cell shape	Cell and nuclear swelling
Plasma membrane blebbing / budding	Patchy chromatin condensation
Chromatin condensation (DNA hyperchromicity)	Swelling of mitochondria
Loss of the structural features of the nucleus	Vacuolization in cytoplasm
Nuclear fragmentation (karyorrhexis)	Plasma membrane rupture
Presence of apoptotic bodies	Dissolution of DNA (karyolysis)
Dilation of the endoplasmic reticulum	Attraction of inflammatory cells
Relatively unchanged cell organelles	
Phagocytosis of cell remnants	
Cell detachment from tissue culture flasks	

Reproduced with permission of the copyright owner. Further reproduction prohibited without permission.

1.2 Pathways of Apoptosis

The pathway that activates the apoptotic response is different in each case, but the response is similar. In most cases, the initial stimuli converge on a common effector pathway, as shown by the ability of Bcl-2 to inhibit apoptosis in response to all signals and the central role of caspase 3 in both the mitochondria-dependent pathway (intrinsic pathway, Fig. 1.1) and the death receptor pathway (extrinsic pathway, Fig. 1.2).

There are two classes of extrinsic interaction by which apoptosis can be induced. In the first class, cell death is induced by a particular stimulus, such as engagement of the T-cell receptor of the Fas/Apo-1/CD95 antigen. In the second class, cell death results from removal of a stimulus, such as IL-2 or IL-3, which normally suppresses apoptosis. Fas/Apo-1/CD95 may interact with other genes that control apoptosis.

1.2.1 Death Receptors

A major pathway that triggers apoptosis in mammalian cells was discovered via the properties of the Fas receptor (Fig. 1.2). Fas ligand (FasL) or an antibody directed against Fas receptor kills cells that express the protein on their surface. The reason is that the antibody-Fas reaction activates Fas, which triggers a downstream pathway for apoptosis. Fas (CD95/APO-1) is a type I membrane protein in the TNF (tumor necrosis factor) family. Fas is a transmembrane protein which possesses characteristic cysteine-rich repeats in its extracellular domains. This pathway can be triggered by cell-cell interactions in which the "ligand" on one cell surface interacts with the receptor on the surface of the other cell. Among the members of this family, both Fas- and TNF-receptors can activate apoptosis.

Reproduced with permission of the copyright owner. Further reproduction prohibited without permission.

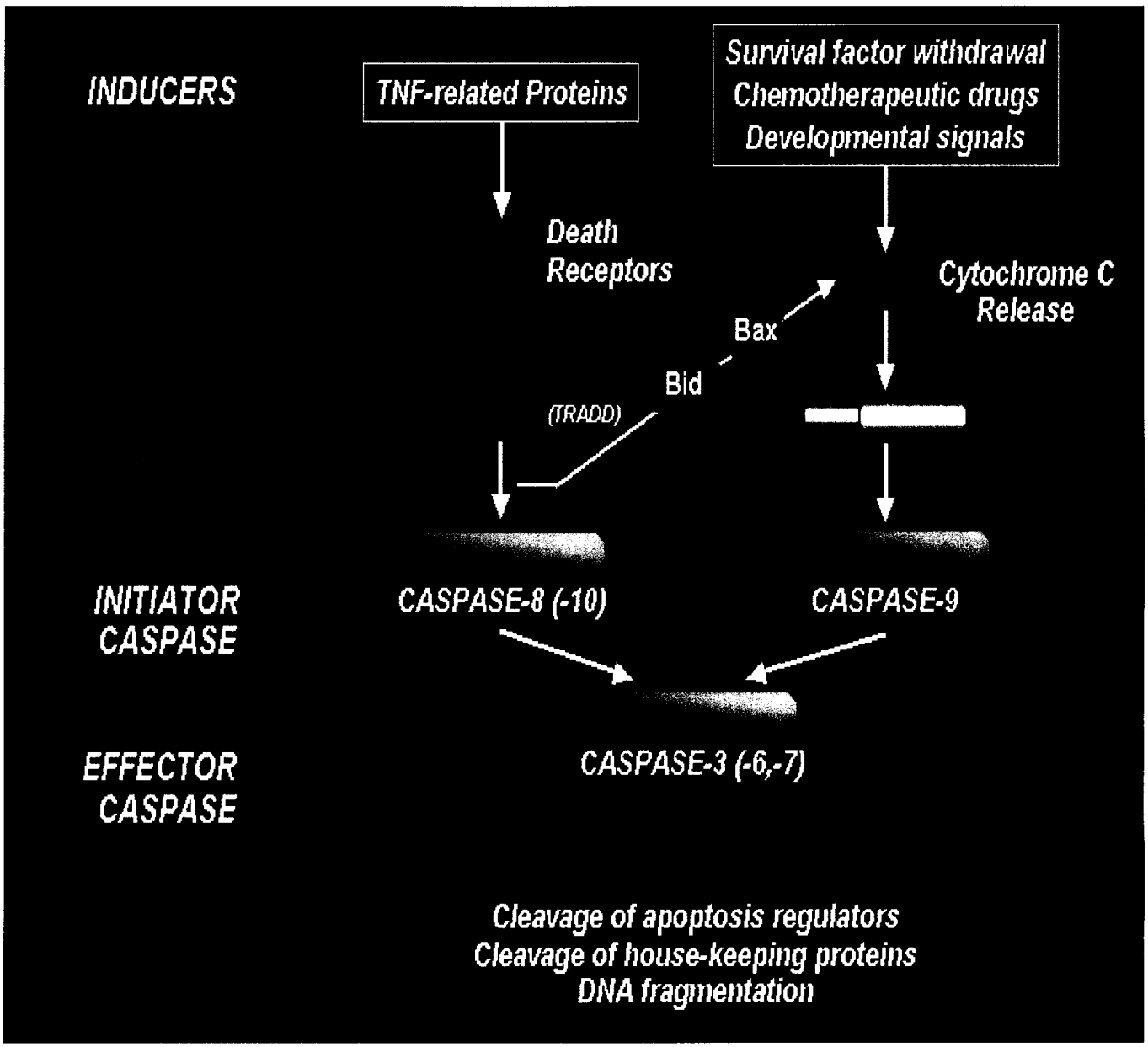

Figure 1.2. The extrinsic death receptor apoptotic pathway.

Abbreviation (alphabetical order): Apaf-1 (apoptotic protease activating factor), FADD (Fas-associated protein with death domain), TNF (tumor necrosis factor), TRADD (TNF receptor associated death domain) (courtesy of Dr. Darzynkiewicz, Z.)

Reproduced with permission of the copyright owner. Further reproduction prohibited without permission.

FasL is a homotrimer, and FasL binding induces trimerization of the Fas receptor. A 65 amino acid intracellular domain near the carboxyl terminus in Fas receptor (130,144), which is called the death domain (DD) (107), trimerizes (Figure 1.3). After trimerization, the DD recruits other DD containing proteins (i.e., FADD, Fas-associated protein with death domain) to the receptor complex. This complex is called the death-inducing signaling complex (DISC). A death effector domain (DED) in FADD is exposed when FADD binds to the death receptor. A DED in FADD binds to a DED in the prodomain of pro-caspase 8 (Figure 1.3). Interaction of two or more pro-caspase 8 molecules causes auto-catalytic activation of caspase 8 molecules, providing a crucial link between Fas and caspase cascades. Through this cascade, the external signal activates caspase 3 and also activates the mitochondrial apoptotic pathway by triggering the release of cytochrome C from the mitochondria with Bid and Bax (Fig. 1.2) (27,40,51,99,122). A detailed description of the cytochrome C-related apoptotic pathways is given in section 1.3.2.

1.2.2 Perforin and Granzymes

Another extrinsic apoptotic pathway is triggered by granzymes (serine proteases), and perforin (a membrane pore-forming protein) found in the lymphocyte granules of activated cytotoxic T lymphocytes and NK (natural killer) cells. Perforin can polymerize into transmembrane pores in the target cell membrane, which facilitates the intra-cellular delivery of the granzymes. Following adhesion of the cytotoxic cell to the target, granzyme B is directly exocytosed and enters the target cells through the perforin pores.

Reproduced with permission of the copyright owner. Further reproduction prohibited without permission.

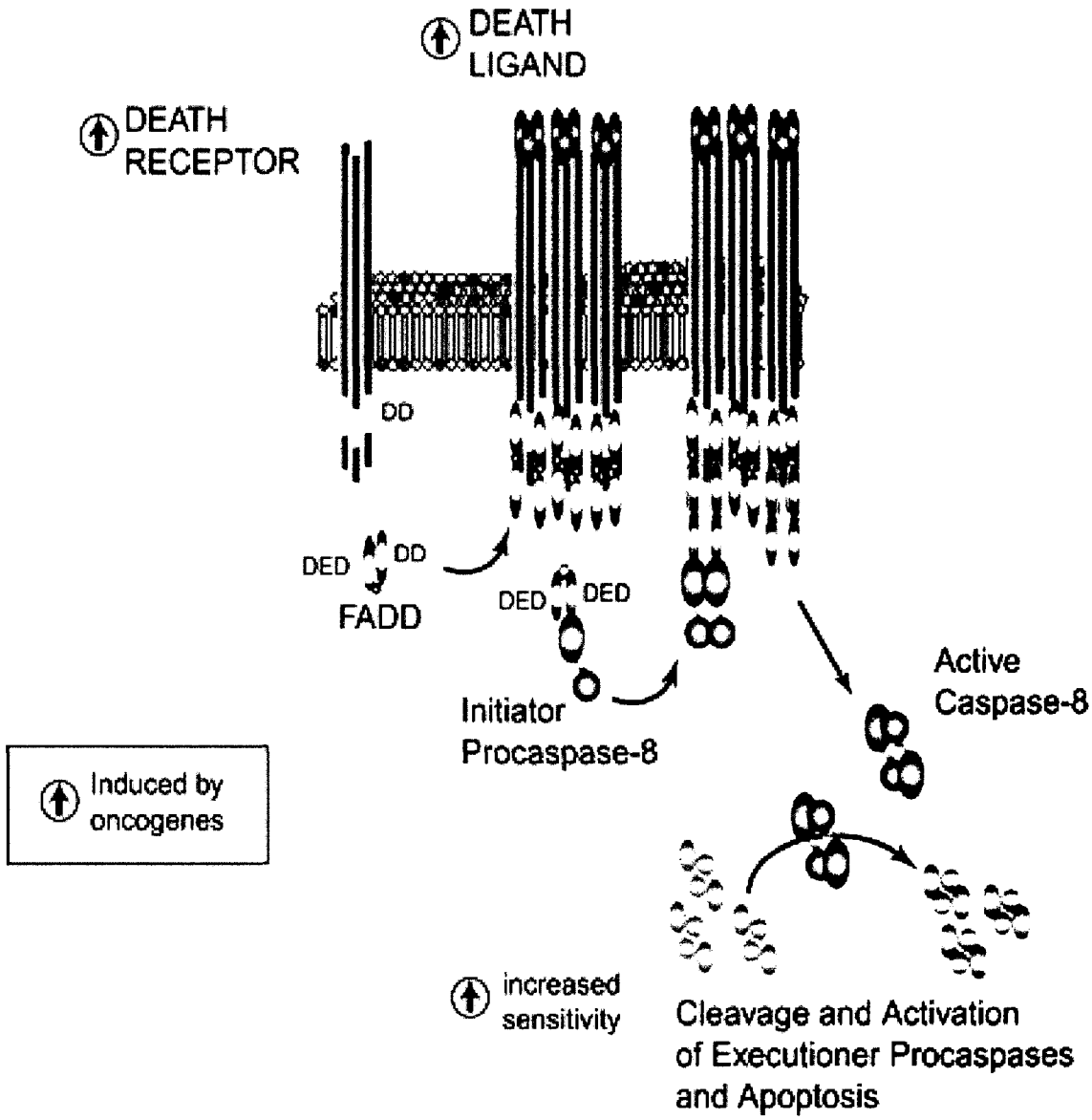

Figure 1.3. Detailed explanation of death receptor oligomerization in extrinsic apoptotic pathway (65)

Abbreviation (alphabetical order): DD (death domain), DED (death effector domain), FADD (Fas-associated protein with death domain)

Reproduced with permission of the copyright owner. Further reproduction prohibited without permission.

The granzymes work on specific substrates involved with cell death by apoptosis in the target cells (89,95). Granzyme B can induce many of the features of apoptosis, including fragmentation of DNA. It activates pro-caspases 3, 6, 7, 8, 9 and 10 (inactive precursors called zymogens) by cleavage to produce the active caspases 3, 6, 7, 8, 9 and 10, respectively (see Table 1.3). When granzyme B is inhibited in the target cells, granzyme A act as the second granzyme system in a family of 11 found in the cytotoxic granules (127,163).

1.2.3 Caspase (ICE) Family

Caspases define a family of aspartate-specific cysteine proteases with multiple roles in the processes of cell differentiation, growth and apoptosis (151). Caspases are pro-enzymes that must be catalytically cleaved at specific Asp amino acids and dimerize with a large and a small subunit to become an active protease. More than 10 mammalian members of the caspase family have been reported so far (Table 1.2). The caspases can be divided into three groups with redundant functions. Caspases 1, 4 and 5 are associated with inflammation (52,70,109); caspases 2, 3 and 7 have been shown to disrupt essential homeostatic pathways and act as effectors or executioner during apoptosis; caspases 6, 8, 9 and 10 act as upstream components or initiators in the apoptosis-related proteolytic cascade (138,173,174). Caspase 3 is derived from the proenzyme CPP32 at the onset of apoptosis and plays a pivotal role in apoptosis (59,134,136,137,138,155). Categorizing caspases by functional domains results in three clusters (174). Caspases 1, 2, 4, 5 and 9 are called CARD (caspase recruitment domain)-caspases; caspases 8 and 10 are called DED-caspases; caspases 3, 6, 7 and 14 are called downstream caspases.

Reproduced with permission of the copyright owner. Further reproduction prohibited without permission.

Table 1.2. Human ICE/CED-3 protease nomenclature and optimal peptide sequences (48,130,148)

New nomenclature	Old nomenclature	Optimal peptide sequences
Caspase-1	ICE	WEHD (Trp-Glu-His-Asp)
Caspase-2	ICH-1, mNedd2	VDVAD (Val-Asp-Val-Ala-Asp)
Caspase-3	CPP32, Yama, Apopain	DEVD (Asp-Glu-Val-Asp)
Caspase-4	TX, ICH-2, ICE_{rel}-II, Caspase-11 (mouse)	WEHD (Trp-Glu-His-Asp)
Caspase-5	TY, ICE_{rel}-III, Caspase-12 (mouse)	WEHD (Trp-Glu-His-Asp)
Caspase-6	Mch2	VEID (Val-Glu-Ile-Asp)
Caspase-7	Mch3, ICE-LAP3, CMH-1	DEVD (Asp-Glu-Val-Asp)
Caspase-8	MACHα1, FLICE, Mch5	LETD (Leu-Glu-Thr-Asp)
Caspase-9	ICE-LAP6, Mch6	LEHD (Leu-Glu-His-Asp)
Caspase-10	Mch4, FLICE-2	DEVD (Asp-Glu-Val-Asp)
Caspase-14	MICE	
General Inhibitor	used frequently with neurons	Boc-D-FMK "BAF"
	synthetic caspase inhibitor	Z-VAD-FMK

Reproduced with permission of the copyright owner. Further reproduction prohibited without permission.

There is a cascade of proteases in which one member activates another by cleaving it (Figs 1.1, 1.2 and Table 1.3). In general, caspases are likely to be activated by other caspases or granzyme B in both a linear sequence and in parallel pathways, which might vary depending on both the apoptotic inducer and the cell type or tissue, but the details are very complex and still not known.

A variety of other substrates are not activated but rather are inactivated by specific caspase cleavage, for example the nuclear lamins, which are part of the intermediate filament network contributing to nuclear envelope integrity and chromatin organization (Table 1.4). Overexpression in cells of uncleavable mutant lamins delayed cell death, demonstrating that lamin cleavage precedes DNA fragmentation and contributes to chromatin condensation and nuclear shrinkage *in vivo*. Cleavage of chromatin at internucleosomal sites depends on activation of a specific endonuclease. CAD (caspase-activated DNase) is a unique nuclease which is usually located in the cytoplasm in an inactive, latent form. CAD is synthesized with two extra amino acids at its N terminus; it makes a complex with ICAD (inhibitor of caspase-activated DNase) and it is stabilized when those extra amino acids are removed. ICAD acts as a chaperone for correct folding of CAD. CAD consists of 342 amino acids, with a 15 amino acid nuclear localization signal at its carboxyl terminus. CAD is activated by caspase 3 cleavage and inactivation of the nuclease inhibitor ICAD which has two DEVD sequences (38,156,195). The activated CAD enters the nucleus and degrades chromosomal DNA (Fig. 1.4). The sequence of murine ICAD is closely homologous to a human protein, DFF-45 (DNA-fragmentation factor 45), which contains caspase 3 sites and is cleaved in apoptosis (38,117,156). DFF consists of two subunits of 45- and 40-kDa

Reproduced with permission of the copyright owner. Further reproduction prohibited without permission.

Table 1.3. Cleavage of caspase precursors by caspases and granzyme B in vivo and/or in vitro (148)

Protease or caspase	Substrate (caspase precursor)
Granzyme B	Caspase 3, 6-10
Caspase-1	Caspase 1, 3, 4
Caspase-3	Caspase 1, 6, 7, 9
Caspase-4	Caspase 1, 4
Caspase-5	Caspase 5
Caspase-6	Caspase 3, 7
Caspase-8	Caspase 3, 4, 7, 9
Caspase-10	Caspase 1, 3, 7

Reproduced with permission of the copyright owner. Further reproduction prohibited without permission.

Table 1.4. Cleavage of caspase substrates in apoptosis (excluding caspase precursors) (148,168)

Substrate	Caspase	Cellular localization of substrate	Consequences of cleavage in apoptosis
Activation of function			
ICAD, DFF	Caspase-3	Cytoplasm	Induction of DNA fragmentation by cleavage of the substrates
Pro-IL-1β	Caspase-1	Cytoplasm	Active IL-1β regulates apoptosis induced by other factors
Interferon-γ Inducing factor	Caspase-1	Cytoplasm	Pro-interleukin-18
PKCδ	Caspase-3	Cytoplasm	Induction of catalytic activity. Contribution to cell death?
SREBPs 1,2	Caspase 3,7	ER/nucleus	Induction of transcription. Suppression of cell lysis?
Bid	Caspase-8	Cytoplasm	Bcl-2 family member. Induction of releases of cytochrome C
Cytosolic phospholipase A2	?	Cytoplasm	Phospholipid metabolism
Inactivation of function			
Cytoskeletal and structural proteins			
Lamins A,B,C	Caspase-6	Nuclear envelope	Loss of nuclear matrix integrity; nuclear disassembly facilitated
Actin	Caspases	Cytoskeleton	?
α-fodrin	Caspase-3-related	Cortical cytoskeleton	Cell shape changes
Gas2	?	Microfilament	Cell shape changes
β-Catenin	?	Plasma membrane	Cell adhesion changes
Gelsolin	Caspase-3	Cytoplasm	Actin-severing protein, membrane blebbing and other morphology features related
Cell cycle and replication			
DNA topo I,II	?	Nuclear scaffold	DNA replication
Mdm2/Hdm2	?	Nucleus	Inhibitor of p53; Loss of cell cycle control
NuMA	?	Nucleus	?
Rb	Caspase-3	Nucleus	Loss of apoptosis suppression?
p21 (Cip1/Waf1)	?		Cdk2 inhibitor
Cdc27	?		Anaphase-promoting complex
Cyclin A	?		Loss of cell cycle control

Reproduced with permission of the copyright owner. Further reproduction prohibited without permission.

Transcription and translation			
U1-70 kDa	Caspase-3	Nucleus	Inhibits RNA splicing
HnRNP C1, C2	Caspase-3 like	Nucleus	?
NF-κB, IκB-α	?		Cytokine and anti-apoptotic genes, inhibitor of NF-κB
DNA cleavage and repair			
PARP	Caspase 1,3,4,6,7	Nucleus	Accelerates DNA fragmentation and Inhibits DNA repair
DNA-PK	Caspase-3	Nucleus	Inhibits DNA repair
Signal transducers			
D4-GDI	Caspase-3	Cytoplasm	Inhibitor of small GTPases, Rho pathway
PITSLRE	Caspase-3 like	Nucleus	Loss of cell cycle regulation
Others			
Huntingtin	Caspase-3?	Cytoplasm	Failure of a subset of neurons to survive
Pro-caspases	Caspases	Cytoplasm	Activated by upstream caspases
Bcl-2		Cytoplasm	Apoptosis inhibitor
Apaf-1	Caspase-3	Cytoplasm	Removal of upstream apoptotic machinery
Hsp90			Involved in Alzheimer's disease
Presenilins			

Abbreviation: ICAD, Inhibitor of caspase-activated DNase; DFF, DNA fragmentation factor; Pro-IL-1β, prointerleukin-1β; IL-1β, interleukin-1β; PKCδ, protein kinase Cδ; SREBPs 1,2, sterol response element binding proteins; PARP, poly (ADP-ribose) polymerase; DNA-PK, DNA-dependent protein kinase; U1-70 kDa, 70-kDa component of the U1 small nuclear ribonucleoprotein; Rb, retinoblastoma protein; PITSLRE, isoforms of the 110-kDa PITSLRE protein kinase family; NuMA, nuclear matrix and mitotic apparatus protein; D4-GDI, GDP dissociation inhibitor type D4, an inhibitor of Rho family GTPases that functions to regulate inflammatory cell activity, is susceptible to cleavage by caspase-3; DNA topo I and II, DNA topoisomerases I and II; hnRNP C1, C2, heteronuclear ribonucleoproteins C1 and C2 (components of the spliceosome believed to participate in pre-mRNA processing); ER, endoplasmic reticulum; MDM-2, mouse double minute-2 protein; Apaf-1, apoptotic protease activating factor.

Reproduced with permission of the copyright owner. Further reproduction prohibited without permission.

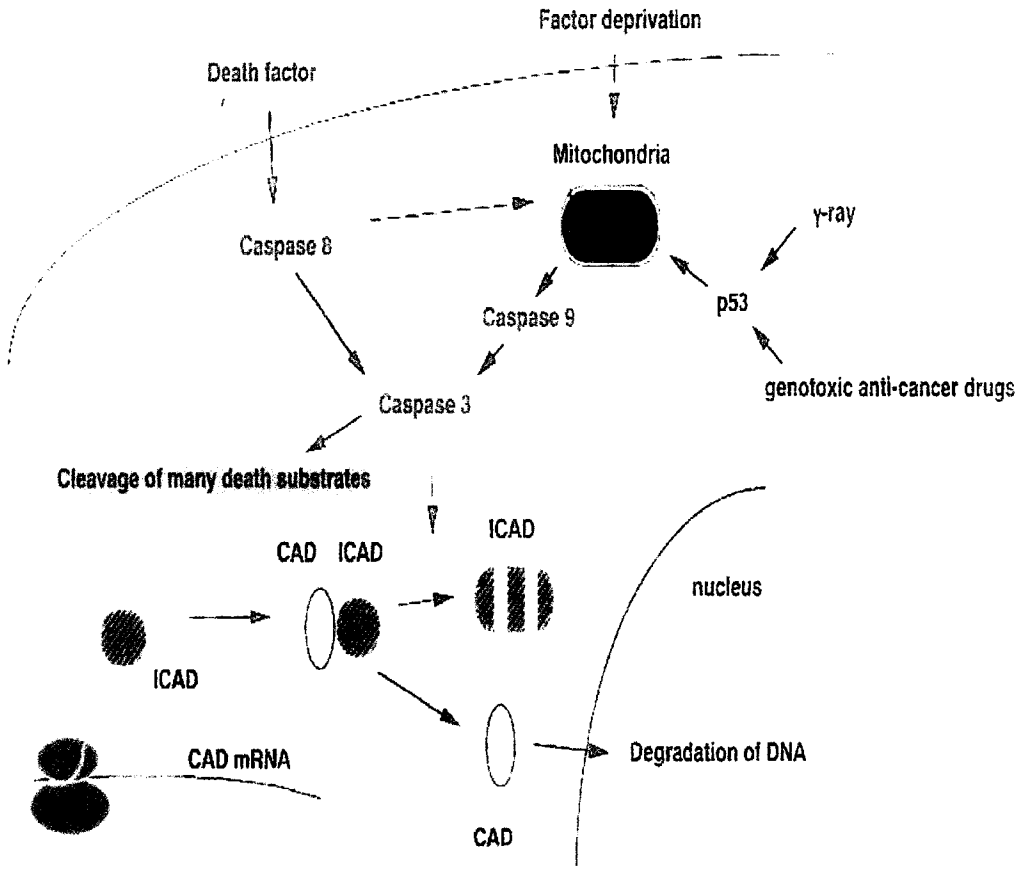

Figure 1.4. A model for CAD-dependent DNA fragmentation during apoptosis (131)

Abbreviation (alphabetical order): CAD (caspase-activated DNase), ICAD (inhibitor of caspase-activated DNase)

Reproduced with permission of the copyright owner. Further reproduction prohibited without permission.

proteins (DFF-45 and DFF-40). Caspase 3 cleaves DFF-45, and DFF-40 (CAD) is activated and cleaves chromosomal DNA in the nucleus (116).

Failure to detect apoptosis with the TUNEL assay may be related to CAD/ICAD. First, when the expression of CAD and ICAD is low, such as in fibroblasts, only a small percentage of TUNEL positive cells is observed. In contrast, lymphoid and myeloid cell lines have a high level of CAD and ICAD expression, and have a massive DNA fragmentation. Second, when caspase 3 is mutated or absent (in cell lines lacking caspase 3 or in caspase 3-null mice), the TUNEL assay does not give a positive population because the CAD/ICAD system is not activated by caspase 3.

Other known substrates inactivated by cleavage are the nuclear enzyme PARP (135,187) and DNA protein kinase (148). Both play roles in DNA repair and PARP has been suggested to suppress the activity of an apoptotic endonuclease by poly ADP-ribosylation. The catalytic domain of PARP is efficiently cleaved from the DNA-binding domain by various caspases. Cleaved PARP is a marker of apoptosis in many mammalian cells. It is possible that PARP cleavage accelerates DNA fragmentation by adversely affecting the DNA repair machinery.

Synthetic caspase inhibitors are very useful for analysis of caspase activity and potential treatment for the chronic diseases characterized by cell death, such as Alzheimer's diseases. A popular method for measuring caspase activity utilizes fluorogenic or chromogenic oligopeptide substrates and inhibitors that enable relatively simple procedures and quickly yield quantitative kinetic data. Optimal peptide sequences (Table 1.2) have been developed that produce maximum specificity. These peptides act as pseudosubstrates for active caspases and become competitive inhibitors. Irreversible

Reproduced with permission of the copyright owner. Further reproduction prohibited without permission.

inhibitors are made by modifying the peptide C-terminal aspartic acid with fluoromethyl ketone (FMK) (172,174). The caspase-3 activity can be monitored in vitro using the fluorogenic peptide substrate carbobenzoxy-Asp-Glu-Val-Asp-7-amino-4-trifluoromethyl coumarin (Z-DEVD-AFC), a variation of the substrate described in the literature (137). This peptide-dye conjugate produces a blue fluorescence upon exposure to near-UV light. Caspase-3 enzymatically cleaves the AFC from the peptide and release free AFC which then produces a blue-green fluorescence. The advantages of using the caspase system for measuring apoptosis are as follows: (i) caspase activity is an early marker for cells entering apoptosis; (ii) caspase is measured fluorometrically for very sensitive and quantitative detection; (iii) the caspase fluorogenic assay is fast, easy, quantitative, and robust; (iv) the FLICA (fluorochrome-labeled inhibitors of caspases) assay with PI can provide cell cycle specific analysis of apoptosis in individual cells.

The realization that many of the caspase substrates are important proteins involved in cell regulation, signaling, DNA repair, homeostasis and cell survival makes it attractive to think that the proteolytic disabling of certain key proteins directly contributes to apoptosis.

1.3 Regulation of Apoptosis

1.3.1 Genes in C. elegans

The control of apoptosis involves components that inhibit the pathway as well as those that activate it. This first became clear from the genetic analysis of cell death in *C. elegans*, where mutants were found that either activate or inactivate cell death. Cell death

Reproduced with permission of the copyright owner. Further reproduction prohibited without permission.

occurs at precisely defined times during the developmental program, and all the dead cells show the classic signs of apoptosis. The entire cell-elimination process in *C. elegans* has three distinct phases – killing the cell, phagocytosis of the corpse, and digestion of the engulfed cell constituents. The expression of specific genes is important in each phase.

Three genes [*egl-1* (egg laying defective), *ced-3* (cell death abnormal), and *ced-4*] are required for apoptosis in *C. elegans (17,24,25)*. Loss-of-function mutations in any of these genes result in the survival of the cells that are supposed to die. The *ced-3* gene encodes a member of the caspase family. The mammalian homologue of *Ced-4* is *Apaf-1* (200). *ced-9* is another gene which is required for apoptosis control. It is the *C. elegans* counterpart of human *bcl-2 (80)*. *ced-9* blocks apoptosis during development in *C. elegans* embryos, apparently by encoding a protein that inhibits activation of *ced-3* and *ced-4*. When Egl-1 binds Ced-9, the complex of Ced-9 and Ced-4 loosens and releases Ced-4. This makes Ced-4 oligomerize, which is followed by the activation of Ced-3. The proper control of apoptosis may therefore involve a balance between activation and inhibition of this pathway (107).

ced-1, ced-2, ced-5, ced-6, ced-7, ced-10, and ced-12 encode proteins that change the properties of the outer surface of the dead cell's plasma membrane, flagging the cell for phagocytosis (79). Group 1 is composed of *ced-1, ced-6,* and *ced-7*. Ced-1 and Ced-7 recognize the corpse and may be involved in phosphatidylserine-induced engulfment. Ced-6 transfers the signals from Ced-1. Group 2 consists of *ced-2, ced-5, ced-10*, and *ced-12*. They are involved in cytoskeletal reorganization during phagocytosis.

Reproduced with permission of the copyright owner. Further reproduction prohibited without permission.

1.3.2 Bcl-2 family in mammalian cells

Studies using *C. elegans* have provided clear evidence for cell death by an active process dependent on the activity of particular genes (24,37). Many studies have confirmed that expression of the proto-oncogene *bcl-2* can suppress apoptosis in a wide variety of cultured cell types (82). In myeloid leukemic cells, a high resistance to induction of apoptosis by a variety of cancer chemotherapy compounds, irradiation, and heat shock was associated with a high level of expression of *bcl-2* (119). Screening for expression of *bcl-2* may be useful to characterize leukemia and other types of cancer cells regarding their susceptibility to induction of apoptosis by different cytotoxic anticancer agents.

The bcl-2 family of proteins acts as critical regulators of pathways that are involved in apoptosis, functioning either to inhibit or to promote cell death. Thus, the bcl-2 family members are divided into two major sub-families, which are composed of anti-apoptotic and pro-apoptotic bcl-2 members (Table 1.5). Group I (anti-apoptotic) members possess four conserved α-helix bcl-2 homology (BH) domains named BH1, BH2, BH3, and BH4 as well as C-terminal hydrophobic membrane localizing domain. Group II (pro-apoptotic) members lack BH4 but have the other domains. A more diverse group III (pro-apoptotic) consists of members with only BH3 domain (78).

The ratio between the anti-apoptotic and pro-apoptotic members determines the fate of the cells after receiving a death signal. Bcl-2 family members form homodimers or heterodimers with other bcl-2 family members. When bcl-2 forms heterodimers with Bax, it prevents Bax proteins from forming pores in the mitochondria membrane (Fig. 1.1). Thus, if bcl-2 is overexpressed, apoptosis is likely to be inhibited, but if bcl-2 is

Reproduced with permission of the copyright owner. Further reproduction prohibited without permission.

Table 1.5. Anti-apoptotic and pro-apoptotic BCL-2 family members (99)

		Members
Anti-apoptotic	Mammalian	BCL-2, BCL-X_L, BCL-W, MCL-1, A1/BFL-1, BOO/DIVA, NR-13
	Viral	E1B-19K, BHRF1, KS-BCL-2, ORF16, LMW5-HL
	C. elegans	CED-9
Pro-apoptotic	Mammalian	BAX, BAK, BOK/MTD, BCL-X_S
	BH3-only	BID, BAD, BIK/NBK, BLK, HRK, BIM/BOD, BNIP3, NIX
	C. elegans	EGL-1

Reproduced with permission of the copyright owner. Further reproduction prohibited without permission.

silenced (92) or Bax or other pro-apoptotic members are overexpressed, such as in response to DNA damage, apoptosis is likely to occur.

The separation of anti-apoptotic and pro-apoptotic members in the absence of a death signal is important for regulating the efficient response to apoptosis and avoiding unnecessary formation of multimers. Anti-apoptotic proteins are integral membrane proteins found mostly in the mitochondria, endoplastic reticulum (ER), or nuclear membrane (13,76,98). Some pro-apoptotic proteins are found in the cytosol or the cytoskeleton. After an apoptosis signal, pro-apoptotic proteins (e.g., Bax) integrates into the mitochondrial outer membrane followed by the exposure of its amino terminal domain from a closed configuration (27,85,192). In the carboxyl terminal hydrophobic domain, the removal of this domain inhibits the redistribution during apoptosis and inhibits apoptotic activity of Bax (192).

Bid is a 'BH3 domain only' pro-apoptotic member, which acts as a linker between an extrinsic death signal and the mitochondrial apoptotic pathway by regulating cytochrome C release (Fig. 1.2). It inactivates bcl-2 and activates Bax (185). A death signal from the Fas receptor activates caspase 8 and activated caspase 8 cleaves cytosolic p22 Bid. The truncated p15 Bid (tBid) inserts into the mitochondrial outer membrane where it causes the release of cytochrome C (68,108,122). The released cytochrome C binds to Apaf-1 (apoptotic protease activating factor-1). The N-terminal region of the inactive monomeric form of Apaf-1 interacts with the WD domains in the C-terminal region (Fig. 1.5). Binding of cytochrome C to the WD region unfolds Apaf-1 and exposes

Reproduced with permission of the copyright owner. Further reproduction prohibited without permission.

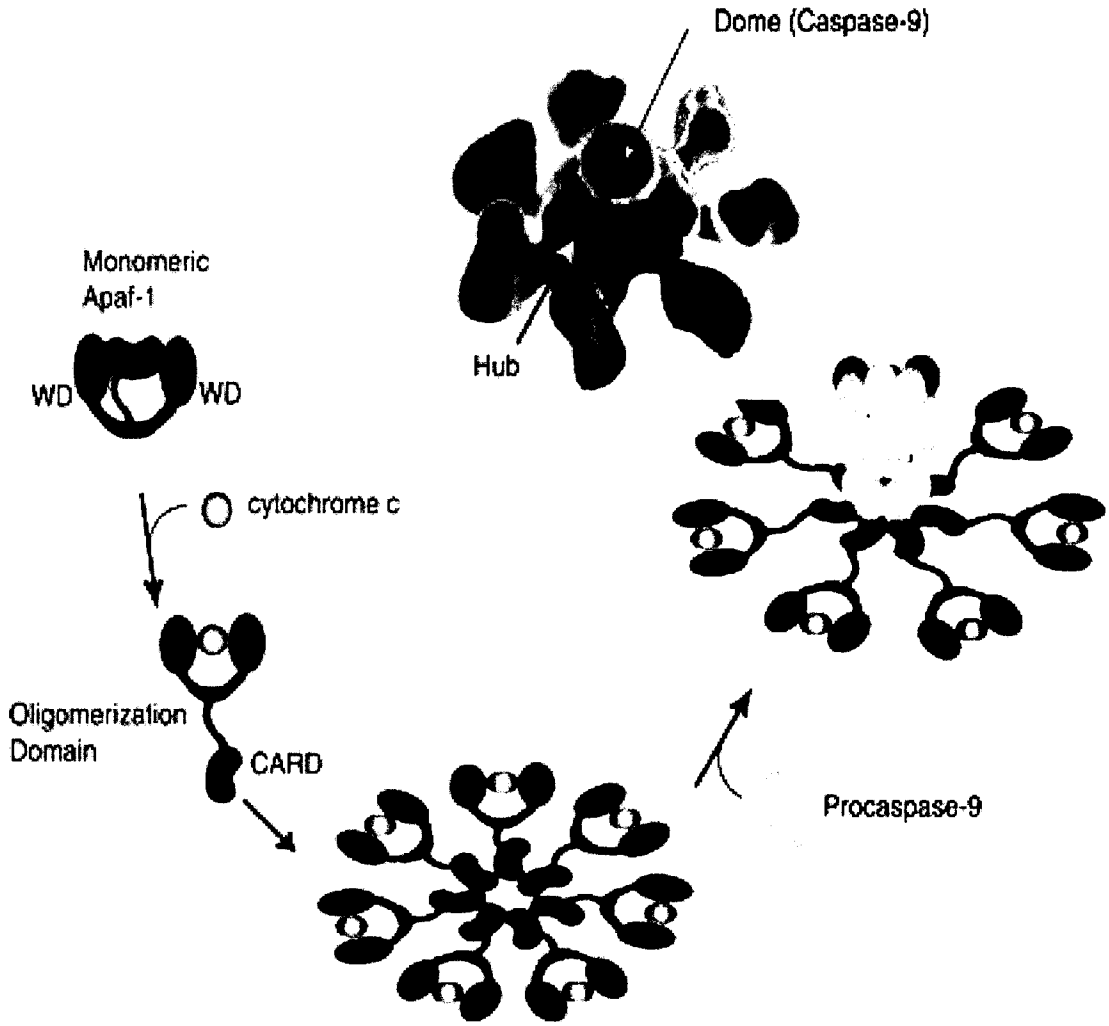

Figure 1.5. The structure of apoptosome (65)

Abbreviation (alphabetical order): Apaf-1 (apoptotic protease activating factor), CARD (caspase recruitment domain)

Reproduced with permission of the copyright owner. Further reproduction prohibited without permission.

an oligomerization domain. A heptamer of Apaf-1 and cytochrome C is formed and stabilized by dATP or ATP. This heptamer combines with pro-caspase 9 to form a complex, called the apoptosome, by interaction of caspase recruitment domains (CARDs). The aggregation of pro-caspase 9 activates caspase 9, which is followed by the activation of caspase 3 (Fig.1.1 and Fig.1.2) (110,115,200). Bcl-2 and Bcl-X_L act as anti-apoptotic molecules that sequester BH-3 only pro-apoptotic family members in stable multimers, repressing the activation of Bax or Bak.

Calcium (Ca^{2+}) stimulus induces the formation of membrane permeability transition (PT) pore in the mitochondria, which is composed of the adenine nucleotide translocator (ANT), Bax and the voltage-dependent anion channel (VDAC) (161,162,177). This channel allows water and solutes to enter the mitochondrion, which is followed by mitochondrial swelling and the release of cytochrome C (Fig.1.1) (66,199). This phenomenon can be blocked by the PT pore inhibitor cyclosporin A. In contrast to calcium stimulus, growth factor withdrawal causes non-specific rupture of the mitochondrial outer membrane and cytochrome C release following mitochondrial swelling resulting from defective exchange of ADP and hyperpolarization of the inner membrane (Fig. 1.6) (181).

Reproduced with permission of the copyright owner. Further reproduction prohibited without permission.

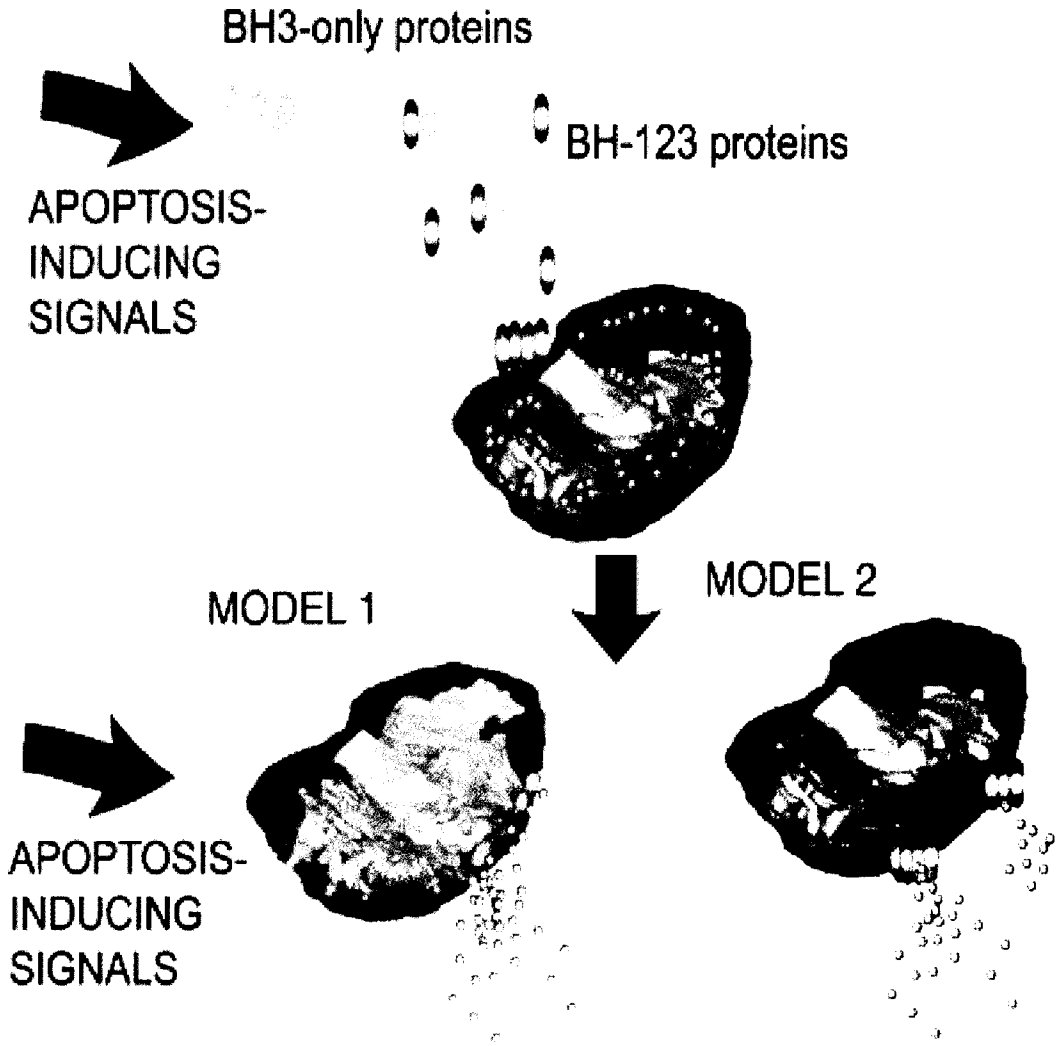

Figure 1.6 Two mechanisms of mitochondrial outer membrane permeabilization (65)

Reproduced with permission of the copyright owner. Further reproduction prohibited without permission.

1.3.3 p53

The p53 tumor suppressor protein is a short-lived protein which is induced and stabilized in the cellular response to ionizing radiation, genotoxic agents, oxidative stress, hypoxia and oncogene expression. Wild-type p53 is inactivated by mutations or deletions in many types of human cancer cells (143). Mutations and deletions in the *p53* gene are also common in human myeloid leukemia cell lines (169).

p53 is a tetrameric transcription factor with a central DNA binding domain that recognizes an interrupted palindromic 10 bp motif (14,54,72,124,129). p53 activates transcription at promoters that contain multiple copies of these p53-responsive motifs. The immediate N-terminal region provides the transactivation domain, which interacts directly with TBP (the TATA box-binding protein) (49,152). This region of p53 is also a target for other proteins that interact with it, including cellular oncoprotein Mdm2 and the adenovirus oncoprotein E1B 55kDa.

Mdm2 is a cellular protein that inhibits p53 activity by binding to the N-terminus and blocking transactivation (125). p53 induces transcription of *Mdm2*, so the interaction between p53 and Mdm2 forms an autoregulatory negative feedback loop in which the two components limit each other's activities. Mdm2 controls p53 function by inhibition of p53-mediated transcriptional activity and promotion of p53 degradation. The interaction of E1B 55kDa with p53 enables adenovirus to block p53 action, which is an essential part of its transforming capacity. *mdm2* null mice (but p53 normal) die during embryogenesis, but the simultaneous elimination of p53 rescued the lethality (22,93,126). Thus, p53 is active and lethal in the absence of Mdm2.

Reproduced with permission of the copyright owner. Further reproduction prohibited without permission.

In its function as a transcription factor in response to DNA damage, p53 activates several genes related to (i) cell cycle arrest in G_1 phase (CDKN1A (p21/WAF-1/CIP1) a cyclin-dependent kinase inhibitor which inhibits the cell cycle progression by binding to and inhibiting the activity of cyclin/Cdk complexes), (ii) DNA repair (PCNA and GADD45), and (iii) activation (*APAF-1,* BAX and Fas) and/or repression (*bcl-2*) of certain genes for induction of apoptosis after excessive DNA damage (66,106,153). p53 may also induce apoptosis by a mechanism independent of transcriptional activation (10).

p53 also has the ability to bind to damaged DNA. The C-terminal domain recognizes and binds to short (<40 base) single-stranded regions of DNA and to mismatches generated by very short (1-3 base) deletions and insertions of bases (91,104).

All the transforming forms of p53 turned out to be mutant forms of the protein. They fall into the category of dominant negative mutants, which function by overwhelming the wild-type protein and preventing it from functioning. The most common form of a dominant negative mutant is one that forms a heteromeric protein containing both mutant and wild type subunits, in which the wild-type subunits are unable to function. p53 probably exists as a tetramer. Oligomerization requires the C-terminal region (107). When mutant and wild-type subunits of p53 oligomerize, the tetramer takes up the mutant conformation.

Wild-type p53 mediates apoptosis in normal hemopoietic cells deprived of viability-inducing cytokines or treated with different cytotoxic agents. This was confirmed by showing that thymocytes from wild-type p53-deficient mice compared to thymocytes from normal mice were more resistant to γ-irradiation-induced apoptosis and to induction of apoptosis by other DNA-damaging compounds (15,121). The involvement

Reproduced with permission of the copyright owner. Further reproduction prohibited without permission.

of wild-type p53 in apoptosis was also indirectly suggested from experiments showing that DNA damaging agents can induce an increase in expression of wild-type p53 (121). Wild-type p53 is involved in the process of apoptosis in normal hemopoietic cells, which suggests a similar role for p53 in other normal cell types. However, the fact that hemopoietic cells from p53-deficient mice were not completely resistant to induction of apoptosis, the ability to induce apoptosis in leukemic cells lacking p53, such as HL-60 (191), and the similar susceptibility of thymocytes from normal and p53-deficient mice to dexamethasone-induced apoptosis (15,121) show that there are also p53-independent pathways for induction of apoptosis.

1.3.4 c-myc

The *myc* family of proto-oncogenes produces DNA binding proteins, which can heterodimerize to form transcriptional activators or repressors. Their regulation in proliferation, differentiation and apoptosis is very complex. The best characterized is *c-myc*, whose expression is maintained throughout the cell cycle in normal proliferating fibroblasts and elevated by several mechanisms. When cells are deprived of serum or growth factors, downregulation of *c-myc* may cause them to arrest in G_1 and certain nonmalignant factor-dependent myeloid cell lines and Rat-1 fibroblasts may undergo apoptosis (41,167). Deregulated expression of c-*myc* in myeloid leukemic cells coexpressing mutant p53 did not result in enhancement of susceptibility to apoptosis, showing that mutant p53 suppressed the apoptosis-enhancing effect of deregulated *c-myc* (119,120). In addition to enhancing apoptosis or sensitizing cells to apoptotic stimuli by a p53-dependent mechanism, deregulated *c-myc* can also induce cell proliferation and

Reproduced with permission of the copyright owner. Further reproduction prohibited without permission.

inhibit differentiation. The *bcl-2* gene can also suppress the apoptosis-enhancing effects of deregulated *c-myc*. The *c-myc* gene and mutant p53 can therefore cooperate in tumor development as occurs with *c-myc* and *bcl-2* (119,120,167). In addition to the *c-myc*-dependent pathways, there are also *c-myc*-independent pathways that regulate apoptosis. Dexamethasone-induced apoptosis in a human T cell lymphoblastic leukemia resulted in decreased expression of *c-myc* and deregulated expression of *c-myc* in these cells actually inhibited induction of apoptosis by dexamethasone (67).

How does c-myc promote two such opposite functions as proliferation and death? In the absence of growth factors (and hence low myc expression), the default for mammalian cells is to block in G_0; similarly the default condition with c-myc expression could be apoptosis. The actual signal is controlled by the balance between apoptosis-suppressing molecules such as mutant p53, Bcl-2 and Bcl-XL, and apoptosis-inducing molecules such as p53, c-myc and Bax. Without an apoptotic inducer, apoptosis-suppressing molecules are dominant and the default signal becomes proliferation. With an apoptotic inducer, apoptosis-inducing molecules are dominant and the default signal becomes apoptosis.

1.3.5 Inhibitors of apoptosis

Extrinsic and intrinsic apoptotic signals are processed and regulated by molecules such as Apaf-1, Bcl-2 family members and IAPs. Anti-apoptotic Bcl-2 proteins regulate the release of cytochrome C and IAPs regulate the cascade of catalytic processing of pro-caspases. The inhibitors of each specific reaction are very important as research tools and as clinical drugs to inhibit cell death *in vivo*. The first apoptotic inhibitor, crmA, was

Reproduced with permission of the copyright owner. Further reproduction prohibited without permission.

identified in the cowpox virus as a self-defense system against the apoptotic machinery of infected cells. A variety of inhibitors, which are the products of viral and cellular genes and artificial caspase inhibitors (e.g., FLICA), repress the function of several apoptosis members, especially caspases (Table 1.6) (6,31,34,35,85,164,165,182).

1.4 Brief Summary

Two major apoptotic pathways have been discovered so far. The first pathway is the 'intrinsic apoptotic pathway' (Fig.1.1). It is stimulated by cellular stress from many inducers such as cytotoxic agents, growth factor deprivation, ionizing radiation and mitogenic oncogenes. These stimuli and the interaction of Bcl-2 family members, especially pro-apoptotic Bcl-2 members, promote the release of cytochrome C into the cytosol. Cytochrome C and Apaf-1 form an oligomeric complex called the apoptosome with pro-caspase 9, which then activates caspase 9, the initiator caspase (Fig.1.5). Activated caspase 9 starts the downstream activation of apoptosis by activating caspase 3, the main effector caspase. Activated caspase-3 cleaves ICAD and releases CAD. Activated CAD starts the degradation of DNA into nucleosomal fragments (116,117), which is detected by the DNA ladder assay and TUNEL (Fig.1.4).

The second pathway is the 'extrinsic apoptotic pathway' (Fig.1.2). It is stimulated by extracellular binding of death receptors such as Fas/CD95/APO-1 with their respective ligands. When ligands bind the receptor, the receptors undergo oligomerization, DD in the receptor recruits other DD containing adapters (i.e., FADD). This complex is called

Reproduced with permission of the copyright owner. Further reproduction prohibited without permission.

Table 1.6. Inhibition of mammalian caspases, Bax and others by viral, mammalian caspases inhibitors and chemical inhibitors (6,31,34,35,85,164,165,182)

	Inhibitors
BAX	cycloheximide
Caspase 1	crm A, synthetic caspase inhibitor
Caspase 2	synthetic caspase inhibitor
Caspase 3	Viral p35, XIAP, synthetic caspase inhibitor
Caspase 4	synthetic caspase inhibitor
Caspase 5	crm A, synthetic caspase inhibitor
Caspase 6	Viral p35, synthetic caspase inhibitor
Caspase 7	XIAP, synthetic caspase inhibitor
Caspase 8	crm A, Viral p35, synthetic caspase inhibitor
Caspase 9	synthetic caspase inhibitor
Caspase 10	synthetic caspase inhibitor
Granzyme B	PI-9/GBI
IAP	Smac/DIABLO (inhibitor of inhibitors)
PT pore	cyclosporin A

Abbreviation and explanation: crm A, cowpox virus product cytokine response modifier A; p35, baculoviral protein; IAP, inhibitor of apoptosis; XIAP, X-linked inhibitor-of-apoptosis protein; Synthetic caspase inhibitor, developed based on the substrate cleavage sites of the caspases; PI-9, cytotoxic lymphocyte serpin protease inhibitor 9, close relative of crm A; GBI, granzyme B inhibitor; Smac, second mitochondria-derived activator of caspases; DIABLO, direct IAP binding protein with low pI; PT pore, permeability transition pore.

Reproduced with permission of the copyright owner. Further reproduction prohibited without permission.

DISC. A DED in FADD is exposed when FADD binds to the death receptor. A DED in FADD binds to a DED in the prodomain of pro-caspase 8. Combining two pro-caspase 8 molecules together induces autocatalytic activity forming caspase 8 molecules, providing a crucial link between Fas/CD95/APO-1 and caspase cascades (Fig.1.3). These activated caspases activate effector caspases 3, 6 and 7. Thus, death receptors function as a passage for the transmission of extracellular death signal to the cytosol. Moreover, activated initiator caspase 8 activates cytosolic Bid. The activated Bid (tBid) inserts into the mitochondrial outer membrane where it causes the release of cytochrome C. The released cytochrome C is involved in the same procedures as in the intrinsic pathway. Finally both branched signals combine in the effector caspase 3 step. Two major and one minor branched apoptotic pathways with different triggers converge at a caspase 3 step and execute apoptosis.

1.5 Hyperthermia-Induced Apoptosis

Cells that are heated to a few degrees above physiological temperatures (hyperthermia) undergo apoptosis and become sensitive to radiotherapy and many antitumor agents. Radiotherapy in combination with hyperthermia or antitumor agents can improve therapy, so the cellular response to hyperthermia is of great clinical interest.

1.5.1 Morphology and DNA Fragmentation

The light microscopic and ultrastructural appearances of cells undergoing apoptosis induced by hyperthermia are identical to those induced by a wide variety of other agents. As is the case with apoptosis in general, hyperthermia induces a series of

Reproduced with permission of the copyright owner. Further reproduction prohibited without permission.

apoptotic phenomena such as chromatin condensation, convolution of the nuclear and cell membranes, fragmentation of the nucleus and formation of apoptotic bodies. DNA extracted from cells undergoing hyperthermia-induced apoptosis also shows the same selective cleavage into oligonucleosomal-sized DNA fragments as usual.

1.5.2 Kinetics

Induction of apoptosis by hyperthermia occurs very rapidly. In the intestinal crypts of rats and in cultures of murine mastocytoma for example, significantly elevated levels of apoptosis are observed immediately after the completion of a 30 min period of 43 or 44 °C heating (2,75). Apoptosis peaks in mastocytoma cultures at between 2 and 4 h, and then decreases as the apoptotic bodies undergo secondary necrosis and are degraded to debris. By 24 h, apoptotic counts have returned to levels approaching control values (75). Apoptotic bodies formed in culture are not phagocytosed and eventually undergo spontaneous degeneration. While the lag period (time between completion of heating and onset of apoptosis) varies among different cell types, apoptotic inducer and detection methods used, once underway, the kinetics of the apoptotic process itself appears to be similar. Cells undergoing apoptosis in vivo following hyperthermic treatment are rapidly phagocytosed and digested by nearby resident cells or macrophages and all evidence for their occurrence in tissues may be lost within about 8 to 12 h (102).

1.5.3 Sensitivity of cells to apoptotic induction

One of the more interesting findings to have come out of studies of hyperthermia-induced apoptosis is that the sensitivity to apoptotic induction varies enormously from

Reproduced with permission of the copyright owner. Further reproduction prohibited without permission.

cell type to cell type. Understanding why some cell types are sensitive or resistant to apoptotic induction is important as a reduced capacity of cells to undergo apoptosis appears to be associated with the development of cancer and may also be an important factor in cancer treatment failures. What makes a cell sensitive to induction of apoptosis by hyperthermia or other agents is not clear at present. However, it appears that most of the extremely heat-sensitive cell lines have a lymphoid origin, grow as suspension cultures and have low levels of constitutively expressed heat shock proteins and *bcl-2 (102).*

1.5.4 Heat Dose or Thermal Dose Equivalent

The cell survival curves for heat are similar in shape to those obtained for x-rays (an initial shoulder followed by an exponential region), except that the time of exposure to the elevated temperature replaces the absorbed dose of x-rays. The similarity in the shape of the cell-survival curves for heat and x-rays may be misleading, however, since the amount of energy involved in cell inactivation is a thousand times greater for heat than for x-rays. This reflects the different mechanisms involved in cell killing by heat and x-rays (73). The slope of an Arrhenius plot of various levels of hyperthermia gives the activation energy of the chemical process involved in the cell killing. The similarity of the activation energy for protein denaturation to the activation energy for heat cytotoxicity, calculated from the Arrhenius analysis, led to the hypothesis that the target for heat cell killing may be a protein or proteins. The structural chromosomal proteins, nuclear matrix, cytoskeleton, repair enzymes and membrane components have all been identified as possible targets that are denatured by hyperthermia (73).

Reproduced with permission of the copyright owner. Further reproduction prohibited without permission.

The effects of heat are primarily dependent on time of heating at a given temperature. The relationship between treatment time and temperature for a biological isoeffect (the Arrhenius plot) has been confirmed for a variety of normal tissues and tumors. A marked change of slope occurs somewhere between 42 °C and 43 °C (188). Above this transition temperature the slope is consistent for a variety of cells and tissues. For temperature above 43 °C, it is generally agreed that a 1°C rise of temperature is equivalent to a reduction of time by a factor of 2 to give equal killing (Eq.1.1) (28).

$$\frac{t_2}{t_1} = 2^{T_1 - T_2} \qquad \text{(Equation 1.1)}$$

where $t_1$and t_2 are the heating times at temperatures T_1 and T_2 respectively, to produce equal cell killing, e.g. 43 °C for 60 min equals 44 °C for 30 min equals 45 °C for 15 min. For temperatures below the transition temperature an increase in temperature by 1°C requires that time be decreased by a factor of 4 to 6 (Eq.1.2) (28).

$$\frac{t_2}{t_1} = (4 to 6)^{T_1 - T_2} \qquad \text{(Equation 1.2)}$$

Therefore, when defining thermal doses in hyperthermic studies, both the time and temperature of heating are equally important determinants. The equivalent heating time at 43 °C (the heat dose or thermal dose equivalent) may be calculated from one or the other of these expressions or a combination of both. In principle, at least, the heat dose

Reproduced with permission of the copyright owner. Further reproduction prohibited without permission.

associated with a changing temperature may be calculated as the sum of equivalent heating times at 43 °C for each temperature (73,157).

1.5.5 Mechanisms of hyperthermia-induced apoptosis

When cultured cells are subjected to elevated temperatures, they respond by synthesizing a small number of highly conserved stress proteins, commonly called heat shock proteins (hsps). In vertebrate species, this stress-induced transcriptional enhancement is due to the activation of heat shock transcription factor 1 (HSF1), which is capable of specifically binding heat shock element (HSE). When cells are stressed, homotrimerized HSF1 translocates into the nucleus and is then hyperphosphorylated (77,194,201). The hsps, which are also expressed constitutively in cells, play an important role in normal cell physiology as well as heat shock. One of their more important functions is to protect organisms from the toxic effects of heating. They fulfill this function by binding to and stabilizing unfolded or partially denatured proteins, thus preventing the formation of damaging aggregates. Furthermore, the synthesis of hsps correlates with thermotolerance. Cell death from hyperthermia can result from necrosis or apoptosis, depending on the severity of the heat stress. There may be a critical temperature above which cells respond by necrosis rather than apoptosis.

1.6 The time-course of apoptosis

The fraction of cells undergoing programmed cell death or apoptosis at a particular time-point is valuable information to evaluate the effectiveness of therapy for a

Reproduced with permission of the copyright owner. Further reproduction prohibited without permission.

variety of diseases. Induction of apoptosis occurs at different rates depending on the cell line and apoptotic inducer. For example, significantly elevated levels of apoptosis are observed immediately after the completion of a 30 min period of 43° or 44°C heating or 6.25-μg/ml etoposide treatments in HL-60 cells (see Chapter 3 and 6). However, because apoptosis is a kinetic event, this estimation of the percentage or fraction of apoptotic cells (apoptotic index, AI) can be inaccurate and underestimated by the disintegration of apoptotic cells. Moreover, each apoptotic assay can detect apoptotic cells only in specific time-windows based on its detection method (e.g. caspases, TUNEL, annexin V, etc). The time window depends on the time of appearance of apoptotic cells after the inducing event and the length of time before apoptotic cells disintegrate in culture or are phagocytosed *in vivo*, or are no longer responsive to the specific assay. The cell type and apoptotic inducer also make the length of the time-window variable. Once the individual cells pass the specific time-window of the assay they are not counted as apoptotic cells. For example, the fraction of apoptosis after hyperthermia peaks at between 2 and 4 h in HL-60 cells, and then decreases as the apoptotic cells pass through the time-window of each assay (see Chapter 4). This underestimation of apoptosis is a serious disadvantage in interpreting apoptosis induction by therapeutic agents.

The total amount of apoptosis occurring during or after the treatment is much more valuable information than the apoptotic index. Two different approaches have been used to obtain a more accurate assessment of the incidence of apoptosis. One is to halt the apoptotic disintegration process and the other is to calculate the disintegration population. The purpose of both methods is to calculate the cumulative apoptotic index (CAI)

Reproduced with permission of the copyright owner. Further reproduction prohibited without permission.

(149,165). The fluorescent inhibitor of caspases (FLICA) FAM-VAD-FMK (6,164) was used to arrest cells in apoptosis, thereby preventing their disintegration or exit from the time-window of the assay (166). FAM-VAD-FMK is the fluorochrome (FAM)-labeled inhibitors of caspases (FLICA), which through the fluoromethylketone (FMK) element bind to the active center of the activated caspases. The peptide element of these inhibitors defines their specificity; VAD (Val-Ala-Asp) is generic to most caspases. However, the FLICA assay has several disadvantages. First, the continuous existence of inhibitor can affect the kinetics of apoptosis induction, the cell cycle, and other cell signaling and metabolic activities. Second, the FLICA assay is applicable only in the analysis of caspase-mediated apoptosis. Third, the existence of additional binding sites for FLICA could result in the overestimation of CAI. Fourth, this assay should be carefully tested for the proper concentration of FLICA to block the progression of apoptosis. In the second approach for CAI, a non-cycling cell line was used so there are no new cells resulting from cell division. Thus, the comparison of cell number before and after a treatment allow one to calculate the disintegrated cells and correct for them (149). This method is not good for cycling cells, though.

1.7 Purpose of the Project

Early studies of apoptosis focused on the isolation of mutants for understanding the role of genes alone and finding the homologs between species. This step could be called a 'one dimensional analysis' because it was the step to identify all members in the field or prepare to isolate the building blocks in a genomic view. Subsequent research

Reproduced with permission of the copyright owner. Further reproduction prohibited without permission.

tried to discover the functional relationship between genes, understand the connections in signal transduction, and categorize each member of a certain group. This work can be considered as making a network of interactions in a proteomic view. It could be called a 'two dimensional analysis' or 'qualitative analysis' because it was a necessary step to develop a big picture of apoptosis. In the future, understanding of apoptosis must expand to include other cellular phenomena such as proliferation with each cell cycle phase, differentiation, mutation, and senescence in a cytomic view. This might be known as 'three dimensional analysis' or 'quantitative analysis'. Cytomics is the functional relationships between the cell (Cytome) and the metabolic pathways (Proteomics-proteome) resulting from genetic control mechanisms (Genomics-genome) - some relate Cytomics to what is being termed functional genomics.

In the past study of cancer therapy, the end point was usually focused on the shrinkage of tumor volume. However, cancer could relapse with only a few cancer cells surviving after therapy. As the knowledge of genes involved in apoptosis grows, there is a need for new tools and models for evaluating therapy at the individual cell level with the change of status of multiple genes. In the present study, I have developed three techniques; an 'apoptotic quotient calculation' to estimate the amount of apoptosis from each cell cycle phase, a 'CAI estimation model' to calculate the CAI with time course AI data, and a 'cell cycle progression model' to understand and evaluate apoptosis and its interaction with cell proliferation.

Reproduced with permission of the copyright owner. Further reproduction prohibited without permission.

The apoptotic quotient calculation is for estimating how many apoptotic cells come from each cell cycle phase. This calculation is performed with Multi-2D® and Multicycle® software.

To overcome the disadvantages of FLICA and non-cycling cell assays for estimating the cumulative apoptotic index (CAI), as described above, I developed the CAI estimation model to estimate CAI by the kinetics of apoptosis. Based on measuring apoptotic index (AI) at multiple time points after a treatment, the kinetics of apoptosis can be explained as follows: First, the cells which start apoptosis early exit the time-window early ('first in, first out'). Second, the time-window (T_w) is constant in a particular system. Third, the shape of the AI time-dependent graph is a guideline for how many phases of apoptosis exist. When the graph is symmetrical (the apoptotic induction rate (AIR_i) is equal to the decreasing rate), apoptosis take place in a uni-phasic manner. If not, it could bi- or multi-phasic. Fourth, the apoptotic induction rate (AIR_i) of each phase is calculated. Fifth, the length of each phase (T_i) is calculated.

In order to obtain a comprehensive understanding of the effects of a treatment on apoptosis and cell cycle alterations, I developed a cell cycle progression model, which determined other important cell parameters. The number of cells counted at each time point, the number of induced apoptotic cells at each time point by AI and CAI, and the change of cell number in each cell cycle phase between every time point were measured, analyzed, and calculated based on the explanation and equations in the Materials and Methods section (Chapter 2). A cell cycle progression model was used to calculate all constants and variables, including the number of apoptotic cells from each cell cycle

Reproduced with permission of the copyright owner. Further reproduction prohibited without permission.

phase, the existence of cell cycle blocks with cell cycle progression, and cell cycle-specific resistance or sensitivity to apoptosis. I defined several parameters for explaining the model, which are the *apoptotic quotient (ApQ)*, *apoptosis probability index (API)*, *efflux coefficient (EC)* and the degree of sensitivity. *ApQ* represents the amount of apoptosis for each cell cycle phase. *API* represents the number of apoptotic cells expected in each phase if the treatment is not cell cycle specific. *EC* represents the existence of blocks in cell cycle phases. The degree of sensitivity indicates whether specific cell cycle phases are sensitive or resistant to an apoptotic agent. This study could be extended to an analysis of cell cycle progression and apoptosis changes in mutants, and could help to understand the molecular basis of cell cycle and apoptosis interactions by diverse mutations in genes regulating cell cycle and apoptosis.

Reproduced with permission of the copyright owner. Further reproduction prohibited without permission.

Reference List

1. Afanasyev VN, Korol BA, Matylevich NP, Pechatnikov VA, Umansky SR: The use of flow cytometry for the investigation of cell death. Cytometry 14:603-609, 1993.

2. Allan DJ, Harmon BV: The morphologic categorization of cell death induced by mild hyperthermia and comparison with death induced by ionizing radiation and cytotoxic drugs. Scan Electron Microsc Pt 3:1121-1133, 1986.

3. Barry MA, Behnke CA, Eastman A: Activation of programmed cell death (apoptosis) by cisplatin, other anticancer drugs, toxins, and hyperthermia. Biochem Pharmacol 40:2353-2362, 1990.

4. Barry MA, Reynolds JE, Eastman A: Etoposide-induced apoptosis in human HL-60 cells is associated with intracellular acidification. Cancer Res 53:2349-2357, 1993.

5. Bassnett S, Reinisch L, Beebe DC: Intracellular pH measurement using single excitation-dual emission fluorescence ratios. Am J Physiol 258:C171-C1781990.

6. Bedner E, Smolewski P, Amstad P, Darzynkiewicz Z: Activation of caspases measured in situ by binding of fluorochrome- labeled inhibitors of caspases (FLICA): correlation with DNA fragmentation. Exp Cell Res 259:308-313, 2000.

7. Ben-Sasson SA, Sherman Y, Gavrieli Y: Identification of dying cells--in situ staining. Methods Cell Biol 46:29-39, 1995.

8. Bowen C, Spiegel S, Gelmann EP: Radiation-induced apoptosis mediated by retinoblastoma protein. Cancer Res 58:3275-3281, 1998.

9. Bradbury DA, Simmons TD, Slater KJ, Crouch SP: Measurement of the ADP:ATP ratio in human leukaemic cell lines can be used as an indicator of cell viability, necrosis and apoptosis. J Immunol Methods 240:79-92, 2000.

10. Caelles C, Helmberg A, Karin M: p53-dependent apoptosis in the absence of transcriptional activation of p53-target genes. Nature 370:220-223, 1994.

11. Castedo M, Hirsch T, Susin SA, Zamzani N, Marchetti P, Macho A, Kroemer G: Sequential acquisition of mitochondrial and plasma membrane alterations during early lymphocyte apoptosis. J Immunol 157:512-521, 1996.

12. Chen YC, Lin-Shiau SY, Lin JK: Involvement of reactive oxygen species and caspase 3 activation in arsenite-induced apoptosis. J Cell Physiol 177:324-333, 1998.

13. Chittenden T, Harrington EA, O'Connor R, Flemington C, Lutz RJ, Evan GI, Guild BC: Induction of apoptosis by the Bcl-2 homologue Bak. Nature 374:733-736, 1995.

Reproduced with permission of the copyright owner. Further reproduction prohibited without permission.

14. Cho Y, Gorina S, Jeffrey PD, Pavletich NP: Crystal structure of a p53 tumor suppressor-DNA complex: Understanding tumorigenic mutations. Science 265:346-355, 1994.

15. Clarke AR, Purdie CA, Harrison DJ, Morris RG, Bird CC, Hooper ML, Wyllie AH: Thymocyte apoptosis induced by p53-dependent and independent pathways. Nature 362:849-852, 1993.

16. Clodi K, Kliche KO, Zhao S, Weidner D, Schenk T, Consoli U, Jiang S, Snell V, Andreeff M: Cell-surface exposure of phosphatidylserine correlates with the stage of fludarabine-induced apoptosis in chronic lymphocytic leukemia and expression of apoptosis-regulating genes. Cytometry 40:19-25, 2000.

17. Conradt B, Horvitz HR: The C. elegans protein EGL-1 is required for programmed cell death and interacts with the Bcl-2-like protein CED-9. Cell 93:519-529, 1998.

18. Darzynkiewicz Z, Bruno S, Del Bino G, Gorczyca W, Hotz MA, Lassota P, Traganos F: Features of apoptotic cells measured by flow cytometry. Cytometry 13:795-808, 1992.

19. Darzynkiewicz Z, Juan G, Li X, Gorczyca W, Murakami T, Traganos F: Cytometry in cell necrobiology: Analysis of apoptosis and accidental cell death (necrosis). Cytometry 27:1-20, 1997.

20. Darzynkiewicz Z, Li X, Gong J: Assays of cell viability : Discrimination of cells dying by apoptosis. Methods Cell Biol 41:15-38, 1994.

21. Davis MH, Altschuld RA, Jung DW, Brierley GP: Estimation of intramitochondrial pCa and pH by fura-2 and 2,7 biscarboxyethyl-5(6)-carboxyfluorescein (BCECF) fluorescence. Biochem Biophys Res Commun 149:40-45, 1987.

22. de Rozieres S, Maya R, Oren M, Lozano G: The loss of mdm2 induces p53-mediated apoptosis. Oncogene 19:1691-1697, 2000.

23. Del Bino G, Bruno S, Yi PN, Darzynkiewicz Z: Apoptotic cell death triggered by camptothecin or teniposide: The cell cycle specificity and effects of ionizing radiation. Cell Prolif Nov. 25:537-548, 1992.

24. del Peso L, Gonzalez VM, Inohara N, Ellis RE, Nunez G: Disruption of the CED-9.CED-4 complex by EGL-1 is a critical step for programmed cell death in Caenorhabditis elegans. J Biol Chem 275:27205-27211, 2000.

25. del Peso L, Gonzalez VM, Nunez G: Caenorhabditis elegans EGL-1 disrupts the interaction of CED-9 with CED-4 and promotes CED-3 activation. J Biol Chem 273:33495-33500, 1998.

26. Depraetere V: "Eat me" signals of apoptotic bodies. Nat Cell Biol 2:E1042000.

27. Desagher S, Osen-Sand A, Nichols A, Eskes R, Montessuit S, Lauper S, Maundrell K, Antonsson B, Martinou JC: Bid-induced conformational change of Bax is responsible for mitochondrial cytochrome c release during apoptosis. J Cell Biol 144:891-901, 1999.

28. Dewey WC, Hopwood LE, Sapareto SA, Gerweck LE: Cellular responses to combinations of hyperthermia and radiation. Radiology 123:463-474, 1977.

Reproduced with permission of the copyright owner. Further reproduction prohibited without permission.

29. Dive C, Gregory CD, Phipps DJ, Evans DL, Milner AE, Wyllie AH: Analysis and discrimination of necrosis and apoptosis (programmed cell death) by multiparameter flow cytometry. Biochim Biophys Acta 1133:275-285, 1992.

30. Dobrowsky E, Newell K, Tannock IF: The potential of lactate and succinate to kill nutrient deprived tumor cells by intracellular acidification. Int J Radiat Oncol Biol Phys 20:275-279, 1991.

31. Du C, Fang M, Li Y, Li L, Wang X: Smac, a mitochondrial protein that promotes cytochrome c-dependent caspase activation by eliminating IAP inhibition. Cell 102:33-42, 2000.

32. Dubrez L, Goldwasser F, Genne P, Pommier Y, Solary E: The role of cell cycle regulation and apoptosis triggering in determining the sensitivity of leukemic cells to topoisomerase I and II inhibitors. Leukemia 9:1013-1024, 1995.

33. Eastman A: Assays for DNA fragmentation, endonucleases, and intracellular pH and Ca2+ associated with apoptosis. Methods Cell Biol 46:41-55, 1995.

34. Ekert PG, Silke J, Vaux DL: Caspase inhibitors. Cell Death Differ 6:1081-1086, 1999.

35. Ekert PG, Silke J, Vaux DL: Inhibition of apoptosis and clonogenic survival of cells expressing crmA variants: optimal caspase substrates are not necessarily optimal inhibitors. EMBO J 18:330-338, 1999.

36. Elliott MJ, Stribinskiene L, Lock RB: Expression of Bcl-2 in human epithelial tumor (HeLa) cells enhances clonogenic survival following exposure to 5-fluoro-2'-deoxyuridine or staurosporine, but not following exposure to etoposide or doxorubicin. Cancer Chemother Pharmacol 41:457-463, 1998.

37. Ellis RE, Yuan JY, Horvitz HR: Mechanisms and functions of cell death. Annu Rev Cell Biol 7:663-698, 1991.

38. Enari M, Sakahira H, Yokoyama H, Okawa K, Iwamatsu A, Nagata S: A caspase-activated DNase that degrades DNA during apoptosis, and its inhibitor ICAD. Nature 391:43-50, 1998.

39. Endlich B, Radford IR, Forrester HB, Dewey WC: Computerized video time-lapse microscopy studies of ionizing radiation- induced rapid-interphase and mitosis-related apoptosis in lymphoid cells. Radiat Res 153:36-48, 2000.

40. Eskes R, Desagher S, Antonsson B, Martinou JC: Bid induces the oligomerization and insertion of Bax into the outer mitochondrial membrane. Mol Cell Biol 20:929-935, 2000.

41. Evan GI, Wyllie AH, Gilbert CS, Littlewood TD, Land H, Brooks M, Waters CM, Penn LZ, Hancock DC: Induction of apoptosis in fibroblasts by *c-myc* and *bcl-2* proto-oncogenes. Cell 69:119-128, 1992.

42. Facompre M, Wattez N, Kluza J, Lansiaux A, Bailly C: Relationship between cell cycle changes and variations of the mitochondrial membrane potential induced by etoposide. Mol Cell Biol Res Commun 4:37-42, 2000.

43. Fadok VA, Bratton DL, Rose DM, Pearson A, Ezekewitz RA, Henson PM: A receptor for phosphatidylserine-specific clearance of apoptotic cells. Nature 405:85-90, 2000.

Reproduced with permission of the copyright owner. Further reproduction prohibited without permission.

44. Fairbairn JJ, Khan MW, Ward KJ, Loveridge BW, Fairbairn DW, O'Neill KL: Induction of apoptotic cell DNA fragmentation in human cells after treatment with hyperthermia. Cancer Lett 89:183-188, 1995.

45. Falcieri E, Luchetti F, Burattini S, Canonico B, Santi S, Papa S: Lineage-related sensitivity to apoptosis in human tumor cells undergoing hyperthermia. Histochem Cell Biol 113:135-144, 2000.

46. Fearnhead HO, Chwalinski M, Snowden RT, Ormerod MG, Cohen GM: Dexamethasone and etoposide induce apoptosis in rat thymocytes from different phases of the cell cycle. Biochem Pharmacol 48:1073-1079, 1994.

47. Ferlini C, DiCesare S, Rainaldi G, Malorni W, Samoggia P, Biselli R, Fattorossi A: Flow cytometric analysis of the early phases of apoptosis by cellular and nuclear techniques. Cytometry 24:106-115, 1996.

48. Fernandes-Alnemri T, Litwack G, Alnemri ES: Mch2, a new member of the apoptotic Ced-3/Ice cysteine protease gene family. Cancer Res 55:2737-2742, 1995.

49. Fields S, Jang SK: Presence of a potent transcription activating sequence in the p53 protein. Science 249:1046-1049, 1990.

50. Fiers W, Beyaert R, Declercq W, Vandenabeele P: More than one way to die: apoptosis, necrosis and reactive oxygen damage. Oncogene 18:7719-7730, 1999.

51. Finucane DM, Bossy-Wetzel E, Waterhouse NJ, Cotter TG, Green DR: Bax-induced caspase activation and apoptosis via cytochrome c release from mitochondria is inhibitable by Bcl-xL. J Biol Chem 274:2225-2233, 1999.

52. Flavell RA, Su MS, Livingston DJ, Harding MW, Ku G, Lippke JA, Kuida K: Altered cytokine export and apoptosis in mice deficient in Interleukin-1 beta converting enzyme. Science 267:2000-2003, 1995.

53. Formigli L, Papucci L, Tani A, Schiavone N, Tempestini A, Orlandini GE, Capaccioli S, Orlandini SZ: Aponecrosis: morphological and biochemical exploration of a syncretic process of cell death sharing apoptosis and necrosis. J Cell Physiol 182:41-49, 2000.

54. Friedman PN, Chen X, Bargonetti J, Prives C: The p53 protein is an unusually shaped tetramer that binds directly to DNA. Proc Natl Acad Sci U S A 90:3319-3323, 1993.

55. Fujimura M, Morita-Fujimura Y, Kawase M, Copin JC, Calagui B, Epstein CJ, Chan PH: Manganese superoxide dismutase mediates the early release of mitochondrial cytochrome C and subsequent DNA fragmentation after permanent focal cerebral ischemia in mice. J Neurosci 19:3414-3422, 1999.

56. Gavrieli Y, Sherman Y, Ben-Sasson SA: Identification of programmed cell death in situ via specific labeling of nuclear fragmentation. J Cell Biol 119:493-501, 1992.

57. Gold R, Schmied M, Giegerich G, Breitschopf H, Hartung HP, Toyka KV, Lassmann H: Differentiation between cellular apoptosis and necrosis by the combined use of in situ tailing and nick translation techniques. Lab Invest 71:219-225, 1994.

Reproduced with permission of the copyright owner. Further reproduction prohibited without permission.

58. Gold R, Schmied M, Rothe G, Zichler H, Breitschopf H, Wekerle H, Lassmann H: Detection of DNA fragmentation in apoptosis: application of in situ nick translation to cell culture systems and tissue sections. J Histochem Cytochem 41:1023-1030, 1993.

59. Goldberg YP, Nicholson DW, Rasper DM, Kalchman MA, Koide HB, Graham RK, Bromm M, Kazemi-Esfarjani P, Thornberry NA, Vaillancourt JP, Hayden MR: Cleavage of huntingtin bt apopain, a proapoptotic cysteine protease, is modulated by the polyglutamine tract. Nat Genet 13:442-449, 1996.

60. Gorczyca W, Gong J, Ardelt B, Traganos F, Darzynkiewicz Z: The cell cycle related differences in susceptibility of HL-60 cells to apoptosis induced by various antitumor agents. Cancer Res 53:3186-3192, 1993.

61. Gorczyca W, Gong J, Darzynkiewicz Z: Dectection of DNA strand breaks in individual apoptotic cells by the in situ terminal deoxynucleotidyl transferase and nick translation assays. Cancer Res 53:1945-1951, 1993.

62. Gorman AM, Hirt UA, Zhivotovsky B, Orrenius S, Ceccatelli S: Application of a fluorometric assay to detect caspase activity in thymus tissue undergoing apoptosis in vivo. J Immunol Methods 226:43-48, 1999.

63. Goto A, Shomori K, Ohkumo T, Tanaka F, Sato K, Ito H: Hyperthermia-induced apoptosis occurs both in a p53 gene-dependent and - independent manner in three human gastric carcinoma cell lines. Oncol Rep 6:335-339, 1999.

64. Grasl-Kraupp B, Ruttkay-Nedecky B, Koudelka H, Bukowska K, Bursch W, Schulte-Hermann R: In situ detection of fragmented DNA (TUNEL assay) fails to discriminate among apoptosis, necrosis, and autolytic cell death: a cautionary note. Hepatology 21:1465-1468, 1995.

65. Green DR, Evan GI: A matter of life and death. Cancer Cell 1:19-30, 2002.

66. Green DR, Reed JC: Mitochondria and apoptosis. Science 281:1309-1312, 1998.

67. Gregory CD: Apoptosis and the immune response. Wiley-Liss, New York, 1995.

68. Gross A, Yin XM, Wang K, Wei MC, Jockel J, Milliman C, Erdjument-Bromage H, Tempst P, Korsmeyer SJ: Caspase cleaved BID targets mitochondria and is required for cytochrome c release, while BCL-XL prevents this release but not tumor necrosis factor-R1/Fas death. J Biol Chem 274:1156-1163, 1999.

69. Grynkiewicz G, Poenie M, Tsien RY: A new generation of Ca^{2+}indicators with greatly improved fluorescence properties. J Biol Chem 260, No.6:3440-3450, 1985.

70. Gu Y, Kuida K, Tsutsui H, Ku G, Hsiao K, Fleming MA, Hayashi N, Higashino K, Okamura H, Nakanishi K, Kurimoto M, Tanimoto T, Flavell RA, Sato V, Harding MW, Livingston DJ, Su MS: Activation of interferon-gamma inducing factor mediated by interleukin-1beta converting enzyme. Science 275:206-209, 1997.

71. Haapajarvi T, Kivinen L, Heiskanen A, des BC, Datto MB, Wang XF, Laiho M: UV radiation is a transcriptional inducer of p21(Cip1/Waf1) cyclin- kinase inhibitor in a p53-independent manner. Exp Cell Res 248:272-279, 1999.

Reproduced with permission of the copyright owner. Further reproduction prohibited without permission.

72. Halazonetis TD, Kandil AN: Conformational shifts propagate from the oligomerization domain of p53 to its tetrameric DNA binding domain and restore DNA binding to select p53 mutants. EMBO J 12:5057-5064, 1993.

73. Hall EJ: Radiobiology for the Radiobiologist. 4th Edition. J.B. Lippencott Co., Philadelphia, PA, 1994.

74. Hara S, Halicka HD, Bruno S, Gong J, Traganos F, Darzynkiewicz Z: Effect of protease inhibitors on early events of apoptosis. Exp Cell Res 223:372-384, 1996.

75. Harmon BV, Corder AM, Collins RJ, Gobe GC, Allen J, Allan DJ, Kerr JFR: Cell death induced in a murine mastocytoma by 42-47° C heating in vitro: Evidence that the form of death changes from apoptosis to necrosis above a critical heat load. Int J Radiat Biol 58:845-858, 1990.

76. Harris MH, Thompson CB: The role of the Bcl-2 family in the regulation of outer mitochondrial membrane permeability. Cell Death Differ 7:1182-1191, 2000.

77. He L, Fox MH: Activation of heat-shock transcription factor 1 in heated Chinese hamster ovary cells is dependent on the cell cycle and is inhibited by sodium vanadate. Radiat Res 151:283-292, 1999.

78. Hengartner MO: The biochemistry of apoptosis. Nature 407:770-776, 2000.

79. Hengartner MO: Apoptosis: corralling the corpses. Cell 104:325-328, 2001.

80. Hengartner MO, Horvitz HR: C. elegans cell survival gene ced-9 encodes a functional homolog of the mammalian proto-oncogene bcl-2. Cell 76:665-676, 1994.

81. Hickman JA: Apoptosis induced by anticancer drugs. Cancer Metastasis Rev 11:121-139, 1992.

82. Hockenbery D, Nunez G, Milliman C, Schreiber RD, Korsmeyer SJ: Bcl-2 is an inner mitochondrial membrane protein that blocks programmed cell death. Nature 348:334-336, 1990.

83. Holler N, Zaru R, Micheau O, Thome M, Attinger A, Valitutti S, Bodmer JL, Schneider P, Seed B, Tschopp J: Fas triggers an alternative, caspase-8-independent cell death pathway using the kinase RIP as effector molecule. Nat Immunol 1:489-495, 2000.

84. Hotz MA, Gong J, Traganos F, Darzynkiewicz Z: Flow cytometric detection of apoptosis: Comparison of the assays of in situ DNA degradation and chromatin changes. Cytometry 15:237-244, 1994.

85. Hsu YT, Wolter KG, Youle RJ: Cytosol-to-membrane redistribution of Bax and Bcl-X(L) during apoptosis. Proc Natl Acad Sci U S A 94:3668-3672, 1997.

86. Huang Y, Chan AML, Liu Y, Wang X, Holbrook NJ: Serum withdrawal and etoposide induce apoptosis in human lung carcinoma cell line A549 via distinct pathways. Apoptosis 2:1997.

Reproduced with permission of the copyright owner. Further reproduction prohibited without permission.

87. Hug H, Los M, Hirt W, Debatin KM: Rhodamine 110-linked amino acids and peptides as substrates to measure caspase activity upon apoptosis induction in intact cells. Biochemistry 38:13906-13911, 1999.

88. Inomata M, Saijo N, Kawashima K, Kaneko A, Fujiwara Y, Kunikane H, Tanaka Y: Induction of apoptosis in cultured retinoblastoma cells by the protein phosphatase inhibitor, okadaic acid. J Cancer Res Clin Oncol 121:729-738, 1995.

89. Irmler M, Hertig S, MacDonald HR, Sadoul R, Becherer JD, Proudfoot A, Solari R, Tschopp J: Granzyme A is an interleukin 1 beta-converting enzyme. J Exp Med 181:1917-1922, 1995.

90. Isola R, Falchi AM, Diana A, Diaz G: Probing mitochondrial probes. Cytometry 41:1482000.

91. Jayaraman J, Prives C: Activation of p53 sequence-specific DNA binding by short single strands of DNA requires the p53 C-terminus. Cell 81:1021-1029, 1995.

92. Jiang M, Milner J: Bcl-2 constitutively suppresses p53-dependent apoptosis in colorectal cancer cells. Genes Dev 17:832-837, 2003.

93. Jones SN, Roe AE, Donehower LA, Bradley A: Rescue of embryonic lethality in Mdm2-deficient mice by absence of p53. Nature 378:206-208, 1995.

94. Kaganab VE, Fabisiaka JP, Shvedovad AA, Tyurinaal YY, Tyurinal VA, Schorbc NF, Kawaia K: Oxidative signaling pathway for externalization of plasma membrane phosphatidylserine during apoptosis [In Process Citation]. FEBS Lett 477:1-7, 2000.

95. Kam CM, Hudig D, Powers JC: Granzymes (lymphocyte serine proteases): characterization with natural and synthetic substrates and inhibitors. Biochim Biophys Acta 1477:307-323, 2000.

96. Katschinski DM, Boos K, Schindler SG, Fandrey J: Pivotal role of reactive oxygen species as intracellular mediators of hyperthermia-induced apoptosis. J Biol Chem 275:21094-21098, 2000.

97. Kerr JFR, Winterford CM, Harmon BV: Apoptosis: Its significance in cancer and cancer therapy. Cancer 73:2013-2026, 1994.

98. Kiefer MC, Brauer MJ, Powers VC, Wu JJ, Umansky SR, Tomei LD, Barr PJ: Modulation of apoptosis by the widely distributed Bcl-2 homologue Bak. Nature 374:736-739, 1995.

99. Korsmeyer SJ, Wei MC, Saito M, Weiler S, Oh KJ, Schlesinger PH: Pro-apoptotic cascade activates BID, which oligomerizes BAK or BAX into pores that result in the release of cytochrome c. Cell Death Differ 7:1166-1173, 2000.

100. Kressel M, Groscurth P: Distinction of apoptotic and necrotic cell death by in situ labelling of fragmented DNA. Cell Tissue Res 278:549-556, 1994.

101. Lattanzio FA, Jr.: The effects of pH and temperature on fluorescent calcium indicators as determined with chelex-100 and EDTA buffer systems. Biochem Biophys Res Commun 171:102-108, 1990.

Reproduced with permission of the copyright owner. Further reproduction prohibited without permission.

102. Lavin MF, Watters D: Programmed cell death: the cellular and molecular biology of apoptosis. Harwood academic publishers, Unied States, 1993.

103. Lecoeur H, Prevost MC, Gougeon ML: Oncosis is associated with exposure of phosphatidylserine residues on the outside layer of the plasma membrane: a reconsideration of the specificity of the annexin V/propidium iodide assay. Cytometry 44:65-72, 2001.

104. Lee S, Elenbaas B, Levine A, Griffith J: p53 and its 14 kDa C-terminal domain recognize primary DNA damage in the form of insertion/deletion mismatches. Cell 81:1013-1020, 1995.

105. Leist M, Nicotera P: Apoptosis versus necrosis: the shape of neuronal cell death. Results Probl Cell Differ 24:105-135, 1998.

106. Levine AJ: p53, the cellular gatekeeper for growth and division. Cell 88:323-331, 1997.

107. Lewin B: Genes IV. Oxford University Press, Oxford NewYork Tokyo, 1997.

108. Li H, Zhu H, Xu CJ, Yuan J: Cleavage of BID by caspase 8 mediates the mitochondrial damage in the Fas pathway of apoptosis. Cell 94:491-501, 1998.

109. Li P, Allen H, Banerjee S, Franklin S, Herzog L, Johnston C, McDowell J, Paskind M, Rodman L, Salfeld J: Mice deficient in IL-1 beta-converting enzyme are defective in production of mature IL-1 beta and resistant to endotoxic shock. Cell 80:401-411, 1995.

110. Li P, Nijhawan D, Budihardjo I, Srinivasula SM, Ahmad M, Alnemri ES, Wang X: Cytochrome c and dATP-dependent formation of Apaf-1/caspase-9 complex initiates an apoptotic protease cascade. Cell 91:479-489, 1997.

111. Li WX, Chen CH, Ling CC, Li GC: Apoptosis in heat-induced cell killing: The protective role of hsp70 and the sensitization effect of the c-*myc* gene. Radiat Res 145:324-330, 1996.

112. Li X, Melamed MR, Darzynkiewicz Z: Detection of apoptosis and DNA replication by differential labeling of DNA strand breaks with fluorochromes of different color. Exp Cell Res 222:28-37, 1996.

113. Lipton SA, Bossy-Wetzel E: Dueling activities of AIF in cell death versus survival: DNA binding and redox activity. Cell 111:147-150, 2002.

114. Liu J, Bhalgat M, Zhang C, Diwu Z, Hoyland B, Klaubert DH: Fluorescent molecular probes V: a sensitive caspase-3 substrate for fluorometric assays. Bioorg Med Chem Lett 9:3231-3236, 1999.

115. Liu X, Kim CN, Yang J, Jemmerson R, Wang X: Induction of apoptotic program in cell-free extracts: requirement for dATP and cytochrome c. Cell 86:147-157, 1996.

116. Liu X, Li P, Widlak P, Zou H, Luo X, Garrard WT, Wang X: The 40-kDa subunit of DNA fragmentation factor induces DNA fragmentation and chromatin condensation during apoptosis. Proc Natl Acad Sci U S A 95:8461-8466, 1998.

117. Liu X, Zou H, Slaughter C, Wang X: DFF, a heterodimeric protein that functions downstream of caspase-3 to trigger DNA fragmentation during apoptosis. Cell 89:175-184, 1997.

Reproduced with permission of the copyright owner. Further reproduction prohibited without permission.

118. Lock RB, Stribinskiene L: Dual modes of death induced by etoposide in human epithelial tumor cells allow Bcl-2 to inhibit apoptosis without affecting clonogenic survival. Cancer Res 56:4006-4012, 1996.

119. Lotem J, Sachs L: Regulation by bcl-2, c-myc and p53 of susceptibility to induction of apoptosis by heat shock and cancer chemotherapy compounds in differentiation-competent and defective myeloid leukemic cells. Cell Growth Differ 4:41-47, 1993.

120. Lotem J, Sachs L: A mutant p53 antagonizes the deregulated c-myc-mediated enhancement of apoptosis and decrease in leukemogenicity. Proc Natl Acad Sci U S A 92:9672-9676, 1995.

121. Lowe SW, Schmitt EM, Smith SW, Osborne BA, Jacks T: p53 is required for radiation-induced apoptosis in mouse thymocytes. Nature 362:847-849, 1993.

122. Luo X, Budihardjo I, Zou H, Slaughter C, Wang X: Bid, a Bcl2 interacting protein, mediates cytochrome c release from mitochondria in response to activation of cell surface death receptors. Cell 94:481-490, 1998.

123. Macho A, Decaudin D, Castedo M, Hirsch T, Susin SA, Zamzami N, Kroemer G: Chloromethyl-X-Rosamine is an aldehyde-fixable potential-sensitive fluorochrome for the detection of early apoptosis. Cytometry 25:333-340, 1996.

124. McLure KG, Lee PW: p53 DNA binding can be modulated by factors that alter the conformational equilibrium. EMBO J 18:763-770, 1999.

125. Michael D, Oren M: The p53-Mdm2 module and the ubiquitin system. Semin Cancer Biol 13:49-58, 2003.

126. Montes de Oca LR, Wagner DS, Lozano G: Rescue of early embryonic lethality in mdm2-deficient mice by deletion of p53. Nature 378:203-206, 1995.

127. Mullbacher A, Ebnet K, Blanden RV, Hla RT, Stehle T, Museteanu C, Simon MM: Granzyme A is critical for recovery of mice from infection with the natural cytopathic viral pathogen, ectromelia. Proc Natl Acad Sci U S A 93:5783-5787, 1996.

128. Musgrove E, Rugg C, Hedley D: Flow cytometric measurement of cytoplasmic pH: A critical evaluation of available fluorochromes. Cytometry 7:347-355, 1986.

129. Nagaich AK, Zhurkin VB, Durell SR, Jernigan RL, Appella E, Harrington RE: p53-induced DNA bending and twisting: p53 tetramer binds on the outer side of a DNA loop and increases DNA twisting. Proc Natl Acad Sci U S A 96:1875-1880, 1999.

130. Nagata S: Apoptosis by death factor. Cell 88:355-365, 1997.

131. Nagata S: Apoptotic DNA fragmentation. Exp Cell Res 256:12-18, 2000.

132. Nakano H, Kurihara K, Okamoto M, Tone S, Shinohara K: Heat-induced apoptosis and p53 in cultured mammalian cells. Int J Radiat Biol 71:519-529, 1997.

133. Nakano H, Shinohara K: X-ray-induced cell death: Apoptosis and necrosis. Radiat Res 140:1-9, 1994.

Reproduced with permission of the copyright owner. Further reproduction prohibited without permission.

134. Nasir J, Goldberg YP, Hayden MR: Huntington disease: new insights into the relationship between CAG expansion and disease. Hum Mol Genet 5:1431-1435, 1996.

135. Nicholson DW: ICE/CED3-like proteases as therapeutic targets for the control of inappropriate apoptosis. Nat Biotechnol 14:297-301, 1996.

136. Nicholson DW: Caspase structure, proteolytic substrates, and function during apoptotic cell death. Cell Death Differ 6:1028-1042, 1999.

137. Nicholson DW, Ali A, Thornberry NA, Vaillancourt JP, Ding CK, Gallant M, Gareau Y, Griffin PR, Labelle M, Lazebnik YA: Identification and inhibition of the ICE/CED-3 protease necessary for mammalian apoptosis. Nature 376:37-43, 1995.

138. Nicholson DW, Thornberry NA: Caspases: killer proteases. Trends Biochem Sci 22:299-306, 1997.

139. Nicotera P, Leist M, Ferrando-May E: Apoptosis and necrosis: different execution of the same death. Biochem Soc Symp 66:69-73, 1999.

140. O'Brien MC, Healy SF, Jr., Raney SR, Hurst JM, Avner B, Hanly A, Mies C, Freeman JW, Snow C, Koester SK, Bolton WE: Discrimination of late apoptotic/necrotic cells (type III) by flow cytometry in solid tumors. Cytometry 28:81-89, 1997.

141. O'Brien V, Frisch SM, Juliano RL: Expression of the integrin α5 subunit in HT29 colon carcinoma cells suppresses apoptosis triggered by serum deprivation. Exp Cell Res 224:208-213, 1996.

142. O'Connor L, Harris AW, Strasser A: CD95 (Fas/APO-1) and p53 signal apoptosis independently in diverse cell types. Cancer Res 60:1217-1220, 2000.

143. Oren M: p53: The ultimate tumor suppressor gene? FASEB J 6:3169-3176, 1992.

144. Park A, Baichwal VR: Systematic mutational analysis of the death domain of the tumor necrosis factor receptor 1-associated protein TRADD. J Biol Chem 271:9858-9862, 1996.

145. Perkins CL, Fang G, Kim CN, Bhalla KN: The role of Apaf-1, caspase-9, and bid proteins in etoposide- or paclitaxel-induced mitochondrial events during apoptosis. Cancer Res 60:1645-1653, 2000.

146. Pinkoski MJ, Green DR: Fas ligand, death gene. Cell Death Differ 6:1174-1181, 1999.

147. Porter AG, Janicke RU: Emerging roles of caspase-3 in apoptosis. Cell Death Differ 6:99-104, 1999.

148. Porter AG, Ng P, Jänicke RU: Death substrates come alive. BioEssays 19:501-507, 1997.

149. Prieto A, Diaz D, Barcenilla H, Garcia-Suarez J, Reyes E, Monserrat J, San Antonio E, Melero D, De La HA, Orfao A, Alvarez-Mon M: Apoptotic rate: A new indicator for the quantification of the incidence of apoptosis in cell cultures. Cytometry 48:185-193, 2002.

Reproduced with permission of the copyright owner. Further reproduction prohibited without permission.

150. Radford IR, Murphy TK, Radley JM, Ellis SL: Radiation response of mouse lymphoid and myeloid cell lines. Part II. Apoptotic death is shown by all lines examined. Int J Radiat Biol 65:217-227, 1994.

151. Raff M: Cell suicide for beginners. Nature 396:119-122, 1998.

152. Raycroft L, Wu HY, Lozano G: Transcriptional activation by wild-type but not transforming mutants of the p53 anti-oncogene. Science 249:1049-1051, 1990.

153. Reed JC: Bcl-2 family proteins. Oncogene 17:3225-3236, 1998.

154. Rijkers GT, Justement LB, Griffioen AW, Cambier JC: Improved method for measuring intracellular Ca^{++} with Fluo-3. Cytometry 11:923-927, 1990.

155. Rotonda J, Nicholson DW, Fazil KM, Gallant M, Gareau Y, Labelle M, Peterson EP, Rasper DM, Ruel R, Vaillancourt JP, Thornberry NA, Becker JW: The three-dimensional structure of apopain/CPP32, a key mediator of apoptosis. Nat Struct Biol 3:619-625, 1996.

156. Sakahira H, Enari M, Nagata S: Cleavage of CAD inhibitor in CAD activation and DNA degradation during apoptosis. Nature 391:96-99, 1998.

157. Sapareto SA, Dewey WC: Thermal dose determination in cancer therapy. Int J Radiat Oncol Biol Phys 10:787-800, 1984.

158. Searle J, Kerr JFR, Bishop C: Necrosis and apoptosis: Distinct modes of cell death with fundamentally different significance. Pathology Annual 17:229-259, 1982.

159. Seki H, Kanegane H, Iwai K, Konno A, Ohta K, Yachie A, Taniguchi N, Miyawaki T: Ionizing radiation induces apoptotic cell death in human TcR-gamma/δ^+ T and natural killer cells without detectable p53 protein. Eur J Immunol 24:2914-2917, 1994.

160. Sellins K, Cohen JJ: Hyperthermia induces apoptosis in thymocytes. Radiat Res 126:88-95, 1991.

161. Shimizu S, Ide T, Yanagida T, Tsujimoto Y: Electrophysiological study of a novel large pore formed by Bax and the voltage-dependent anion channel that is permeable to cytochrome c. J Biol Chem 275:12321-12325, 2000.

162. Shimizu S, Narita M, Tsujimoto Y: Bcl-2 family proteins regulate the release of apoptogenic cytochrome c by the mitochondrial channel VDAC. Nature 399:483-487, 1999.

163. Shresta S, Graubert TA, Thomas DA, Raptis SZ, Ley TJ: Granzyme A initiates an alternative pathway for granule-mediated apoptosis. Immunity 10:595-605, 1999.

164. Smolewski P, Bedner E, Du L, Hsieh TC, Wu JM, Phelps DJ, Darzynkiewicz Z: Detection of caspases activation by fluorochrome-labeled inhibitors: Multiparameter analysis by laser scanning cytometry. Cytometry 44:73-82, 2001.

165. Smolewski P, Grabarek J, Lee BW, Johnson GL, Darzynkiewicz Z: Kinetics of HL-60 cell entry to apoptosis during treatment with TNF- alpha or camptothecin assayed by the stathmo-apoptosis method. Cytometry 47:143-149, 2002.

Reproduced with permission of the copyright owner. Further reproduction prohibited without permission.

166. Smolewski P, Grabarek J, Phelps DJ, Darzynkiewicz Z: Stathmo-apoptosis: arresting apoptosis by fluorochrome-labeled inhibitor of caspases. Int J Oncol 19:657-663, 2001.

167. Strasser A, Harris AW, Bath ML, Cory S: Novel primitive lymphoid tumors induced in transgenic mice by cooperation between *myc* and *bcl-2*. Nature 348:331-333, 1990.

168. Stroh C, Schulze-Osthoff K: Death by a thousand cuts: an ever increasing list of caspase substrates. Cell Death Differ 5:997-1000, 1998.

169. Sugimoto K, Toyoshima H, Sakai R, Miyagawa K, Hagiwara K, Ishikawa F, Takaku F, Yazaki Y, Hirai H: Frequent mutations in the p53 gene in human myeloid leukemia cell lines. Blood 79:2378-2383, 1992.

170. Takano YS, Harmon BV, Kerr JFR: Apoptosis induced by mild hyperthermia in human and murine tumour cell lines: A study using electron microscopy and DNA gel electrophoresis. J Pathol 163:329-336, 1991.

171. Takasu T, Lyons JC, Park HJ, Song CW: Apoptosis and perturbation of cell cycle progression in an acidic environment after hyperthermia. Cancer Res 58:2504-2508, 1998.

172. Talanian RV, Quinlan C, Trautz S, Hackett MC, Mankovich JA, Banach D, Ghayur T, Brady KD, Wong WW: Substrate specificities of caspase family proteases. J Biol Chem 272:9677-9682, 1997.

173. Thornberry NA, Lazebnik Y: Caspases: enemies within. Science 281:1312-1316, 1998.

174. Thornberry NA, Rano TA, Peterson EP, Rasper DM, Timkey T, Garcia-Calvo M, Houtzager VM, Nordstrom PA, Roy S, Vaillancourt JP, Chapman KT, Nicholson DW: A combinatorial approach defines specificities of members of the caspase family and granzyme B. Functional relationships established for key mediators of apoptosis. J Biol Chem 272:17907-17911, 1997.

175. Tolskaya EA, Romanova LI, Kolesnikova MS, Ivannikova TA, Agol VI: Final checkpoint in the drug-promoted and poliovirus-promoted apoptosis is under post-translational control by growth factors. J Cell Biochem 63:422-431, 1996.

176. Tsujimoto Y: Apoptosis and necrosis: intracellular ATP level as a determinant for cell death modes. Cell Death Differ 4:429-434, 1997.

177. Tsujimoto Y, Shimizu S: VDAC regulation by the Bcl-2 family of proteins. Cell Death Differ 7:1174-1181, 2000.

178. van Engeland M, Nieland LJW, Ramaekers FCS, Schutte B, Reutelingsperger CPM: Annexin V-affinity assay: A review on an apoptosis detection system based on phosphatidylserine exposure. Cytometry 31:1-9, 1998.

179. van Engeland M, Ramaekers FCS, Schutte B, Reutelingsperger CPM: A novel assay to measure loss of plasma membrane asymmetry during apoptosis of adherent cells in culture. Cytometry 24:131-139, 1996.

180. van Erp PEJ, Jansen MJJM, de Jongh GJ, Boezeman JBM, Schalkwijk J: Ratiometric measurement of intracellular pH in cultured human keratinocytes using carboxy-SNARF-1 and flow cytometry. Cytometry 12:127-132, 1991.

Reproduced with permission of the copyright owner. Further reproduction prohibited without permission.

181. Vander Heiden MG, Chandel NS, Schumacker PT, Thompson CB: Bcl-xL prevents cell death following growth factor withdrawal by facilitating mitochondrial ATP/ADP exchange. Mol Cell 3:159-167, 1999.

182. Verhagen AM, Ekert PG, Pakusch M, Silke J, Connolly LM, Reid GE, Moritz RL, Simpson RJ, Vaux DL: Identification of DIABLO, a mammalian protein that promotes apoptosis by binding to and antagonizing IAP proteins. Cell 102:43-53, 2000.

183. Vidair CA, Wang Z, Dewey WC: Noninvolvement of the heat-induced increase in the concentration of intracellular free Ca^{2+} in killing by heat and induction of thermotolerance. Radiat Res 124:156-164, 1990.

184. Vreeswijk MP, Westland BE, Hess MT, Naegeli H, Vrieling H, van Zeeland AA, Mullenders LH: Impairment of nucleotide excision repair by apoptosis in UV-irradiated mouse cells. Cancer Res 58:1978-1985, 1998.

185. Wang K, Yin XM, Chao DT, Milliman CL, Korsmeyer SJ: BID: a novel BH3 domain-only death agonist. Genes Dev 10:2859-2869, 1996.

186. Wang Y, Rea T, Bian J, Gray S, Sun Y: Identification of the genes responsive to etoposide-induced apoptosis: application of DNA chip technology. FEBS Lett 445:269-273, 1999.

187. Wang ZQ, Auer B, Stingl L, Berghammer H, Haidacher D, Schweiger M, Wagner EF: Mice lacking ADPRT and poly(ADP-ribosyl)ation develop normally but are susceptible to skin disease. Genes Dev 9:509-520, 1995.

188. Westra A, Dewey WC: Variation in sensitivity to heat shock during the cell-cycle of chinese hamster ovary cells in vitro. Int J Radiat Biol 19:467-477, 1971.

189. Wieder ED, Fox MH: The role of intracellular free calcium in the cellular response to hyperthermia. Int J Hyperthermia 11:733-742, 1995.

190. Wieder ED, Hang H, Fox MH: Measurement of intracellular pH using flow cytometry with carboxy-SNARF-1. Cytometry 14:916-921, 1993.

191. Wolf D, Rotter V: Major deletions in the gene encoding the p53 tumor antigen cause lack of p53 expression in HL-60 cells. Proc Natl Acad Sci U S A 82:790-794, 1985.

192. Wolter KG, Hsu YT, Smith CL, Nechushtan A, Xi XG, Youle RJ: Movement of Bax from the cytosol to mitochondria during apoptosis. J Cell Biol 139:1281-1292, 1997.

193. Woods CM, Zhu J, McQueney PA, Bollag D, Lazarides E: Taxol-induced mitotic block triggers rapid onset of a p53-independent apoptotic pathway. Mol Med 1:506-526, 1995.

194. Wu C: Heat shock transcription factors: Structure and regulation. Annu Rev Cell Dev Biol 11:441-469, 1995.

195. Wyllie A: Apoptosis. An endonuclease at last. Nature 391:20-21, 1998.

196. Wyllie AH, Kerr JFR, Currie AR: Cell death: The significance of apoptosis. Int Rev Cytol 68:251-306, 1980.

Reproduced with permission of the copyright owner. Further reproduction prohibited without permission.

197. Yonezawa M, Otsuka T, Kato T, Moriyama A, Kato KH, Asai K, Matsui N: Hyperthermic induction of apoptosis in malignant fibrous histiocytoma cells: possible involvement of a p53-independent pathway in the induction of bax gene. J Orthop Sci 7:117-122, 2002.

198. Yu Y, Little JB: p53 is involved in but not required for ionizing radiation-induced caspase-3 activation and apoptosis in human lymphoblast cell lines. Cancer Res 58:4277-4281, 1998.

199. Zamzami N, Brenner C, Marzo I, Susin SA, Kroemer G: Subcellular and submitochondrial mode of action of Bcl-2-like oncoproteins. Oncogene 16:2265-2282, 1998.

200. Zou H, Henzel WJ, Liu X, Lutschg A, Wang X: Apaf-1, a human protein homologous to C.elegans CED-4, participates in cytochrome C-dependent activation of caspase-3. Cell 90:405-413, 1997.

201. Zou J, Guo Y, Guettouche T, Smith DF, Voellmy R: Repression of heat shock transcription factor HSF1 activation by HSP90 (HSP90 complex) that forms a stress-sensitive complex with HSF1. Cell 94:471-480, 1998.

Reproduced with permission of the copyright owner. Further reproduction prohibited without permission.

CHAPTER 2

MATERIALS AND METHODS

2.1 Cell Lines and Cell Culture

Human promyelocytic leukemic HL-60 cells and HCW-2 cells, a variant of the human HL-60 cell line that is resistant to apoptosis, were kindly provided by Z. Darzynkiewicz (New York Medical College, Hawthorne, NY) and E.A. Hendrickson (Brown University, Providence, RI). The HL-60 cell lines lack the expression of p53 due to major deletions in the gene (8). The resistance to apoptosis characteristic of HCW-2 cells results from being unable to release cytochrome C into the cytosol after apoptotic stimuli (4,5).

The HL-60 cells were routinely grown in RPMI1640 medium (GIBCO/BRL Life Technologies, Inc., Grand Island, NY) supplemented with 10 % fetal bovine serum (Nova-Tech, Inc., Grand Island, NE) and 100-units/ml penicillin, 100 μg/ml streptomycin (GIBCO/BRL Life Technologies, Inc., Grand Island, NY), and 2 mM L-glutamine (Sigma Chemical Co., St. Louis, MO). They were grown in suspension in 25 cm^2 flasks (Greiner Labortechnik, CELLSTAR) in a humidified incubator at 37 °C in a 5 % CO_2 environment. HL-60 cell densities in stock cultures were kept below 6 x 10^5 cells/ml.

Reproduced with permission of the copyright owner. Further reproduction prohibited without permission.

2.2 Induction of Apoptosis by Hyperthermia

Appropriate numbers of cells were inoculated into T25 flasks 22-26 hrs before heating so that approximately 1 x 10^6 exponentially growing cells were present at the time of heating. Cells were heated at 45 °C (± 0.1 °C) for 15 min or 30 min, then incubated at 37 °C for various times or heated at different temperatures for different times for isodose experiments. At selected times cells were collected, centrifuged and fixed (see below).

2.3 Induction of Apoptosis by Chemical Treatments

Cells treated with etoposide, an inhibitor of topoisomerase II (Sigma Chemical Co., St. Louis, MO), were used for a positive control. The stock solution of 625-μg/ml etoposide in dimethylsulfoxide (DMSO) was stored at -20 °C until used. Etoposide was added to 1 x 10^6 cells in the flask at a final concentration of 6.25-μg/ml (approximately 10.6 μM) in the medium. After 3 hr of incubation at 37 °C, cells were collected, centrifuged and fixed (see below).

2.4 TUNEL Assay

After the induction of apoptosis, cells were fixed in freshly prepared 0.5 % paraformaldehyde solution (pH 7.4) at 4° C for 15 min in the dark, centrifuged, then fixed in ice-cold 70 % ethanol and stored in a freezer overnight. The cells were labeled for apoptosis with the "*In Situ* Cell Death Detection Kit, Fluorescein" (Roche Diagnostics Corporation, Roche Applied Science, Indianapolis, IN) according to recommended

Reproduced with permission of the copyright owner. Further reproduction prohibited without permission.

procedures with modifications in permeabilization time and temperature to improve results. Briefly, fixed cells were centrifuged and washed once in phosphate-buffered saline (PBS) containing 1% bovine serum albumin (BSA), then resuspended in 2 ml permeabilization buffer (0.1% Triton X-100 and 0.1% sodium citrate in PBS) for 25 min at room temperature and washed twice in 0.2 ml PBS/1% BSA. The cells were resuspended in 50 µl TUNEL reaction mixture (TdT enzyme and labeling solution) and incubated for 60 min at 37 °C in a humidified dark atmosphere in an incubator. The labeled cells were washed once in 0.1% Triton X-100 in PBS and washed again in PBS/1% BSA, then resuspended in 0.5 ml ice-cold PBS containing 2.5-µg/ml Propidium Iodide (PI) and 40 kunits units RNase A (Sigma Chemical Co., St. Louis, MO) for at least 30 min. The stained cells were filtered through 40-µm-nylon mesh (Small Parts Inc., Miami Lakes, FL) before flow cytometry analysis.

2.5 Bromodeoxyuridine (BrdU) labeling assay

For the pulse labeling of BrdU, 50 µl of BrdU (Sigma Chemical Co., St. Louis, MO) stock solution (1 mM) was added to a flask of 10^5 cells/ml, giving 10 µM BrdU final concentration. The cells were incubated for 30 min at 37° C and washed twice with 5 ml pre-warmed medium and incubated for 3 hr with 6.25-µg/ml etoposide. Cells were fixed in ice-cold 70 % ethanol and stored in a cold room (4° C) overnight. Fixed cells were centrifuged and washed once in 2 ml PBS, then resuspended in 0.7 ml of denaturation solution (0.2 mg/ml pepsin in 2 N HCl) for 15 min at 37 °C in the dark and suspended with 1.88 ml 1M Tris buffer (Trizma base, Sigma Chemical Co.) to terminate the hydrolysis and washed in 2 ml PBS. The cells were resuspended in 100-µl anti-BrdU

Reproduced with permission of the copyright owner. Further reproduction prohibited without permission.

antibody (DakoCytomation, Carpinteria, CA) with 1:30 dilution in TBFP permeable buffer (0.5 % Tween-20, 1 % bovine serum albumin and 1 % fetal bovine serum in PBS) and incubated for 25 min at room temperature in the dark and washed in 2 ml PBS. The primary antibody-labeled cells were resuspended in 200 µl Alexa Fluor® $F(ab')_2$ fragment of goat anti-mouse IgG (H+L) (2 mg/mL) (Molecular Probes, Eugene, OR) with 1:200 dilution in TBFP permeable buffer and incubated for 25 min at room temperature in the dark and washed in 2 ml PBS, then resuspended in 0.5 ml PBS containing 10 µg/ml PI and 40 Kunits units RNase A at least 30 min before analysis by flow cytometry. The stained cells were filtered through 40-µm-nylon mesh (Small Parts Inc., Miami Lakes, FL) before flow cytometry analysis.

2.6 Flow Cytometry Analysis

All cell samples were analyzed with a Coulter EPICS V cell sorter (Coulter, Miami, FL) interfaced to a Cicero data acquisition and display system (DakoCytomation, Inc., Fort Collins, CO) using 500 mW at 488 nm. Integral green fluorescence (IGFL) was measured between 515 and 530 nm and integral red fluorescence (IRFL) was measured above 610 nm. Fluorescence histograms were gated on forward angle light scattering to exclude debris and clumped cells. Gating on peak versus integral fluorescence of the propidium iodide signal was set to eliminate clumped cells.

Reproduced with permission of the copyright owner. Further reproduction prohibited without permission.

2.7 Computer and software packages

DNA histograms and dual parameter (bivariate) histograms were analyzed using the Cicero data acquisition and display system software as well as Multi-2D® and Multicycle® (Phoenix Flow Systems, San Diego, CA) software. The regression analysis and calculation were performed with SigmaPlot® and Microsoft Excel® software. The programs were executed on a personal computer.

2.8 Quantitative Analysis of Data

To determine the fraction of the population that was undergoing apoptosis, a region was placed around the apoptotic population on a bivariate histogram. The Cicero program calculates the number of cells in the selected region. To determine the cell cycle distribution of the normal or non-apoptotic cell population, the data in a region of the bivariate histogram containing non-apoptotic cells were saved by the Multi-2D program as a single-parameter DNA histogram. The saved file was analyzed with Multicycle for the cell cycle distribution (Fig. 2.1).

2.9 Cell Division Rate Measurement

Cell division rates were measured using the number of cells counted with a Particle Data Cell Counter (Micromeritics Instrument Corporation, Norcross, GA). The number of cells after time t in a population of N_0 cells is calculated, assuming exponential growth, by Equation 2.1.

Reproduced with permission of the copyright owner. Further reproduction prohibited without permission.

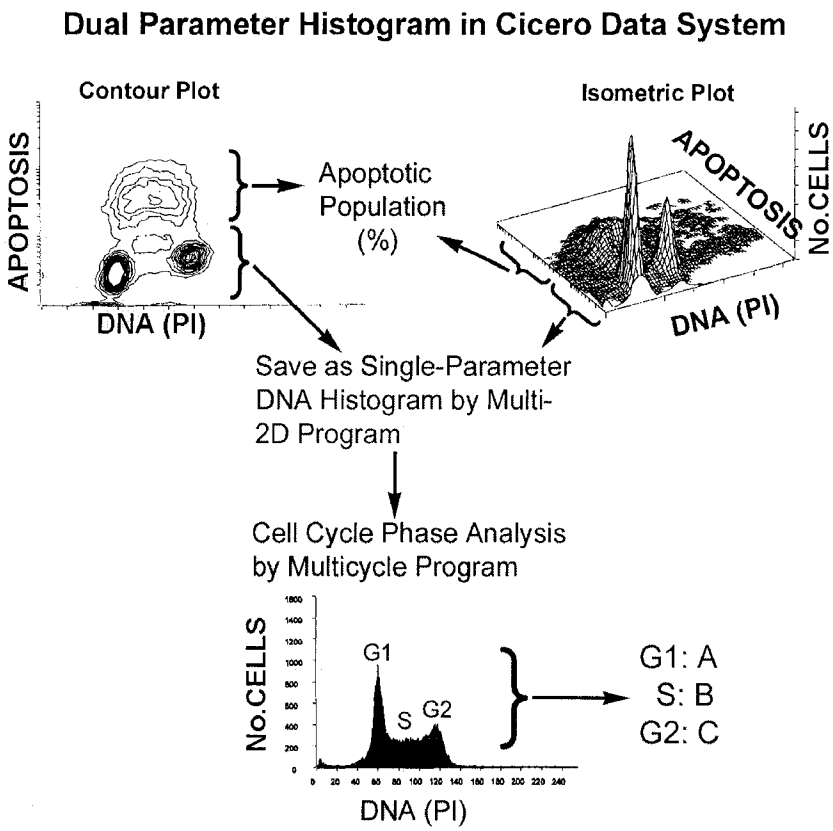

Figure 2.1. The procedure for analyzing the cell cycle population with Multicycle® and Multi-2D® software.

Reproduced with permission of the copyright owner. Further reproduction prohibited without permission.

$$N_t = N_0 e^{bt} \quad \text{(Equation 2.1)}$$

After counting the number of cells at each time point, the cell division rate, *b*, between each time point was calculated from Eq. 2.2 or by a nonlinear regression of the cell growth curve with SigmaPlot® software.

$$b = \frac{1}{t}\ln(\frac{N_t}{N_0}) \quad \text{(Equation 2.2)}$$

2.10 Potential Doubling Time (T_{pot}) Method

T_{pot} is a measure of cell cycle time that takes into account growth fraction but not cell loss. By measuring the relative movement of the BrdU positive population, potential doubling time (*Tpot*) was calculated by Eq. 2.3.

$$T_{pot} = \lambda * \frac{T_S}{LI} \quad \text{(Equation 2.3)}$$

Where T_s is the length of S phase, *LI* (labeling index) is the fraction of cells synthesizing DNA, and λ is a correction factor for the nonlinear distribution of cells through the cell cycle (2,6,7). T_s can be measured by the relative movement of the BrdU labeled cells and culture time. The relative movement (*RM*) was calculated by Eq. 2.4.

$$RM = \frac{F_L - F_{G1}}{F_{G2/M} - F_{G1}} \quad \text{(Equation 2.4)}$$

Where F_L is the mean IRFL (fluorescence intensity from PI staining) of the BrdU labeled cells. F_{G1} and $F_{G2/M}$ are the mean IRFL of G_1 and G_2/M cells, respectively. F_L at time 0 is

Reproduced with permission of the copyright owner. Further reproduction prohibited without permission.

approximately half way between F_{G1} and $F_{G2/M}$; thus RM_0 (the relative movement at time zero) is assumed to be 0.5 in Eq. 2.5.

$$T_S = \frac{1 - RM_0}{RM_t - RM_0} * t = \frac{0.5}{RM_t - 0.5} * t \qquad \text{(Equation 2.5)}$$

Where RM_t is the relative movement at time t and t is the sampling time. LI is calculated by the fraction of cells labeled with BrdU. λ is assumed to be one (2).

2.11 Equations for Cell Growth and Cell Disintegration

The relationship between cell production and cell loss is expressed by Eq. 2.6 (7).

$$\Delta[\text{Growth}] = \Delta[\text{Cell Production}] - \Delta[\text{Cell Loss}] \qquad \text{(Equation 2.6)}$$

where Δ[Cell Production] is the number of cells produced by cell division and Δ[Cell Loss] is the number of cells disintegrated by apoptosis in a time Δt. The rate of change in the number of apoptotic inducer-treated cells is assumed to be proportional to the number of N cells at any given time. This assumption is expressed by the differential equation (Eq. 2.7), which is modified from a previously published model (3).

$$\frac{dN(t)}{dt} = N(t) * [b(t) - k(t)] \qquad \text{(Equation 2.7)}$$

where $N(t)$ is the number of cells at time t, and $b(t)$ and $k(t)$ represent the division and disintegration rates of cells at time t, respectively.

Reproduced with permission of the copyright owner. Further reproduction prohibited without permission.

2.12 Cell Cycle Progression Model

Based on the Multicycle analysis of the cell cycle distributions, the change in the number of cells in each phase of the cell cycle after heat shock or etoposide treatment was calculated. A model was developed to analyze the progression of cells into different compartments (Fig. 2.2). α_1 is the probability of G_1 cells undergoing apoptosis, α_2 is the probability of G_1 cells progressing to S phase, and α_3 is the probability of G_1 cells remaining in G_1 without undergoing apoptosis or progression. Similarly, β and γ represent probabilities for transitions for S and G_2/M phase cells respectively. A, B, and C are used to represent G_1, S and G_2/M phases for simplicity in the equations. G_2 and M are included in a single phase since they are not resolved in DNA histograms. A_0, B_0 and C_0 are the initial number of cells for each population. A_t, B_t and C_t are the final number of cells for each population in the cell cycle phases. For each experiment, the initial total number of cells is normalized to 30,000. The following conditions pertain:

$$\begin{aligned} \alpha_1 + \alpha_2 + \alpha_3 &= 1 \\ \beta_1 + \beta_2 + \beta_3 &= 1 \\ \gamma_1 + \gamma_2 + \gamma_3 &= 1 \end{aligned} \qquad \text{(Equation 2.8)}$$

The number of cells undergoing apoptosis is given in Eq.2.9, where ΔAI represents the increasing number of cells undergoing apoptosis and K is the number of cells that have disintegrated. ΔAI and K are calculated with the CAI estimation model (see chapter 4).

$$A_0\alpha_1 + B_0\beta_1 + C_0\gamma_1 = \Delta AI + K \qquad \text{(Equation 2.9)}$$

Reproduced with permission of the copyright owner. Further reproduction prohibited without permission.

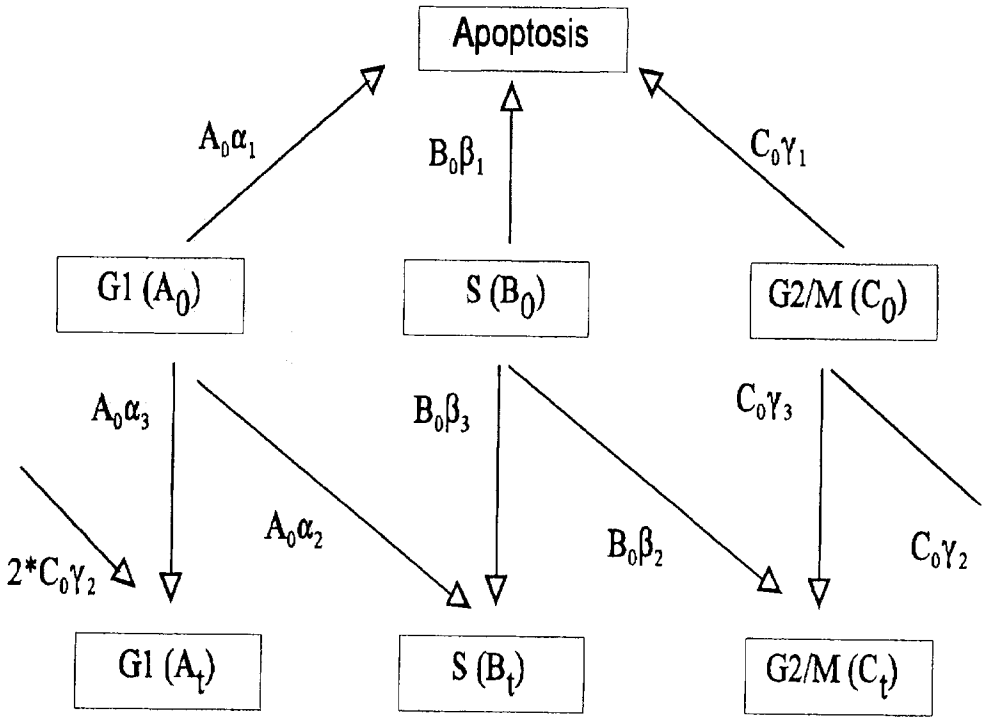

Figure 2.2. The cell cycle progression model. Only three phases are represented because G_2 and M cannot be distinguished in DNA histograms. Cells initially in G_1, S or G_2/M phases (A_0, B_0 and C_0) may progress to the next phase, undergo apoptosis, or remain in the same phase. The number of non-apoptotic cells in each phase at a time t after treatment by heat or drugs is A_t, B_t and C_t. Cells may also enter the apoptosis compartment from any phase. The transition probabilities are α_1, β_1 and γ_1.

Reproduced with permission of the copyright owner. Further reproduction prohibited without permission.

The cell cycle progression model was developed to analyze the distribution of cells in apoptosis and in the cell cycle after heating or treatment by etoposide. It is based on the number of cells in each cell cycle phase and the number of apoptotic cells before and after treating the cells with an agent that causes apoptosis. By comparing the differences between the initial and final number of cells in each cell cycle phase with the number of apoptotic cells from each cell cycle phases, α_i, β_i and γ_i can be determined. The final number of cells in each phase (A_t, B_t and C_t) is calculated by adding the population remaining in G_1, S or G_2/M to the population moving in from the previous phase (Eq. 2.10). Note that for each cell progressing from C (G2/M) in Fig. 2.2, two cells enter G_1 because the number of cells doubles in mitosis.

$$\begin{aligned} A_t &= A_0\alpha_3 + 2C_0\gamma_2 = A_0(1-\alpha_1-\alpha_2) + 2C_0\gamma_2 \\ B_t &= B_0\beta_3 + A_0\alpha_2 = B_0(1-\beta_1-\beta_2) + A_0\alpha_2 \\ C_t &= C_0\gamma_3 + B_0\beta_2 = C_0(1-\gamma_1-\gamma_2) + B_0\beta_2 \end{aligned} \qquad \text{(Equation 2.10)}$$

The population of cells in each phase of the cell cycle depends on both influx from the previous phase and efflux into the next phase as well as apoptosis occurring in that phase (Fig.2.2). Equation 2.11 defines these relationships. The calculation of efflux and influx is performed with the non-apoptotic population only. I define these calculated values as *Efflux Coefficients (EC)*. When the value of EC is greater than zero, cell cycle progression from that phase is dominant and when EC is smaller than zero, cell cycle delay or block in that phase is dominant. If EC_{G1}, EC_S and $EC_{G2} > 0$,

Reproduced with permission of the copyright owner. Further reproduction prohibited without permission.

$$EC_{G1} = \frac{1}{N_0}(A_0\alpha_2 - 2C_0\gamma_2) > 0$$
$$EC_S = \frac{1}{N_0}(B_0\beta_2 - A_0\alpha_2) > 0 \qquad \text{(Equation 2.11)}$$
$$EC_{G2} = \frac{1}{N_0}(C_0\gamma_2 - B_0\beta_2) > 0$$

Efflux > Influx, indicating Cell Cycle Progression

If EC_{G1}, EC_S and EC_{G2} in Eq. 2.12. < 0,

$$EC_{G1} = \frac{1}{N_0}(A_0\alpha_2 - 2C_0\gamma_2) < 0$$
$$EC_S = \frac{1}{N_0}(B_0\beta_2 - A_0\alpha_2) < 0 \qquad \text{(Equation 2.12)}$$
$$EC_{G2} = \frac{1}{N_0}(C_0\gamma_2 - B_0\beta_2) < 0$$

Efflux < Influx, indicating Cell Cycle Block

I developed a technique called the apoptotic quotient calculation for measuring α_1, β_1 and γ_1 directly from flow cytometry data. The population of apoptotic cells overlaps with the non-apoptotic population when single parameter DNA histograms are measured with paraformaldehyde fixation (1). Formaldehyde is a cross-linking fixative, which makes the cells rigid by covalently linking many surface proteins, as well as DNA. The application of the CAI estimation model helps to avoid the double counting and overlapping of apoptotic populations. The cell cycle distributions of non-apoptotic cells (A_t, B_t and C_t) were measured by Multicycle from the single parameter data derived from a bivariate histogram (Fig. 2.1). The total number of cells in each compartment (A_{Tot}, B_{Tot}

Reproduced with permission of the copyright owner. Further reproduction prohibited without permission.

and C_{Tot}) was determined from a Multicycle analysis of the DNA histograms that include both apoptotic and non-apoptotic cells. The frequency of apoptotic cells for each cell cycle position (ApQ_{G1}, ApQ_S and ApQ_{G2}) was calculated by comparing the non-apoptotic population with the total number of cells in each cell cycle compartment. Equation 2.13 gives the cell cycle distributions of the apoptotic cells ApQ_{G1}, ApQ_S and ApQ_{G2}.

$$\begin{aligned} Ap_{G1} &= A_{Tot} - A_t \\ Ap_S &= B_{Tot} - B_t \\ Ap_{G2} &= C_{Tot} - C_t \end{aligned} \qquad \text{(Equation 2.13)}$$

Thus,

$$\begin{aligned} \alpha_1 (= ApQ_{G1}) &= Ap_{G1} / A_0 \\ \beta_1 (= ApQ_S) &= Ap_S / B_0 \\ \gamma_1 (= ApQ_{G2}) &= Ap_{G2} / C_0 \end{aligned} \qquad \text{(Equation 2.14)}$$

With this model we can determine α_1, β_1 and γ_1 and define them as the *apoptotic quotient (ApQ)* from each cell cycle phase. Other variables can be calculated by using Eq. 2.8 and Eq. 2.10.

If α_1, β_1 and γ_1 are all the same, then cells in each cell cycle phase are equally sensitive to the induction of apoptosis by a particular agent. In this case, by rearranging Eq. 2.9:

$$\begin{aligned} & A_0\alpha_1 + B_0\alpha_1 + C_0\alpha_1 = \Delta AI + K \\ & \alpha_1 (A_0 + B_0 + C_0) = \Delta AI + K \\ & \therefore \alpha_1 = \beta_1 = \gamma_1 = \frac{\Delta AI + K}{A_0 + B_0 + C_0} = API \end{aligned} \qquad \text{(Equation 2.15)}$$

Reproduced with permission of the copyright owner. Further reproduction prohibited without permission.

We define α_1, β_1 and γ_1 from Eq.2.15 as *Apoptosis Probability Indices (API)*. The biological significance of this condition is that cells in all three cell cycle phases have the same sensitivity to undergo apoptosis.

2.13 Comparison of Cell Cycle Progression Data

From Eq. 2.8, Eq. 2.9, Eq. 2.10, Eq. 2.11 and Eq. 2.12, we can determine whether G_1, S and G_2/M phase cells undergo apoptosis or cell cycle delays based on the values of *ApQ* and *EC*. In particular, by comparing *ApQ* with *API*, one can determine whether cells are more sensitive to apoptosis in a particular cell cycle phase. In other words, if *ApQ* is greater than *API* for each cell cycle phase in cells treated by an apoptotic agent, then these cells are more sensitive to that apoptotic agent than predicted by Eq. 2.15. If *ApQ* equals *API*, the cells are not unusually sensitive to the apoptotic agent in that cell cycle phase. If *ApQ* is smaller than *API*, the cells are resistant to the apoptotic agent. In conclusion, with this method you can tell (i) how many cells undergo apoptosis (by *ApQ*), (ii) how many cells progress from or remain in each cell cycle phase (by α_2, β_2, γ_2 and α_3, β_3, γ_3), (iii) how sensitive cells are to undergo apoptosis in each cell cycle phase (by comparing *ApQ* and *API*) and (iv) the existence of cell cycle blocks (by the interpretation of *EC*). These definitions and interpretations are summarized in Table 2.1 – 2.3.

Reproduced with permission of the copyright owner. Further reproduction prohibited without permission.

Table 2.1

The explanation for terms used previously

Terms	Explanation
ApQ	Apoptotic Quotient, the probability of apoptosis in each cell cycle phase measured by comparing the cell cycle phase distribution for non-apoptotic cells and the entire cell population (i.e., ApQ_{G1}, ApQ_S and ApQ_{G2})
API	Apoptosis Probability Index, the expected probability for apoptotic cells when cells in each cell cycle phase have the same probability to undergo apoptosis (i.e., $API_{G1}=API_S=API_{G2}$)
EC	Efflux Coefficient, the difference between efflux (apoptosis and progression to the next phase) and influx (progression from previous phase) (i.e., EC_{G1}, EC_S and EC_{G2})

Reproduced with permission of the copyright owner. Further reproduction prohibited without permission.

Table 2.2

Interpretation of Efflux Coefficient (*EC*) for each cell cycle phase cells

EC	Efflux or Influx	Comments
Greater than zero	Efflux > Influx	No Cell Cycle Block
Smaller than zero	Efflux < Influx	Cell Cycle Block
Equal to zero	Efflux = Influx	Stationary State

Note: *EC*, Efflux coefficient from Eq.2.11 and Eq.2.12; Efflux, the number of cells leaving phase through apoptosis and progression; Influx, the number of cells progressing from previous phase.

Reproduced with permission of the copyright owner. Further reproduction prohibited without permission.

Table 2.3

Comparison between *ApQ* and *API* for each cell cycle phase cells with respect to their sensitivity to undergo apoptosis

ApQ and *API*	Sensitive or Resistant
$ApQ > API$	Sensitive
$ApQ < API$	Resistant
$ApQ = API$	No Specific Sensitivity

Note: *ApQ*, Apoptosis quotient from Eq.2.13 and Eq.2.14; *API*, Apoptosis probability indices from Eq.2.15.

Reproduced with permission of the copyright owner. Further reproduction prohibited without permission.

Reference List

1. Bedner E, Li X, Kunicki J, Darzynkiewicz Z: Translocation of Bax to mitochondria during apoptosis measured by laser scanning cytometry. Cytometry 41:83-88, 2000.

2. Begg AC, McNally NJ, Shrieve DC, Kärcher H: A method to measure the duration of DNA synthesis and the potential doubling time from a single sample. Cytometry 6:620-626, 1985.

3. Conolly RB, Kimbell JS: Computer simulation of cell growth governed by stochastic processes: application to clonal growth cancer models. Toxicol Appl Pharmacol 124:284-295, 1994.

4. Han Z, Bhalla K, Pantazis P, Hendrickson EA, Wyche JH: Cif (Cytochrome c efflux-inducing factor) activity is regulated by Bcl- 2 and caspases and correlates with the activation of Bid. Mol Cell Biol 19:1381-1389, 1999.

5. Han Z, Li G, Bremner TA, Lange TS, Zhang G, Jemmerson R, Wyche JH, Hendrickson EA: A cytosolic factor is required for mitochondrial cytochrome c efflux during apoptosis. Cell Death Differ 5:469-479, 1998.

6. Liao KH, Gustafson DL, Fox MH, Chubb LS, Reardon KF, Yang RS: A biologically based model of growth and senescence of Syrian hamster embryo (SHE) cells after exposure to arsenic. Environ Health Perspect 109:1207-1213, 2001.

7. Steel GG: Basic theory of growing cell populations. In: Growth Kinetics of Tumors:cell population kinetics in relation to the growth and treatment of cancer, Anonymous Clarendon Press, Oxford, 1977, pp. 56-85.

8. Wolf D, Rotter V: Major deletions in the gene encoding the p53 tumor antigen cause lack of p53 expression in HL-60 cells. Proc Natl Acad Sci U S A 82:790-794, 1985.

Reproduced with permission of the copyright owner. Further reproduction prohibited without permission.

CHAPTER 3

ANALYSIS OF CELL CYCLE DEPENDENT APOPTOSIS AND CELL CYCLE BLOCKS INDUCED BY ETOPOSIDE IN HL-60 AND HCW-2 CELLS

3.1 Introduction

Apoptosis is an important mode of cell killing for therapy of a variety of diseases. Molecular methods of measuring apoptosis, such as caspase activity, PARP cleavage, and the presence of DNA ladders, can provide qualitative information regarding induction of apoptosis by various agents. Flow cytometry methods can supply more quantitative information regarding cell cycle-dependent apoptosis and help achieve an understanding of apoptotic processes at the level of individual cells. Since many therapeutic agents also cause cell cycle blocks, it is important to try to separate out cell cycle perturbations from apoptosis in specific phases of the cell cycle.

Flow cytometry can be used to measure the distribution of cells through the cell cycle by measuring the DNA content of individual cells. With standard procedures for measuring the cell cycle with flow cytometry, apoptotic cells could be counted as cell cycle arrested cells because apoptotic cells remain in the cell cycle phase in which they entered apoptosis. This would mask information about cell cycle progression and arrest

Reproduced with permission of the copyright owner. Further reproduction prohibited without permission.

of non-apoptotic cells due to the treatment. For a more complete analysis, bivariate histograms of DNA content versus apoptosis can be analyzed to provide information on both cell cycle progression and cell cycle specific apoptosis (7,17,19,27).

A quantitative and mathematical analysis of the relationship between cell cycle specific apoptosis and cell cycle progression has not yet been developed. Such an analysis may be useful in studies exploring the cell cycle response to therapeutic drugs. Cancer cells frequently abrogate cell cycle checkpoints while normal cells activate their checkpoints in response to DNA damaging agents. The differences between normal and cancer cells to a therapeutic treatment could be better understood with the new model proposed in this dissertation.

To achieve a more accurate analysis of cell cycle progression, arrest and apoptosis, I developed an apoptotic quotient calculation to estimate the amount of apoptosis from each cell cycle phase and a cell progression model to understand and evaluate apoptosis and its interaction with cell proliferation by calculating the presence of cell cycle delays along with cell cycle progression and cell cycle-specific resistance or sensitivity to apoptosis. I defined several parameters for explaining the model (see Chapter 2), which are the *apoptotic quotient (ApQ)*, *apoptosis probability index (API)*, *efflux coefficient (EC)* and *the degree of sensitivity*. *ApQ* represents the amount of apoptosis for each cell cycle phase, *API* represents the number of apoptotic cells expected in each cell cycle phase if the treatment is not cell cycle specific, *EC* indicates the presence of cell cycle blocks, and *the degree of sensitivity* indicates whether an apoptosis-inducing agent is cell cycle phase specific or not.

Reproduced with permission of the copyright owner. Further reproduction prohibited without permission.

In this study, the cell progression model was tested in two different circumstances: (i) the induction of S-phase specific apoptosis with etoposide in HL-60 cells, and (ii) the induction of cell cycle blocks with etoposide in an apoptosis-resistant cell line (HCW-2) analyzed with BrdU incorporation. The number of apoptotic cells after treatment with etoposide was measured by the TUNEL assay and propidium iodide labeling using flow cytometry. It is assumed that the cells do not undergo disintegration from late-stage apoptosis during the course of the experiments.

3.2 Materials and Methods

In order to test the modeling approach to analyze apoptosis and cell cycle delays described in Chapter 2, a system was necessary which would induce a large amount of apoptosis in a cell cycle-dependent manner. Human myelogenous leukemic HL-60 cells were used since they readily undergo apoptosis in response to a variety of chemical and physical agents (1,2,6,7,9,12,16,17,18,23,25,28,30,34). S-phase specific apoptosis was induced with the topoisomerase II inhibitor, etoposide (2,12,13,26,30,34). Etoposide is a good positive control for analyzing the effects of other apoptotic stimuli on apoptosis and cell cycle delays. HCW-2 cells, an apoptotic resistant variant of HL-60 cells (20,21,22), were used to analyze cell cycle progression and delays without the complications of apoptosis. HCW-2 cells are resistant to apoptosis because they are unable to release cytochrome C into the cytosol after apoptotic stimuli (20,21,22). The cell progression model was used to calculate cell cycle specific apoptosis and delays. BrdU labeling experiments were done to calculate the potential doubling time (T_{pot}) of cells after

Reproduced with permission of the copyright owner. Further reproduction prohibited without permission.

treatment. The general description for the experimental assays and model was explained in Chapter 2. The specific details are provided in figure and table legends.

3.3 Results

3.3.1 Etoposide-induced Apoptosis in HL-60 Cells

HL-60 cells were treated with 6.25-μg/ml etoposide, and then incubated at 37°C for 3 hr before measuring apoptosis with the TUNEL assay. Results from an experiment which illustrates the apoptotic population are shown in Fig. 3.1. The peak on the left in each histogram (in Fig. 3.1A and Fig. 3.1C) represents the cells in G_1 phase and the peak on the right represents primarily the cells in G_2 and M phases. Since the G_2 and M phase cells have the same DNA content, they cannot be distinguished with PI staining. Cells between the two peaks are S phase cells, which have DNA content between that of G1, and G_2/M phase cells. A comparison of Fig. 3.1B and Fig. 3.1D shows that etoposide causes apoptosis to occur principally in S phase cells.

The DNA histograms in Fig. 3.1A and 3.1C look similar even though a large fraction of cells are apoptotic in the etoposide-treated sample because cells were fixed with paraformaldehyde, a cross-linking agent that prevents the degraded DNA in apoptotic cells from leaking out of the cells. Thus, the apoptotic population was not recognized in univariate DNA histograms (Fig. 3.1A and Fig. 3.1C). To quantitatively describe the percentage of cells in each phase of the cell cycle in Fig. 3.1A, the DNA histograms were analyzed using Multicycle® software. Because the DNA histogram in

Reproduced with permission of the copyright owner. Further reproduction prohibited without permission.

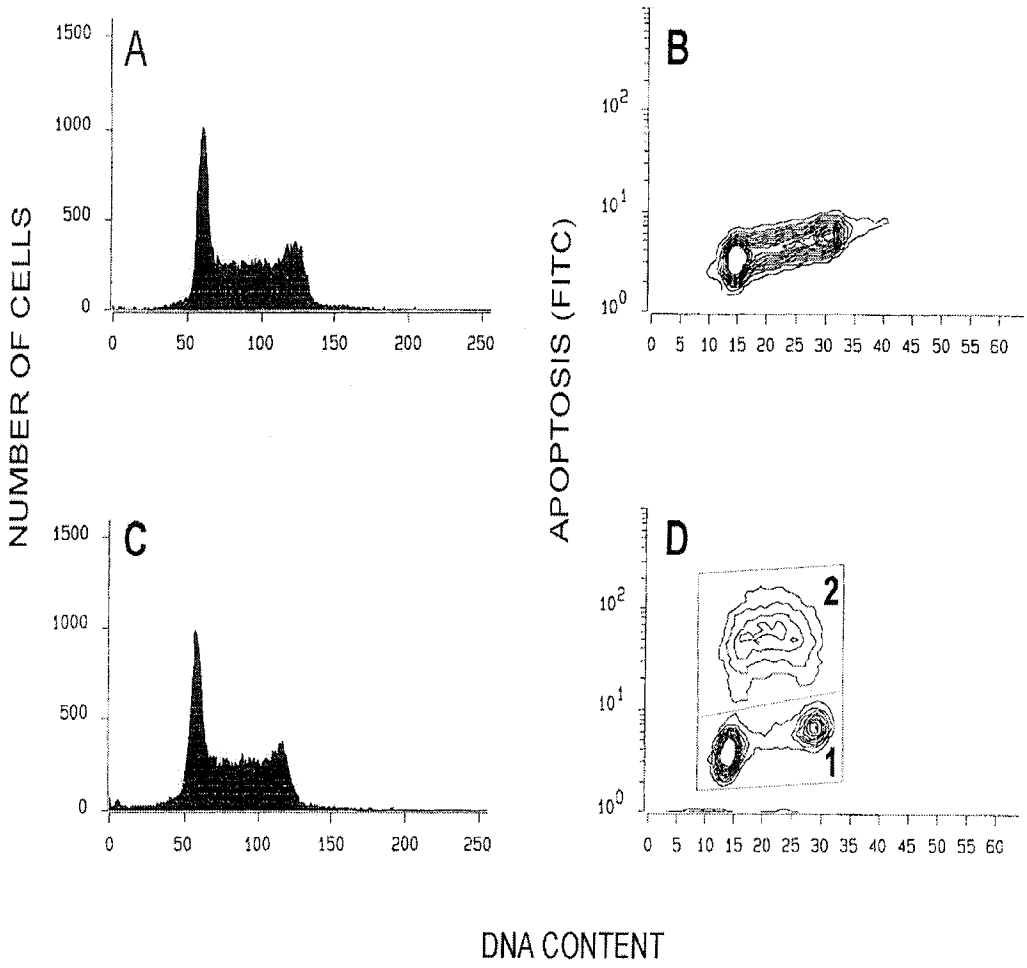

Figure 3.1. Cell cycle distribution of control and etoposide-treated (6.25-μg/ml for 3 hr) HL-60 cells and dual parameter histograms showing apoptosis (FITC) and DNA content (IRFL) for control and etoposide-treated cells. (A) DNA histogram for control cells. (B) TUNEL assay for control cells. (C) DNA histogram for etoposide-treated cells. (D) TUNEL assay for etoposide-treated cells. In (B) and (D), the Y-axis represents the fluorescence intensity of FITC-labeled dUTP incorporated into DNA breaks which are characteristic of apoptotic cells.

Reproduced with permission of the copyright owner. Further reproduction prohibited without permission.

Fig. 3.1C includes the apoptotic population, they cannot be used for analyzing the cell cycle distribution of the non-apoptotic cells.

The number of cells in each cell cycle phase, including apoptotic and non-apoptotic cells, however, could be analyzed by Multi-2D® and Multicycle® software (Fig. 2.1 and Fig. 3.1D). To quantitatively describe the percentage of non-apoptotic cells in each phase of the cell cycle for an etoposide-treated sample, the data from dual parameter histograms for the non-apoptotic population (Region 1, Fig. 3.1D) were saved as single-parameter DNA histograms by the Multi-2D® program and were then analyzed using Multicycle® software. After the numbers of cells for both figures were analyzed from Fig. 3.1C and 3.1D using Multicycle® software, the data from Region 1 in Fig. 3.1D could be subtracted to get the number of apoptotic cells from each cell cycle phase (Eq. 2.14).

The number of cells in each cell cycle phase and the number of apoptotic cells (Region 2, Fig.3.1D) for control and etoposide-treated cells are shown in Fig.3.2. The number of cells in S phase decreased drastically concomitant with a large increase in the apoptotic population. It is apparent that the apoptotic population mainly came from S phase cells after treatment with etoposide.

From Eq. 2.15, α_1, β_1 and γ_1 (Fig. 2.2) can be calculated. α_1, β_1 and γ_1 calculated in this way are defined as the *Apoptotic Quotient (ApQ)* in Table 3.1. *ApQ* is a measure of the probability of apoptosis from each cell cycle phase after treatment. Data from Multicycle analysis and the calculated results with comments are shown in Table 3.1. These results show that 78 % of S phase cells underwent apoptosis at 3 hr after etoposide

Reproduced with permission of the copyright owner. Further reproduction prohibited without permission.

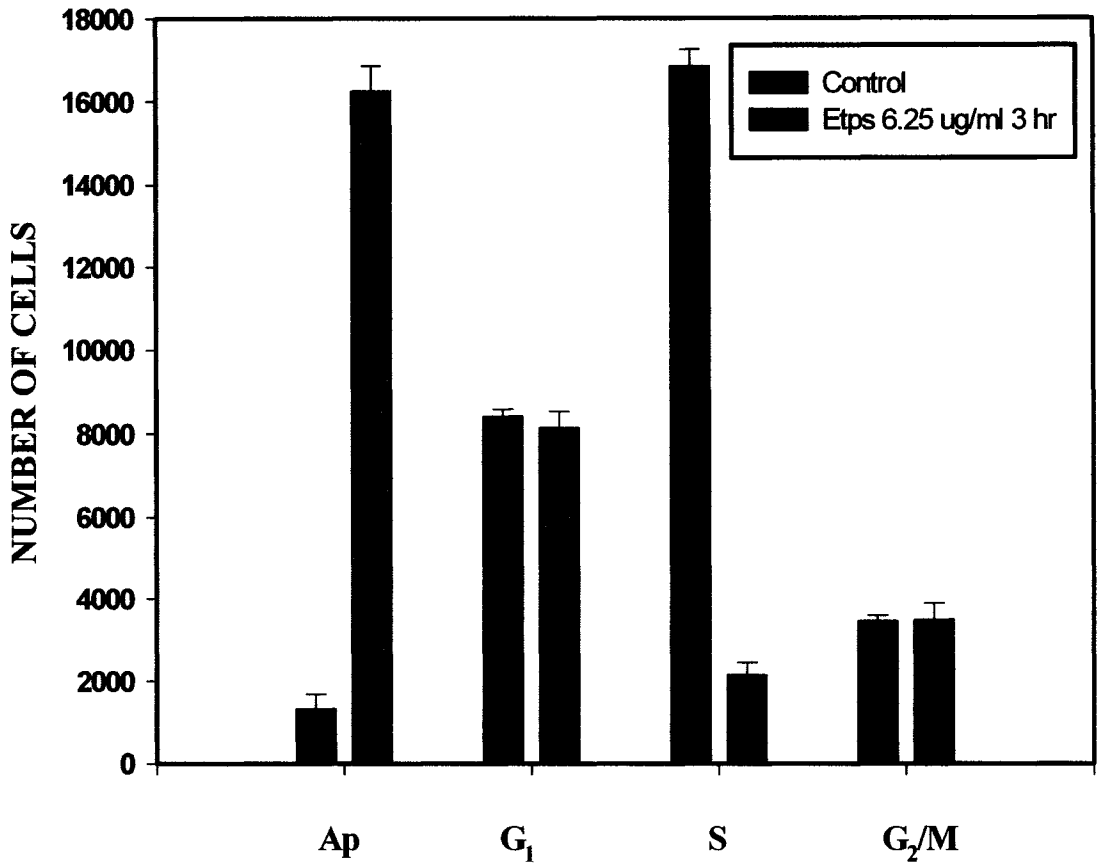

Figure 3.2. The number of apoptotic cells and the cell cycle phase distributions of non-apoptotic cells before and after a 3 hr treatment with 6.25-μg/ml etoposide in HL-60 cells. Ap: apoptosis; control, untreated cells. The error bar represents the standard error of the mean. These data are based on five different experiments. The number of cells in each phase are calculated by analyzing the cell cycle distributions with Multicycle®. Control cells are from histrograms such as a Figure 3.1.A. Non-apoptotic cell cycle distributions are from Figure 3.1.D region 1. The total number of cells is 30,000.

Reproduced with permission of the copyright owner. Further reproduction prohibited without permission.

Table 3.1 The effects of a 3 hr, 6.25 μg/ml etoposide on the cell cycle distribution and apoptosis in HL-60 cells, including an analysis of the efflux coefficient and apoptosis probability index (API) as described.

		Control	Etoposide-treated sample
Time (hr)		0	3
Cell Numbers		30000	32707
Cumulative Apoptotic Index		0	17718
Non-Apoptotic Cells	G_1	8792	8876
	S	17608	2323
	G_2/M	3600	3790
Apoptotic Quotient (ApQ)	G_1	-	0.314
	S	-	0.784
	G_2/M	-	0.319
Cell Progression (α_2, β_2, γ_2)	α_2	-	0.292
	β_2	-	0.230
	γ_2	-	0.752
Apoptotic Probability Index (API)		-	0.591
Interpretation of Efflux Coefficient (EC)	G_1	-	Block
	S	-	NB
	G_2/M	-	Block
Sensitivity by comparison between ApQ and API	G_1	-	R
	S	-	S
	G_2/M	-	R

Reproduced with permission of the copyright owner. Further reproduction prohibited without permission.

treatment, while 31 % of G_1 phase cells and 32 % of G2/M phase cells underwent apoptosis. Control cells without etoposide had a low level of apoptosis (4.38 ± 1.19 %) after 3 hr culture. When the model was calculated, the number of apoptotic cells in the control sample was neglected.

If cells in each cell cycle phase are equally likely to undergo apoptosis from an apoptotic inducer, then the probabilities for undergoing apoptosis should be equal ($\alpha_1 = \beta_1 = \gamma_1$). I defined these equalities as *Apoptosis Probability Indices (API)*. The *API* gives the theoretical probability of cells undergoing apoptosis from each cell cycle phase with the same sensitivity, as described by Eq. 2.16. A comparison of *ApQ* (experimental results) and *API* (theoretical expectation) shows whether cells are more sensitive to undergoing apoptosis from a particular cell cycle phase than expected theoretically. Thus, etoposide, an inhibitor of topoisomerase II, specifically killed the S phase cells (Fig. 3.3 and Table 3.1). If the mechanism of a drug is unknown, this approach could provide a good first step for understanding the mechanism of the drug. Results in Table 3.1 show that G_1 and G_2/M phase cells are resistant and S phase cells are sensitive to apoptosis. A graphical representation of the values of *ApQ* and *API* is given in Fig. 3.3.

Interpretation of the values of *Efflux Coefficient (EC)* (Eq. 2.12 and Eq. 2.13) in Fig. 3.3 and Table 3.1 indicates that cells are blocked in G_1 and G_2/M but not in S phase. The probability of progression (α_2, β_2, and γ_2) in Table 3.1 and the probability of remaining in the phase (α_3, β_3, and $\gamma 3$) could be calculated by using the values of *ApQ*, Eq. 2.9 and Eq. 2.11. These experimental results can explain the probability of cell cycle progression and cell cycle delay.

Reproduced with permission of the copyright owner. Further reproduction prohibited without permission.

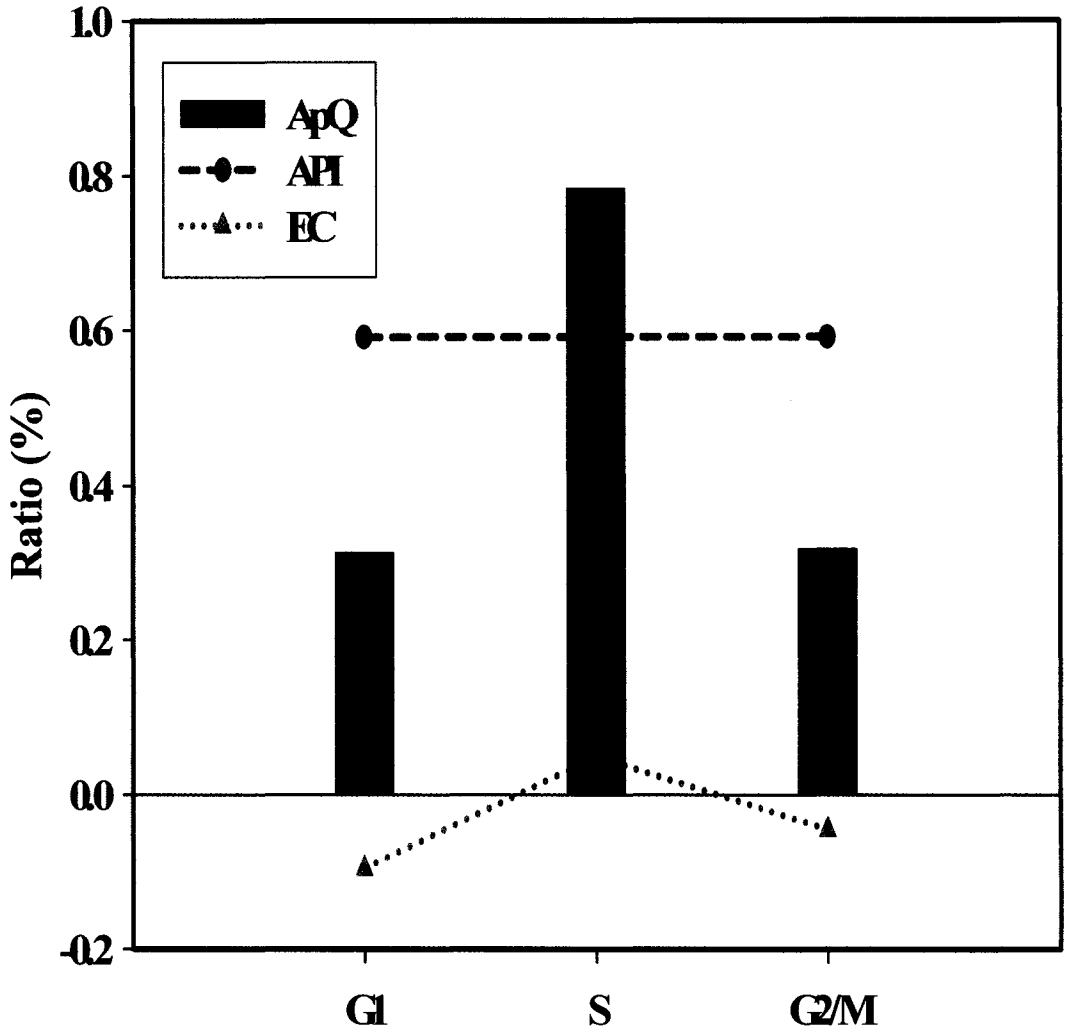

Figure 3.3. The percentage of ApQ, API and EC at each cell cycle phase in HL-60 cells. Cells were treated with 6.25μg/ml etoposide for 3 hrs.

Reproduced with permission of the copyright owner. Further reproduction prohibited without permission.

Cyclin B1 is the mitotic cyclin whose level increases drastically in G_2 phase. Cyclin B1 interacts with Cdc2 kinase (CDK1), one of the cyclin-dependent kinases. Camptothecin (topoisomerase I inhibitor) and etoposide treatment showed unscheduled early transient increases in the activity of cyclin B1/Cdc 2 kinase, which is associated with Cdc2 tyrosine phosphorylation without alteration of Cdc2 or cyclin B1 protein levels (32). These data indicate that when cells were cultured with etoposide, heavily damaged S phase cells underwent apoptosis during S phase or S phase cells which survived the etoposide progressed to the next cell cycle and blocked at the G_2/M checkpoint, cells in G_2/M phase tried finish their cell cycle and blocked at the G_1 checkpoint, and G_1 cells blocked at the G_1 checkpoint.

In this study it was assumed that the disintegration of cells by apoptosis did not take place because the collection time was not long enough. This assumption will be explained in detail in Chapter 4. Briefly, the time-window of the apoptotic assay and the time for apoptotic cell disintegration to begin are greater than the experiment time. Thus, the apoptotic index (AI) was equal to the cumulative apoptotic index (CAI) and parameter K in Eq. 2.10 was equal to zero. Apoptotic cells induced by etoposide treatment could be accumulated and counted at the collection time without the loss of any cells to disintegration from late-stage apoptosis.

3.3.2 HCW-2 cells with 6.25-μg/ml etoposide

When HL-60 cells are labeled with BrdU and then treated with agents that induce apoptosis, the progression of the BrdU positive population is affected by apoptosis.

Reproduced with permission of the copyright owner. Further reproduction prohibited without permission.

HCW-2 cells were used to demonstrate cell cycle progression, arrest and potential doubling time without complications due to apoptosis. HCW-2 cells were pulse-labeled with BrdU for 30 min, incubated with 6.25-μg/ml etoposide for 3 hr, washed with medium and incubated for various times at 37°C. Control samples were pulse-labeled with BrdU but without etoposide treatment and were harvested at the same time points. Results from an experiment which illustrates the cell cycle distributions are shown in Fig.3.4. Control samples had very similar DNA histograms at all time points, while etoposide-treated samples had delayed progression and cell cycle arrest. Cells were delayed progressing through S phase at 6, 9 and 12 hr samples and cells were arrested in G_2 phase at all time points.

The movement of BrdU-labeled populations of control and etoposide-treated HCW-2 cells are shown in Fig.3.5. BrdU-labeled control cells had a normal cell cycle distribution and cell cycle progression. BrdU-labeled S phase cells divided and first appeared in G_1 phase as a BrdU-labeled population at 3 hr and this population increased at later times. After 24 hr the control cells had two cycling cell cycle populations, a BrdU-positive and a BrdU-negative population. In contrast, the etoposide-treated cells did not begin to divide and appear as BrdU-labeled G_1 phase cells until 12 hr and was still a very small population after 24 hr. Thus, HCW-2 cells had a delayed progression and G_2 cell cycle block for at least 12 hr after drug removal. The total number of control and etoposide-treated cells are shown in Fig. 3.6. HCW-2 cells treated with 6.25-μg/ml etoposide for 3 hr did not have significant cell division for 24 hr. The percentage of cells in each cell cycle phase for control cells at each time point are shown in Fig.3.7. The

Reproduced with permission of the copyright owner. Further reproduction prohibited without permission.

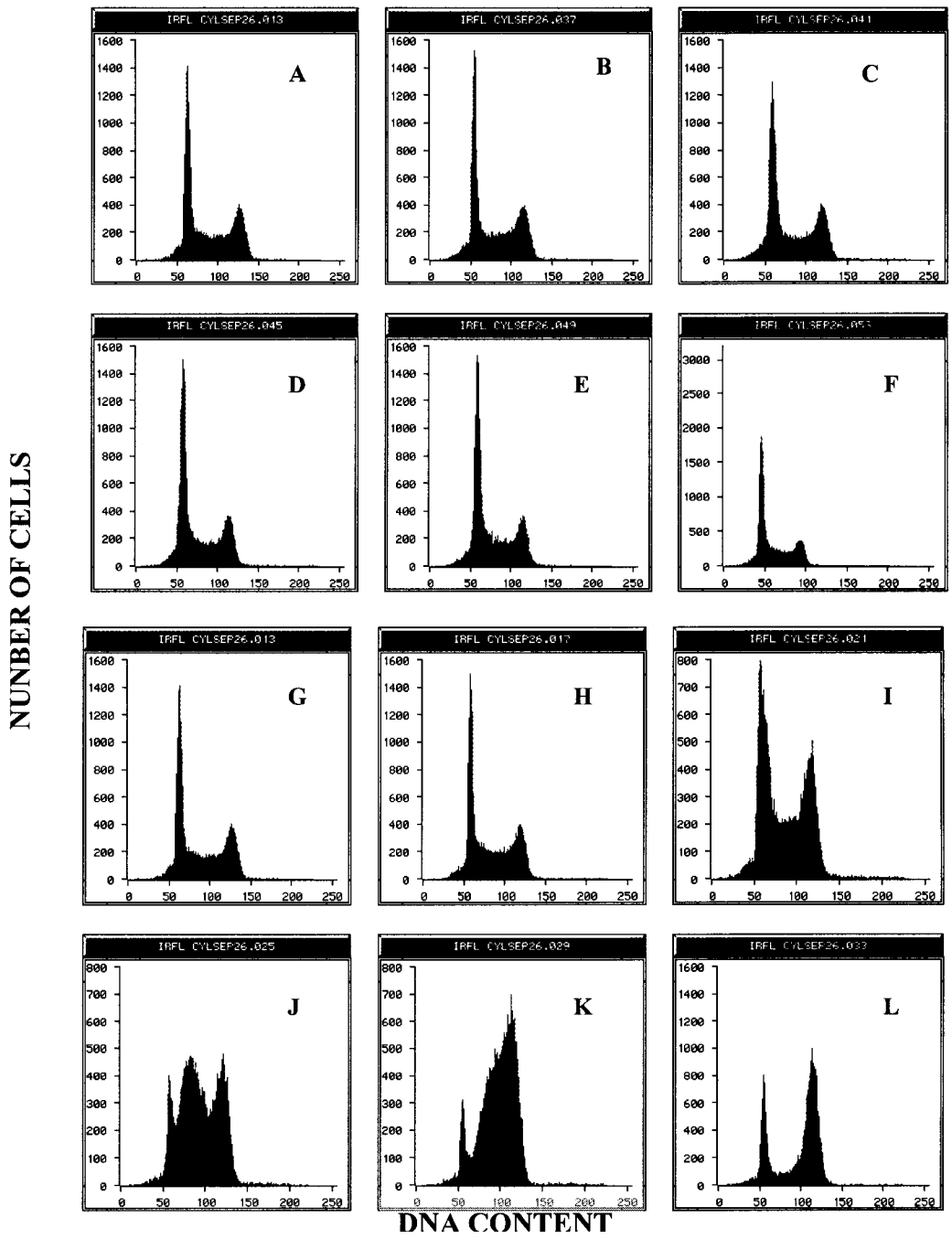

Figure 3.4 Cell cycle distributions of control and etoposide-treated (6.25-μg/ml for 3 hr) HCW-2 cells. (A-F) 0, 3, 6, 9, 12, 24 hr DNA histogram for control cells. (G) 0 hr DNA histogram for control cells (H-L) 3 hr etoposide treatment plus 0, 3, 6, 9, 21 hr DNA histogram.

Reproduced with permission of the copyright owner. Further reproduction prohibited without permission.

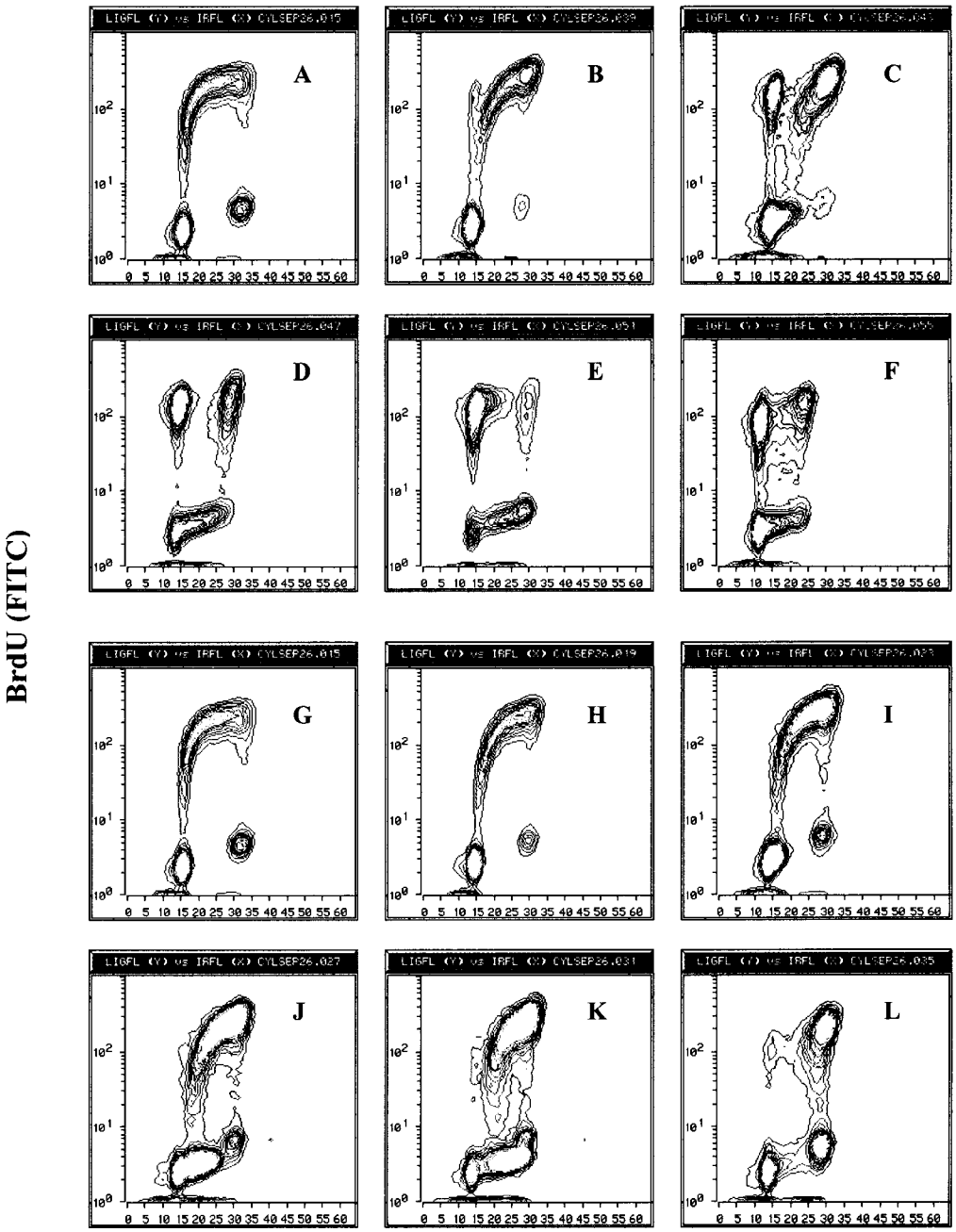

Figure 3.5 BrdU positive and negative cell distribution of control and etoposide-treated (6.25-μg/ml for 3 hr) HCW-2 cells in dual parameter histograms. (A-F) 0, 3, 6, 9, 12, 24 hr dual parameter histogram for control cells. (G) 0 hr dual parameter histogram for control cells (H-L) 3 hr etoposide treatment plus 0, 3, 6, 9, 21 hr dual parameter histogram.

Reproduced with permission of the copyright owner. Further reproduction prohibited without permission.

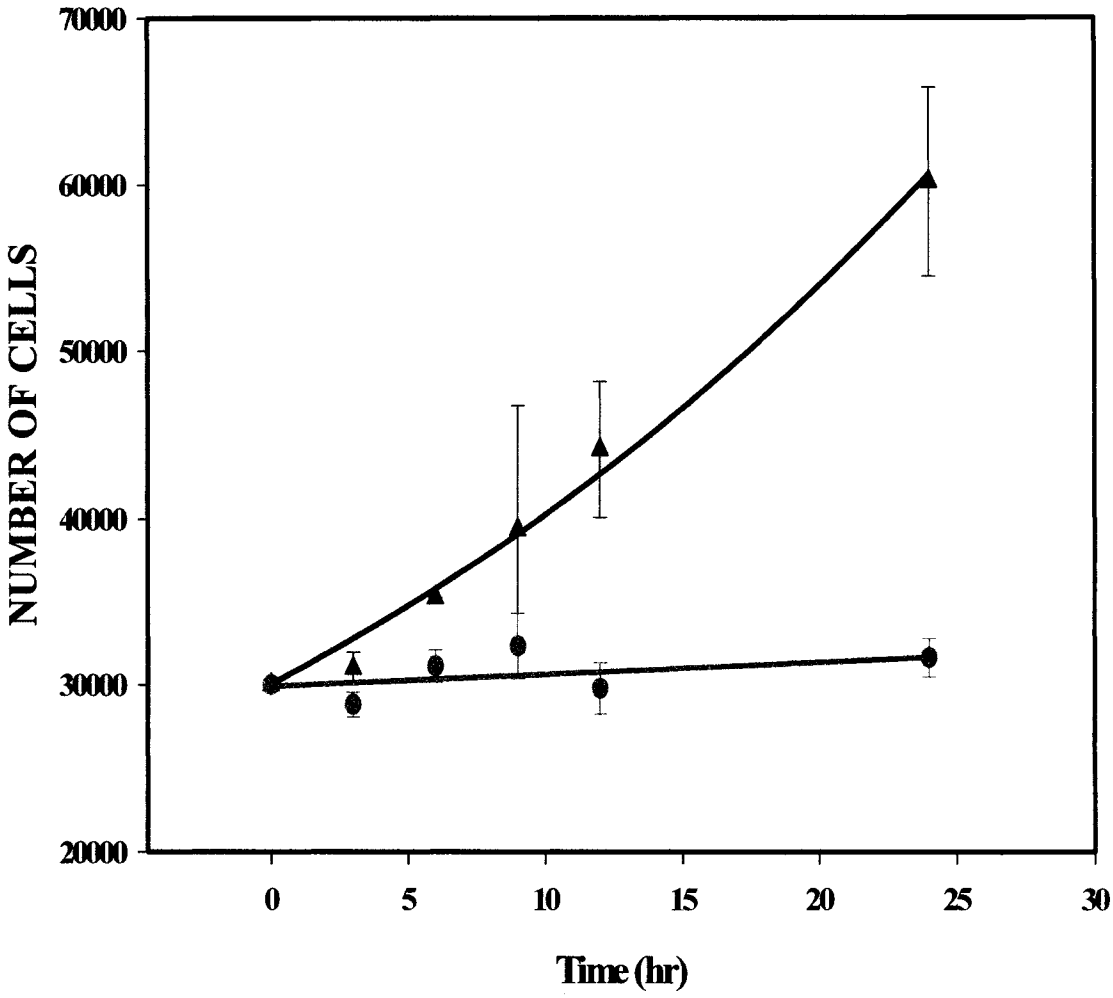

Figure 3.6 The change in number of HCW-2 cells as a function of time after 6.25-µg/ml-etoposide treatments. Cell numbers are counted at sample collection time. The dots represent measured values with error bars representing ± one standard error. The line represents the result of nonlinear regression from the exponential equation N_t = 30037*exp (0.0292*time) for control cells and N_t = 29908*exp (0.0023*time) for etoposide-treated cells. This regression had a standard error of estimate equal to 3694 and 2276 cells for each samples.

Reproduced with permission of the copyright owner. Further reproduction prohibited without permission.

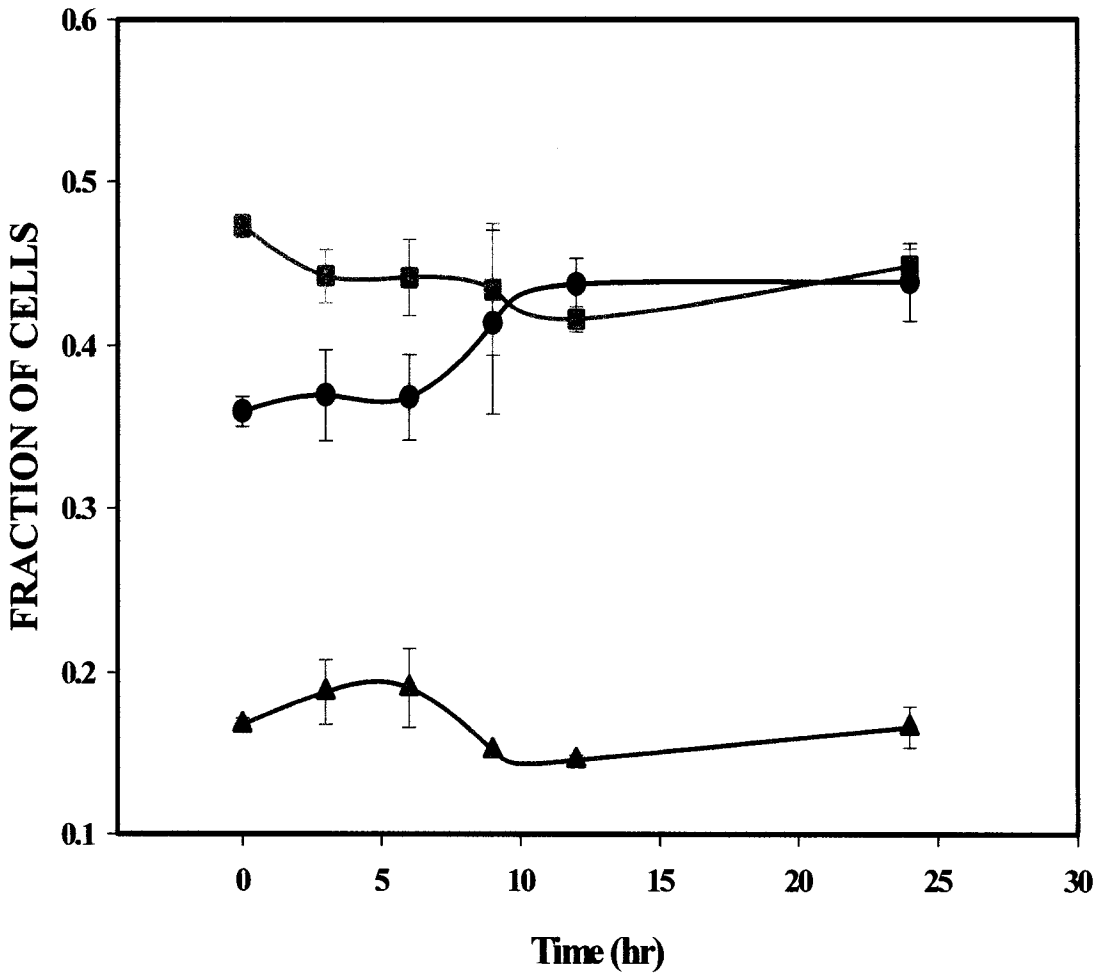

Figure 3.7 The percentage of HCW-2 control cells in each cell cycle phase. The error bars represent the standard error of the mean. These data are based on at least three different experiments. (•): G_1 phase cells; (■): S phase cells; (▲): G_2/M phase cells.

Reproduced with permission of the copyright owner. Further reproduction prohibited without permission.

percentages in S and G_2/M phase remained nearly constant and the percentage in G_1 phase slightly increased. The number of cells in each cell cycle phase for etoposide-treated cells are shown in Fig.3.8. The number of G_1 phase cells started to decrease after etoposide treatment and reached the lowest point by 12 hr, then increased by 24 hr. The number of S phase cells increased and reached a peak at 9 hr and then decreased. The number of G_2/M phase cells remained stable for 6 hr, and then increased until 24 hr. After 3 hr etoposide treatment G_1 and S phase cells slowly progressed to the next cell cycle phase and accumulated in G_2/M phase for at least 24 hrs. It is apparent that cells block at the G_2 checkpoint after treatment with etoposide in HCW-2 cells.

T_{pot} is a measure of cell cycle time that takes into account cell growth fraction, but not cell loss. By measuring the relative movement of BrdU positive cells, potential doubling time (*Tpot*) was calculated as described in Chapter 2. T_{pot} was calculated with previously reported methods (3,35,36,40). A linear regression is analyzed by SigmaPlot® software. A linear regression function was used to predict the relationship between the data curve and sampling time *t*. Tpot for control and etoposide-treated sample are shown in Fig.3.9, Table 3.2 and Table 3.3. The line represents the result of linear regression (Tpot = a*t + b) Tpot = 0.895*t + 12.5 for control cells and Tpot = 1.13*t + 22.6 for etoposide-treated cells. The slopes of the curves in Fig.3.9 are similar, but the difference in the intercepts shows the effect of etoposide treatment. The early cell cycle delay by etoposide was shown at 6 hr (3 + 3 hr).

In the analysis of HCW-2 data with the cell progression model, ApQ is zero without apoptosis. When control and etoposide-treated (6.25-μg/ml, 3 hr) HCW-2 cells were labeled with the TUNEL assay, a TUNEL positive population was not detected

Reproduced with permission of the copyright owner. Further reproduction prohibited without permission.

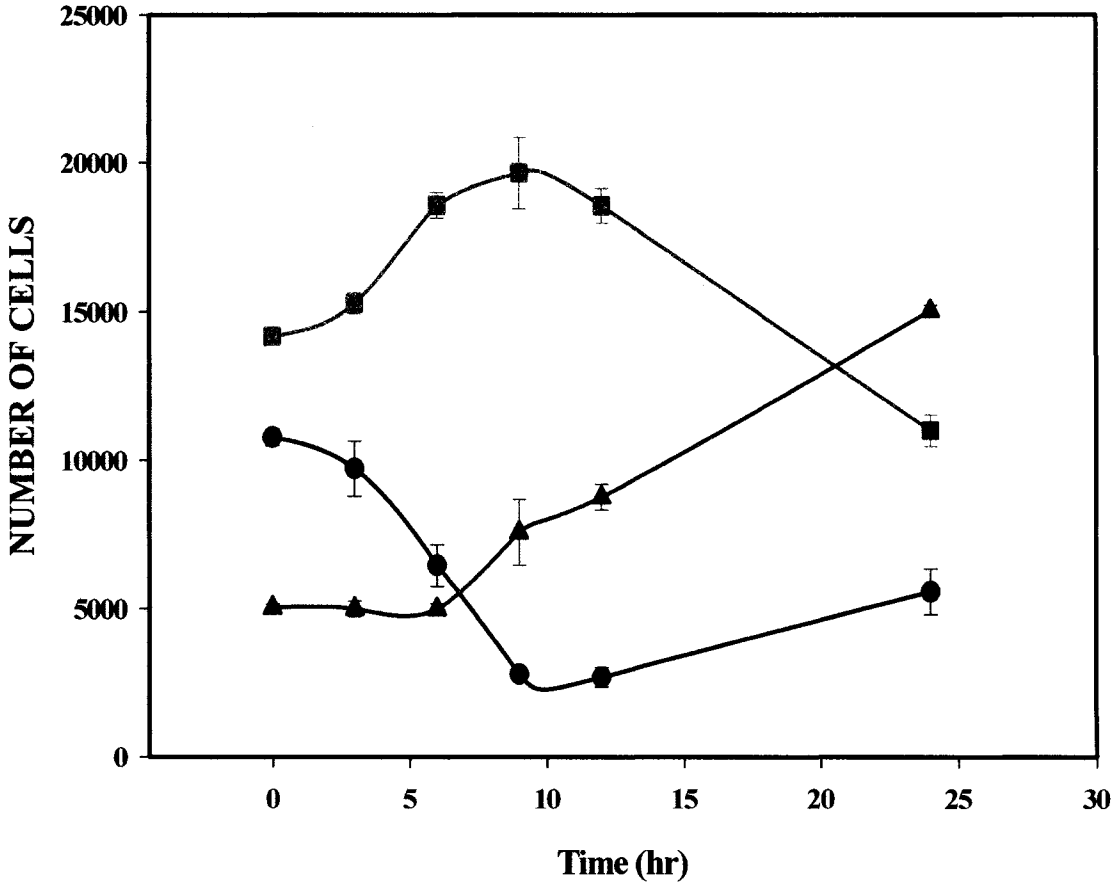

Figure 3.8 The number of HCW-2 cells in each cell cycle phase after treatment with 6.25-μg/ml etoposide for 3 hrs. The number of cells at 0 hr represents control cells. The error bar represents the standard error of the mean. These data are based on three or more different experiments. (•): G_1 phase cells; (■): S phase cells; (▲): G_2/M phase cells.

Reproduced with permission of the copyright owner. Further reproduction prohibited without permission.

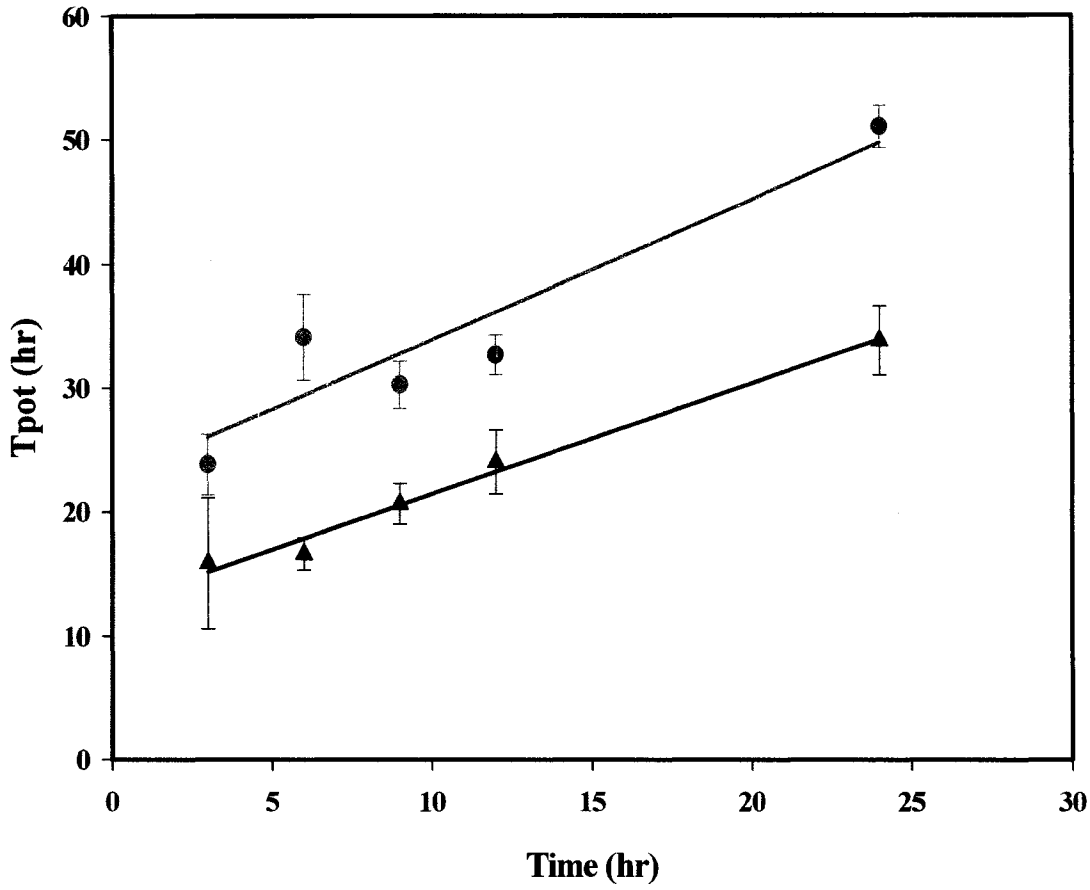

Figure 3.9 The changes of potential doubling time (T_{pot}) for Control and etoposide-treated HCW-2 cells with 6.25-μg/ml for 3 hr. Control T_{pot} (▲): BrdU pulse-labeled for 30 min without etoposide treatment; Etps T_{pot} (●): BrdU pulse-labeled for 30 min, etoposide-treated for 3 hr and post culture without etoposide. The error bar represents the standard error of the mean. The line represents the result of linear regression Tpot = 0.895*t + 12.5 for control cells and Tpot = 1.13*t + 22.6 for etoposide-treated cells.

Reproduced with permission of the copyright owner. Further reproduction prohibited without permission.

Table 3.2 The BrdU pulse-labeled data for control HCW-2 cells, including an analysis of cell progression model and potential doubling time. The data were measured directly by the experiments or calculated indirectly by interpolation.

		Pulse-labeled Population								
Time (hr)		0	3	6	9	12	15*	18*	21*	24
Cell Numbers		30038	32788	35790	39066	42643	46547	50808	55460	60537
Cell Cycle phase	G_1	10662	12046	13891	16028	18266	20424	22418	24342	26525
	S	14297	14558	15447	16735	18269	19952	21800	24000	26982
	G_2/M	5079	6184	6452	6303	6108	6171	6590	7118	7030
Cell Progression (α_2, β_2, γ_2)	α_2	-	0.386	0.345	0.318	0.307	0.309	0.320	0.329	0.327
	β_2	-	0.270	0.225	0.202	0.202	0.217	0.235	0.238	0.208
	γ_2	-	0.541	0.485	0.508	0.567	0.639	0.691	0.706	0.713
Relative Movement		0.51	0.71	0.86	0.93	1.00	-	-	-	1.34
Potential Doubling Time (Tpot)		-	15.86	16.60	20.64	24.00	-	-	-	33.84

* Interpolated values

Reproduced with permission of the copyright owner. Further reproduction prohibited without permission.

Table 3.3 The BrdU pulse-labeled data for etoposide-treated HCW-2 cells, including an analysis of cell progression model and potential doubling time. The data were measured directly by the experiments or calculated indirectly by interpolation.

		Control	Etoposide 3 hr plus Post Culture							
Time (hr)		0	3	6	9	12	15*	18*	21*	24
Cell Numbers		29909	30116	30324	30534	30746	30959	31173	31389	31606
Cell Cycle phase	G_1	11644	8469	5932	4072	2918	2483	2771	3770	5459
	S	13714	16422	18293	19291	19395	18599	16914	14365	10991
	G_2/M	4551	5225	6099	7171	8433	9877	11488	13254	15156
Cell Progression (α_2, β_2, γ_2)	α_2	-	0.308	0.349	0.384	0.387	0.295	0.057	0.00	0.00
	β_2	-	0.064	0.066	0.070	0.076	0.085	0.098	0.117	0.148
	γ_2	-	0.046	0.040	0.034	0.029	0.025	0.022	0.019	0.016
Interpretation of Efflux Coefficient (EC)	G_1	-	NB	NB	NB	NB	NB	Block	Block	Block
	S	-	Block	Block	Block	Block	NB	NB	NB	NB
	G_2/M	-	Block	Block	Block	Block	Block	Block	Block	Block
Relative Movement		0.51	0.63	0.67	0.78	0.85	-	-	-	0.99
Potential Doubling Time (Tpot)		-	23.80	34.11	30.25	32.67	-	-	-	50.98

* Interpolated values

Abbreviation and explanation: NB; no cell cycle block.

Reproduced with permission of the copyright owner. Further reproduction prohibited without permission.

(data not shown). Interpretation of the values of *Efflux Coefficient (EC)* in Table 3.3 indicates that when cells were treated with 6.25-μg/ml etoposide for 3 hr and then cultured without drug, cells are blocked in G_2/M for at least 24 hr, delayed in S phase for the first 15 hr and delayed in G_1 after 18 hr. These results indicate that etoposide activates both the S phase checkpoint and G_2 checkpoint as a result of DNA damage, but does not activate the G_1 checkpoint, probably because p53 is inactivated in these cells.

3.4 Discussion

A variety of approaches have been used to analyze cell cycle responses to physical and chemical agents, such as cell cycle simulation (38), kinetic analysis of drug-induced cell cycle perturbations (39) and potential doubling time with cell loss (4) and population growth (5,37). Another approach is to measure the changes in the cell cycle and killing effects by the treatment (31). Recently, a non-cycling cell population was used to calculate the disintegration of apoptotic cells by comparing the number of cells before and after treatment (29). Another approach used a caspase inhibitor to halt the disintegration of apoptotic cells to calculate the cumulative apoptotic index (33). However, these previous approaches did not provide a comprehensive analysis of cell cycle arrest, progression, cell cycle-specific sensitivity and degree of apoptosis from each cell cycle phase. In this Chapter, I measured, analyzed and calculated all of these parameters with the model described in Chapter 2.

When cells undergo apoptosis, the length of the process is dependent on the cell line and the apoptotic inducer. Apoptosis in HL-60 cells is usually rapid (a few hours)

Reproduced with permission of the copyright owner. Further reproduction prohibited without permission.

and involves a large fraction of the cells. Cells treated with camptothecin, a DNA topoisomerase I inhibitor, exhibited about 50 % apoptosis during the initial 8 hr at a rate of about 7 % of the cells undergoing apoptosis per hour. After 8 hr, cells entered apoptosis for up to 48 hr at a rate of about 1 % of cells per hour (33). Cells progressing through S phase were selectively susceptible to apoptosis when treated with camptothecin, teniposide, amsacrine, mitoxantrone, H7 (protein kinase C inhibitor) and hydroxyurea (17). Several studies demonstrated selective apoptosis of S-phase cells and the relative resistance of G_1 or G_0 cells during treatments with this inhibitor (8,11,24).

In this study, apoptosis of HL-60 cells was induced by treatment with the DNA topoisomerase II inhibitor, etoposide. TUNEL and bivariate histogram with PI showed S-phase specific apoptosis (Fig. 3.1 and 3.3). I developed the *apoptotic quotient calculation* to estimate the amount of apoptosis from each cell cycle phase and a *cell progression model* to analyze the existence of cell cycle-specific sensitivity with the treatment and cell cycle arrest. Also, the model can calculate cell cycle progression between each phase and the number of cells remaining in each phase.

The results reported here support previous results that apoptotic HL-60 cells mainly came from S phase (77.9 % = S phase apoptosis/total apoptosis) after etoposide treatment (15). Though only a small number of cells undergo apoptosis in G_1 (15.6 % = G_1 phase apoptosis/total apoptosis) and G_2/M (6.5 % = G_2/M phase apoptosis/total apoptosis) phases, it is significant. These results also show that HL-60 cells treated with 6.25-μg/ml etoposide for 3 hr are blocked in G_1 and G_2/M phases. G_1 arrest is greater than G_2/M arrest, because the number of cells progressing to G_1 phase is greater than the number of cells to G_2/M phase after the big loss of S phase cells. The G_2/M arrest is not large when

Reproduced with permission of the copyright owner. Further reproduction prohibited without permission.

it is compared to heat shock-induced G_2/M block, maybe due to the nature of S-phase specific topoisomerase-induced apoptosis. This cell cycle arrest may permit DNA repair prior to mitosis. It was previously reported that a larger G_2 arrest resulted from a lower concentration of etoposide treatment (10,14). Apoptosis could be induced following G_2 block with prolonged drug-treatment time at relatively low drug-concentrations (10,14). DNA damage induced by higher doses of etoposide could trigger cell suicide through apoptosis directly, without cell progression to G_2. This phenomenon may be referred to as interphase cell death (34).

The comparison of ApQ and API show that G_1 and G_2/M phase in HL-60 cells are resistant to etoposide and S phase cells are sensitive. This indicates that S phase cells are the main target of etoposide. This observation is consistent with the increased sensitivity of S phase cells to etoposide reported in the literature (8,11,24). The degree of the block and sensitivity to apoptosis could be changed based on the drug concentration and treatment time (10).

HCW-2 cells treated with etoposide had an early S phase arrest, a late G_1 phase arrest, a continuous G_2/M phase block and increasing T_{pot}. Cell growth after etoposide was minimal. The T_{pot} increased in control cells due to contact inhibition at higher cell concentrations. However, the T_{pot} increased in etoposide-treated cells due to delays in cell cycle progression without apoptosis.

The major differences between the parental cell line (HL-60 cells) and mutant cell line (HCW-2 cells) after 6.25-μg/ml etoposide treatment for 3 hr are proliferation rate, cell cycle phase fractions, cell progression, and apoptosis. HL-60 cells had a larger increase in G_1 cells than HCW-2 cells when total number of cells is compared. The rate

Reproduced with permission of the copyright owner. Further reproduction prohibited without permission.

of progression from S to G_2/M (β_2) and cell division (γ_2) decreased substantially after etoposide treatment (Table 3.3) compared to HL-60 cells (Table 3.1) and control HCW-2 cells (Table 3.2). HCW-2 cells had a more complete G_2/M cell cycle arrest than HL-60 cells. Although HCW-2 cells do not have an apoptotic population because of the lack of cytochrome C release from mitochondria, HCW-2 cells should have the same amount of DNA damage to S phase cells by etoposide when compared to HL-60 cells.

Thus, heavily damaged S phase HL-60 cells are able to undergo apoptosis and these are removed from the population. However, HCW-2 cells do not undergo apoptosis so the extensive DNA damage causes a pronounced block in G_2 and the cells can attempt to repair the damage. It is interesting to note that even the cells that were in G_1 at the time of etoposide treatment subsequently move slowly through S phase and are also delayed in G_2 (Fig. 3.5).

In summary, the results reported here show that complicated patterns of apoptosis and cell cycle perturbations occur after etoposide treatment. The model I developed allows a more comprehensive analysis of these patterns.

3.5 Appendix

The following is a brief description of the cell progression model procedure.

1) During the Experiment
   a) Count the cell number before and after
   b) Measure the amount of apoptosis and cell cycle phases with TUNEL or any apoptotic methods by bivariate analysis in fixation with paraformaldehyde and ethanol
2) Data Analysis and Optimization
   a) Total cell number: Calculate the coefficients of exponential growth curve based on measured cell number with curve fitting software (SigmaPlot®, control and several time points)
   b) Apoptotic, Non-apoptotic and total population: Analyze the apoptotic, non-apoptotic and total number of cells in each cell cycle phase before and after treatment at every time point
      i) Data analysis with Multi-2D® and Multicycle® software.

Reproduced with permission of the copyright owner. Further reproduction prohibited without permission.

ii) Calculate the coefficients by curve fitting software (SigmaPlot®)

c) Calculate the *CAI* by *AI* curve and determine the cell disintegration rate based on *CAI* and *AI* curve

i) Calculate the *CAI* with Equations in chapter 4

ii) Calculate the coefficients by curve fitting software (SigmaPlot®)

3) Calculate *ApQ, API*, each cell progression rate (α_2, β_2 and γ_2), and *EC* based on equations in Materials and Methods

4) Analyze the final results and comment on the data

Reproduced with permission of the copyright owner. Further reproduction prohibited without permission.

Reference List

1. Aroor AR, Baker RC: Ethanol-induced apoptosis in human HL-60 cells. Life Sci 61:2345-2350, 1997.

2. Barry MA, Reynolds JE, Eastman A: Etoposide-induced apoptosis in human HL-60 cells is associated with intracellular acidification. Cancer Res 53:2349-2357, 1993.

3. Begg AC, McNally NJ, Shrieve DC, Kärcher H: A method to measure the duration of DNA synthesis and the potential doubling time from a single sample. Cytometry 6:620-626, 1985.

4. Bertuzzi A, Gandolfi A, Sinisgalli C, Starace G, Ubezio P: Cell loss and the concept of potential doubling time. Cytometry 29:34-40, 1997.

5. Cain SJ, Chau PC: Transition probability cell cycle model. Part II--Non-balanced growth. J Theor Biol 185:69-79, 1997.

6. Darzynkiewicz Z, Bruno S, Del Bino G, Gorczyca W, Hotz MA, Lassota P, Traganos F: Features of apoptotic cells measured by flow cytometry. Cytometry 13:795-808, 1992.

7. Del Bino G, Bruno S, Yi PN, Darzynkiewicz Z: Apoptotic cell death triggered by camptothecin or teniposide: The cell cycle specificity and effects of ionizing radiation. Cell Prolif Nov. 25:537-548, 1992.

8. Del Bino G, Darzynkiewicz Z: Camptothecin, teniposide, or 4'-(9-acridinylamino)-3-methanesulfon-m- anisidide, but not mitoxantrone or doxorubicin, induces degradation of nuclear DNA in the S phase of HL-60 cells. Cancer Res 51:1165-1169, 1991.

9. Del Bino G, Darzynkiewicz Z, Degraef C, Mosselmans R, Fokan D, Galand P: Comparison of methods based on annexin-V binding, DNA content or TUNEL for evaluating cell death in HL-60 and adherent MCF-7 cells. Cell Prolif 32:25-37, 1999.

10. Del Bino G, Skierski JS, Darzynkiewicz Z: The concentration-dependent diversity of effects of DNA topoisomerase I and II inhibitors on the cell cycle of HL-60 cells. Exp Cell Res 195:485-491, 1991.

11. Deptala A, Li X, Bedner E, Cheng W, Traganos F, Darzynkiewicz Z: Differences in induction of p53, p21WAF1 and apoptosis in relation to cell cycle phase of MCF-7 cells treated with camptothecin. Int J Oncol 15:861-871, 1999.

12. Dubrez L, Goldwasser F, Genne P, Pommier Y, Solary E: The role of cell cycle regulation and apoptosis triggering in determining the sensitivity of leukemic cells to topoisomerase I and II inhibitors. Leukemia 9:1013-1024, 1995.

13. Dynlacht JR, Earles M, Henthorn J, Seno JD: Different patterns of DNA fragmentation and degradation of nuclear matrix proteins during apoptosis induced by radiation, hyperthermia or etoposide. Radiat Res 154:515-530, 2000.

Reproduced with permission of the copyright owner. Further reproduction prohibited without permission.

14. Facompre M, Wattez N, Kluza J, Lansiaux A, Bailly C: Relationship between cell cycle changes and variations of the mitochondrial membrane potential induced by etoposide. Mol Cell Biol Res Commun 4:37-42, 2000.

15. Frey T: Correlated flow cytometric analysis of terminal events in apoptosis reveals the absence of some changes in some model systems. Cytometry 28:253-263, 1997.

16. Gong J, Li X, Darzynkiewicz Z: Different patterns of apoptosis of HL60 cells induced by cycloheximide and camptothecin. J Cell Physiol 157:263-270, 1993.

17. Gorczyca W, Gong J, Ardelt B, Traganos F, Darzynkiewicz Z: The cell cycle related differences in susceptibility of HL-60 cells to apoptosis induced by various antitumor agents. Cancer Res 53:3186-3192, 1993.

18. Gorczyca W, Melamed MR, Darzynkiewicz Z: Apoptosis of S-phase HL60 cells induced by DNA topoisomerase inhibitors: detection of DNA strand breaks by flow cytometry using the in situ nick translation assay. Toxicol Lett 67:249-258, 1993.

19. Halicka HD, Seiter K, Feldman EJ, Traganos F, Mittelman A, Ahmed T, Darzynkiewicz Z: Cell cycle specificity of apoptosis during treatment of leukemias. Apoptosis 2:1997.

20. Han Z, Bhalla K, Pantazis P, Hendrickson EA, Wyche JH: Cif (Cytochrome c efflux-inducing factor) activity is regulated by Bcl- 2 and caspases and correlates with the activation of Bid. Mol Cell Biol 19:1381-1389, 1999.

21. Han Z, Chatterjee D, Early J, Pantazis P, Hendrickson EA, Wyche JH: Isolation and characterization of an apoptosis-resistant variant of human leukemia HL-60 cells that has switched expression from Bcl-2 to Bcl-xL. Cancer Res 56:1621-1628, 1996.

22. Han Z, Li G, Bremner TA, Lange TS, Zhang G, Jemmerson R, Wyche JH, Hendrickson EA: A cytosolic factor is required for mitochondrial cytochrome c efflux during apoptosis. Cell Death Differ 5:469-479, 1998.

23. Kawasaki K, Murakami T, Ita M, Sasaki K, Furukawa S: KRN5500, a novel antitumor agent, induces apoptosis or cell differentiation in HL-60 cells. Cytometry 39:211-216, 2000.

24. Li X, Darzynkiewicz Z: The Schrodinger's cat quandary in cell biology: integration of live cell functional assays with measurements of fixed cells in analysis of apoptosis. Exp Cell Res 249:404-412, 1999.

25. Martin SJ, Lennon SV, Bonham AM, Cotter TG: Induction of apoptosis (programmed cell death) in human leukemic HL-60 cells by inhibition of RNA or protein synthesis. J Immunol 145:1859-1867, 1990.

26. Martins LM, Mesner PW, Kottke TJ, Basi GS, Sinha S, Tung JS, Svingen PA, Madden BJ, Takahashi A, McCormick DJ, Earnshaw WC, Kaufmann SH: Comparison of caspase activation and subcellular localization in HL-60 and K562 cells undergoing etoposide-induced apoptosis. Blood 90:4283-4296, 1997.

27. Murakami T, Li X, Gong J, Bhatia U, Traganos F, Darzynkiewicz Z: Induction of apoptosis by 5-azacytidine: drug concentration-dependent differences in cell cycle specificity. Cancer Res 55:3093-3098, 1995.

Reproduced with permission of the copyright owner. Further reproduction prohibited without permission.

28. Palissot V, Liautaud-Roger F, Carpentier Y, Dufer J: Image cytometry of early nuclear events during apoptosis induced by camptothecin in HL-60 leukemic cells. Cytometry 25:341-348, 1996.

29. Prieto A, Diaz D, Barcenilla H, Garcia-Suarez J, Reyes E, Monserrat J, San Antonio E, Melero D, De La HA, Orfao A, Alvarez-Mon M: Apoptotic rate: A new indicator for the quantification of the incidence of apoptosis in cell cultures. Cytometry 48:185-193, 2002.

30. Ritke MK, Rusnak JM, Lazo JS, Allan WP, Dive C, Heer S, Yalowich JC: Differential induction of etoposide-mediated apoptosis in human leukemia HL60 and K562 cells. Mol Pharmacol 46:605-611, 1994.

31. Sena G, Onado C, Cappella P, Montalenti F, Ubezio P: Measuring the complexity of cell cycle arrest and killing of drugs: kinetics of phase-specific effects induced by taxol. Cytometry 37:113-124, 1999.

32. Shimizu T, O'Connor PM, Kohn KW, Pommier Y: Unscheduled activation of cyclin B1/Cdc2 kinase in human promyelocytic leukemia cell line HL60 cells undergoing apoptosis induced by DNA damage. Cancer Res 55:228-231, 1995.

33. Smolewski P, Grabarek J, Lee BW, Johnson GL, Darzynkiewicz Z: Kinetics of HL-60 cell entry to apoptosis during treatment with TNF- alpha or camptothecin assayed by the stathmo-apoptosis method. Cytometry 47:143-149, 2002.

34. Solary E, Bertrand R, Pommier Y: Apoptosis induced by DNA topoisomerase I and II inhibitors in human leukemic HL-60 cells. Leuk Lymphoma 15:21-32, 1994.

35. Steel GG: Basic theory of growing cell populations. In: Growth Kinetics of Tumors:cell population kinetics in relation to the growth and treatment of cancer, Anonymous Clarendon Press, Oxford, 1977, pp. 56-85.

36. Terry NH, White RA, Meistrich ML, Calkins DP: Evaluation of flow cytometric methods for determining population potential doubling times using cultured cells. Cytometry 12:234-241, 1991.

37. Torricelli A, Bisiach M, Spinelli L, Ubezio P: From flow cytometric BrdUrd data to cell population growth and doubling time. Cytometry 29:222-232, 1997.

38. Ubezio P: Cell cycle simulation for flow cytometry. Comput Methods Programs Biomed 31:255-266, 1990.

39. Ubezio P, Filippeschi S, Spinelli L: Method for kinetic analysis of drug-induced cell cycle perturbations. Cytometry 12:119-126, 1991.

40. White RA, Meistrich ML: A comment on "A method to measure the duration of DNA synthesis and the potential doubling time from a single sample". Cytometry 7:486-490, 1986.

Reproduced with permission of the copyright owner. Further reproduction prohibited without permission.

CHAPTER 4

The Estimation of Cumulative Apoptotic Index (CAI) by Time-lapse Apoptotic Index (AI)

4.1 Introduction

The degree of programmed cell death or apoptosis at a particular time point (apoptotic index or AI) is useful information to assess therapy for a variety of diseases, but the total percentage of cells undergoing apoptosis during the treatment is much more useful information than the AI at a particular time point. Because apoptosis is a kinetic event, an estimation of the percentage or fraction of apoptotic cells can be inaccurate and underestimated by the disintegration of apoptotic cells. Moreover, each assay can detect apoptotic cells only in a specific time-window based on the properties of the assay (e.g., caspases, TUNEL, annexin V, etc). For example, the presence of phosphatidylserine on the outer plasma membrane, which can be labeled with annexin V, is an early event. When combined with PI staining, early apoptotic cells are annexin V positive and PI negative while late apoptotic cells are annexin V positive and PI positive. Thus, the time window for early apoptosis constitutes the time when cells are annexin V positive and PI negative. The cell type and apoptotic inducer also make the length of the time-window variable. Once individual cells pass the specific time-window of the assay they are not

Reproduced with permission of the copyright owner. Further reproduction prohibited without permission.

counted as apoptotic cells until they disintegrate in the late stages of apoptosis. This underestimation of apoptosis has a couple of critical disadvantages in apoptosis research. First, the underestimation affects the assessment of the relationship between drug dose and cell death. When the cumulative apoptotic index (CAI) is used for the dose dependence of apoptosis, the results are more accurate. Second, the change in the number of apoptotic cells in each time interval cannot be calculated using AI. Thus, time-dependent kinetic analysis of apoptosis is not available. Cell cycle analysis combined with CAI can provide greater insight into the kinetics of apoptosis as well as cell cycle progression.

Previously, two different methods were used to obtain a more accurate assessment of the incidence of apoptosis. One is to halt the apoptotic disintegration process and the other is to calculate the disintegration population. The ultimate goal of both methods is to calculate the CAI (8,10). In the first method, known as stathmo-apoptosis, the fluorescent inhibitor of caspases (FLICA) FAM-VAD-FMK (1,9) was used to arrest cells in apoptosis, thereby preventing their disintegration, passage and exit from the time-window of the assay (11). FLICA binds to the active center of the activated caspases through the fluoromethylketone (FMK) portion. The peptide portion of these inhibitors defines their specificity; VAD (Val-Ala-Asp) is generic to most caspases (Table 1.2) (7). However, the FLICA assay has several disadvantages: first, the continuous existence of the inhibitor can affect the kinetics of apoptosis phenomena, including loss of integrity of the plasma membrane, cell cycle, and other cell signaling and metabolic events. Second, the FLICA assay is applicable only in the analysis of caspase-mediated apoptosis. Third, the existence of additional binding sites for FLICA could result in an overestimation of CAI.

Reproduced with permission of the copyright owner. Further reproduction prohibited without permission.

Fourth, this assay should be carefully tested to get the proper concentration of FLICA to completely block progression of apoptosis.

In the second approach for CAI, a non-cycling cell line was used. When analyzing the apoptotic mechanism in a non-cycling cell population, there is no newly dividing cell population. Thus, the comparison of cell numbers at two different time points allows one to calculate the disintegrated cells (8). This method also has some disadvantages: first, the method can only be used for non-cycling cells. Second, even though the addition of disintegrated cells to AI at each time point gives better AI data, it still cannot directly explain CAI because the end of the time-window in this technique is not necessarily the same as the starting time of disintegration. This technique is only useful if the apoptosis process take place very fast and apoptotic integration finishes before the sampling time. The gaps between them could cause an underestimation of AI.

To overcome these disadvantages of FLICA and non-cycling cell assays for estimating CAI, I propose a new model to estimate CAI using the AI kinetics data based on measuring AI at multiple time points. Previously, apoptosis induction by TNF-α plus cycloheximide and camptothecin treatment occurred in two phases with different apoptosis induction rates as measured by FLICA (10). Thus, I assume that apoptosis may progress with multiple phases and the time-window (T_w) is constant in all phases. Several variables are also introduced: the apoptotic induction rate (percent apoptotic cells / hour) (AIR_i, i= *1, 2, 3 etc*) and the time of each phase (T_i, i= *1, 2, 3 etc*). To better understand each case of multi-phasic apoptosis, general calculations and graphs of AI and CAI are presented.

Reproduced with permission of the copyright owner. Further reproduction prohibited without permission.

The kinetics of apoptosis are explained as follows: first, the shape of the AI time-dependent curve is a guideline for how many phases of apoptosis exist. When the graph is symmetrical, apoptosis take place in a uni-phasic mode. If not, it could have bi- or multi-phasic modes. Second, the number of plateau regions indicates how many different apoptotic phases exist. One plateau or peak indicates there is at least one phase in AI data. Third, the time-window (T_w), which can be different in different assays and different cell lines, is calculated. Fourth, the apoptotic induction rate (AIR_i, *i= 1, 2, 3 etc*) of each phase is calculated. Fifth, the length of each phase (T_i, *i= 1, 2, 3 etc*) is calculated. There are three assumptions which I have made for the CAI estimation. First, cells which start apoptosis early exit the time-window early (first in, first out). Second, the time-window is a constant width within each phase. Third, the apoptotic induction rate (AIR_i) is equal to the rate of movement out of the time window. Thus, it should show a linear symmetrical shape in each individual phase. This analysis is very similar to the concept of Fraction of Labeled Mitoses curves (6) where cells move into and out of a mitotic window, but in this case they are apoptotic windows and multiple phases can exist.

4.2 Materials and Methods

The general information for the experiments was explained in Chapter 2 Materials and Methods. Detailed and specific information is provided in figure and table legends.

Reproduced with permission of the copyright owner. Further reproduction prohibited without permission.

4.3 Results

4.3.1 Uni-phasic apoptosis

The major characteristic of uni-phasic apoptosis is the existence of linear symmetry in the AI curve. Uni-phasic apoptosis has one plateau or peak and one AIR_1. Uni-phasic apoptosis has three coefficients: AIR_1, T_w, and T_1. The shapes of AI and CAI curve have two general cases which are dependent on the relationship between T_w and T_1 (Figure 4.1 and Figure 4.2).

4.3.1.1 Case I. If $T_w < T_1$

As an example, when AIR_1 equals 6, T_w equals 8, and T_1 equals 12, the calculation data (top) and resulting shapes of the AI and CAI curves (bottom) are as shown in Fig.4.1. The duration of the plateau area is the difference between T_w and T_1. The first decrease in AI begins at the endpoint of T_1. The calculation is performed with Eq. 4.1.

$$\begin{aligned} AI1 &= CAI1 = AIR_1 * t \\ AI2 &= AIR_1 * T_w \\ AI3 &= AIR_1 * (T_w + T_1 - t) \\ CAI2 &= AIR_1 * T_1 \end{aligned} \qquad \text{(Equation 4.1)}$$

4.3.1.2 Case II. If $T_w >= T_1$

When AIR_1 equals 6, T_w equals 12, and T_1 equals 8, the calculation data (top) and shapes of the AI and CAI curves (bottom) are as shown in Fig.4.2. The duration of the plateau is the difference between T_w and T_1. The first decrease in AI begins at the endpoint of T_w. The calculation is performed with Eq. 4.2. The AI curves with different CAI in cases I and II give the same results even though different coefficients are used.

Reproduced with permission of the copyright owner. Further reproduction prohibited without permission.

Time													AI	CAI
1	6												6	6
2	6	6											12	12
3	6	6	6										18	18
4	6	6	6	6									24	24
5	6	6	6	6	6								30	30
6	6	6	6	6	6	6							36	36
7	6	6	6	6	6	6	6						42	42
8	6	6	6	6	6	6	6	6					48	48
9		6	6	6	6	6	6	6	6				48	54
10			6	6	6	6	6	6	6	6			48	60
11				6	6	6	6	6	6	6	6		48	66
12					6	6	6	6	6	6	6	6	48	72
13						6	6	6	6	6	6	6	42	72
14							6	6	6	6	6	6	36	72
15								6	6	6	6	6	30	72
16									6	6	6	6	24	72
17										6	6	6	18	72
18											6	6	12	72
19												6	6	72
20													0	72

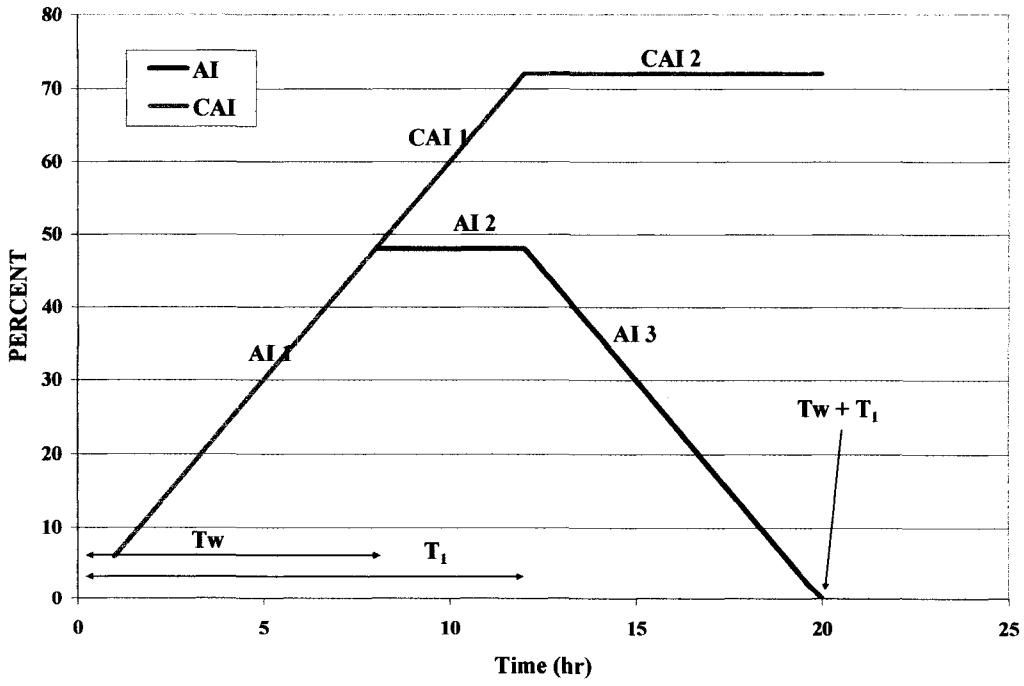

Figure 4.1 The AI and CAI curves for uni-phasic apoptosis for uni-phasic apoptosis curve if $T_w < T_1$, $AIR_1=6$, $T_w=8$, and $T_1=12$. Top: data format and calculation. Bottom: uni-phasic apoptosis curve.

Reproduced with permission of the copyright owner. Further reproduction prohibited without permission.

Time									AI	CAI
1	6								6	6
2	6	6							12	12
3	6	6	6						18	18
4	6	6	6	6					24	24
5	6	6	6	6	6				30	30
6	6	6	6	6	6	6			36	36
7	6	6	6	6	6	6	6		42	42
8	6	6	6	6	6	6	6	6	48	48
9	6	6	6	6	6	6	6	6	48	48
10	6	6	6	6	6	6	6	6	48	48
11	6	6	6	6	6	6	6	6	48	48
12	6	6	6	6	6	6	6	6	48	48
13		6	6	6	6	6	6	6	42	48
14			6	6	6	6	6	6	36	48
15				6	6	6	6	6	30	48
16					6	6	6	6	24	48
17						6	6	6	18	48
18							6	6	12	48
19								6	6	48
20									0	48

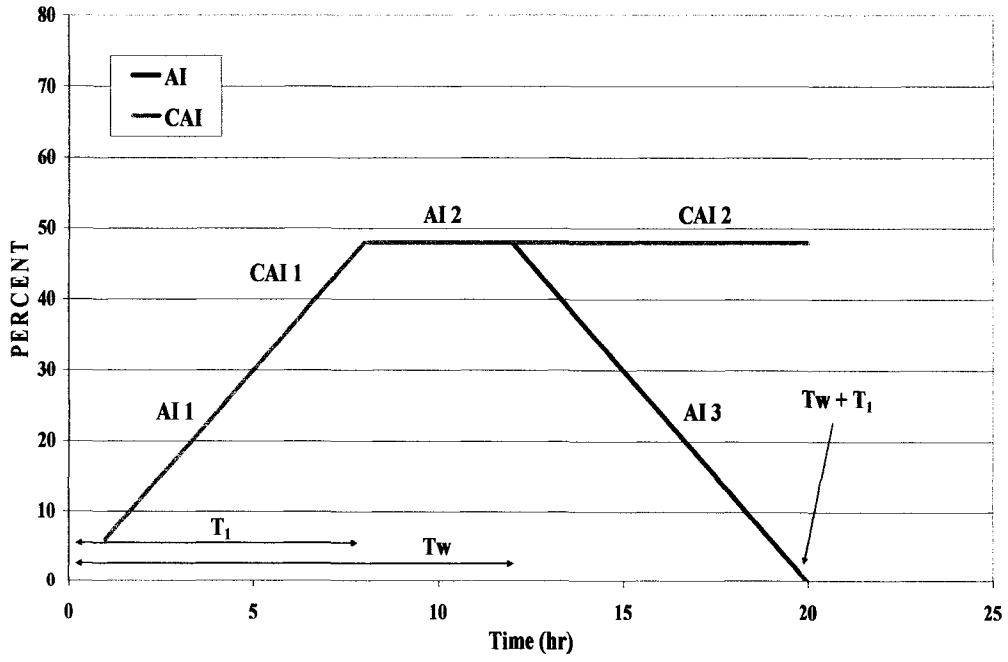

Figure 4.2 The AI and CAI curves for uni-phasic apoptosis for uni-phasic apoptosis curve if $T_w >= T_1$, $AIR_1=6$, $T_w=12$, and $T_1=8$. Top: data format and calculation. Bottom: uni-phasic apoptosis curve.

Reproduced with permission of the copyright owner. Further reproduction prohibited without permission.

Thus, when CAI is calculated from the AI curve, the calculation has to be done using both cases. For the decision of right CAI, the comparison of CAI is performed when dose of treatment is doubled or tripled.

$$\begin{aligned} AI1 &= CAI1 = AIR_1 * t \\ AI2 &= AIR_1 * T_1 \\ AI3 &= AIR_1 * (T_w + T_1 - t) \\ CAI2 &= AIR_1 * T_1 \end{aligned} \qquad \text{(Equation 4.2)}$$

4.3.2 Bi-phasic apoptosis

The major characteristics of bi-phasic apoptosis are non-symmetrical curves and the existence of two plateaus in the AI curve. Bi-phasic apoptosis has five coefficients: AIR_1, AIR_2, T_w, T_1 and T_2. The AI and CAI curves have four general cases which are dependent on two relationships between T_w and T_1, and between (T_w+T_1) and (T_1+T_2).

4.3.2.1 Case I. If $T_w < T_1$, $(T_w+T_1) < (T_1+T_2)$

When AIR_1 equals 6, AIR_2 equals 2, T_w equals 8, T_1 equals 10, and T_2 equals 12, the data and AI (blue solid line) and CAI (pink solid line) curves are as shown in Fig.4.3. To calculate the CAI curve, the first phase of apoptosis had to be estimated using symmetry considerations. AI increased at a rate of AIR_1 until the beginning of the first AI plateau was located. This point was the endpoint of T_w. Next, the first point where AI started decreasing was located. This point was the endpoint of T_1. Then a curve was calculated that decreased at the same rate as the initial increase (AIR_1). This symmetrical curve constituted the first phase of apoptosis (green dashed curve). Next the first phase curve was subtracted from the actual AI curve, resulting in the second phase curve (red

Reproduced with permission of the copyright owner. Further reproduction prohibited without permission.

t																			AI	CAI	1st	2nd
1	6																		6	6	6	
2	6	6																	12	12	12	
3	6	6	6																18	18	18	
4	6	6	6	6															24	24	24	
5	6	6	6	6	6														30	30	30	
6	6	6	6	6	6	6													36	36	36	
7	6	6	6	6	6	6	6												42	42	42	
8	6	6	6	6	6	6	6	6											48	48	48	
9		6	6	6	6	6	6	6	6										48	54	48	
10			6	6	6	6	6	6	6	6									48	60	48	0
11				6	6	6	6	6	6	6	2								44	62	42	2
12					6	6	6	6	6	6	2	2							40	64	36	4
13						6	6	6	6	6	2	2	2						36	66	30	6
14							6	6	6	6	2	2	2	2					32	68	24	8
15								6	6	6	2	2	2	2	2				28	70	18	10
16									6	6	2	2	2	2	2	2			24	72	12	12
17										6	2	2	2	2	2	2	2		20	74	6	14
18											2	2	2	2	2	2	2	2	16	76	0	16
19												2	2	2	2	2	2	2	16	78		16
20													2	2	2	2	2	2	16	80		16
21														2	2	2	2	2	16	82		16
22															2	2	2	2	16	84		16
23																2	2	2	14	84		14
24																	2	2	12	84		12
25																		2	10	84		10
26																			8	84		8
27																			6	84		6
28																			4	84		4
29																			2	84		2
30																			0	84		0

Figure 4.3 (A) The data for calculating AI and CAI curves for bi-phasic apoptosis when bi-phasic apoptosis curve if $T_w < T_1$, $(T_w+T_1) < (T_1+T_2)$, a=6, b=2, T_w=8, T_1=10 and T_2=12.

Reproduced with permission of the copyright owner. Further reproduction prohibited without permission.

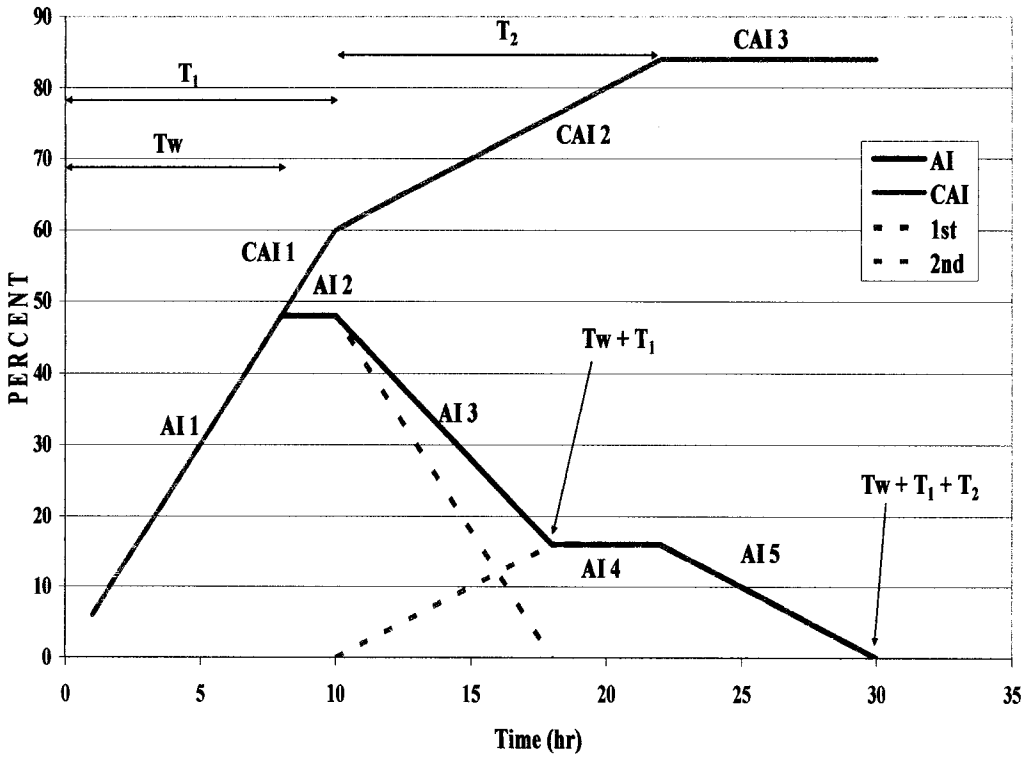

Figure 4.3 (B) The AI and CAI curves for bi-phasic apoptosis if $T_w < T_1$, $(T_w+T_1) < (T_1+T_2)$, a=6, b=2, T_w=8, T_1=10 and T_2=12.

Reproduced with permission of the copyright owner. Further reproduction prohibited without permission.

dashed curve). The length of the first plateau is the difference between T_w and T_1. The length of the second plateau is the difference between (T_w+T_1) and (T_1+T_2). The first point where AI decreased is the endpoint of T_1 and the second point of decreasing AI after second plateau is the endpoint of T_2. The calculation was performed with Eq. 4.3.

$$
\begin{aligned}
&AI1 = CAI1 = AIR_1 * t \\
&AI2 = AIR_1 * Tw \\
&AI3 = AIR_1 * (Tw + T_1 - t) + AIR_2 * (t - T_1) \\
&AI4 = AIR_2 * Tw \\
&AI5 = AIR_2 * (Tw + T_1 + T_2 - t) \\
&CAI2 = AIR_1 * T_1 + AIR_2 * (t - T_1) \\
&CAI3 = AIR_1 * T_1 + AIR_2 * T_2
\end{aligned}
\qquad \text{(Equation 4.3)}
$$

4.3.2.2 Case II. If Tw < T_1, (T_w+T_1) >= (T_1+T_2)

When AIR_1 equals 6, AIR_2 equals 2, T_w equals 8, T_1 equals 10, and T_2 equals 6, the data and shapes of AI (blue solid line) and CAI (pink solid line) curves are as shown in Fig.4.4. To calculate the CAI, the first phase of apoptosis had to be estimated. The same procedure was used as with the previous case. However, there is no second plateau because (T_w+T_1) is greater than (T_1+T_2). The first point where AI decreased is the endpoint of T_1 and the second rate-changing point is the endpoint of T_2. The third rate-changing point is the endpoint of sum (T_w+T_1). The second and third rate-changing points are not noticeable in the experimental data. Thus, the calculation has to be performed with possible cases for the estimation of T_2. The calculation was done using Eq. 4.4. The first phase of apoptosis is shown with the green dashed curve and the second phase of apoptosis is shown with the red dashed curve.

Reproduced with permission of the copyright owner. Further reproduction prohibited without permission.

t																AI	CAI	1st	2nd
1	6															6	6	6	
2	6	6														12	12	12	
3	6	6	6													18	18	18	
4	6	6	6	6												24	24	24	
5	6	6	6	6	6											30	30	30	
6	6	6	6	6	6	6										36	36	36	
7	6	6	6	6	6	6	6									42	42	42	
8	6	6	6	6	6	6	6	6								48	48	48	0
9		6	6	6	6	6	6	6	6							48	54	48	0
10			6	6	6	6	6	6	6	6						48	60	48	0
11				6	6	6	6	6	6	6	2					44	62	42	2
12					6	6	6	6	6	6	2	2				40	64	36	4
13						6	6	6	6	6	2	2	2			36	66	30	6
14							6	6	6	6	2	2	2	2		32	68	24	8
15								6	6	6	2	2	2	2	2	28	70	18	10
16									6	6	2	2	2	2	2	24	72	12	12
17										6	2	2	2	2	2	18	72	6	12
18											2	2	2	2	2	12	72	0	12
19												2	2	2	2	10	72	0	10
20													2	2	2	8	72	0	8
21														2	2	6	72	0	6
22															2	4	72	0	4
23																2	72	0	2
24																0	72	0	0
25																0	72		
26																0	72		
27																0	72		
28																0	72		
29																0	72		
30																0	72		

Figure 4.4 (A) The data for calculating AI and CAI curves for bi-phasic apoptosis when bi-phasic apoptosis curve if $T_w < T_1$, $(T_w+T_1) >= (T_1+T_2)$, a=6, b=2, T_w=8, T_1=10 and T_2=6.

Reproduced with permission of the copyright owner. Further reproduction prohibited without permission.

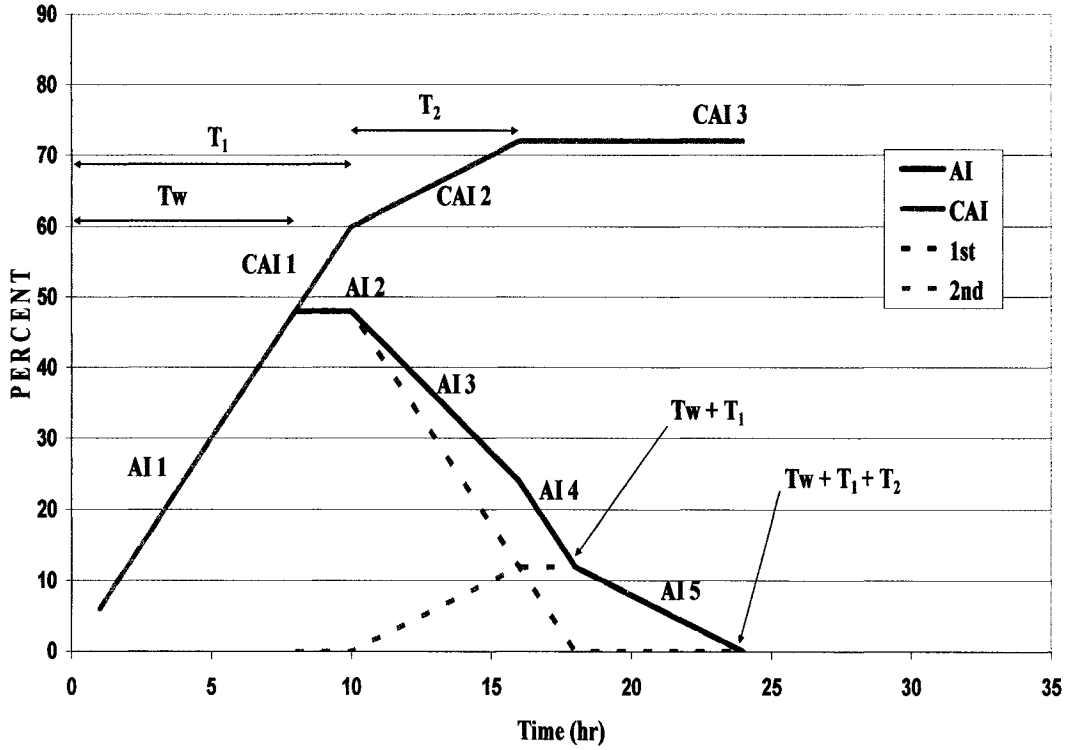

Figure 4.4 (B) The AI and CAI curves for bi-phasic apoptosis if $T_w < T_1$, $(T_w+T_1) >= (T_1+T_2)$, a=6, b=2, T_w=8, T_1=10 and T_2=6.

Reproduced with permission of the copyright owner. Further reproduction prohibited without permission.

$$
\begin{aligned}
AI1 &= CAI1 = AIR_1 * t \\
AI2 &= AIR_1 * Tw \\
AI3 &= AIR_1 * (Tw + T_1 - t) + AIR_2 * (t - T_1) \\
AI4 &= AIR_1 * (Tw + T_1 - t) + AIR_2 * T_2 \\
AI5 &= AIR_2 * (Tw + T_1 + T_2 - t) \\
CAI2 &= AIR_1 * T_1 + AIR_2 * (t - T_1) \\
CAI3 &= AIR_1 * T_1 + AIR_2 * T_2
\end{aligned}
\qquad \text{(Equation 4.4)}
$$

4.3.2.3 Case III. If Tw >= T_1, (T_w+T_1) < (T_1+T_2)

When AIR_1 equals 6, AIR_2 equals 2, T_w equals 10, T_1 equals 8, and T_2 equals 12, the data and AI (blue solid line) and CAI (pink solid line) curves are as shown in Fig.4.5. To calculate the CAI curve, the first phase of apoptosis had to be estimated using symmetry considerations. AI increased at a rate of AIR_1 until the beginning of the first change in slope was located. This point was the endpoint of T_1. Next, the first point where AI started decreasing was located. This point was the endpoint of T_w. Then a curve was calculated that decreased at the same rate as the initial increase (AIR_1). This symmetrical curve constituted the first phase of apoptosis (green dashed curve). Next the first phase curve was subtracted from the actual AI curve, resulting in the second phase curve (red dashed curve). The length of the first plateau is the difference between T_w and T_1. The length of the second plateau is the difference between (T_w+T_1) and (T_1+T_2). The first point where AI decreased is the endpoint of T_w and the second point of decreasing AI after the second plateau is the endpoint of T_2. The calculation was performed with Eq. 4.5.

Reproduced with permission of the copyright owner. Further reproduction prohibited without permission.

t																		AI	CAI	1st	2nd
1	6																	6	6	6	
2	6	6																12	12	12	
3	6	6	6															18	18	18	
4	6	6	6	6														24	24	24	
5	6	6	6	6	6													30	30	30	
6	6	6	6	6	6	6												36	36	36	0
7	6	6	6	6	6	6	6											42	42	42	0
8	6	6	6	6	6	6	6	6										48	48	48	0
9	6	6	6	6	6	6	6	6	2									50	50	48	2
10	6	6	6	6	6	6	6	6	2	2								52	52	48	4
11		6	6	6	6	6	6	6	2	2	2							48	54	42	6
12			6	6	6	6	6	6	2	2	2	2						44	56	36	8
13				6	6	6	6	6	2	2	2	2	2					40	58	30	10
14					6	6	6	6	2	2	2	2	2	2				36	60	24	12
15						6	6	6	2	2	2	2	2	2	2			32	62	18	14
16							6	6	2	2	2	2	2	2	2	2		28	64	12	16
17								6	2	2	2	2	2	2	2	2	2	24	66	6	18
18									2	2	2	2	2	2	2	2	2	20	68	0	20
19										2	2	2	2	2	2	2	2	20	70	0	20
20											2	2	2	2	2	2	2	20	72	0	20
21												2	2	2	2	2	2	18	72	0	18
22													2	2	2	2	2	16	72	0	16
23														2	2	2	2	14	72	0	14
24															2	2	2	12	72	0	12
25																2	2	10	72	0	10
26																	2	8	72	0	8
27																		6	72	0	6
28																		4	72		4
29																		2	72		2
30																		0	72		0

Figure 4.5 (A) The data for calculating AI and CAI curves for bi-phasic apoptosis when bi-phasic apoptosis curve if $T_w >= T_1$, $(T_w+T_1) < (T_1+T_2)$, a=6, b=2, T_w=10, T_1=8 and T_2=12.

Reproduced with permission of the copyright owner. Further reproduction prohibited without permission.

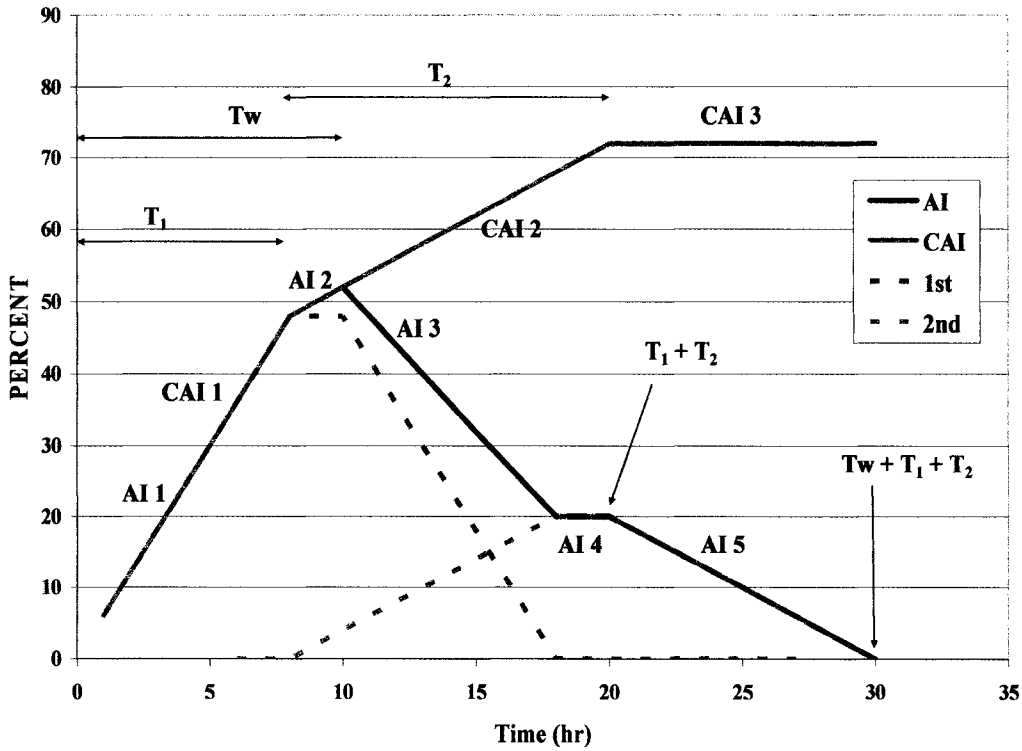

Figure 4.5 (B) The AI and CAI curves for bi-phasic apoptosis if $T_w >= T_1$, $(T_w+T_1) < (T_1+T_2)$, a=6, b=2, T_w=10, T_1=8 and T_2=12.

Reproduced with permission of the copyright owner. Further reproduction prohibited without permission.

$$
\begin{aligned}
AI1 &= CAI1 = AIR_1 * t \\
AI2 &= AIR_1 * T_1 + AIR_2 * (t - T_1) \\
AI3 &= AIR_1 * (Tw + T_1 - t) + AIR_2 * (t - T_1) \\
AI4 &= AIR_2 * Tw \\
AI5 &= AIR_2 * (Tw + T_1 + T_2 - t) \\
CAI2 &= AIR_1 * T_1 + AIR_2 * (t - T_1) \\
CAI3 &= AIR_1 * T_1 + AIR_2 * T_2
\end{aligned}
\qquad \text{(Equation 4.5)}
$$

4.3.2.4 Case IV. If Tw >= T_1, (T_w+T_1) >= (T_1+T_2)

When AIR_1 equals 6, AIR_2 equals 2, T_w equals 10, T_1 equals 8, and T_2 equals 6, the data and shapes of AI (blue solid line) and CAI (pink solid line) curves are as shown in Fig.4.6. To calculate the CAI, the first phase of apoptosis had to be estimated. The same procedure was used as with the previous case. However, there is no second plateau because (T_w+T_1) is greater than (T_1+T_2). The first point where AI decreased is the endpoint of T_w and the second rate-changing point is the endpoint of T_2. The third rate-changing point is the endpoint of sum (T_w+T_1). The second rate-changing point is not noticeable in the experimental data. Thus, the calculation has to be performed with possible cases for the estimation of T_2. The calculation was done using Eq. 4.6. The first phase of apoptosis is the green dashed curve and the second phase of apoptosis is the red dashed curve.

$$
\begin{aligned}
AI1 &= CAI1 = AIR_1 * t \\
AI2 &= AIR_1 * T_1 + AIR_2 * (t - T_1) \\
AI3 &= AIR_1 * (Tw + T_1 - t) + AIR_2 * (t - T_1) \\
AI4 &= AIR_1 * (Tw + T_1 - t) + AIR_2 * T_2 \\
AI5 &= AIR_2 * (Tw + T_1 + T_2 - t) \\
CAI2 &= AIR_1 * T_1 + AIR_2 * (t - T_1) \\
CAI3 &= AIR_1 * T_1 + AIR_2 * T_2
\end{aligned}
\qquad \text{(Equation 4.6)}
$$

Reproduced with permission of the copyright owner. Further reproduction prohibited without permission.

t															AI	CAI	1st	2nd
1	6														6	6	6	
2	6	6													12	12	12	
3	6	6	6												18	18	18	
4	6	6	6	6											24	24	24	
5	6	6	6	6	6										30	30	30	
6	6	6	6	6	6	6									36	36	36	
7	6	6	6	6	6	6	6								42	42	42	
8	6	6	6	6	6	6	6	6							48	48	48	0
9	6	6	6	6	6	6	6	6	2						50	50	48	2
10	6	6	6	6	6	6	6	6	2	2					52	52	48	4
11		6	6	6	6	6	6	6	2	2	2				48	54	42	6
12			6	6	6	6	6	6	2	2	2	2			44	56	36	8
13				6	6	6	6	6	2	2	2	2	2		40	58	30	10
14					6	6	6	6	2	2	2	2	2	2	36	60	24	12
15						6	6	6	2	2	2	2	2	2	30	60	18	12
16							6	6	2	2	2	2	2	2	24	60	12	12
17								6	2	2	2	2	2	2	18	60	6	12
18									2	2	2	2	2	2	12	60	0	12
19										2	2	2	2	2	10	60	0	10
20											2	2	2	2	8	60	0	8
21												2	2	2	6	60	0	6
22													2	2	4	60	0	4
23														2	2	60	0	2
24															0	60	0	0

Figure 4.6 (A) The data for calculating AI and CAI curves for bi-phasic apoptosis when bi-phasic apoptosis curve if $T_w >= T_1$, $(T_w+T_1) >= (T_1+T_2)$, a=6, b=2, T_w=10, T_1=8 and T_2=6.

Reproduced with permission of the copyright owner. Further reproduction prohibited without permission.

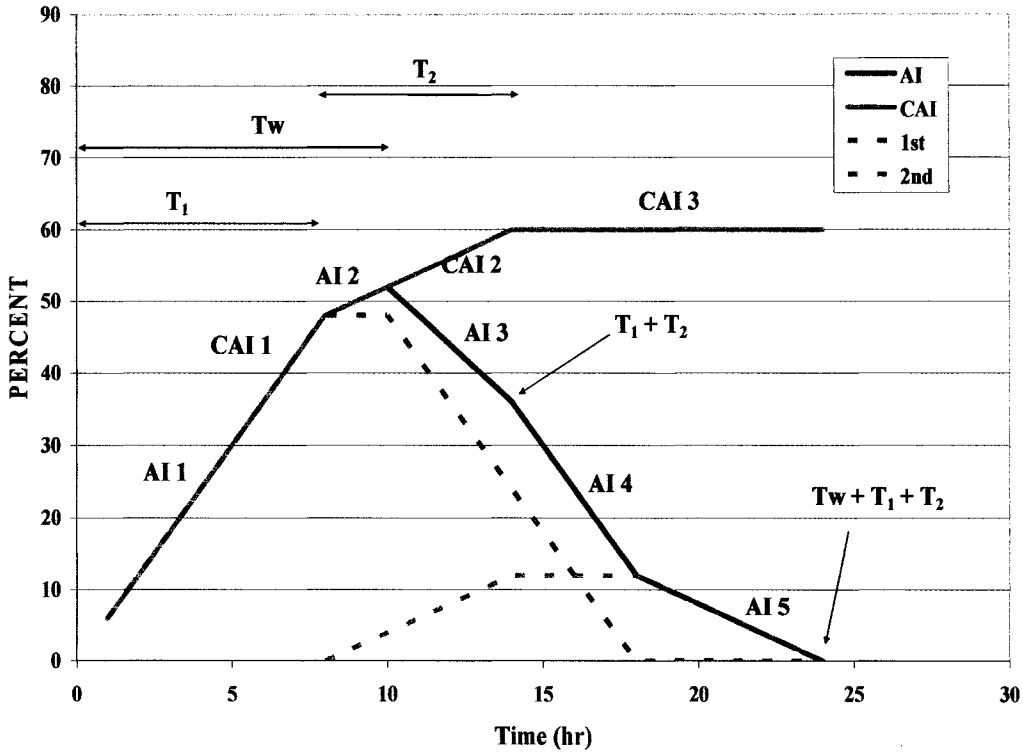

Figure 4.6 (B) The AI and CAI curves for bi-phasic apoptosis if $T_w >= T_1$, $(T_w+T_1) >= (T_1+T_2)$, a=6, b=2, T_w=10, T_1=8 and T_2=6.

Reproduced with permission of the copyright owner. Further reproduction prohibited without permission.

4.3.3 Multi-phasic apoptosis

The shape of AI curve in multi-phasic apoptosis depends on the gap between each phase. Multi-phasic apoptosis has (2n+1) coefficients with n phases, which are apoptotic induction rate (AIR_i, $i=1, 2, 3,$ etc), T_w, the length of phase time (T_i, $i=1, 2, 3,$ etc). When AIR_1 equals 6, AIR_2 equals 5, AIR_3 equals 4, AIR_4 equals 3, AIR_5 equals 2, T_w equals 5, and T_i equals 6, the shapes of AI (light blue solid line) and CAI (pink solid line) curves are as shown in Fig.4.7. To calculate the CAI curve, the first phase of apoptosis had to be estimated using symmetry considerations as previously described. AI increased at a rate of AIR_1 until the beginning of the first change in slope was located. This point was the endpoint of T_w or T_1. Next, the first point where AI started decreasing was located. This point was the endpoint of T_1 *or* T_w. Then a curve was calculated that decreased at the same rate as the initial increase (AIR_1). This symmetrical curve constituted the first phase of apoptosis (red curve). Next the first phase curve was subtracted from the actual AI curve, resulting in the 'AI-1st phase' curve (green dashed curve). The same procedure was repeated for getting the second phase curve (dark blue curve). The rest became the 'AI-1st-2nd phase' curve (dark red curve). These procedures were performed until the shape of deduced curve became symmetrical. Thus, when 'AI-1st phase' curve was analyzed to obtain the second phase curve, if there were no more phases, the remaining 'AI-1st-2nd phase' curve would have the characteristics of a single phase curve with a peak or plateau and a symmetrical shape (Fig 4.1 and Fig 4.2).

Reproduced with permission of the copyright owner. Further reproduction prohibited without permission.

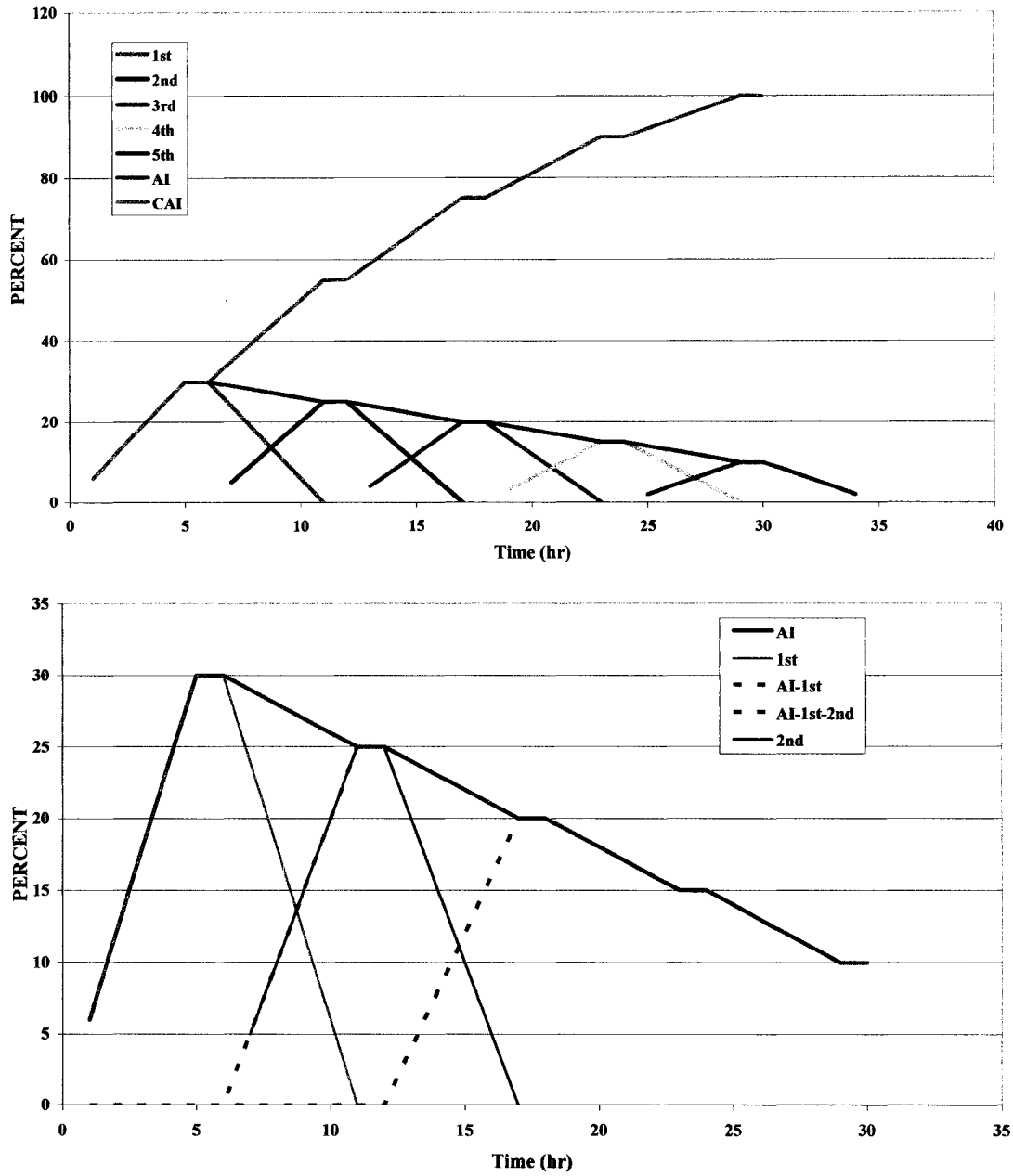

Figure 4.7 The AI and CAI curves for multi-phasic apoptosis. Top: multi-phasic apoptosis curve, AIR_1=6, AIR_2=5, AIR_3=4, AIR_4=3, AIR_5=2, T_w=5, and T_i=6. Bottom: multi-phasic apoptosis curve for calculation step.

Reproduced with permission of the copyright owner. Further reproduction prohibited without permission.

4.3.4 The calculation of CAI by AI from hyperthermia-induced apoptosis

For the analysis of CAI, time-lapse AI data are required. I obtained data from experiments using two different doses of hyperthermia. Dose-dependent data are essential for deducing the CAI because a single dose does not give enough information if CAI is less than 100 percent.

4.3.4.1 45.0 ℃, 15 min time-lapse apoptosis

HL-60 cells were treated with 45.0 °C for 15 min, then incubated at 37 °C until they were fixed and processed for TUNEL analysis. Time-lapse AI data (dark blue rhombus) are shown in Fig. 4.8 (top). When each time-point AI was corrected for unheated control AI, the resulting AI curve was obtained (pink solid line). AI increased at a rate of 4.5 % /hr up to 3 hr, maintained 13 - 14 % for 4 hr, and then started to decrease. It took 14 hrs for AI to decrease from 10 % to 5.5 %. In order to calculate CAI, the first phase curve (green dashed line) has to be determined. The first phase is composed of increasing, plateau and decreasing portions. The increasing portion is 4.5 % /hr for 3 hr, the plateau lasted 4 hrs, and the decreasing portion is linearly symmetrical with the increasing portion. The starting and ending points of the plateau are the endpoint of T_w or T_1. The calculation was done for two cases: in the first case, T_w equals 7, T_1 equals 3 and AIR_1 equals 4.5 % /hr, and in the second case, T_w equals 3, T_1 equals 7 and AIR_1 equals 4.5 % /hr. After the first phase curve was determined, the first phase curve was subtracted from the AI curve (Fig.4.8 top for first case calculation). The rest became the 'AI-1st phase' curve (green solid line). The same procedure was repeated for getting the second

Reproduced with permission of the copyright owner. Further reproduction prohibited without permission.

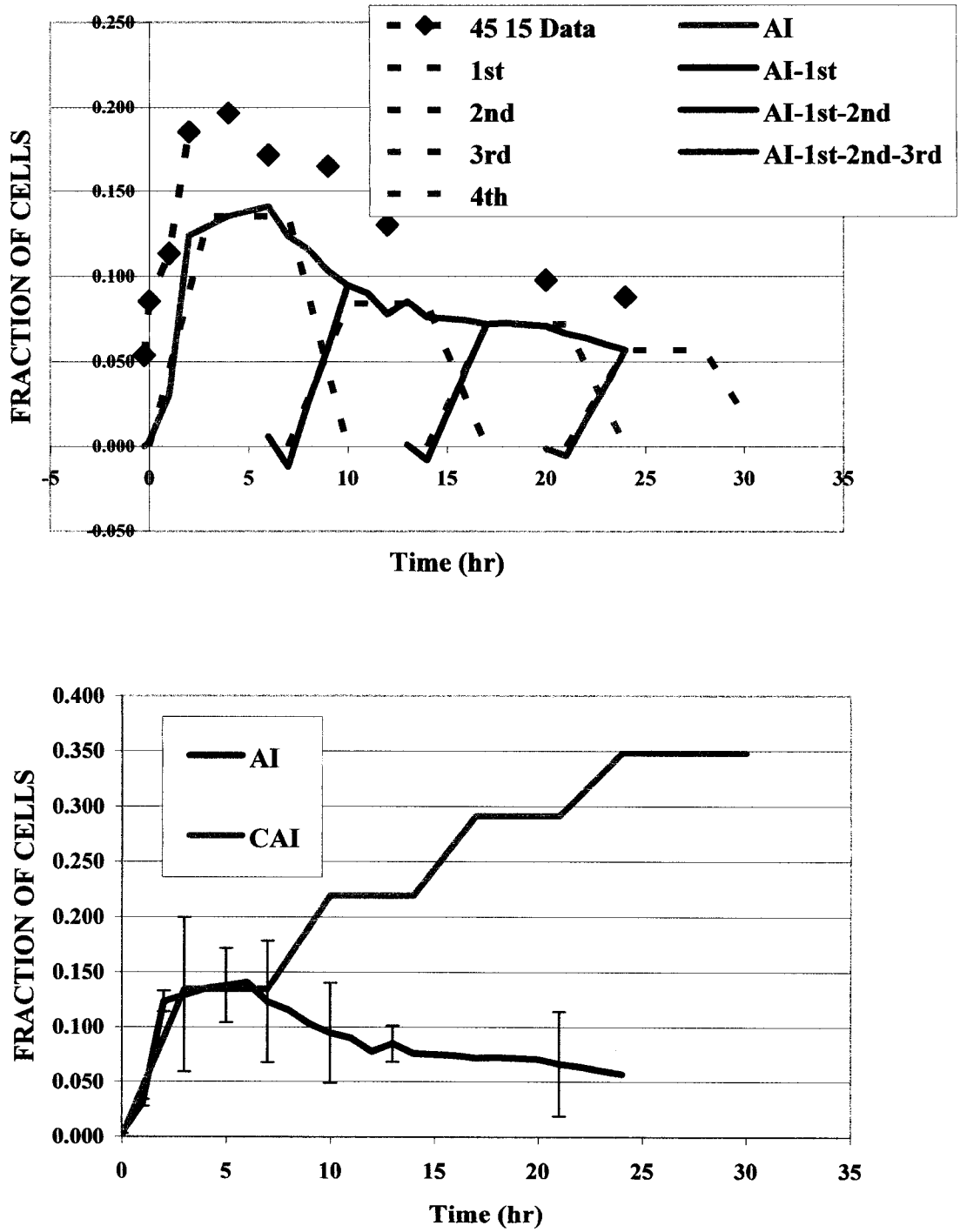

Figure 4.8 The AI and CAI curves for apoptosis from a 45.0 °C, 15 min heat shock. Top: AI data and four phases of apoptosis curves. Bottom: AI and CAI results. The experiments were performed two or more times.

Reproduced with permission of the copyright owner. Further reproduction prohibited without permission.

phase curve (light blue dashed line). The rest became the 'AI-1st-2nd phase' curve (light blue solid line). These procedures were performed until the shape of the subtracted curve became symmetrical. CAI (pink solid line) was calculated based on the model and is shown in Fig.4.8 (bottom). The heat shock for 45.0 °C, 15 min produced 34.8 % cumulated apoptosis during the 24 hr post-culture period. The model predicted four apoptotic phases: first, T_w equals 7, T_1 equals 3 and AIR_1 equals 4.5 % /hr; second, T_w equals 7, T_2 equals 3 and AIR_2 equals 2.8 % /hr; third, T_w equals 7, T_3 equals 3 and AIR_3 equals 2.4 % /hr; and fourth, T_w equals 7, T_4 equals 3 and AIR_4 equals 1.9 % /hr.

4.3.4.2 45.0 ℃, 30 min time-lapse apoptosis

HL-60 cells were treated with 45.0 °C for 30 min, then incubated at 37 °C until they were fixed and processed for TUNEL analysis. Time-lapse AI data (dark blue rhombus) are shown in Fig.4.9 (top). When each time-point AI was corrected for unheated control AI, the resulting AI curve was obtained (orange solid line). AI increased at a rate of 9.9 % /hr up to 4 hr, maintained 39 - 41 % for 6 hr, and then started to decrease. It took 14 hrs for AI to decrease from 39 % to 27.5 %. In order to calculate CAI, the first phase curve (pink dashed line) has to be determined. The first phase is composed of increasing, plateau and decreasing portions. The increasing portion is 9.9 % /hr for 4 hr, the plateau lasted 6 hr and the decreasing portion is linearly symmetrical with the increasing portion. The starting and ending points of the plateau are the endpoint of T_w or T_1. The calculation was done for two cases: in the first case, T_w equals 10, T_1 equals 4 and AIR_1 equals 9.9 % /hr; in the second case, T_w equals 4, T_1 equals 10 and AIR_1 equals 9.9 %/hr. After the first phase was determined, the first phase curve was subtracted from the AI curve (Fig.4.9 top for first case calculation). The rest became the 'AI-1st phase'

Reproduced with permission of the copyright owner. Further reproduction prohibited without permission.

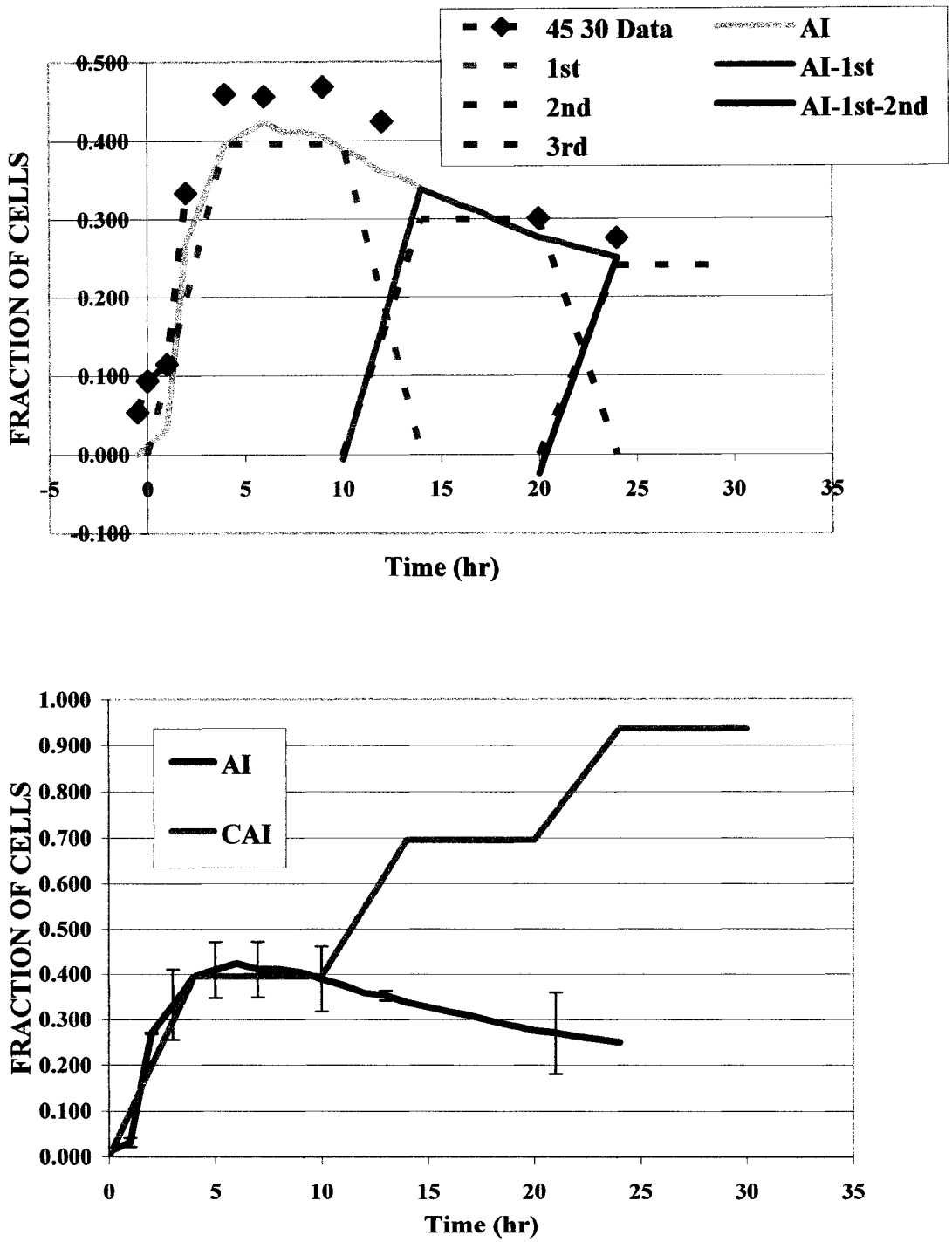

Figure 4.9 The AI and CAI curves for apoptosis from a 45.0 °C, 30 min heat shock. Top: AI data and three phases of apoptosis curves. Bottom: AI and CAI results. The experiments were performed two or more times.

Reproduced with permission of the copyright owner. Further reproduction prohibited without permission.

curve (pink solid line). The same procedure was repeated for getting the second phase curve (light blue dashed line). The rest became the 'AI-1st-2nd phase' curve (light blue solid line). These procedures were performed until the shape of subtracted curve became symmetrical. CAI (pink solid line) was calculated based on the model and shown in Fig.4.9 (bottom). The second case is incorrect because CAI goes over 100 %. The heat shock for 45.0 °C, 30 min produced 93.6 % cumulated apoptosis during the 24 hr post-culture. The model predicted three apoptotic phases: first, T_w equals 10, T_1 equals 4 and AIR_1 equals 9.9 % /hr; second, T_w equals 10, T_2 equals 4 and AIR_2 equals 7.5 % /hr; and third, T_w equals 10, T_3 equals 4 and AIR_3 equals 6.0 % /hr.

4.4 Discussion

Apoptosis is a process of cell death consisting of various cellular activities (caspase activation, annexin V flip-flop, DNA fragmentation, loss of membrane potential, etc.). Each phenomenon is only active and detected by a specific assay for a specific time period, called the time window (T_w). When apoptotic cells pass the time window of the assay, they are no longer detected as apoptotic cells and thus contribute to an underestimation of apoptosis. The existence of a time window in measuring AI is a problem for understanding the kinetics of apoptosis. However, this time-window problem could become an advantage for assessing CAI. I developed a model which can estimate CAI with time-lapse AI data based on the following characteristics of the time window: First, cells which start apoptosis early exit the time-window early ('first in, first out'); second, the time-window is constant for a given cell type with a given inducer of apoptosis; third, the apoptotic induction rate (AIR_i) is equal to the rate of movement out

Reproduced with permission of the copyright owner. Further reproduction prohibited without permission.

of the time window. Thus, it should have a symmetrical shape for each phase of apoptosis. This analysis is very similar to the concept of Fraction of Labeled Mitoses curves (6) where cells move into and out of a mitotic window, but in this case they are apoptotic windows and multiple phases can exist.

A heat shock for 15 min at 45.0 °C produced 34.8 % cumulative apoptotic cells during 24 hr post-culture. Analysis by the model predicted four apoptotic phases: first, T_w equals 7, T_1 equals 3 and AIR_1 equals 4.5 % /hr; second, T_w equals 7, T_2 equals 3 and AIR_2 equals 2.8 % /hr; third, T_w equals 7, T_3 equals 3 and AIR_3 equals 2.4 % /hr; and fourth, T_w equals 7, T_4 equals 3 and AIR_4 equals 1.9 % /hr. A heat shock for 30 min at 45.0 °C produced 93.6 % cumulative apoptotic cells during 24 hr post-culture. The model predicted three apoptotic phases: first, T_w equals 10, T_1 equals 4 and AIR_1 equals 9.9 % /hr; second, T_w equals 10, T_2 equals 4 and AIR_2 equals 7.5 % /hr; and third, T_w equals 10, T_3 equals 4 and AIR_3 equals 6.0 % /hr. When heating time was increased from 15 min to 30 min, CAI increased 2.69 times (34.8 to 93.6 %), T_w increased from 7 hr to 10 hr and T_i increased from 3 hr to 4 hr.

The CAI estimation model revealed important new information about the induction of apoptosis by hyperthermia. When the heat dose was increased from 15 to 30 min, CAI, T_w and T_i were also increased. The increase in CAI and T_i with a larger heat dose resulted in the production of more apoptotic cells and an increase in T_w means that the substrate for the assay existed longer for a greater heat shock.

The analysis also demonstrated that apoptosis developed in several phases with different induction rates, and the AIR_i decreased as the phase number increased. Apoptotic cells in the first phase could be a subpopulation of cells sensitive to the

Reproduced with permission of the copyright owner. Further reproduction prohibited without permission.

specific treatment. For example, S phase cells are sensitive to topoisomerase inhibitors (e.g., camptothecin and etoposide) as well as hyperthermia (2). After the sensitive population underwent apoptosis, the next phase of apoptotic cells could be dependent on several factors, including when damaged cells passed a cell cycle checkpoint after a single treatment (e.g., irradiation with post-culture) or when healthy cells progressed into a sensitive cell cycle phase during continuous treatment (e.g., continuous culture with drugs). Thus, there is a gap between the phases, and the CAI curve increased step-wise instead of continuously. Both continuously increasing and step-wise increasing CAI curves have been reported with FLICA experiments (10).

CAI could also estimate the kinetics of disintegration of apoptotic cells, but the starting point of disintegration could not be determined with our data. Previous approaches for calculating the disintegration of apoptotic cells were done in non-cycling cell populations (8). If one time-window is greater and includes the other time-window, that time-window could include part of the cumulative apoptosis from the other time-window. For example, the loss of membrane integrity is a very late step (3,4,5) and could happen just before disintegration of apoptotic cells. Thus, the time-window for membrane integrity measured by dye exclusion is greater than the time-window for other assays such as TUNEL. In the annexin V assay, control population showed as annexin V (-)/ PI (-) population. Once apoptosis started, early apoptotic population showed as annexin V (+)/ PI (-) and late apoptotic population showed as annexin V (+)/ PI (+). Annexin V (-)/ PI (+) population is the endpoint of this assay. When apoptosis (-)/ PI (+) population in annexin V assay and FLICA assay is measured and plotted, the end point of time-window for apoptosis (-)/ PI (+) population could become a starting point of disintegration.

Reproduced with permission of the copyright owner. Further reproduction prohibited without permission.

Cells treated continuously with 0.15 μM camptothecin and using FLICA had a step-wise increase in the apoptosis (-)/PI (+) population (10). Previously it was reported that the time-window for DNA fragmentation (TUNEL) is not much different than the time-window for the activation of caspases (FLICA) (1). Thus, when the apoptosis (-)/PI (+) population in FLICA assay was analyzed with our model, T_1 was 12 hr and AIR_1 was 5.0 % /hr in the first phase, and T_2 was 12 hr and AIR_2 was 2.5 % /hr in the second phase. The T_w was greater than 48 hr because the graph increased step-wise without a decreasing point. Thus, disintegration did not take place up to 48 hr. This analysis gives 90.0 % CAI. This calculation agrees with their published results using continuous FLICA, which could block apoptosis progression at the caspase activation step and stop apoptosis before the cells disintegrated.

When CAI is compared with clonogenic survival, it should give a much better agreement than comparing AI with clonogenic survival. The existence of non-apoptotic death, or necrotic death by insult could be inferred by a disagreement of CAI and clonogenic survival. This model could also be applied to different types of time-lapse data for calculation of cumulative results. For example, when a particular cyclin is measured with flow cytometry, the cumulative number of cells which express cyclin could be calculated. This calculation could provide information on the fraction of cycling cells in the population. Moreover, the model could analyze how long a specific protein is active or functional and the cumulative amount of protein expression. The average life span of the protein could be calculated because the time-window of this cyclin represents lifetime of this protein. Finally, this model is not limited to certain cell lines and assays,

Reproduced with permission of the copyright owner. Further reproduction prohibited without permission.

does not need special culture treatment, and does not affect the assays, which other assays could do.

4.5 Appendix

The following is a brief description of the 'CAI estimation with AI deduction model' procedure.

1) Determine the first phase curve
   a) Calculate the increasing portion and assume a symmetrical decreasing portion
   b) Find out the starting and ending points of plateau
2) Execute the calculation and analyze with model
   a) Perform the analysis with two cases
      i) T_w=a and T_l=b
      ii) T_w=b and T_l=a
   b) Subtract the first phase curve from the AI curve data
      i) If 'AI-1st phase' curve is symmetrical, this curve is 2nd phase curve
      ii) If 'AI-1st phase' curve is not symmetrical, repeat the procedure for analyzing 2nd phase curve
3) Calculate CAI and present the data

Reproduced with permission of the copyright owner. Further reproduction prohibited without permission.

Reference List

1. Bedner E, Smolewski P, Amstad P, Darzynkiewicz Z: Activation of caspases measured in situ by binding of fluorochrome- labeled inhibitors of caspases (FLICA): correlation with DNA fragmentation. Exp Cell Res 259:308-313, 2000.

2. Dewey WC, Hopwood LE, Sapareto SA, Gerweck LE: Cellular responses to combinations of hyperthermia and radiation. Radiology 123:463-474, 1977.

3. Endlich B, Radford IR, Forrester HB, Dewey WC: Computerized video time-lapse microscopy studies of ionizing radiation- induced rapid-interphase and mitosis-related apoptosis in lymphoid cells. Radiat Res 153:36-48, 2000.

4. Forrester HB, Albright N, Dewey WC, Ling CC: Computerized video time-lapse analysis of apoptosis of REC:Myc cells X- irradiated in different phases of the cell cycle [In Process Citation]. Radiat Res 154:625-639, 2000.

5. Forrester HB, Vidair CA, Albright N, Ling CC, Dewey WC: Using computerized video time lapse for quantifying cell death of X- irradiated rat embryo cells transfected with c-myc or c-Ha-ras. Cancer Res 59:931-939, 1999.

6. Hall EJ: Radiobiology for the Radiobiologist. 4th Edition. J.B. Lippencott Co., Philadelphia, PA, 1994.

7. Porter AG, Ng P, Jänicke RU: Death substrates come alive. BioEssays 19:501-507, 1997.

8. Prieto A, Diaz D, Barcenilla H, Garcia-Suarez J, Reyes E, Monserrat J, San Antonio E, Melero D, De La HA, Orfao A, Alvarez-Mon M: Apoptotic rate: A new indicator for the quantification of the incidence of apoptosis in cell cultures. Cytometry 48:185-193, 2002.

9. Smolewski P, Bedner E, Du L, Hsieh TC, Wu JM, Phelps DJ, Darzynkiewicz Z: Detection of caspases activation by fluorochrome-labeled inhibitors: Multiparameter analysis by laser scanning cytometry. Cytometry 44:73-82, 2001.

10. Smolewski P, Grabarek J, Lee BW, Johnson GL, Darzynkiewicz Z: Kinetics of HL-60 cell entry to apoptosis during treatment with TNF- alpha or camptothecin assayed by the stathmo-apoptosis method. Cytometry 47:143-149, 2002.

11. Smolewski P, Grabarek J, Phelps DJ, Darzynkiewicz Z: Stathmo-apoptosis: arresting apoptosis by fluorochrome-labeled inhibitor of caspases. Int J Oncol 19:657-663, 2001.

Reproduced with permission of the copyright owner. Further reproduction prohibited without permission.

CHAPTER 5

ANALYSIS OF CELL CYCLE DEPENDENT APOPTOSIS AND CELL CYCLE BLOCKS IN HL-60 CELLS AT VARIOUS TIMES AFTER HYPERTHERMIA

5.1 Introduction

Flow cytometry methods can give quantitative information regarding cell cycle-dependent apoptosis and help achieve an understanding of apoptotic kinetics at the level of individual cells. Since many therapeutic agents also cause cell cycle blocks, it is important to try to separate out cell cycle perturbations from apoptosis in specific phases of the cell cycle.

However, because apoptosis is a kinetic event, apoptotic index (AI) at each time-point can be inaccurate and underestimated by the disintegration of apoptotic cells and the specific time-window for the specific assays (e.g., caspases, TdT-mediated dUTP-biotin nick end-labeling or terminal dUTP nick-end labeling (TUNEL), annexin V etc). The cell type and apoptotic inducer also make the length of the time-window variable. Once the individual cells pass each specific time-window of the assay they are not counted as apoptotic cells until they finally disintegrate and are removed from the

Reproduced with permission of the copyright owner. Further reproduction prohibited without permission.

population. This underestimation of apoptosis may lead to problems in understanding the effects of therapeutic agents.

A quantitative and mathematical analysis of the relationship between cell cycle specific apoptosis and cell cycle progression has been developed in previous chapters (Chapter 2). The *apoptotic quotient calculation, CAI (cumulative apoptotic index) estimation model, and cell cycle progression model* could solve this problem and result in a more accurate analysis. Such an analysis may be useful in studies exploring the cell cycle response to therapeutic drugs over an extended period of time. Cancer cells frequently abrogate cell cycle checkpoints while normal cells activate their checkpoints in response to DNA damaging agents. The differences between normal and cancer cells to a therapeutic treatment could be better understood with the new models proposed in this dissertation.

Cells that are heated to a few degrees above physiological temperatures (hyperthermia) undergo apoptosis (1,5,6,7,8,9,10,11,12,13,14,15,16,18,19) and become sensitive to radiotherapy and many antitumor agents. Radiotherapy in combination with hyperthermia or antitumor agents can improve therapy, so the cellular response to hyperthermia is of clinical interest. Induction of apoptosis by hyperthermia occurs very rapidly. Apoptosis peaks in mastocytoma cultures at between 2 and 4 h, and then decreases as the apoptotic bodies undergo secondary necrosis and are degraded to debris. By 24 h, apoptotic counts have returned to levels approaching control values (8). While the lag period (time between completion of heating and onset of apoptosis) varies among different cell types, apoptotic inducer and detection methods used, once underway, the kinetics of the apoptotic process itself appears to be similar.

Reproduced with permission of the copyright owner. Further reproduction prohibited without permission.

In this study, the cell progression model and CAI estimation model were tested in two different circumstances: (i) hyperthermia-induced apoptosis with 45.0 °C, 15 min heat shock in HL-60 cells; and (ii) hyperthermia-induced apoptosis with 45.0 °C, 30 min heat shock in HL-60 cells. The number of apoptotic cells after heat shock was measured by the TUNEL assay and propidium iodide labeling using flow cytometry.

5.2 Materials and Methods

The general information for the experiment was explained in Chapter 2 Materials and Methods. Detailed and specific explanations are provided in figure and table legends.

5.3 Results

5.3.1 Hyperthermia-induced apoptosis with 45.0 °C 15 min heat shock

My goal in this set of experiments was to analyze the changes of cell cycle progression, arrest and apoptosis after a 45.0 °C 15 min heat shock. HL-60 cells were heated at 45.0° C for 15 min and then incubated at 37 °C up to 24 hr to allow apoptosis to develop. The presence of apoptotic cells was measured with the TUNEL method. The DNA histograms from an experiment which illustrate cell cycle delays after heating for 15 min at 45.0° C are shown in Figure 5.1. Cell cycle arrest in G_2/M phase started to appear at 4 hr and was maintained up to 12 hr. The dual-parameter histograms from an experiment which illustrate the apoptotic population for different times after heating are shown in Figure 5.2. An apoptotic population was evident at 1 hr after heating and was

Reproduced with permission of the copyright owner. Further reproduction prohibited without permission.

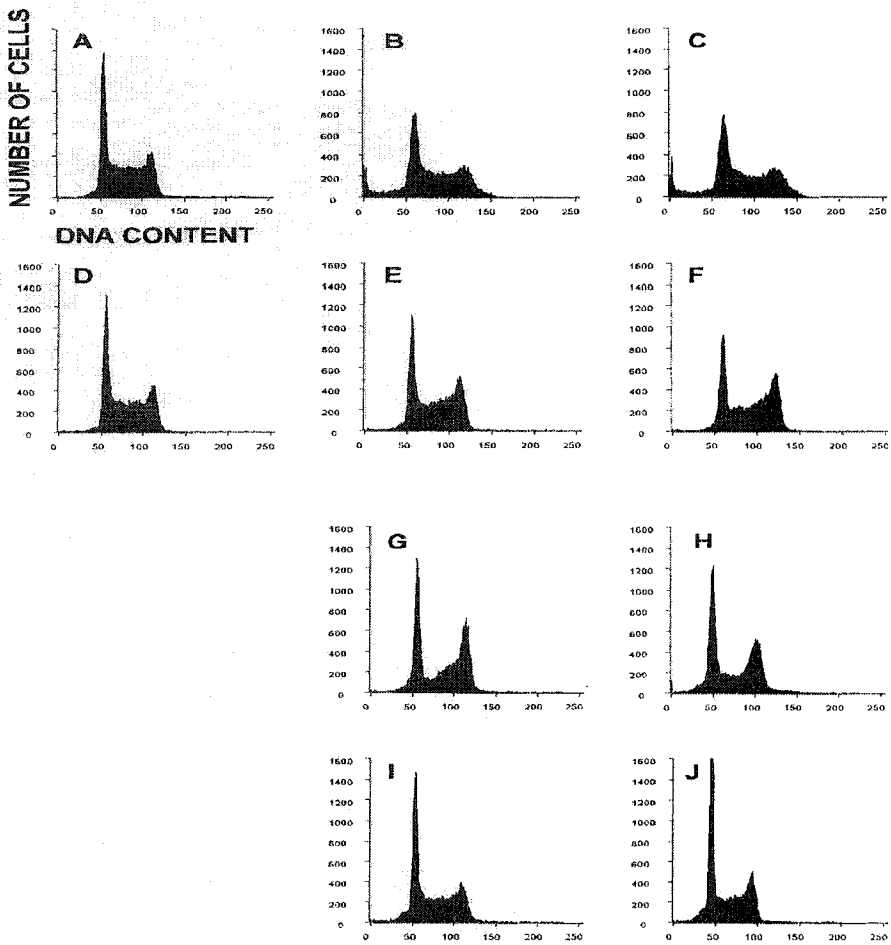

Figure 5.1 Cell cycle distributions for control and heated HL-60 cells at 45.0° C for 15 min. A: control cells ; B: 0 hr at 37° C after heat ; C: 1 hr ; D: 2 hr ; E: 4 hr ; F: 6 hr ; G: 9 hr ; H: 12 hr ; I: 20 hr ; J: 24 hr.

Reproduced with permission of the copyright owner. Further reproduction prohibited without permission.

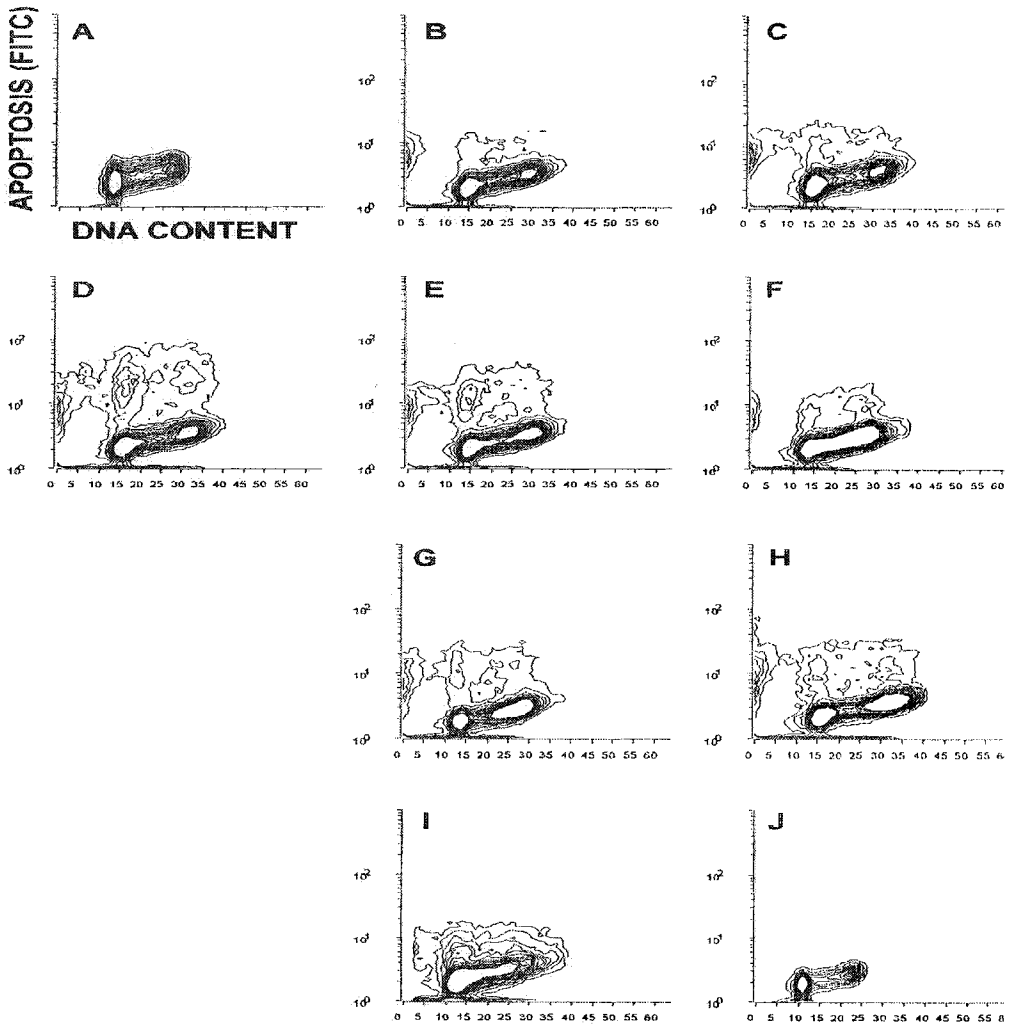

Figure 5.2 Dual parameter histograms showing apoptosis (FITC) and DNA content for control and heated HL-60 cells at 45.0° C for 15 min. A: control cells ; B: 0 hr at 37° C after heat ; C: 1 hr ; D: 2 hr ; E: 4 hr ; F: 6 hr ; G: 9 hr ; H: 12 hr ; I: 20 hr ; J: 24 hr.

Reproduced with permission of the copyright owner. Further reproduction prohibited without permission.

maintained up to 20 hr. Small numbers of apoptotic cells are not shown in the dual-parameter histograms because the contour levels exclude them. It is apparent that the heat treatments caused substantial changes in the cell cycle distribution as well as in the apoptosis index with time after heating. The number of apoptotic cells in each sample was derived from the dual parameter histograms shown in Fig. 5.2. The total number of cells for control and treated samples at each time-point after the treatment is shown in Fig. 5.3.

The number of apoptotic cells were determined using the Cicero data acquisition and display system software installed in a Coulter EPICS V cell sorter (Coulter, Miami, FL) as well as Multi-2D® and Multicycle® (Phoenix Flow Systems, San Diego, CA) software. To quantitatively describe the percentage of cells in each phase of the cell cycle for each time point after the heat treatment shown in Fig. 5.1 and Fig. 5.2, the DNA histograms were analyzed with Multicycle® software. Because the DNA histograms include the apoptotic population, however, they cannot be analyzed directly to determine the fraction of cells in each cell cycle phase for the non-apoptotic cells. To quantitatively describe the cell cycle distribution of the non-apoptotic cells, a gate was drawn around the non-apoptotic population using Multi-2D® and the data within the gate were saved as a single parameter DNA histogram which could then be analyzed by Multicycle®. This analysis then gave the cell cycle distributions of the surviving (non-apoptotic) cells.

The number of non-apoptotic cells in each phase of the cell cycle for each culture time point are shown in Figure 5.4. The number of cells in G_1 phase decreased as time progressed up to 6 hr, increased up to 12 hr, and then remained nearly constant. The

Reproduced with permission of the copyright owner. Further reproduction prohibited without permission.

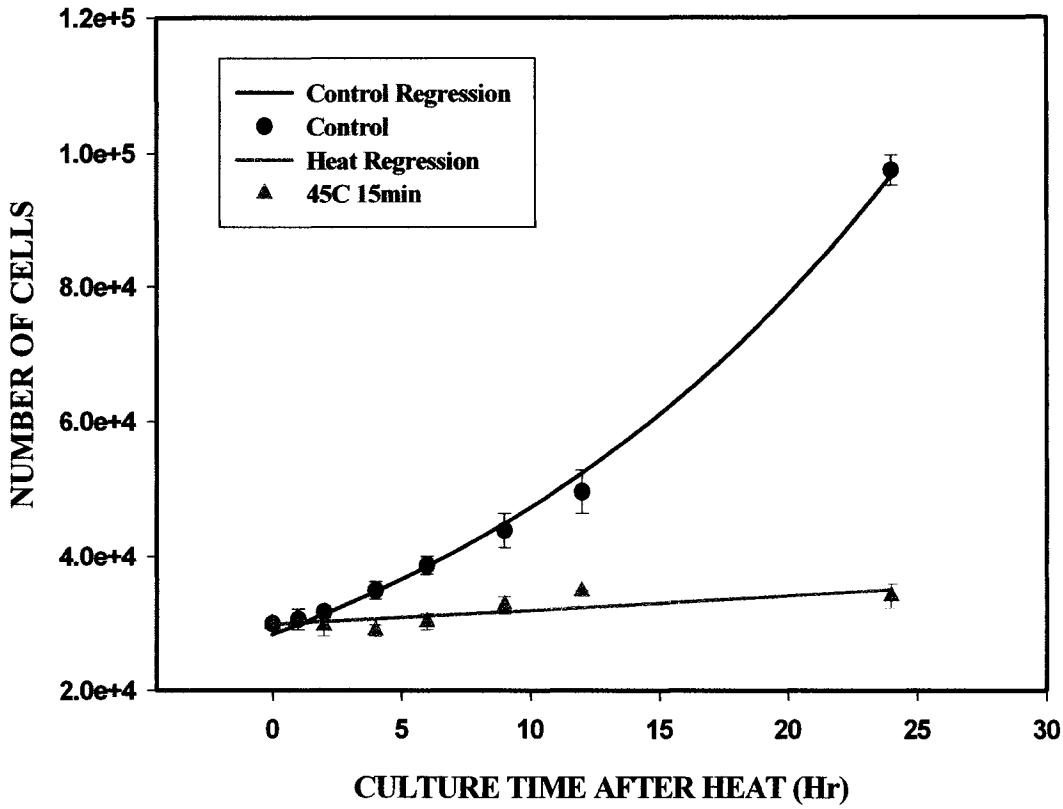

Figure 5.3 The number of HL-60 cells as a function of time after 45.0° C, 15 min heat shock. Cells are counted at sample collection time. The dots represent measured values with error bars representing ± one standard error. The line represents the result of nonlinear regression from the exponential equation N_t = 28363*exp (0.0511*time) for control cells and N_t = 29925*exp (0.0066*time) for heat-treated cells. This regression had a standard error of estimate equal to 3637 and 1660 cells for each samples.

Reproduced with permission of the copyright owner. Further reproduction prohibited without permission.

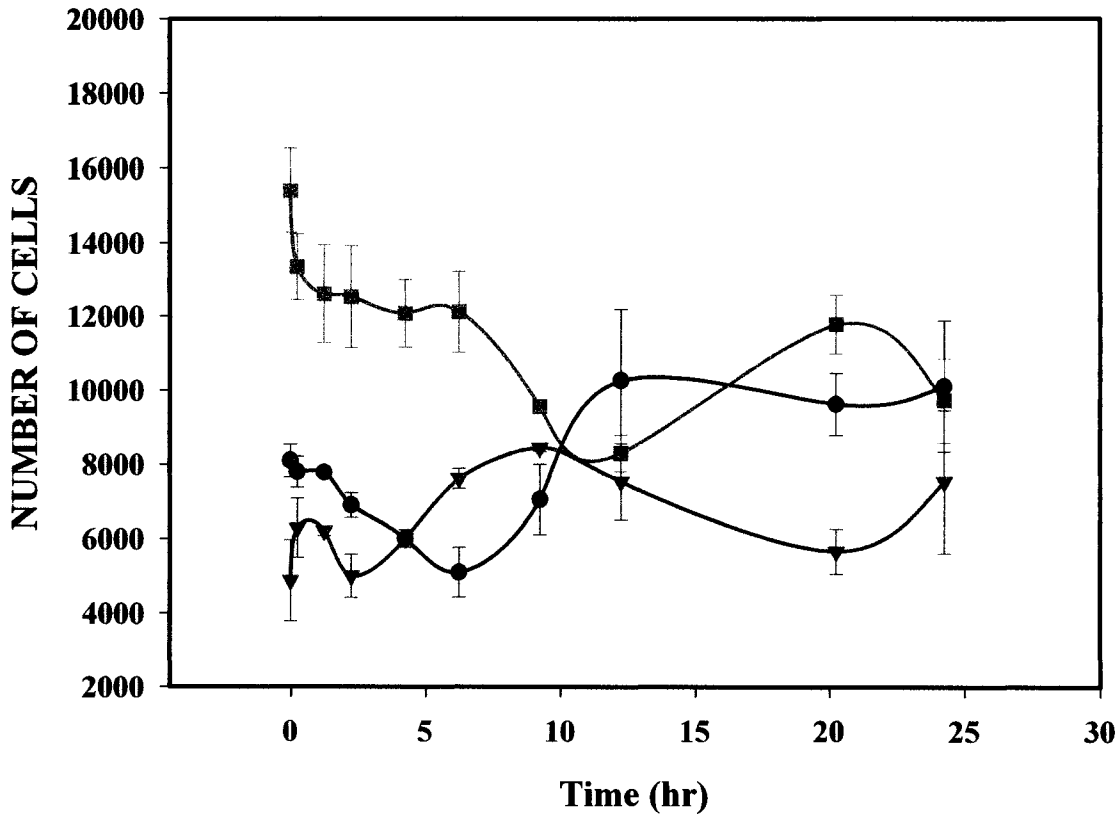

Figure 5.4 The number of non-apoptotic HL-60 cells in each cell cycle phase before and at various times after giving a 45.0° C, 15 min heat shock. Control: untreated cells. The error bars represent the standard error of the mean from at least two experiments. (•): G_1 phase cells; (■): S phase cells; (▲): G_2/M phase cells.

Reproduced with permission of the copyright owner. Further reproduction prohibited without permission.

numbers of cells in G_2/M phase increased just after heat shock and remained nearly constant to 4 hr, increased up to 9 hr, decreased at 20 hr and then increased again. The numbers of cells in S phase decreased just after heat shock and remained nearly constant up to 6 hr, decreased up to 12 hr, and increased at 20 hr and then decreased. From these results, it appears that the main provider for apoptotic population are G_1 and S phase at first part of culture between 0 hr and 12 hr, G_1 and G_2/M phase up to 20 hr. This interpretation is complicated by the fact that there are also apparent cell cycle blocks, especially in G_2/M phase.

The number of apoptotic cells at various times after heating at 45.0 °C for 15 min and calculated CAI results are shown in Fig. 5.5. The apoptotic population reached a peak around 4 hr, decreased up to 12 hr, remained nearly constant to 20 hr and then decreased. The calculated CAI by the *CAI estimation model* described in Chapter 4 was 34.8 %. The CAI graph showed four plateaus at 13.5 %, 21.9 %, 29.1 % and 34.8 %, which represented four phases of apoptosis induction. Analysis by the model calculated four apoptotic phases: first, T_w equals 7, T_1 equals 3 and AIR_1 equals 4.5 % /hr; second, T_w equals 7, T_2 equals 3 and AIR_2 equals 2.8 % /hr; third, T_w equals 7, T_3 equals 3 and AIR_3 equals 2.4 % /hr; and fourth, T_w equals 7, T_4 equals 3 and AIR_4 equals 1.9 % /hr.

To explain these results more completely, the *cell cycle progression model* described in Chapter 2 was used to analyze the data. The *Efflux Coefficient (EC)* was calculated by Eq. 2.11 and 2.12, the *Apoptotic Index (API)* was calculated by Eq. 2.15, and cell cycle distributions were calculated by Multicycle® software. These results along with comments are shown in Table 5.1.

Reproduced with permission of the copyright owner. Further reproduction prohibited without permission.

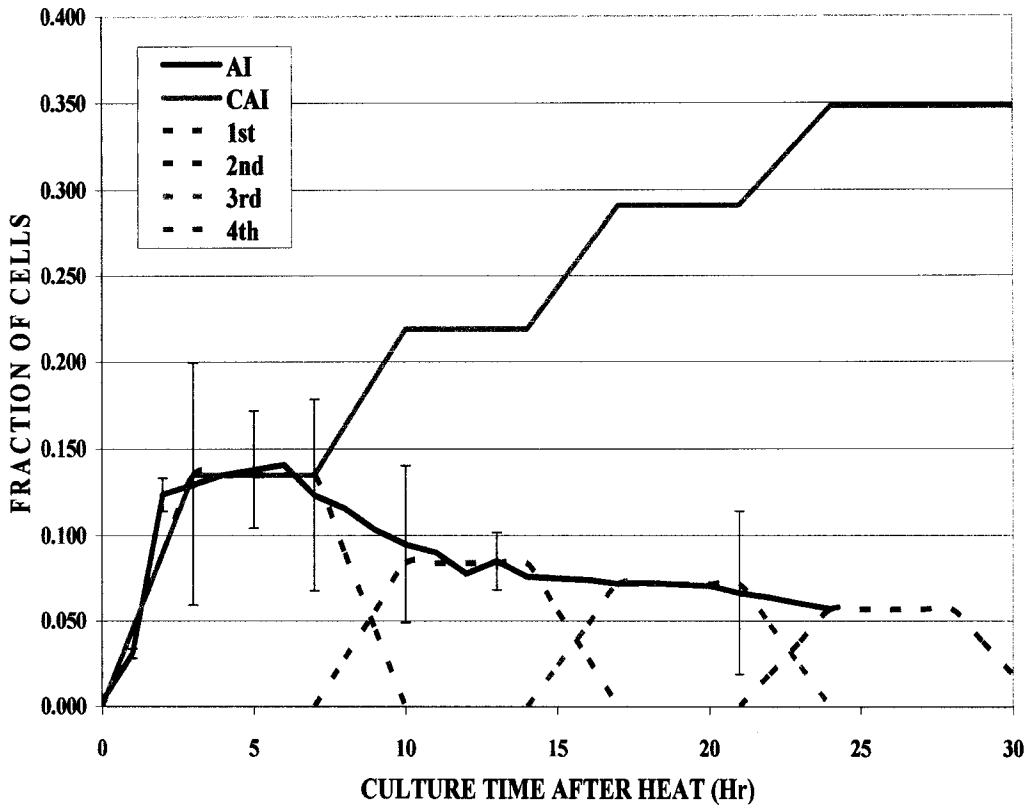

Figure 5.5 The AI of HL-60 at various times at 37° C after heating at 45.0° C for 15 min. AI results represent the mean values and standard error of the mean (SEM) from at least 2 independent experiments. The actual data points in AI curve are the point with error bars. The line between them was interpolated.

Reproduced with permission of the copyright owner. Further reproduction prohibited without permission.

Reproduced with permission of the copyright owner. Further reproduction prohibited without permission.

Table 5.1 The effects of 45.0° C, 15 min heat shock on the cell cycle distribution and apoptosis, including an analysis of the efflux coefficient and apoptosis probability index (API) as described. The data in table are measured directly by the experiments or calculated indirectly by interpolation.

		Control	45.0° C, 15 min Heat-treated sample						
Time (hr)		0	2	4	6	8	10	12	14
Cell Numbers		29926	30323	30726	31134	31548	31967	32392	32822
Cumulative Apoptotic Index		0	2729	4148	4203	5142	7001	7094	7188
Non-Apoptotic Cells	G_1	8394	8061	6377	5814	6465	7798	9694	10894
	S	15798	13605	13439	13141	11369	9019	8047	8208
	G_2/M	5734	5928	6762	7976	8572	8149	7557	6532
Number of Apoptotic Cells at each time point	G_1	-	34	320	18	309	568	30	33
	S	-	250	234	13	371	816	37	30
	G_2/M	-	2445	865	24	259	474	26	31
Apoptotic Quotient (ApQ)	α_1	-	0.004	0.040	0.003	0.053	0.088	0.004	0.003
	β_1	-	0.016	0.017	0.001	0.028	0.072	0.004	0.004
	γ_1	-	0.426	0.146	0.003	0.033	0.055	0.003	0.004
Cell Progression (α_2, β_2, γ_2)	α_2	-	0.130	0.269	0.213	0.00	0.00	0.00	0.00
	β_2	-	0.192	0.155	0.122	0.097	0.041	0.00	0.00
	γ_2	-	0.069	0.068	0.060	0.052	0.049	0.052	0.057
Apoptotic Probability Index (API)		-	0.091	0.051	0.002	0.035	0.070	0.004	0.004
Interpretation of Efflux Coefficient (EC)	G_1	-	NB	NB	NB	Block	Block	Block	Block
	S	-	NB	Block	NB	NB	NB	NB	Block
	G_2/M	-	Block	Block	Block	Block	NB	NB	NB
Sensitivity by comparison between ApQ and API	G_1	-	R	R	S	S	S	R	R
	S	-	R	R	R	R	S	S	S
	G_2/M	-	S	S	S	R	R	R	S

Abbreviation and explanation: NB; no cell cycle block, R; resistant to the treatment in specific cell cycle phase, S; Sensitive to the treatment in specific cell cycle phase

Reproduced with permission of the copyright owner. Further reproduction prohibited without permission.

Table 5.1 Continued...

		45.0° C, 15 min Heat-treated sample				
Time (hr)		16	18	20	22	24
Cell Numbers		33259	33701	34148	34602	35062
Cumulative Apoptotic Index		8880	9807	9937	10727	12202
Non-Apoptotic Cells	G_1	10440	9617	8827	8139	8502
	S	8709	9659	10508	9955	8154
	G_2/M	5230	4618	4876	5781	6204
Number of Apoptotic Cells at each time point	G_1	642	330	39	199	423
	S	473	285	47	319	408
	G_2/M	577	312	44	271	644
Apoptotic Quotient (ApQ)	α_1	0.059	0.032	0.004	0.023	0.052
	β_1	0.058	0.033	0.005	0.030	0.041
	γ_1	0.088	0.060	0.010	0.056	0.111
Cell Progression (α_2, β_2, γ_2)	α_2	0.063	0.132	0.171	0.158	0.016
	β_2	0.00	0.016	0.078	0.155	0.153
	γ_2	0.067	0.085	0.097	0.093	0.080
Apoptotic Probability Index (API)		0.066	0.038	0.005	0.033	0.062
Interpretation of Efflux Coefficient (EC)	G_1	Block	NB	NB	Block	Block
	S	Block	Block	Block	NB	NB
	G_2/M	NB	NB	Block	Block	Block
Sensitivity by comparison between ApQ and API	G_1	R	R	R	R	R
	S	R	R	R	R	R
	G_2/M	S	S	S	S	S

Abbreviation and explanation: NB; no cell cycle block, R; resistant to the treatment in specific cell cycle phase, S; Sensitive to the treatment in specific cell cycle phase

Apoptotic Quotient (ApQ) in Table 5.1. is a measure of the probability of apoptosis from each cell cycle phase after treatment. The number of apoptotic cells from each cell cycle phase for calculating ApQ is shown in Fig. 5.6. Data from Multicycle® analysis and the calculated results with comments are shown in Table 5.1. These results show that the apoptotic population comes from mainly G_2 phase early up to 6 hr, S phase becomes a major supplier between 6 hr and 12 hr, and then all cell cycle phases afterward. Control cells without heat shock had a low level of apoptosis (5.37 ± 2.36 %). When the model was calculated, the number of apoptotic cells in the control sample was subtracted at each time point. Only apoptotic cells produced at each time point were shown in Fig.5.6, resulting in curves with peaks and valleys. The length of each apoptotic phase was 3 hr after 45.0 °C for 15 min heat shock. Then, each phase increased the first 3 hr (peak) and then decreased. The spaces between these peaks were shown as valleys.

Apoptosis Probability Indices (API) gives the theoretical probability of cells undergoing apoptosis from each cell cycle phase with the same sensitivity. A comparison of *ApQ* (experimental results) and *API* (theoretical expectation) shows whether cells are more sensitive to undergoing apoptosis from a particular cell cycle phase than expected theoretically. If any *ApQ* line is located above *API* line (orange solid line), it shows a sensitive population. If it is below, it shows a resistant population. Thus, heat shock at 45.0° C for 15 min specifically killed the G_2/M phase cells early, the G_1 and S phase cells between 6 hr and 12 hr, and the G_2/M phase cells later (Fig.5.7). If the mechanism of an apoptotic inducer is unknown, this approach could provide a good first step for understanding the mechanism of apoptosis.

Reproduced with permission of the copyright owner. Further reproduction prohibited without permission.

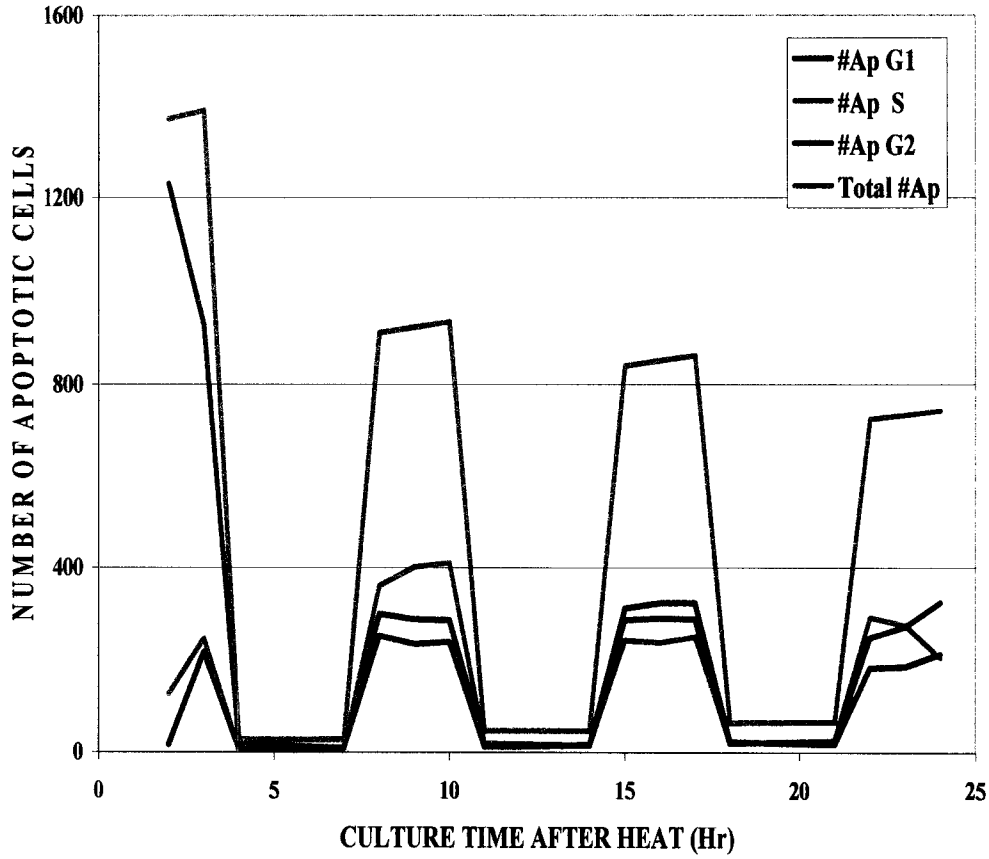

Figure 5.6 The number of apoptotic cells from each cell cycle phases at each time point cultured with various times at 37° C after heating at 45.0° C for 15 min. #Ap G1: number of apoptotic cells from G_1 phase; #Ap S: number of apoptotic cells from S phase; #Ap G2: number of apoptotic cells from G_2/M phase; Total # Ap: sum of apoptotic cells from three cell cycle phase.

Reproduced with permission of the copyright owner. Further reproduction prohibited without permission.

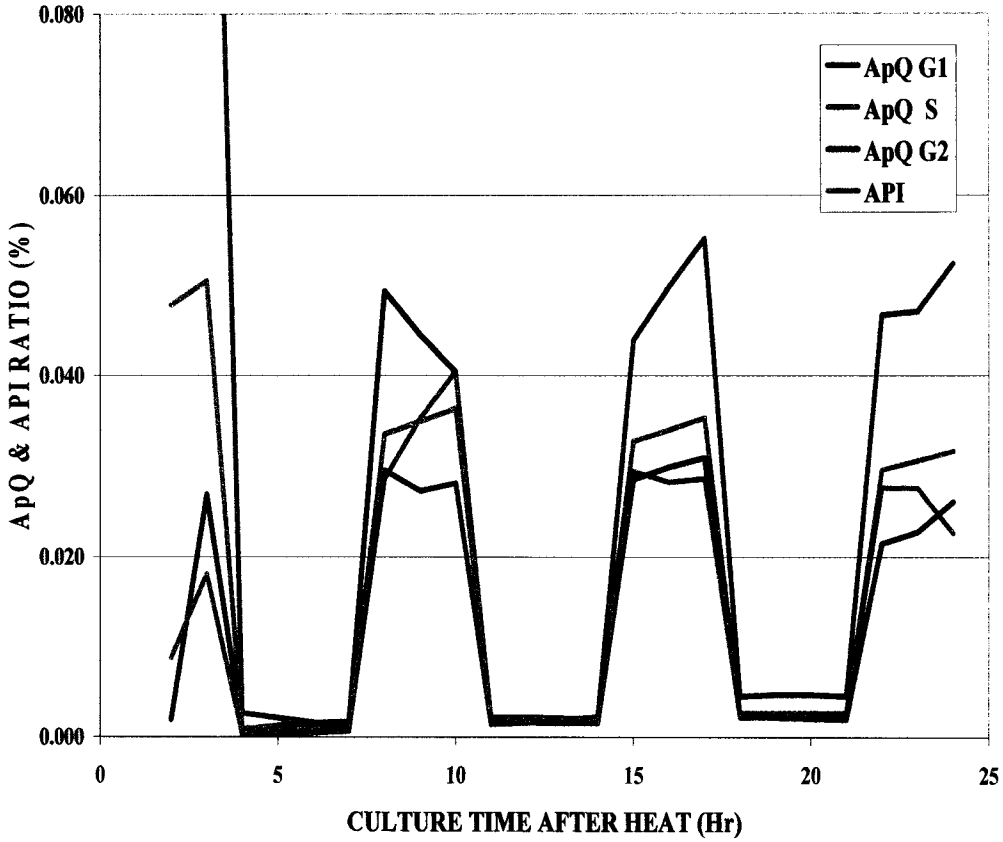

Figure 5.7 The comparison between ApQ and API in each cell cycle phases. Cells were incubated various times at 37° C after heating at 45.0° C for 15 min. ApQ G1: apoptotic quotient in G_1 phase ($\alpha 1$); ApQ S: apoptotic quotient in S phase ($\beta 1$); ApQ G2: apoptotic quotient in G_2/M phase ($\gamma 1$); API: apoptosis probability indices.

Reproduced with permission of the copyright owner. Further reproduction prohibited without permission.

Interpretation of the values of *Efflux Coefficient (EC)* in Fig.5.8 and Table 5.1 indicates that cells are blocked in G_2/M (green solid line) early, G_1 phase (blue solid line) after that, and S (pink solid line) and G2/M later. When these results are combined with CAI and *ApQ* data, they indicate that when cells were heat-shocked at 45.0° C for 15 min, the early apoptotic population came from G_2/M phase blocked cells, the second apoptotic population from G_1 phase with a cell cycle block and S phase with slow progression, a third apoptotic population from G_1 and S phases with cell cycle blocks, and a fourth apoptotic population from S and G_2/M phases with cell cycle blocks. This indicates that there may be at least two different kinds of apoptosis - interphase apoptosis and delayed apoptosis - after heating at 45.0° C for 15 min.

In this study it was assumed that the disintegration of cells by apoptosis did not take place because I do not know the starting point of the time-window for disintegration. However, I could calculate the disintegration graph based on CAI data if I knew the starting point because apoptotic cells, which are induced early, would also start disintegration early.

5.3.2 Hyperthermia-induced apoptosis with 45.0 °C 30 min heat shock

The changes in the apoptotic population and the non-apoptotic population incubated at 37° C up to 24 hrs after a 45.0° C 30 min heat shock was measured in HL-60 cells. The presence of apoptotic cells was measured with the TUNEL method. The DNA histograms from an experiment which illustrate cell cycle delays with culture time after

Reproduced with permission of the copyright owner. Further reproduction prohibited without permission.

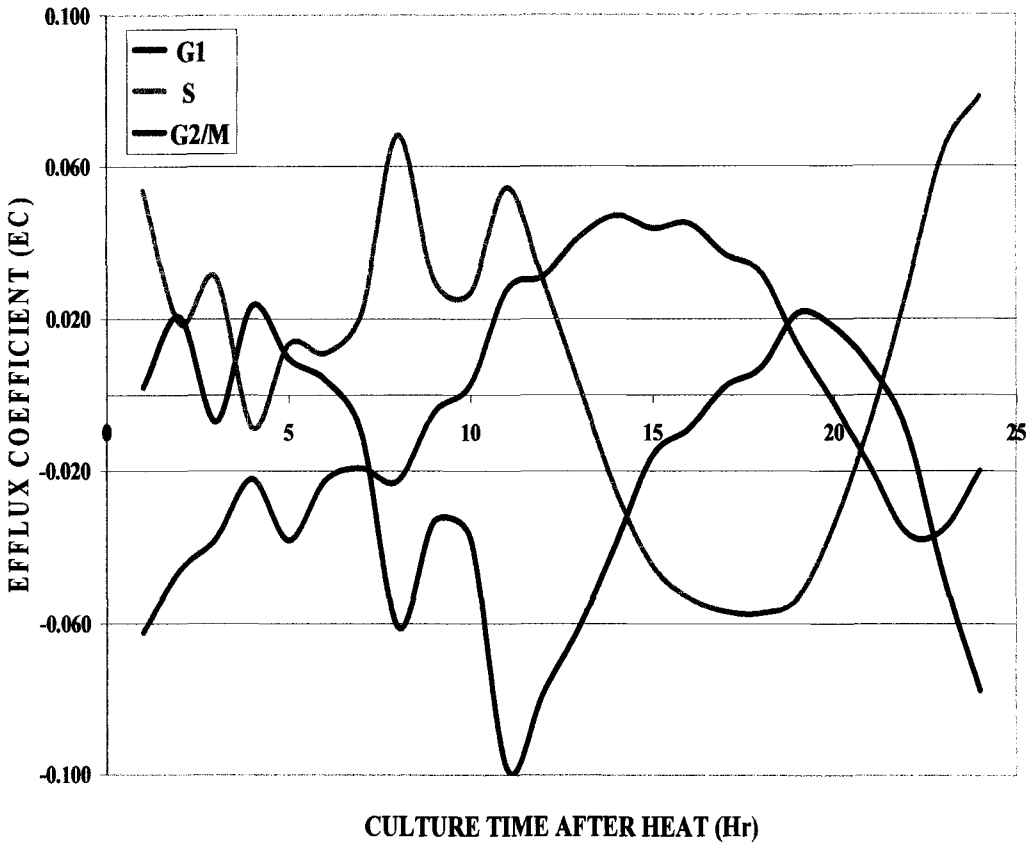

Figure 5.8 The efflux coefficient for each cell cycle phase at various times at 37° C after heating at 45.0° C for 15 min.

Reproduced with permission of the copyright owner. Further reproduction prohibited without permission.

heating are shown in Figure 5.9. The dual-parameter histograms from an experiment which illustrate the apoptotic population for different times after heating are shown in Figure 5.10. It is apparent that the 45.0° C 30 min heat treatments caused substantial changes in the cell cycle distribution as well as in the apoptosis index with time after heating. The number of apoptotic cells in each sample is derived from the dual parameter histograms shown in Fig. 5.10. The total number of cells for control and treated samples at each time-point after the treatment is shown in Fig. 5.11.

To quantitatively describe the percentage of cells in each phase of the cell cycle for each time point after the heat treatment shown in Fig. 5.9 and Fig. 5.10, the DNA histograms were analyzed with Multicycle® software. Because the DNA histograms include the apoptotic population, however, they cannot be analyzed directly to determine the fraction of cells in each cell cycle phase for the non-apoptotic cells. To quantitatively describe the cell cycle distribution of the non-apoptotic cells, a gate was drawn around the non-apoptotic population using Multi-2D® and the data within the gate were saved as a single parameter DNA histogram which could then be analyzed by Multicycle®. This analysis then gave the cell cycle distributions of the surviving (non-apoptotic) cells.

The number of non-apoptotic cells in each phase of the cell cycle for each culture time point are shown in Figure 5.12. The number of cells in G_1 phase decreased as time progressed up to 4 hr, remained nearly constant up to 12 hr, and increased between 12 and 24 hr. The number of cells in G_2/M phase increased to 1 hr, then decreased by 2 hr and remained at that level for 24 hr. The number of cells in S phase decreased rapidly up to 4 hr, remained at that level up to 12 hr, and then further decreased. From these results, it appears that the apoptotic cells come mainly from G1 and S phases between 0 hr and

Reproduced with permission of the copyright owner. Further reproduction prohibited without permission.

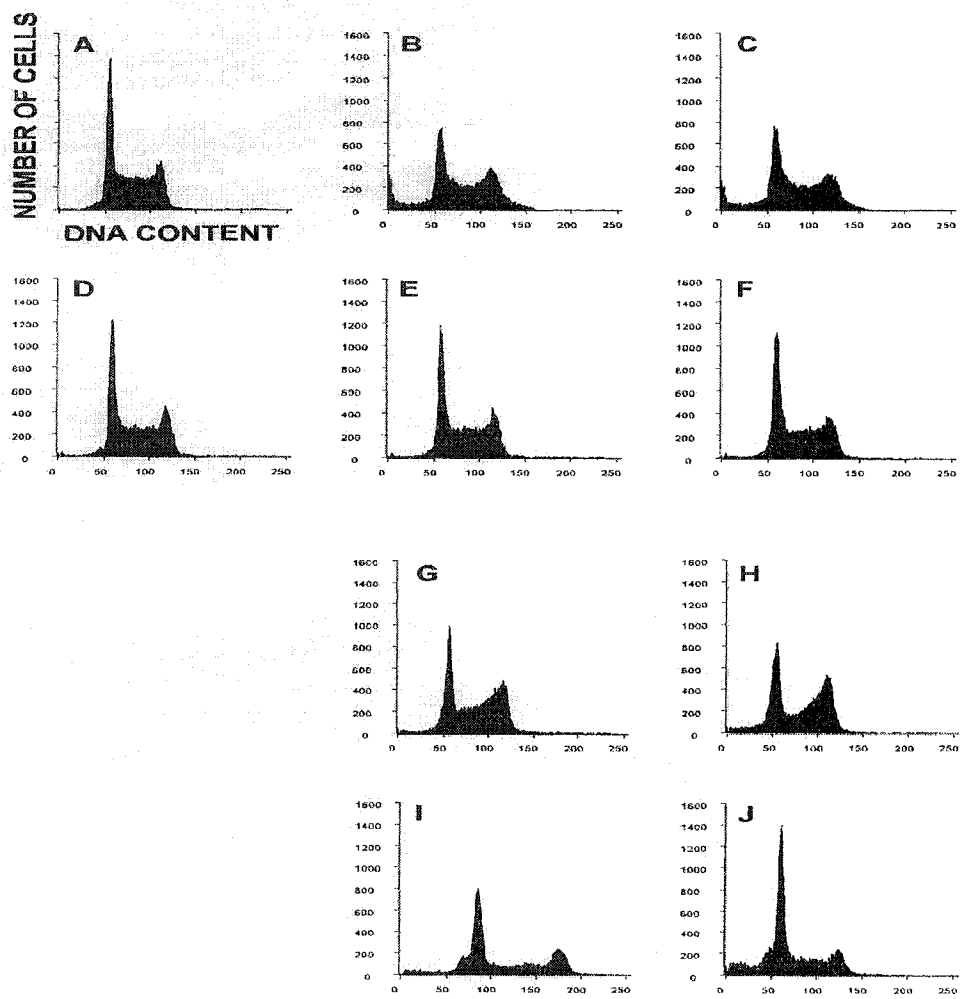

Figure 5.9 Cell cycle distributions for control and heated HL-60 cells at 45.0° C for 30 min. A: control cells ; B: 0 hr at 37° C after heat ; C: 1 hr ; D: 2 hr ; E: 4 hr ; F: 6 hr ; G: 9 hr ; H: 12 hr ; I: 20 hr ; J: 24 hr.

Reproduced with permission of the copyright owner. Further reproduction prohibited without permission.

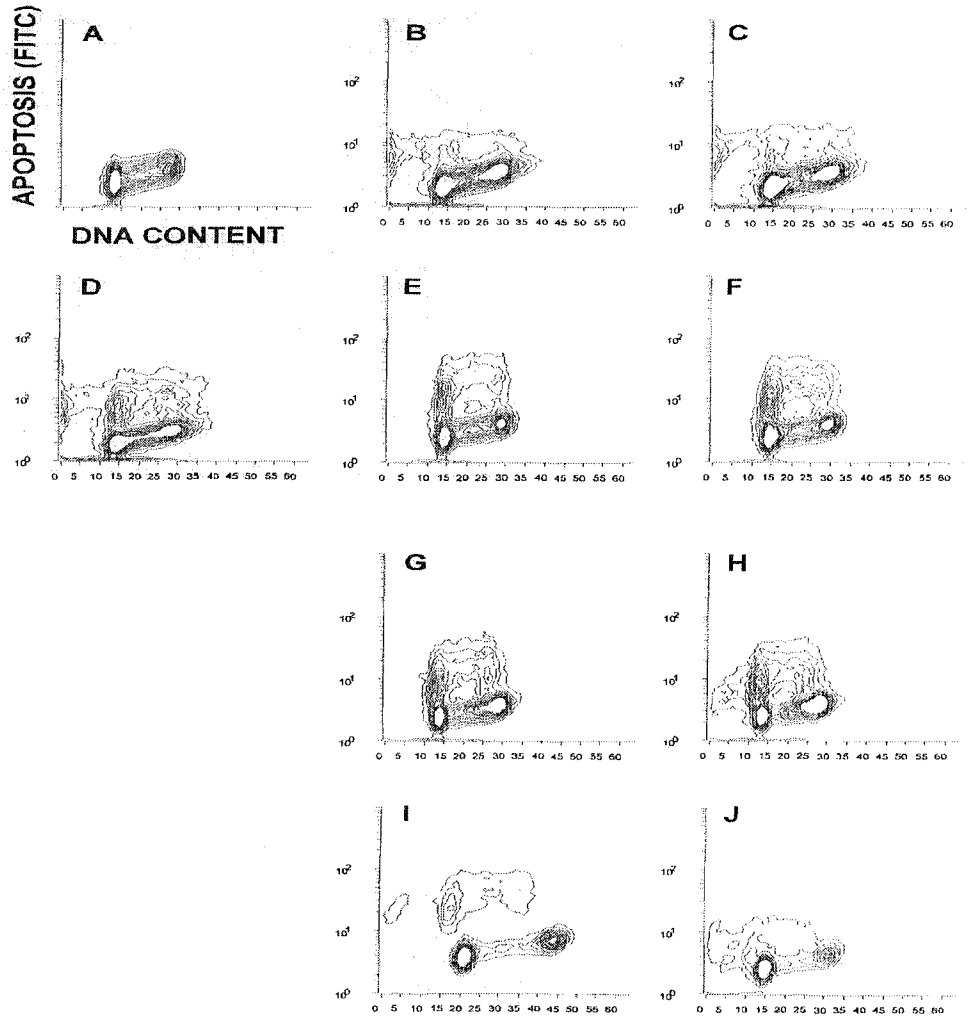

Figure 5.10 Dual parameter histograms showing apoptosis (FITC) and DNA content (IRFL) for control and heated HL-60 cells at 45.0° C for 30 min. A: control cells ; B: 0 hr at 37° C after heat ; C: 1 hr ; D: 2 hr ; E: 4 hr ; F: 6 hr ; G: 9 hr ; H: 12 hr ; I: 20 hr ; J: 24 hr.

Reproduced with permission of the copyright owner. Further reproduction prohibited without permission.

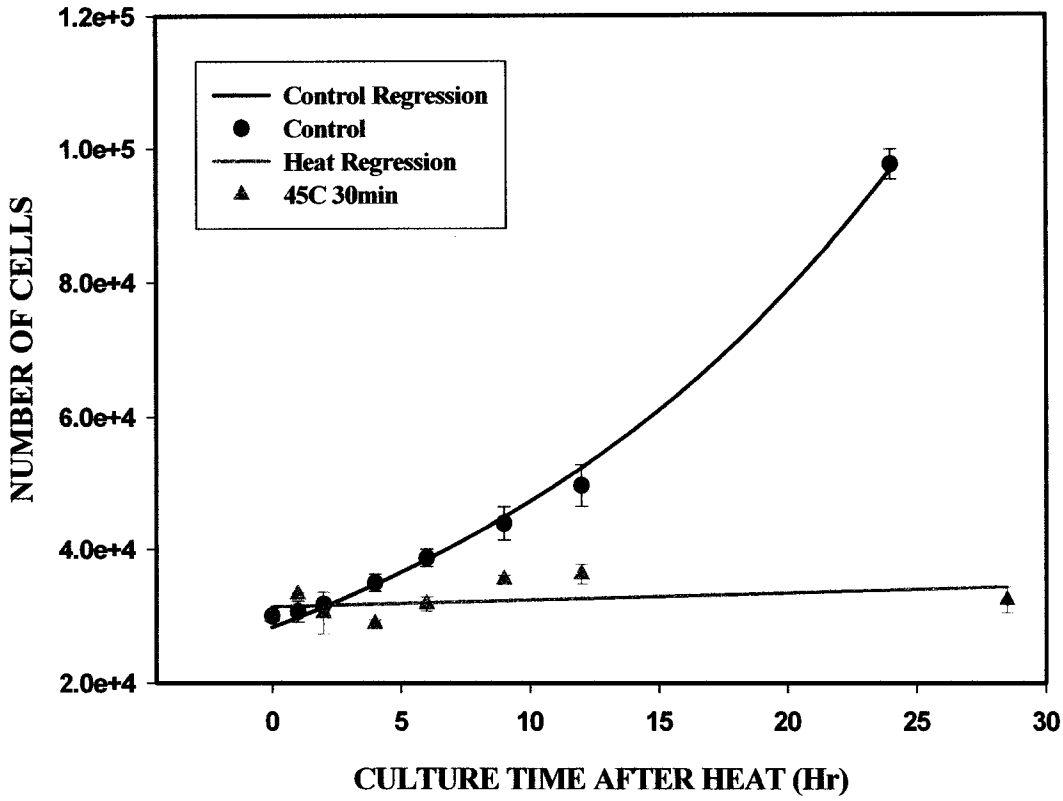

Figure 5.11 The number of HL-60 cells at various times after a 45.0° C, 30 min heat shock. Cell numbers are counted at sample collection time. The dots represent measured values with error bars representing ± one standard error. The line represents the result of nonlinear regression from the exponential equation N_t = 28363*exp (0.0511*time) for control cells and N_t = 31368*exp (0.0031*time) for heat-treated cells. This regression had a standard error of estimate equal to 3637 and 3239 cells for each samples.

Reproduced with permission of the copyright owner. Further reproduction prohibited without permission.

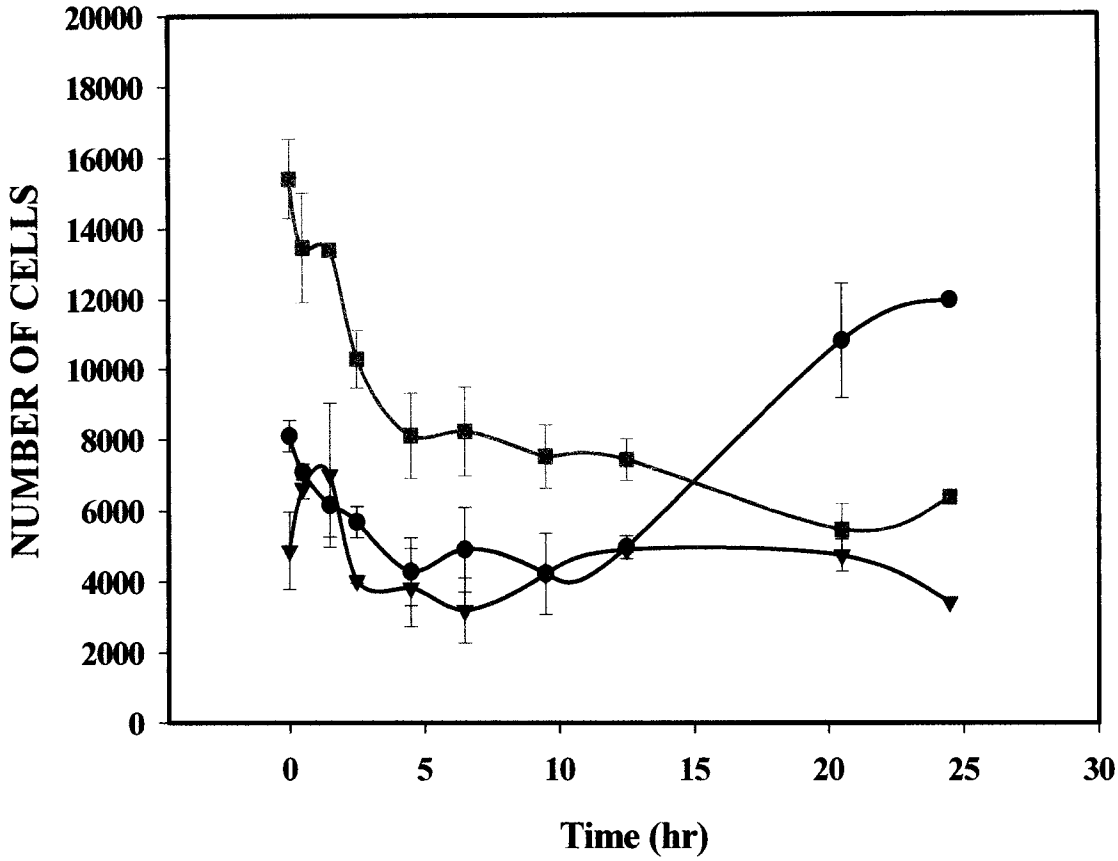

Figure 5.12 The number of non-apoptotic HL-60 cells in each cell cycle phase before and at various times after heating at 45.0° C for 30 min. Control: untreated cells. The error bars represent standard error of the mean from at least two experiments. (•): G_1 phase cells; (■): S phase cells; (▲): G_2/M phase cells.

Reproduced with permission of the copyright owner. Further reproduction prohibited without permission.

4 hr and S phase after that. This interpretation is complicated by the fact that there are also apparent cell cycle blocks.

The number of apoptotic cells and calculated CAI at various times after heating at 45.0 °C for 30 min are shown in Fig. 5.13. The apoptotic population reached a peak around 4 hr, remained nearly constant to 10 hr, and then decreased. The calculated CAI by the *CAI estimation model* described in Chapter 4 was 93.6 %. The CAI graph showed three plateaus at 39.6 %, 69.6 % and 93.6 %, which represented three phases of apoptosis induction. The model calculated three apoptotic phases: first, T_w equals 10, T_1 equals 4 and AIR_1 equals 9.9 % /hr; second, T_w equals 10, T_2 equals 4 and AIR_2 equals 7.5 % /hr; and third, T_w equals 10, T_3 equals 4 and AIR_3 equals 6.0 % /hr.

To explain these results more completely, the *cell cycle progression model* was used to analyze the data. The *Efflux Coefficient (EC)* was calculated by Eq. 2.11 and 2.12, the *Apoptotic Index (API)* was calculated by Eq. 2.15, and cell cycle distributions were calculated by Multicycle® software. These results along with comments are shown in Table 5.2.

Apoptotic Quotient (ApQ) in Table 5.2. is a measure of the probability of apoptosis from each cell cycle phase after treatment. The number of apoptotic cells from each cell cycle phase for calculating ApQ is shown in Fig. 5.14. Data from Multicycle® analysis and the calculated results with comments are shown in Table 5.2. These results show that the main apoptotic population comes from S phase early, from all cell cycle phases after 10 hr, and G_1 and S phases afterward. Control cells without heat shock had a low level of apoptosis (5.38 ± 2.38 %). When the model was calculated, the number of

Reproduced with permission of the copyright owner. Further reproduction prohibited without permission.

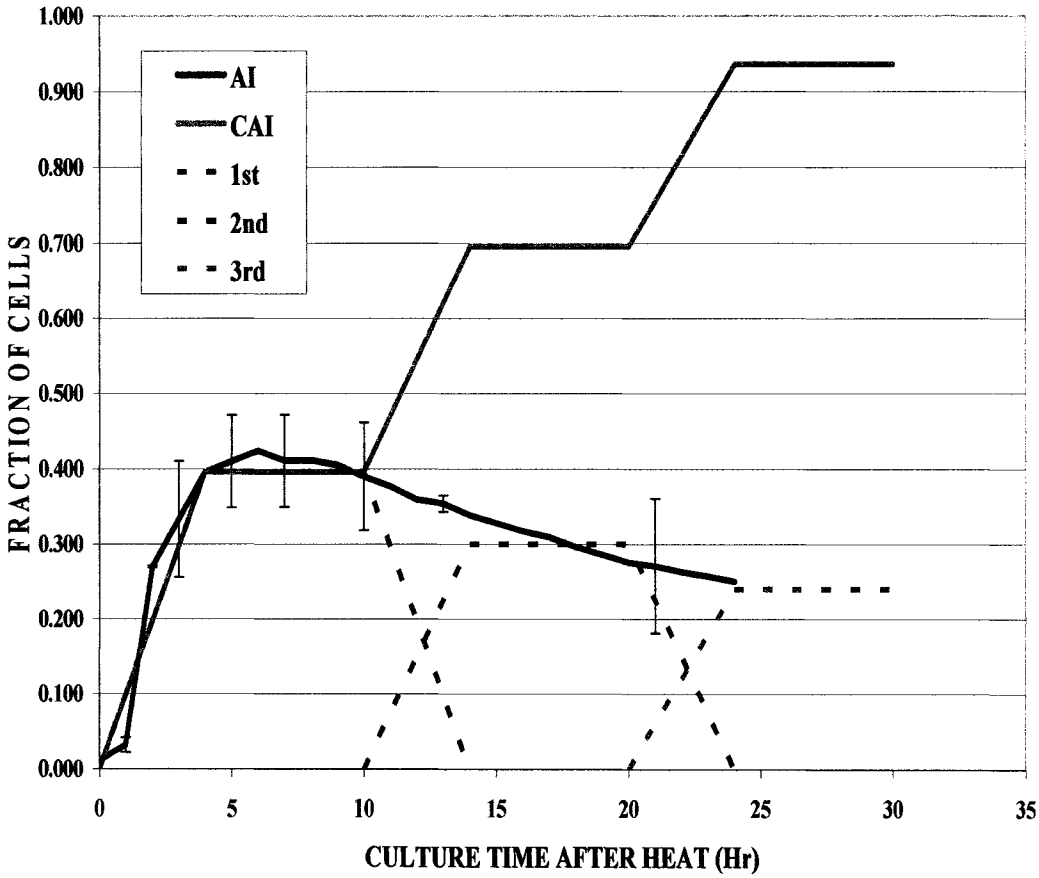

Figure 5.13 The number of apoptotic cells cultured with various times at 37° C after heating at 45.0° C for 30 min. AI results represent the mean values and standard error of the mean (SEM) from at least 2 independent experiments. The actual data points in AI curve are the point with error bars. The line between them was interpolated.

Reproduced with permission of the copyright owner. Further reproduction prohibited without permission.

Reproduced with permission of the copyright owner. Further reproduction prohibited without permission.

Table 5.2 The effects of 45.0° C, 30 min heat shock on the cell cycle distribution and apoptosis, including an analysis of the efflux coefficient and apoptosis probability index (API) as described. The data in table are measured directly by the experiments or calculated indirectly by interpolation.

		Control	45.0° C, 30 min Heat-treated sample						
Time (hr)		0	2	4	6	8	10	12	14
Cell Numbers		31369	31564	31760	31957	32156	32356	32557	32760
Cumulative Apoptotic Index		0	5940	11880	11880	11880	11880	16380	20880
Non-Apoptotic Cells	G_1	8480	7056	5351	5193	5183	5490	4798	4010
	S	16644	13047	9925	9963	9928	9644	7098	4706
	G_2/M	6245	5521	4604	4921	5165	5342	4281	3164
Number of Apoptotic Cells at each time point	G_1	-	965	1305	0	0	0	1430	1465
	S	-	2906	2897	0	0	0	1356	1546
	G_2/M	-	2069	1738	0	0	0	1714	1489
Apoptotic Quotient (ApQ)	α_1	-	0.114	0.185	0	0	0	0.260	0.305
	β_1	-	0.175	0.222	0	0	0	0.141	0.218
	γ_1	-	0.331	0.315	0	0	0	0.321	0.348
Cell Progression (α_2, β_2, γ_2)	α_2	-	0.100	0.112	0.103	0.078	0.018	0.00	0.00
	β_2	-	0.093	0.078	0.052	0.044	0.038	0.089	0.081
	γ_2	-	0.031	0.036	0.043	0.040	0.039	0.038	0.047
Apoptotic Probability Index (API)		-	0.189	0.232	0	0	0	0.220	0.278
Interpretation of Efflux Coefficient (EC)	G_1	-	NB	NB	NB	Block	Block	Block	Block
	S	-	NB	NB	Block	NB	NB	NB	NB
	G_2/M	-	Block	Block	Block	Block	Block	Block	Block
Sensitivity by comparison between ApQ and API	G_1	-	R	R	-	-	-	S	S
	S	-	R	R	-	-	-	R	R
	G_2/M	-	S	S	-	-	-	S	S

Abbreviation and explanation: NB; no cell cycle block, R; resistant to the treatment in specific cell cycle phase, S; Sensitive to the treatment in specific cell cycle phase

Reproduced with permission of the copyright owner. Further reproduction prohibited without permission.

Table 5.2 Continued...

		45.0° C, 30 min Heat-treated sample				
Time (hr)		16	18	20	22	24
Cell Numbers		32963	33169	33375	33582	33791
Cumulative Apoptotic Index		20880	20880	20880	24480	28080
Non-Apoptotic Cells	G_1	4672	5402	6138	4862	3181
	S	4211	3714	3323	2294	1587
	G_2/M	3200	3173	3034	1946	943
Number of Apoptotic Cells at each time point	G_1	0	0	0	1558	1611
	S	0	0	0	1501	1279
	G_2/M	0	0	0	541	710
Apoptotic Quotient (ApQ)	α_1	0	0	0	0.254	0.331
	β_1	0	0	0	0.452	0.557
	γ_1	0	0	0	0.178	0.365
Cell Progression (α_2, β_2, γ_2)	α_2	0.00	0.00	0.00	0.022	0.100
	β_2	0.051	0.042	0.018	0.00	0.00
	γ_2	0.064	0.064	0.065	0.068	0.107
Apoptotic Probability Index (API)		0	0	0	0.289	0.395
Interpretation of Efflux Coefficient (EC)	G_1	Block	Block	Block	Block	NB
	S	NB	NB	NB	Block	Block
	G_2/M	Block	NB	NB	NB	NB
Sensitivity by comparison between ApQ and API	G_1	-	-	-	R	R
	S	-	-	-	S	S
	G_2/M	-	-	-	R	S

Abbreviation and explanation: NB; no cell cycle block, R; resistant to the treatment in specific cell cycle phase, S; Sensitive to the treatment in specific cell cycle phase

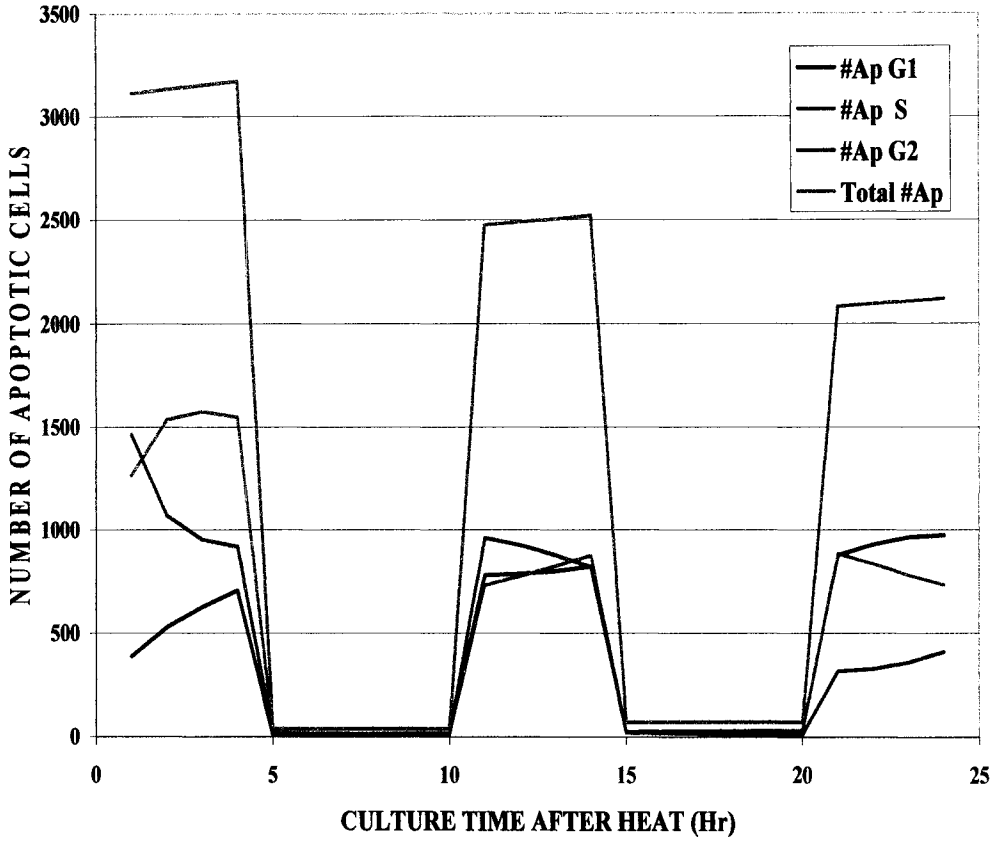

Figure 5.14 The number of apoptotic cells from each cell cycle phase at various times at 37° C after heating at 45.0° C for 30 min. #Ap G1: number of apoptotic cells from G_1 phase; #Ap S: number of apoptotic cells from S phase; #Ap G2: number of apoptotic cells from G_2/M phase; Total # Ap: sum of apoptotic cells from three cell cycle phase.

Reproduced with permission of the copyright owner. Further reproduction prohibited without permission.

apoptotic cells in the control sample was subtracted at each time point. Only apoptotic cells produced at each time point were shown in Fig.5.14, resulting in curves with peaks and valleys. The length of each apoptotic phase was 4 hr after 45.0 °C for 30 min heat shock. Then, each phase increased the first 4 hr (peak) and then decreased. The spaces between these peaks were shown as valleys.

Apoptosis Probability Indices (API) gives the theoretical probability of cells undergoing apoptosis from each cell cycle phase with the same sensitivity. A comparison of *ApQ* (experimental results) and *API* (theoretical expectation) shows whether cells are more sensitive to undergoing apoptosis from a particular cell cycle phase than expected theoretically. If any *ApQ* line is located above *API* line (orange solid line), it shows a sensitive population. If it is located below, it shows a resistant population. Thus, heat shock at 45.0° C for 30 min specifically killed the G_2/M phase cells early and G_1 and G_2/M phase cells between 10 hr and 15 hr, and the S phase cells later (Fig. 5.15).

Interpretation of the values of *Efflux Coefficient (EC)* in Fig. 5.16 and Table 5.2 indicates that cells are blocked in G_2/M up to 15 hr after heating at 45.0° C for 30 min. G_1 phase cells were delayed in by 8 hr and maintained up to 23 hr. A strong cell cycle block point appeared at 12 hr and 18 hr. An S phase cell cycle delay appeared at 21 hr. When these data analyzed with CAI and *ApQ* data, they indicate that when cells were heat-shocked at 45.0° C for 30 min, the early apoptotic population came from G_2/M phase blocked cells and slowly progressing S phase cells, the second apoptotic population came from G_1 and G_2/M phases with a cell cycle block, and the third apoptotic population from

Reproduced with permission of the copyright owner. Further reproduction prohibited without permission.

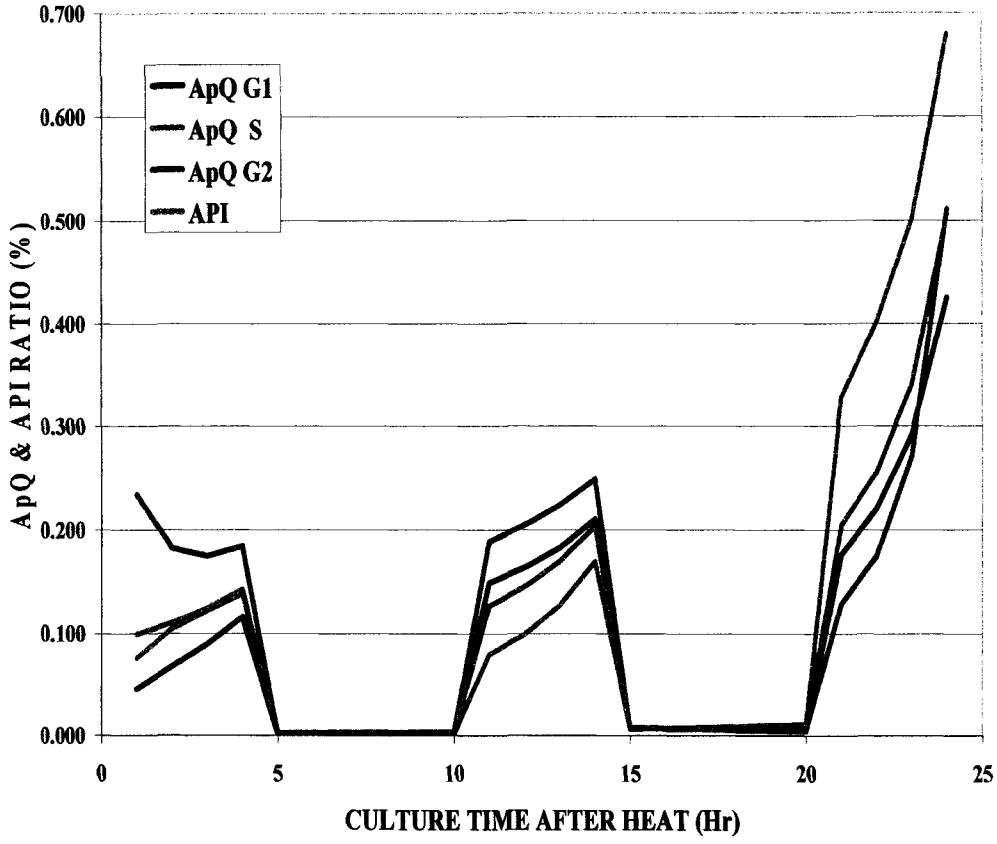

Figure 5.15 The comparison between ApQ and API in each cell cycle phase. Cells are incubated various times at 37° C after heating at 45.0° C for 30 min. ApQ G1: apoptotic quotient in G_1 phase ($\alpha 1$); ApQ S: apoptotic quotient in S phase ($\beta 1$); ApQ G2: apoptotic quotient in G_2/M phase ($\gamma 1$); API: apoptosis probability indices.

Reproduced with permission of the copyright owner. Further reproduction prohibited without permission.

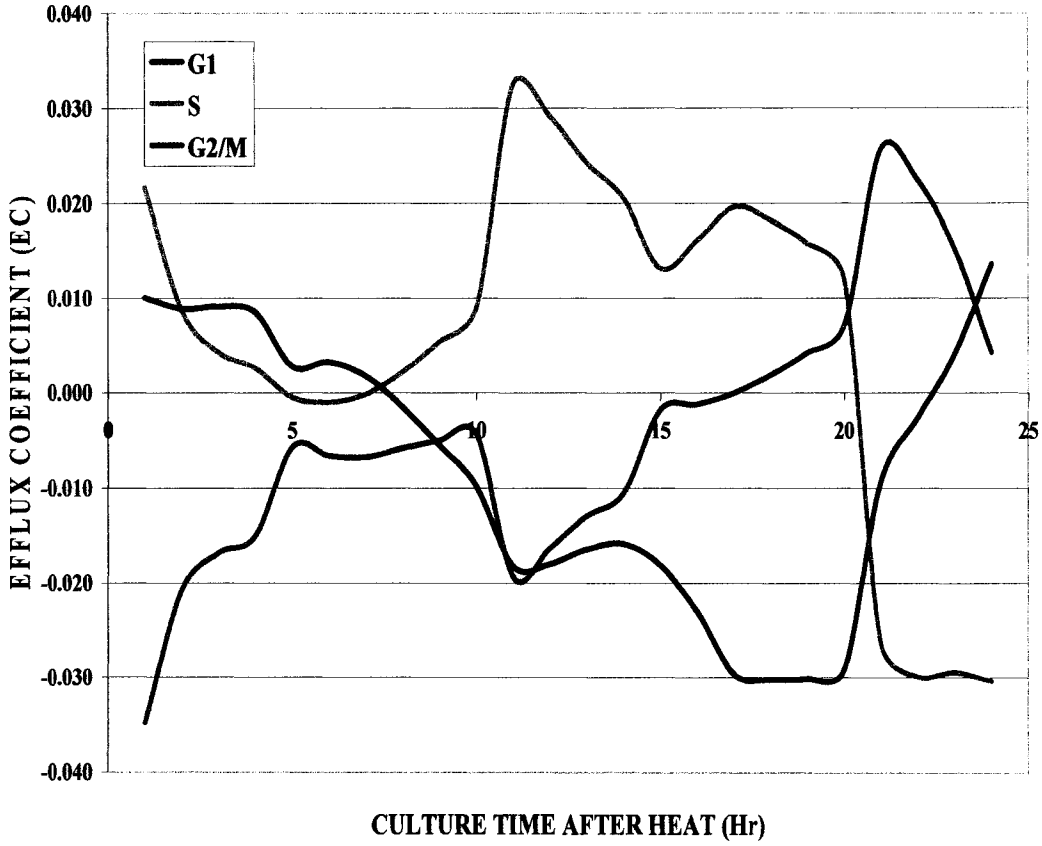

Figure 5.16 The efflux coefficient for each cell cycle phase at various times at 37° C after heating at 45.0° C for 30 min.

Reproduced with permission of the copyright owner. Further reproduction prohibited without permission.

G_1 and S phases with a cell cycle block. This indicates that cell cycle phase specific death showed different patterns with different doses when compared with 45.0° C for 15 min.

In this study it was assumed that the disintegration of cells by apoptosis did not take place because I do not know the starting point of the time-window for disintegration. However, I could calculate the disintegration graph based on CAI data if I knew the starting point because apoptotic cells, which are induced early, would also start disintegration early.

These results indicate that there are significant changes in the response of cells at 7 hr, 15 hr, and 21 hr. A cell cycle block in G_1 starts at 7 hr. A cell cycle block in G_2/M phase ends at 15 hr and apoptosis from all cell cycle phases is shown between 7 hr and 15 hr. The third time point at 21 hr shows the cell cycle block in G_1 and S phase and apoptosis in G_1 and S phases.

5.4 Discussion

In the previous results, hyperthermia induced the apoptotic population mainly from G_1 phase. In this study, apoptosis of HL-60 cells was induced by heat shock treatments at 45.0°C for 15 min or 30 min. DNA histograms, TUNEL and bivariate histogram with PI showed G_1-phase specific apoptosis (Fig. 5.1, 5.2, 5.9 and 5.10). Hyperthermia induced apoptosis not only in G_1 phase but also S and G_2/M phase. These results also show that HL-60 cells are tightly blocked in all cell cycle phases at different times.

After a 45.0°C, 15 min heat shock, early apoptosis came from G_2/M phase cells. This apoptosis may be caused by disruption of microtubular proteins (3). The second

Reproduced with permission of the copyright owner. Further reproduction prohibited without permission.

wave of apoptosis from G_1 phase may be caused by cells in division at the time of heating, which entered G_1 without completing division. The apoptotic population from early S phase may have less time available for the repair of DNA damage before entering into S phase without p53 (17), which leads to problems during replication and causes some kind of interphase death (20). Apoptosis from G_2/M phase after 20 hr may come from cell cycle block with damaged slow moving cells.

After a 45.0°C, 30 min heat shock, early apoptosis came from S and G_2/M phase cells. This apoptosis may be caused by direct damage of cellular proteins for DNA replication machinery and mitosis. The second wave of apoptosis from all cell cycle phases may be due to cells in G_1 and S phases with unrepaired DNA damage (20), and disruption of microtubular proteins in G_2/M phase cells (3). The third wave of apoptosis comes from G_1 and S phases. Cellular damage induced by higher doses of hyperthermia could trigger cell suicide through apoptosis directly, without cell cycle arrest in G_2/M phase (4). After the cells with heavy damage are removed the remaining cells appears to follow the 45.0°C, 15 min heat shock response. The degree of the block and sensitivity to apoptosis could be changed based on the doses of heat and culture time.

These kinds of analysis could be applied to the analysis of differences between normal and cancer cells. A strategy designed to protect normal cells from cycle-dependent lethal agents by exploiting differences in cell cycles of normal and cancer cells is applied for cancer therapy. In the combination of pretreatment and post-treatment, such pretreatment prevents normal cells from entering S or M phase and thus protect them against S-phase- and M-phase-specific agents. For the selective protection of normal cells, several mechanism should be considered as follows; i) Loss of p53-dependent

Reproduced with permission of the copyright owner. Further reproduction prohibited without permission.

checkpoints, ii) growth factor-activated pathways, iii) CDK inhibitors, and iv) drug resistance (2). Toxicity to normal cells is unavoidable if drugs do not have a highly specific cancer cell target. When the differences between normal and cancer cells are maximized with *'cell cycle progression model'*, the side effects are minimized and the better tumor control could be achieved.

Reproduced with permission of the copyright owner. Further reproduction prohibited without permission.

Reference List

1. Barry MA, Behnke CA, Eastman A: Activation of programmed cell death (apoptosis) by cisplatin, other anticancer drugs, toxins, and hyperthermia. Biochem Pharmacol 40:2353-2362, 1990.

2. Blagosklonny MV, Pardee AB: Exploiting cancer cell cycling for selective protection of normal cells. Cancer Res 61:4301-4305, 2001.

3. Coss RA, Dewey WC, Bamburg JR: Effects of hyperthermia on dividing Chinese hamster ovary cells and on microtubules in vitro. Cancer Res 42:1059-1071, 1982.

4. Endlich B, Radford IR, Forrester HB, Dewey WC: Computerized video time-lapse microscopy studies of ionizing radiation- induced rapid-interphase and mitosis-related apoptosis in lymphoid cells. Radiat Res 153:36-48, 2000.

5. Fairbairn JJ, Khan MW, Ward KJ, Loveridge BW, Fairbairn DW, O'Neill KL: Induction of apoptotic cell DNA fragmentation in human cells after treatment with hyperthermia. Cancer Lett 89:183-188, 1995.

6. Gorczyca W, Gong J, Ardelt B, Traganos F, Darzynkiewicz Z: The cell cycle related differences in susceptibility of HL-60 cells to apoptosis induced by various antitumor agents. Cancer Res 53:3186-3192, 1993.

7. Goto A, Shomori K, Ohkumo T, Tanaka F, Sato K, Ito H: Hyperthermia-induced apoptosis occurs both in a p53 gene-dependent and - independent manner in three human gastric carcinoma cell lines. Oncol Rep 6:335-339, 1999.

8. Harmon BV, Corder AM, Collins RJ, Gobe GC, Allen J, Allan DJ, Kerr JFR: Cell death induced in a murine mastocytoma by 42-47° C heating in vitro: Evidence that the form of death changes from apoptosis to necrosis above a critical heat load. Int J Radiat Biol 58:845-858, 1990.

9. He L, Fox MH: Variation of heat shock protein 70 through the cell cycle in HL-60 cells and its relationship to apoptosis. Exp Cell Res 232:64-71, 1997.

10. Li WX, Chen CH, Ling CC, Li GC: Apoptosis in heat-induced cell killing: The protective role of hsp70 and the sensitization effect of the c-*myc* gene. Radiat Res 145:324-330, 1996.

11. Nakano H, Kurihara K, Okamoto M, Tone S, Shinohara K: Heat-induced apoptosis and p53 in cultured mammalian cells. Int J Radiat Biol 71:519-529, 1997.

12. Nishita M, Inoue S, Tsuda M, Tateda C, Miyashita T: Nuclear translocation and increased expression of Bax and disturbance in cell cycle progression without prominent apoptosis induced by hyperthermia. Exp Cell Res 244:357-366, 1998.

Reproduced with permission of the copyright owner. Further reproduction prohibited without permission.

13. Pantazis P, Han Z, Wyche J: Schedule-dependent efficiency of thermochemotherapy in vitro with etoposide and heating at 43 degrees C. Anticancer Res 19:995-998, 1999.

14. Sellins K, Cohen JJ: Hyperthermia induces apoptosis in thymocytes. Radiat Res 126:88-95, 1991.

15. Shchepotin IB, Soldatenkov V, Buras RR, Nauta RJ, Shabahang M, Evans SRT: Apoptosis of human primary and metastatic colon adenocarcinoma cell lines *in vitro* induced by 5-fluorouracil, verapamil, and hyperthermia. Anticancer Res 14:1027-1032, 1994.

16. Takasu T, Lyons JC, Park HJ, Song CW: Apoptosis and perturbation of cell cycle progression in an acidic environment after hyperthermia. Cancer Res 58:2504-2508, 1998.

17. Wolf D, Rotter V: Major deletions in the gene encoding the p53 tumor antigen cause lack of p53 expression in HL-60 cells. Proc Natl Acad Sci U S A 82:790-794, 1985.

18. Yonezawa M, Otsuka T, Kato T, Moriyama A, Kato KH, Asai K, Matsui N: Hyperthermic induction of apoptosis in malignant fibrous histiocytoma cells: possible involvement of a p53-independent pathway in the induction of bax gene. J Orthop Sci 7:117-122, 2002.

19. Zamai L, Falcieri E, Zauli G, Cataldi A, Vitale M: Optimal detection of apoptosis by flow cytometry depends on cell morphology. Cytometry 14:891-897, 1993.

20. Zolzer F, Streffer C: Quiescence in S-phase and G1 arrest induced by irradiation and/or hyperthermia in six human tumour cell lines of different p53 status. Int J Radiat Biol 76:717-725, 2000.

Reproduced with permission of the copyright owner. Further reproduction prohibited without permission.

CHAPTER 6

ANALYSIS OF CELL CYCLE DEPENDENT APOPTOSIS AND CELL CYCLE BLOCKS INDUCED BY DOSE DEPENDENT HYPERTHERMIA IN HL-60 CELLS

6.1 Introduction

Cells that are heated to a few degrees above physiological temperatures (hyperthermia) undergo apoptosis (1,4,5,6,8,9,11,12,13,14,16,17,18,21,22) and become sensitive to radiotherapy and many antitumor agents. Radiotherapy in combination with hyperthermia or antitumor agents can improve therapy, so the cellular response to hyperthermia is of great clinical interest. Induction of apoptosis by hyperthermia occurs very rapidly. Apoptosis peaks in mastocytoma cultures at between 2 and 4 h, and then decreases as the apoptotic bodies undergo secondary necrosis and are degraded to debris. By 24 h, apoptotic counts have returned to levels approaching control values (8). While the lag period (time between completion of heating and onset of apoptosis) varies among different cell types, apoptotic inducer and detection methods used, once underway, the kinetics of the apoptotic process itself appears to be similar (10).

Reproduced with permission of the copyright owner. Further reproduction prohibited without permission.

The slope of an Arrhenius plot of various levels of hyperthermia gives the activation energy of the chemical process involved in the cell killing. The similarity of the activation energy for protein denaturation to the activation energy for heat cytotoxicity, calculated from the Arrhenius analysis, led to the hypothesis that the target for heat cell killing may be protein. The structural chromosomal proteins, nuclear matrix, cytoskeleton repair enzymes and membrane components have all been identified as possible targets that are denatured by hyperthermia (3,7,15,19).

The effects of heat are primarily dependent on time of heating at a given temperature. The relationship between treatment time and temperature for a biological isoeffect (the Arrhenius plot) has been confirmed for a variety of normal tissues and tumors (20). Therefore, when defining thermal doses in hyperthermia studies, both the time and temperature of heating are equally important determinants.

In this study, cell cycle progression and apoptosis were monitored with heating from 5 – 60 min at 45.0 °C in HL-60 cells. The number of apoptotic cells after treatment with heat shock was measured by the TUNEL assay and propidium iodide labeling using flow cytometry.

6.2 Materials and Methods

General information for the experiment was explained in Chapter 2 Materials and Methods. Detailed and specific explanations are provided in figure and table legends.

Reproduced with permission of the copyright owner. Further reproduction prohibited without permission.

6.3 Hyperthermia-induced apoptosis with dose-dependent heat shock at 45.0 °C

My goal in this set of experiments was to analyze the relationship between increasing heating time at 45.0° C and the induction of apoptosis. Because the effects of apoptosis on the cell cycle was studied and analyzed at 45.0° C in previous chapters, I chose 45.0° C to analyze the kinetics of apoptosis. If heating time is doubled at 45.0° C, how is the number of apoptotic cells changed? At shorter than 15 min or longer than 40 min heat shock, could apoptotic population show different relationships?

HL60 cells were heated at various times at 45.0° C and then incubated at 37° C for 12 hr to allow apoptosis to develop. The presence of apoptotic cells was measured with the TUNEL method. The DNA histograms from an experiment which illustrate cell cycle delays for different heat treatment time are shown in Fig. 6.1. The dual-parameter histograms from an experiment which illustrate the apoptotic population for different heat treatment time are shown in Fig. 6.2. Small numbers of apoptotic cells are not shown in the dual-parameter histograms because the contour levels exclude them. It is apparent that the different heat treatments cause substantially different changes in the cell cycle distribution as well as in the apoptosis fraction. The numbers of apoptotic cells in each sample are derived from the dual parameter histograms shown in Fig. 6.2. The total number of cells for control and treated samples after treatment is shown in Fig. 6.3. A 10 min heat shock at 45.0° C reduced cell growth and there was no cell growth after 15 – 60 min of heating.

Reproduced with permission of the copyright owner. Further reproduction prohibited without permission.

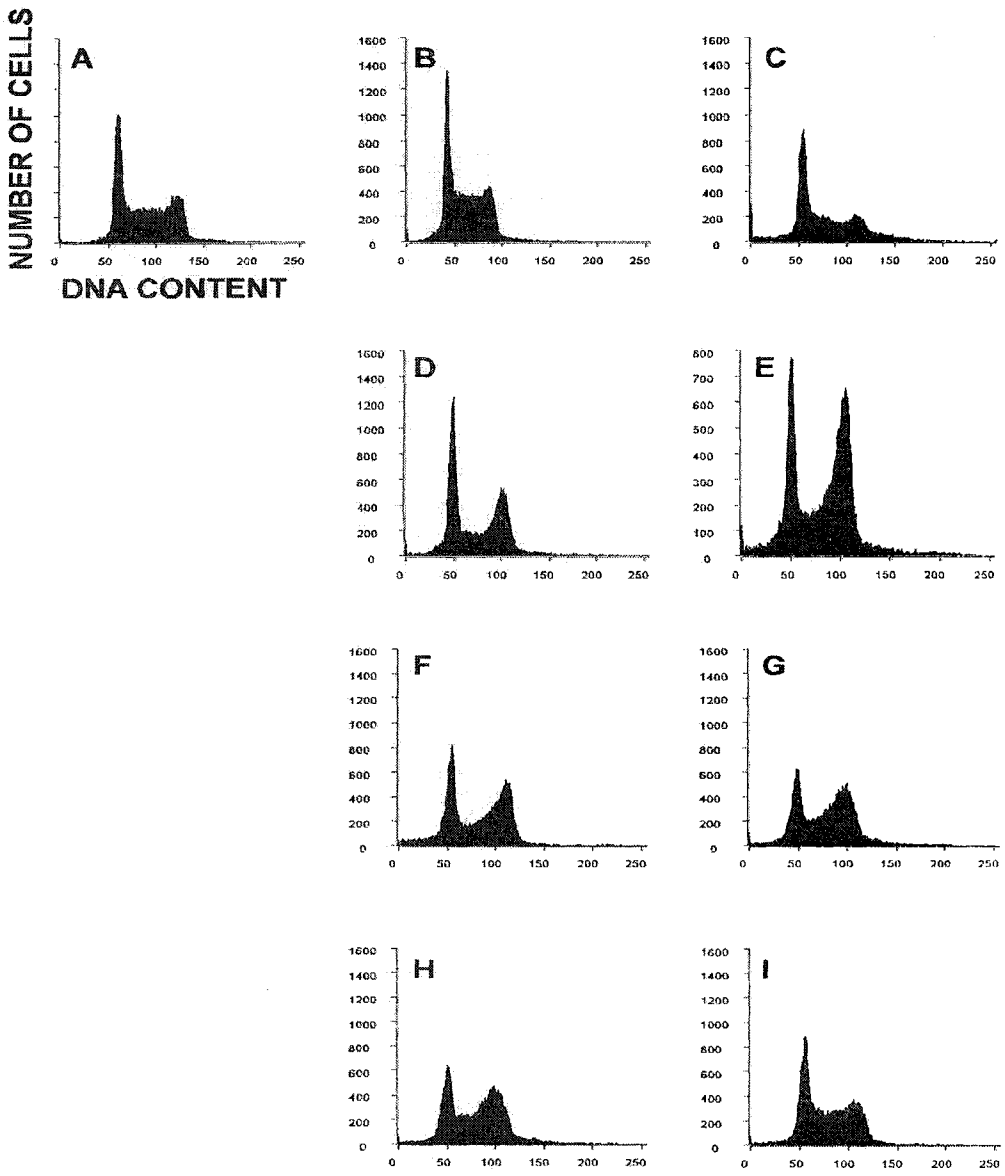

Figure 6.1 Cell cycle distributions of HL-60 cells 12 hr after heating at 45.0° C for various times. (A) control cells, (B) heated 5 min, (C) 10 min, (D) 15 min, (E) 20 min, (F) 30 min, (G) 40 min, (H) 45 min, (I) 60 min.

Reproduced with permission of the copyright owner. Further reproduction prohibited without permission.

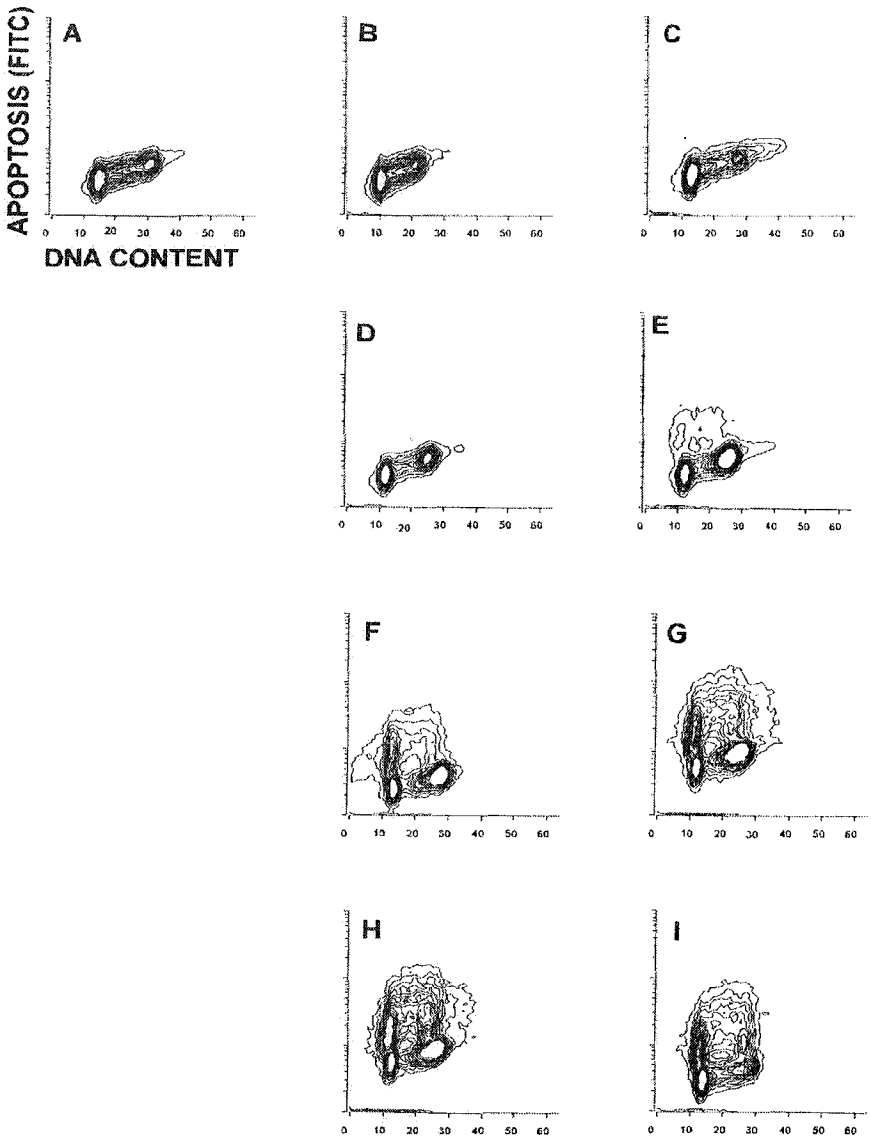

Figure 6.2 Dual parameter histograms of HL-60 cells showing apoptosis (FITC) and DNA content (PI) 12 hr after heating at 45.0° C for various times. (A) control cells, (B) heated 5 min, (C) 10 min, (D) 15 min, (E) 20 min, (F) 30 min, (G) 40 min, (H) 45 min, (I) 60 min.

Reproduced with permission of the copyright owner. Further reproduction prohibited without permission.

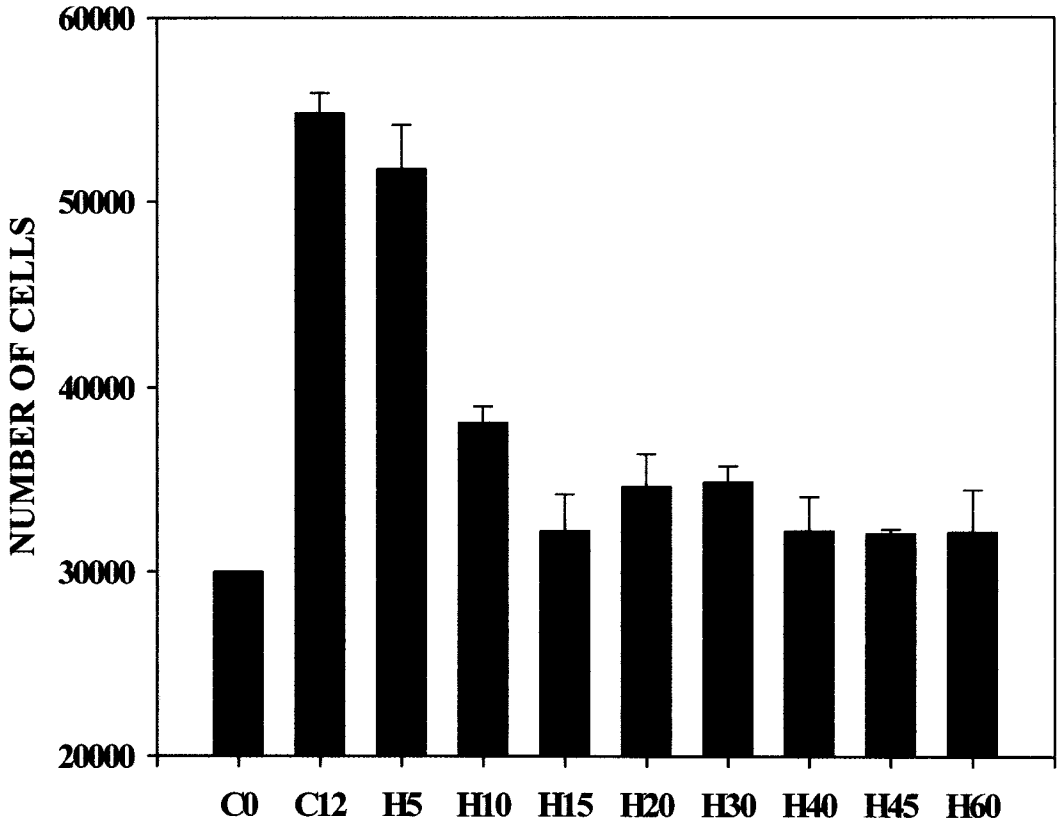

Figure 6.3 The growth of HL-60 cells 12 hr after various heating times at 45.0° C. The bars represent measured values with error bars representing ± one standard error. C0: Control cells at time 0 hr; C12: control cells after 12 hr; H5: 45.0° C heat shock for 5 min; H10: 10 min; H15: 15 min; H20: 20 min; H30: 30 min; H40: 40 min; H45: 45 min; H60: 60 min. These results are based on two or more different experiments.

Reproduced with permission of the copyright owner. Further reproduction prohibited without permission.

The number of apoptotic cells is determined using the Cicero data acquisition and display system software installed in a Coulter EPICS V cell sorter as well as Multi-2D® and Multicycle® software. To quantitatively describe the percentage of cells in each phase of the cell cycle after the different heat treatments shown in Fig. 6.1 and Fig. 6.2, the DNA histograms were analyzed with Multicycle® software. Because the DNA histograms include the apoptotic population, however, they cannot be analyzed directly to determine the fraction of cells in each cell cycle phase for the non-apoptotic cells. To quantitatively describe the cell cycle distribution of the non-apoptotic cells, a gate was drawn around the non-apoptotic population using Multi-2D® and the data within the gate were saved as a single parameter DNA histogram which could then be analyzed by Multicycle®. This analysis then gave the cell cycle distributions of the surviving (non-apoptotic) cells.

The number of non-apoptotic cells in each phase of the cell cycle for each heating time combination is shown in Fig. 6.4. The number of cells in G_1 phase increased as the heating time increased up to 15 min, decreased from 15-45 min and then remained low at 60 min. The number of cells in G_2/M phase increased up to 20 min and then decreased to 60 min. The number of cells in S phase decreased up to 40 min and then remained the same. From these results, it appears that apoptotic cells mainly come from S phase between 5 min and 20 min and from all cell cycle phases between 20 min and 60 min. This interpretation is complicated by the fact that there are also apparent cell cycle blocks. After 15 min at 45.0° C, cells blocked in G_1 and G_2/M phase and S phase decreased compared to control. After 40 to 60 min at 45.0° C, the number of non-apoptotic cells from every cell cycle phase decreased.

Reproduced with permission of the copyright owner. Further reproduction prohibited without permission.

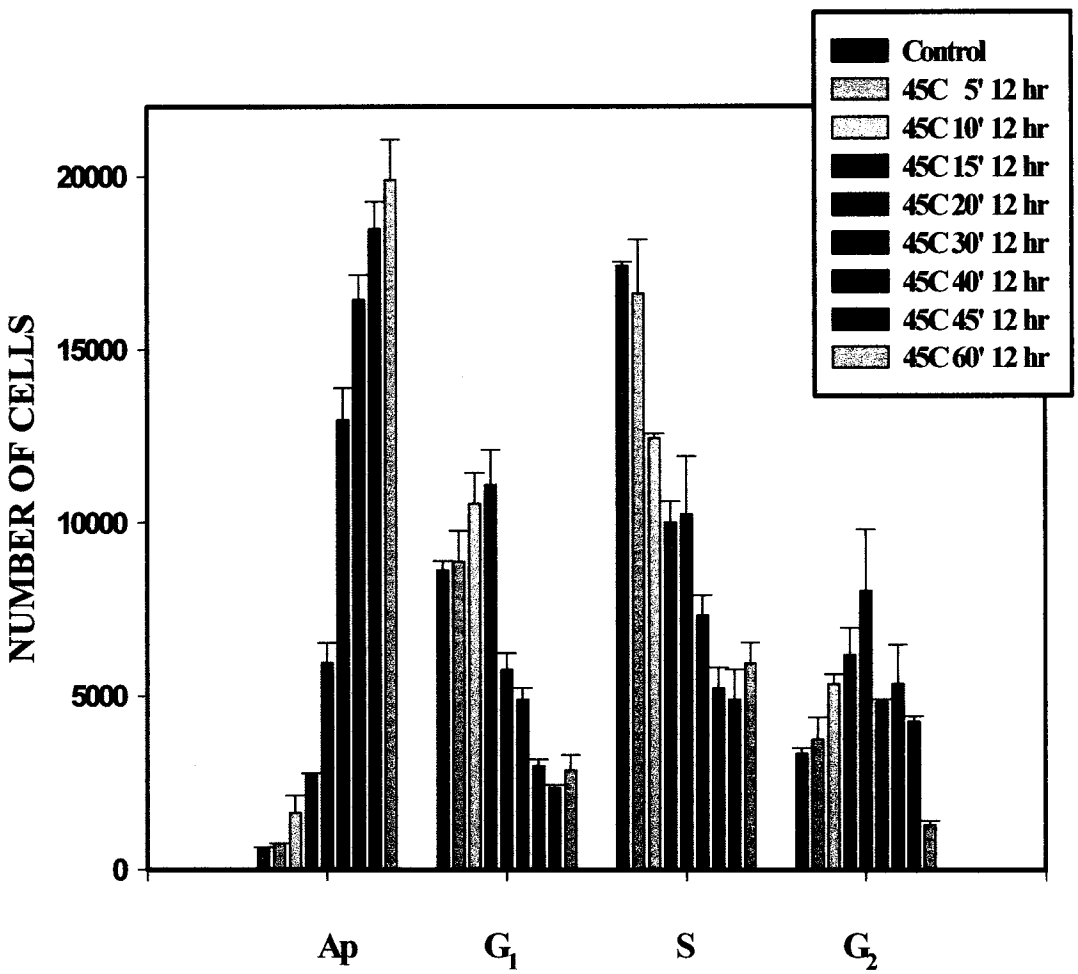

Figure 6.4 The number of non-apoptotic HL-60 cells in different cell cycle phases 12 hr after different heating times at 45.0° C heat shock. Control: untreated cells. The error bars represent standard error of the mean (SEM). These results are based on two or more different experiments.

Reproduced with permission of the copyright owner. Further reproduction prohibited without permission.

The number of apoptotic cells from a sample heated with different conditions is given in Fig. 6.5. The apoptotic population followed a sigmoid curve when the heating time increased. The early range between 5 min and 20 min shows lower rate due to the no accumulation of damage and the mid range between 20 min and 45 min shows the effective cell killing by apoptosis. When these data were transformed to surviving fraction, they showed an apoptosis-resistant population at 45 and 60 min heat shock. To better understand the kinetics of apoptotic cells, the number of apoptotic cells at various times following 45.0° C 15 and 30 min heat shock are shown in Fig. 6.6. The early increase in apoptosis would reach a higher level and the plateau would be maintained for a longer period of time as heating time increased.

The number of non-apoptotic G_1 phase cells increased over control G_1 cells at 12 hr after 5, 10 and 15 min heat shock at 45.0° C and decreased at longer heating times (Fig. 6.7). The number of non-apoptotic S phase cells decreased as the heating time increased at 45.0° C (Fig. 6.8). The number of non-apoptotic G_2/M phase cells increased after 5, 10, 15 and 20 min at 45.0° C, and decreased at longer heating times (Fig. 6.9).

To better understand the kinetics of non-apoptotic cells, the number of non-apoptotic G_1 cells at various times following 45.0° C 15 and 30 min heat shock are shown in Fig. 6.10. The longer the heating time, the larger the decrease in G_1 cells and the longer the time needed to return to control level. The number of non-apoptotic S phase cells at various times after heating for 15 or 30 min at 45.0° C is shown in Fig. 6.11. There was a rapid initial decrease followed by a plateau from 1-6 hrs after a 15 min 45.0° C heat shock and 4-9 hrs after a 30 min 45.0° C heat shock.

Reproduced with permission of the copyright owner. Further reproduction prohibited without permission.

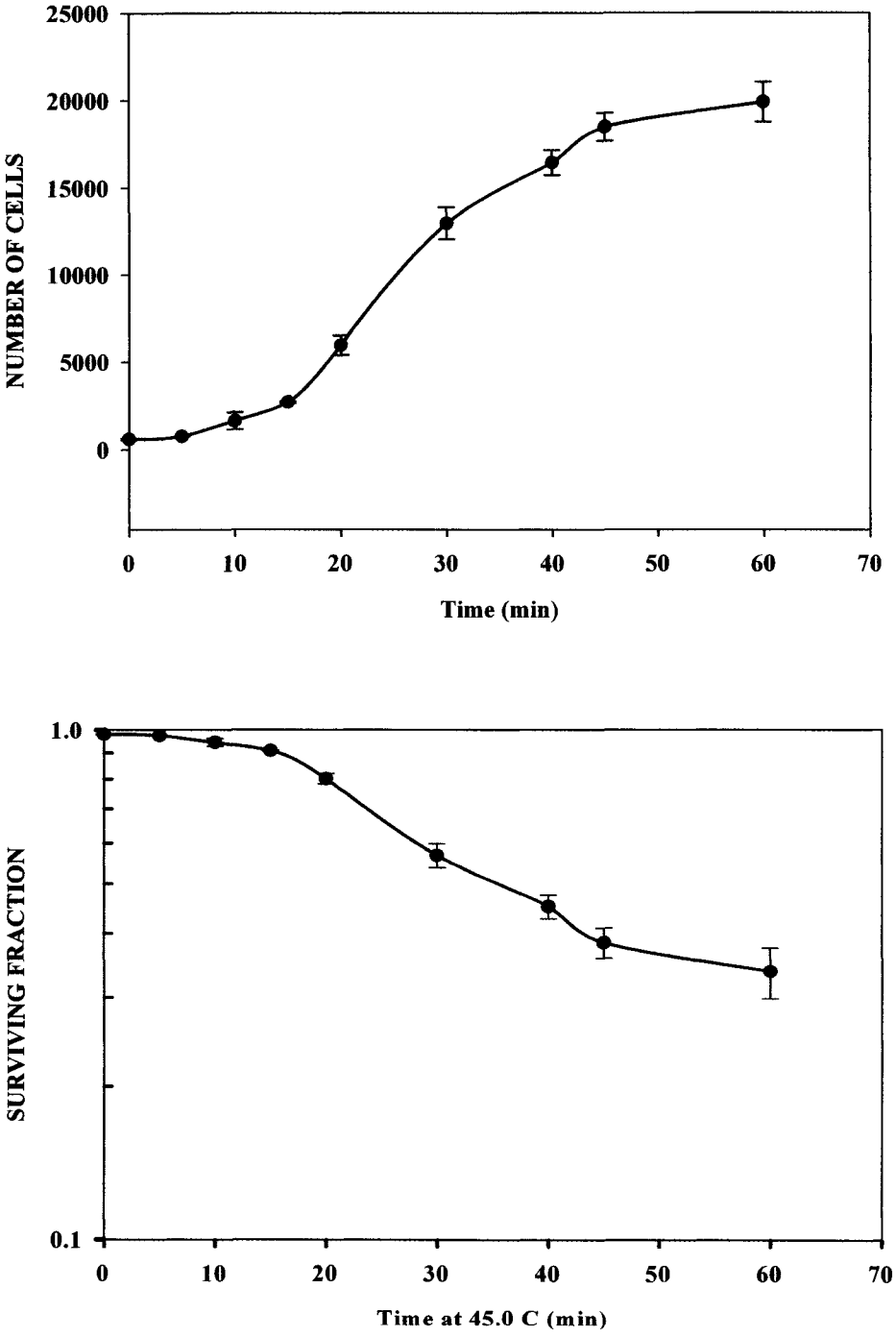

Figure 6.5 The number of apoptotic cells (top) and the survival (bottom) after various heating times at 45.0° C followed by 12 hr culture at 37° C. The results represent the mean values and standard error of the mean (SEM) from two or more independent experiments. 30,000 cells were analyzed at each time point.

Reproduced with permission of the copyright owner. Further reproduction prohibited without permission.

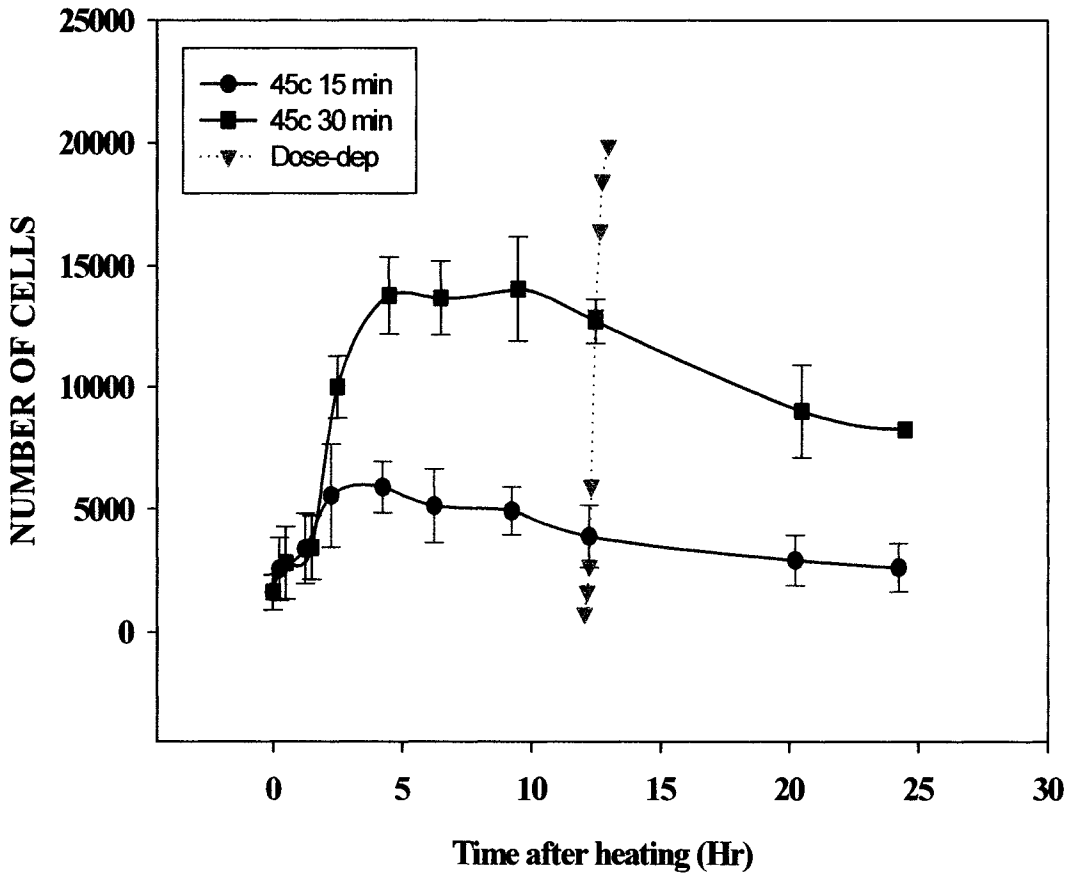

Figure 6.6 The number of apoptotic cells at various times after heating at 45.0° C for 15 min (•) or 30 min (■). Also shown for comparison are the numbers of apoptotic cells (▼) after 12 hr for 5, 10, 15, 20, 30, 40, 45 and 60 min heating at 45.0° C.

Reproduced with permission of the copyright owner. Further reproduction prohibited without permission.

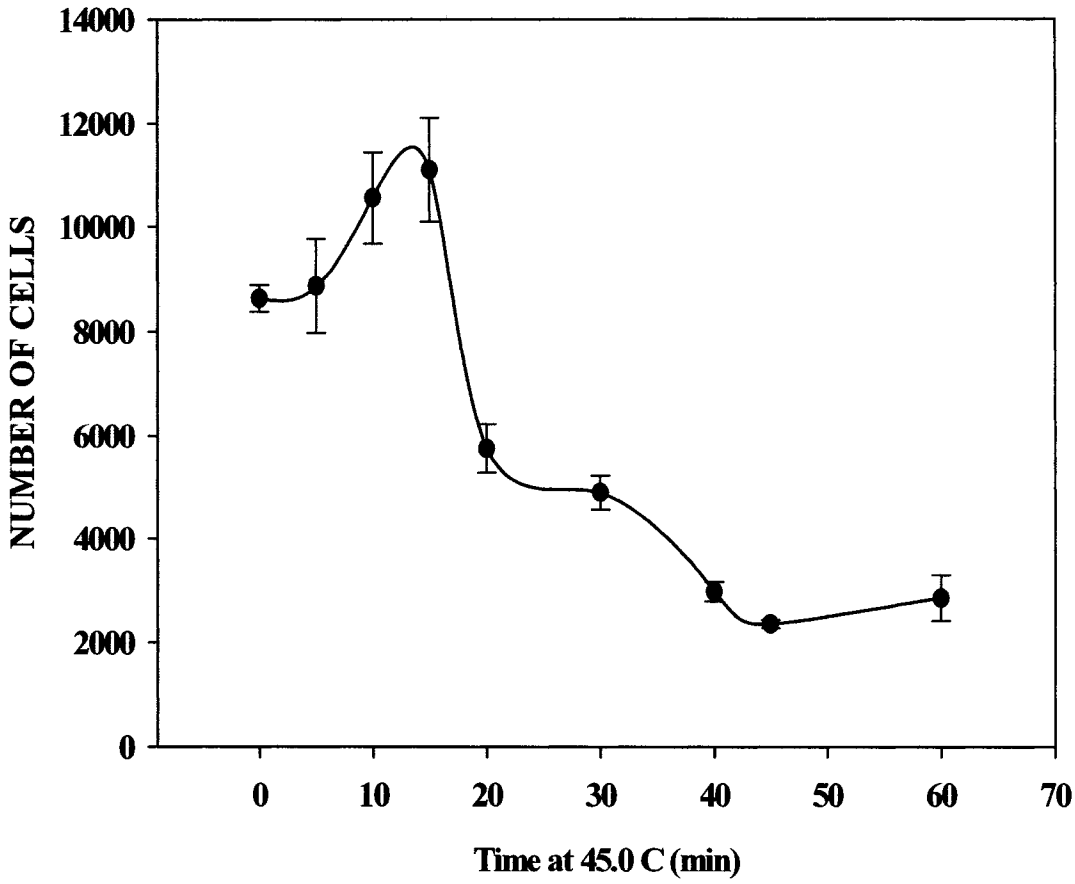

Figure 6.7 The number of non-apoptotic G_1 phase cells after various heating times at 45.0° C followed by 12 hr at 37° C. The results represent the mean values and standard error of the mean (SEM) from at least 2 independent experiments.

Reproduced with permission of the copyright owner. Further reproduction prohibited without permission.

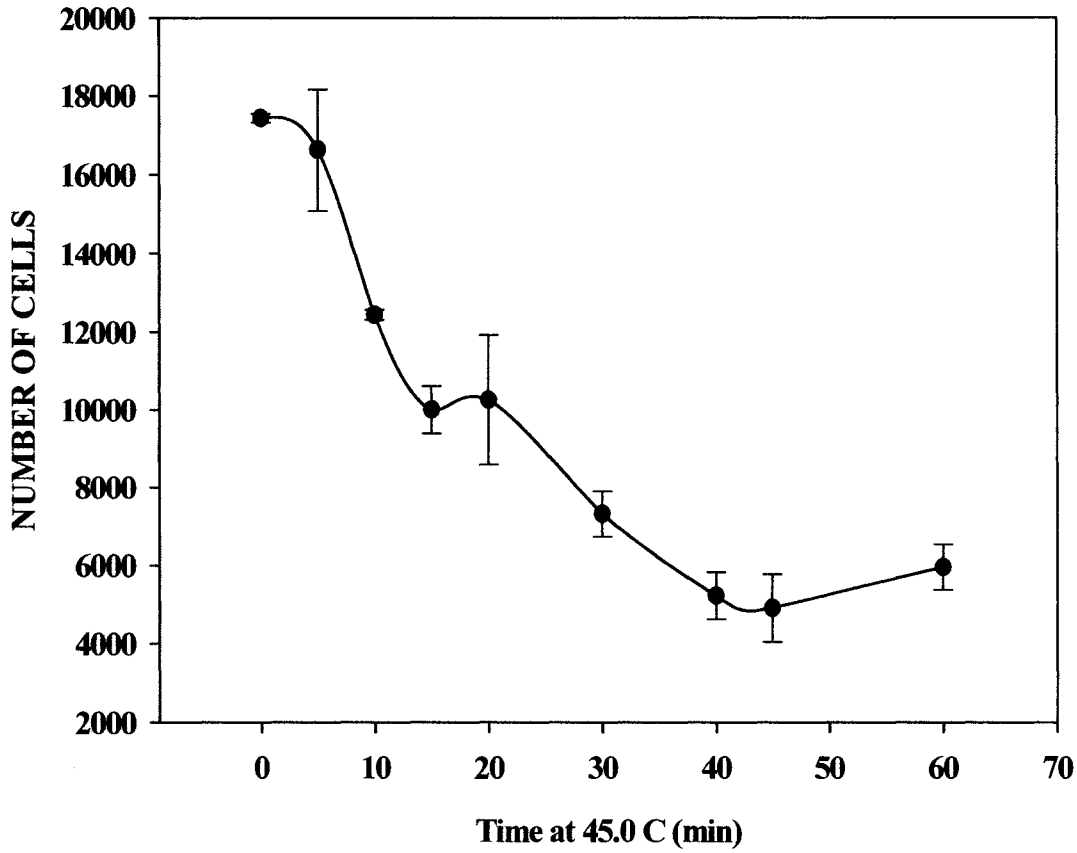

Figure 6.8 The number of non-apoptotic S phase cells after various heating times at 45.0° C followed by 12 hr at 37° C. The results represent the mean values and standard error of the mean (SEM) from at least 2 independent experiments.

Reproduced with permission of the copyright owner. Further reproduction prohibited without permission.

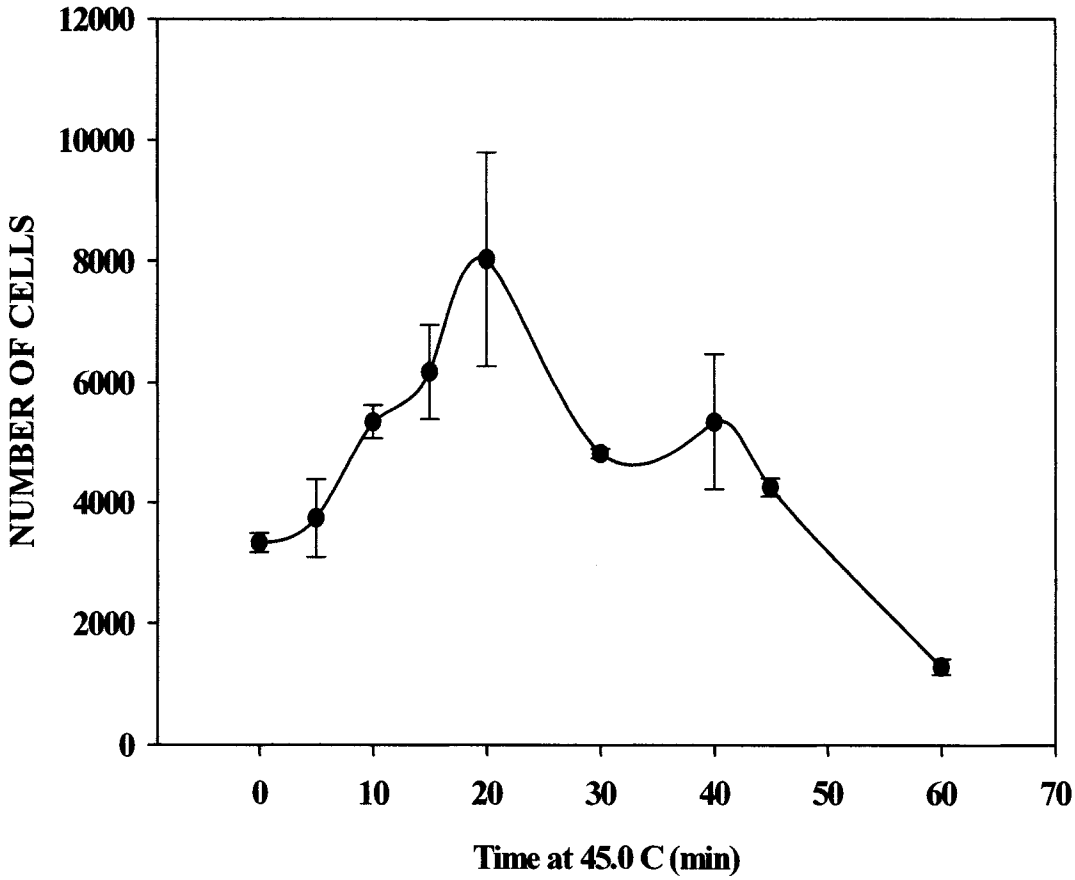

Figure 6.9 The number of non-apoptotic G_2/M phase cells after various heating times at 45.0° C followed by 12 hr at 37° C. The results represent the mean values and standard error of the mean (SEM) from at least 2 independent experiments.

Reproduced with permission of the copyright owner. Further reproduction prohibited without permission.

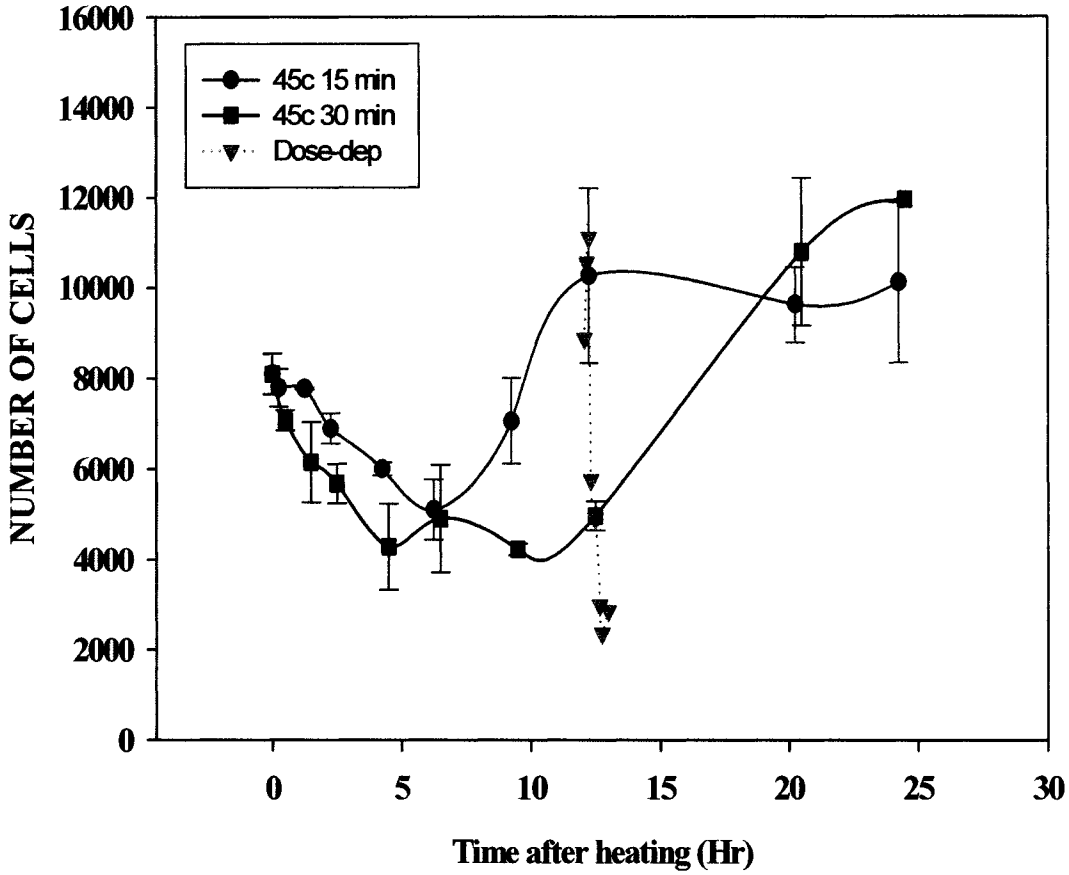

Figure 6.10 The number of non-apoptotic G_1 phase cells at various times after heating at 45.0° C for 15 min (•) or 30 min (■). Also shown for comparison are the numbers of non-apoptotic G_1 phase cells (▼) after 12 hr for 5, 10, 15, 20, 30, 40, 45 and 60 min heating at 45.0° C.

Reproduced with permission of the copyright owner. Further reproduction prohibited without permission.

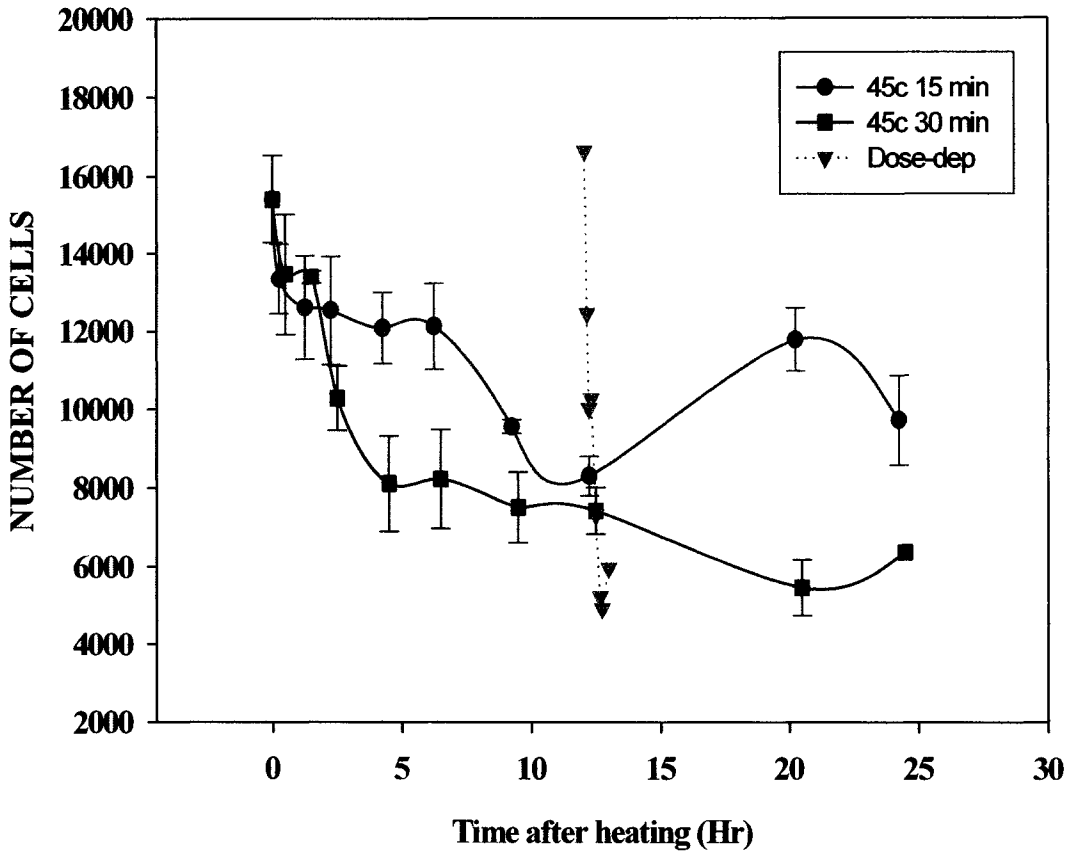

Figure 6.11 The number of non-apoptotic S phase cells at various times after heating at 45.0° C for 15 min (•) or 30 min (■). Also shown for comparison are the numbers of non-apoptotic S phase cells (▼) after 12 hr for 5, 10, 15, 20, 30, 40, 45 and 60 min heating at 45.0° C.

Reproduced with permission of the copyright owner. Further reproduction prohibited without permission.

The maximum decrease was dose-dependent. The number of non-apoptotic G_2/M cells oscillated in a dose-dependent manner with time after heating (Fig. 6.12).

Overall, a mild heat shock (45.0° C, 5-20 min) caused the accumulation of cells in G_1 and G_2/M phases after 12 hr at 37° C whereas a severe heat shock (45.0° C, 20-60 min) reduced the number of non-apoptotic cells in all phases because the apoptotic populations are increased. The fraction of apoptotic cells increased exponentially as expected based on survival curves as the heating time increased to 45 min at 45.0° C, though there was apparently a greater amount of necrosis and less apoptosis at 45.0° C for 60 min. This indicates that there may be at least two different transition points when the heat dose is increased up to necrotic-dominant point.

6.4 Discussion

In the previous results, hyperthermia induced the apoptotic population mainly from G_1 phase (2,5). In this study, hyperthermia induced apoptosis not only in G_1 phase but also S phase. These results also show that HL-60 cells are tightly blocked in G_1 and G_2/M phases. Even if S phase cells undergo apoptosis after a heat shock, it is not large enough to affect G_2 arrest like the etoposide results. This cell cycle arrest may permit DNA repair or renaturing for denatured protein prior to mitosis after mild heat shock. Apoptosis could be induced following a G_2/M block with prolonged culture. Cellular damage induced by higher doses of hyperthermia could trigger cell

Reproduced with permission of the copyright owner. Further reproduction prohibited without permission.

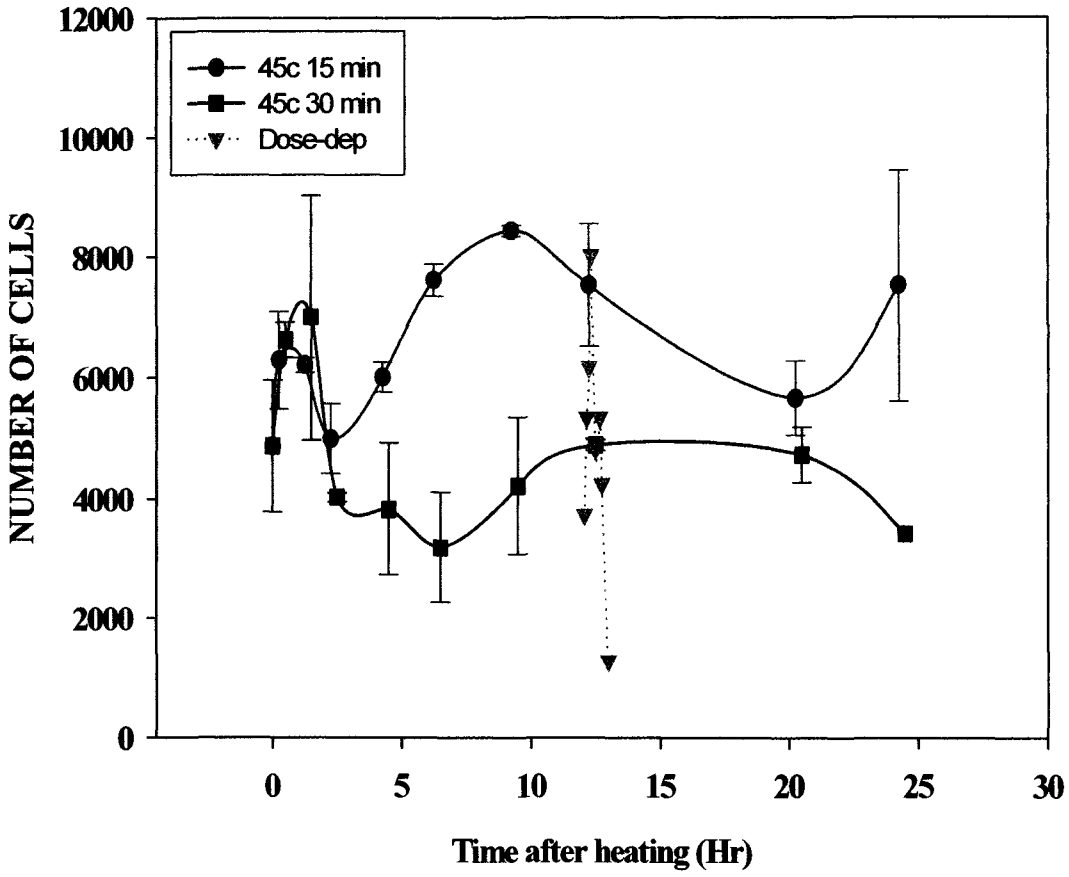

Figure 6.12 The number of non-apoptotic G_2/M phase cells at various times after heating at 45.0° C for 15 min (•) or 30 min (■). Also shown for comparison are the numbers of non-apoptotic G_2/M phase cells (▼) after 12 hr for 5, 10, 15, 20, 30, 40, 45 and 60 min heating at 45.0° C.

Reproduced with permission of the copyright owner. Further reproduction prohibited without permission.

suicide through apoptosis directly, without cell cycle arrest at G_2/M phase. The degree of the block and sensitivity to apoptosis could be changed based on the doses of heat and culture time.

The graph of AI as a function of heating time (Fig. 6.5) showed three regions: the first range between 5 min and 20 min shows lower rate due to the no accumulation of damage and the mid range between 20 min and 45 min shows the effective cell killing by apoptosis. When these data were transformed to surviving fraction, they showed an apoptosis-resistant population at 45 and 60 min heat shock.

The time-dependent changes of non-apoptotic cells showed similar patterns between mild and severe heat shocks. The pattern from severe heat shock was similar to the pattern of mild heat shock in all cell cycle phases but the changes were greater. Based on this concept, if a couple of time-dependent plots (45.0° C 15 and 30 min time-dependent non-apoptotic graphs) and a couple of data points (dose-dependent data at 45.0° C) were obtained, the non-apoptotic graph of different heating time could be estimated.

The apoptotic population came from S phase cells after mild heat shock and from all cell cycle phases after severe heat shock. These results indicate that there are significant changes in the response of cells after 15-30 min at 45.0° C, and after 45 min at 45.0° C. Between 15 and 30 min of heating there was a transition from cell cycle blocks to apoptosis in G_1 and S phase and a maximum cell cycle block in G_2/M phase. Between 45 and 60 min of heating there were significant changes in all cell

Reproduced with permission of the copyright owner. Further reproduction prohibited without permission.

cycle phases, probably representing a change in cell killing from apoptosis to necrosis or some other mode of cell death.

Reproduced with permission of the copyright owner. Further reproduction prohibited without permission.

Reference List

1. Barry MA, Behnke CA, Eastman A: Activation of programmed cell death (apoptosis) by cisplatin, other anticancer drugs, toxins, and hyperthermia. Biochem Pharmacol 40:2353-2362, 1990.

2. Del Bino G, Li X, Traganos F, Darzynkiewicz Z: Altered susceptibility of differentiating HL60 cells to apoptosis induced by antitumor drugs. Leukemia 8:281-288, 1994.

3. Dewey WC, Hopwood LE, Sapareto SA, Gerweck LE: Cellular responses to combinations of hyperthermia and radiation. Radiology 123:463-474, 1977.

4. Fairbairn JJ, Khan MW, Ward KJ, Loveridge BW, Fairbairn DW, O'Neill KL: Induction of apoptotic cell DNA fragmentation in human cells after treatment with hyperthermia. Cancer Lett 89:183-188, 1995.

5. Gorczyca W, Gong J, Ardelt B, Traganos F, Darzynkiewicz Z: The cell cycle related differences in susceptibility of HL-60 cells to apoptosis induced by various antitumor agents. Cancer Res 53:3186-3192, 1993.

6. Goto A, Shomori K, Ohkumo T, Tanaka F, Sato K, Ito H: Hyperthermia-induced apoptosis occurs both in a p53 gene-dependent and - independent manner in three human gastric carcinoma cell lines. Oncol Rep 6:335-339, 1999.

7. Hall EJ: Radiobiology for the Radiobiologist. 4th Edition. J.B. Lippencott Co., Philadelphia, PA, 1994.

8. Harmon BV, Corder AM, Collins RJ, Gobe GC, Allen J, Allan DJ, Kerr JFR: Cell death induced in a murine mastocytoma by 42-47° C heating in vitro: Evidence that the form of death changes from apoptosis to necrosis above a critical heat load. Int J Radiat Biol 58:845-858, 1990.

9. He L, Fox MH: Variation of heat shock protein 70 through the cell cycle in HL-60 cells and its relationship to apoptosis. Exp Cell Res 232:64-71, 1997.

10. Katschinski DM, Boos K, Schindler SG, Fandrey J: Pivotal role of reactive oxygen species as intracellular mediators of hyperthermia-induced apoptosis. J Biol Chem 275:21094-21098, 2000.

11. Li WX, Chen CH, Ling CC, Li GC: Apoptosis in heat-induced cell killing: The protective role of hsp70 and the sensitization effect of the c-*myc* gene. Radiat Res 145:324-330, 1996.

12. Nakano H, Kurihara K, Okamoto M, Tone S, Shinohara K: Heat-induced apoptosis and p53 in cultured mammalian cells. Int J Radiat Biol 71:519-529, 1997.

Reproduced with permission of the copyright owner. Further reproduction prohibited without permission.

13. Nishita M, Inoue S, Tsuda M, Tateda C, Miyashita T: Nuclear translocation and increased expression of Bax and disturbance in cell cycle progression without prominent apoptosis induced by hyperthermia. Exp Cell Res 244:357-366, 1998.

14. Pantazis P, Han Z, Wyche J: Schedule-dependent efficiency of thermochemotherapy in vitro with etoposide and heating at 43 degrees C. Anticancer Res 19:995-998, 1999.

15. Roti Roti JL, Turkel N: Heat-shock-induced changes in nuclear protein and cell killing in thermotolerant HeLa cells. Radiat Res 138:286-290, 1994.

16. Sellins K, Cohen JJ: Hyperthermia induces apoptosis in thymocytes. Radiat Res 126:88-95, 1991.

17. Shchepotin IB, Soldatenkov V, Buras RR, Nauta RJ, Shabahang M, Evans SRT: Apoptosis of human primary and metastatic colon adenocarcinoma cell lines *in vitro* induced by 5-fluorouracil, verapamil, and hyperthermia. Anticancer Res 14:1027-1032, 1994.

18. Takasu T, Lyons JC, Park HJ, Song CW: Apoptosis and perturbation of cell cycle progression in an acidic environment after hyperthermia. Cancer Res 58:2504-2508, 1998.

19. VanderWaal R, Thampy G, Wright WD, Roti Roti JL: Heat-induced modifications in the association of specific proteins with the nuclear matrix. Radiat Res 145:746-753, 1996.

20. Westra A, Dewey WC: Variation in sensitivity to heat shock during the cell-cycle of chinese hamster ovary cells in vitro. Int J Radiat Biol 19:467-477, 1971.

21. Yonezawa M, Otsuka T, Kato T, Moriyama A, Kato KH, Asai K, Matsui N: Hyperthermic induction of apoptosis in malignant fibrous histiocytoma cells: possible involvement of a p53-independent pathway in the induction of bax gene. J Orthop Sci 7:117-122, 2002.

22. Zamai L, Falcieri E, Zauli G, Cataldi A, Vitale M: Optimal detection of apoptosis by flow cytometry depends on cell morphology. Cytometry 14:891-897, 1993.

Reproduced with permission of the copyright owner. Further reproduction prohibited without permission.

CHAPTER 7

ANALYSIS OF CELL CYCLE DEPENDENT APOPTOSIS AND CELL CYCLE BLOCKS INDUCED BY ISO-DOSE HYPERTHERMIA IN HL-60 CELLS

7.1 Introduction

Cells that are heated to a few degrees above physiological temperatures (hyperthermia) undergo apoptosis (2,4,5,6,8,9,10,11,12,13,15,16,17,20,21). The slope of an Arrhenius plot of various levels of hyperthermia gives the activation energy of the chemical process involved in the cell killing. The similarity of the activation energy for protein denaturation to the activation energy for heat cytotoxicity, calculated from the Arrhenius analysis, led to the hypothesis that the target for heat cell killing may be protein. The structural chromosomal proteins, nuclear matrix, cytoskeleton repair enzymes and membrane components have all been identified as possible targets that are denatured by hyperthermia (3,7,14,18).

The effects of heat are primarily dependent on time of heating at a given temperature. The relationship between treatment time and temperature for a biological isoeffect (the Arrhenius plot) has been confirmed for a variety of normal tissues and tumors (19). A marked change of slope occurs somewhere between 42 °C

Reproduced with permission of the copyright owner. Further reproduction prohibited without permission.

and 43 °C (3). Above this transition temperature the slope is consistent for a variety of cells and tissues. For temperature above 43 °C, it is generally agreed that a 1 °C rise of temperature is equivalent to a reduction of time by a factor of 2 to give equal killing. For temperatures below the transition temperature an increase in temperature by 1 °C requires that time be decreased by a factor of 4 to 6 (3). Therefore, when defining thermal doses in hyperthermia studies, both the time and temperature of heating are equally important determinants.

In this study, cell cycle progression and apoptosis were monitored in heating with five different iso-dose temperature-time heat treatments in HL-60 cells. The number of apoptotic cells after treatment with heat shock was measured by the TUNEL assay and propidium iodide labeling using flow cytometry.

7.2 Materials and Methods

General information for the experiment was explained in Chapter 2 Materials and Methods. Detailed and specific explanations are provided in figure and table legends.

7.3 Hyperthermia-induced apoptosis with iso-dose heat shock

Previous studies have indicated that hyperthermia kills cells by apoptosis at temperatures below about 43-44° C but kills primarily by necrosis at higher temperatures (1,3,5,8,9,17). My goal in this set of experiments was to more closely

Reproduced with permission of the copyright owner. Further reproduction prohibited without permission.

analyze the relationship between increasing temperature and the induction of apoptosis. Arrhenius analysis of fibroblast cells heated at various temperatures for different times gives the activation energy of the chemical processes involved in cell killing from the slope of the curve (3). Arrhenius curves generally have a marked change of slope or breakpoint between 42° C and 43° C, which has been taken as evidence that there is a different mode of cell death at temperatures below this temperature than above it (7). The slopes of the Arrhenius curves indicate that, for temperatures above the breakpoint, heating time must be reduced by a factor of 2 for each 1° C increase in temperature to get equivalent cell killing. For temperatures below the transition temperature, an increase in temperature of 1° C requires that time be decreased by a factor of 4 to get equivalent cell killing. Based on the above information, I chose five different temperatures ranging from 42° to 46° C and reduced the heating times 2-fold for each 1° C increase in temperature. This should give an iso-dose at temperatures of 43° C and above and result in an equivalent number of apoptotic cells for each heat treatment. If apoptosis is reduced at higher temperatures, the number of apoptotic cells should be reduced at the higher temperatures.

HL60 cells were heated at various times and temperatures and then incubated at 37° C for 6 hr to allow apoptosis to develop. The presence of apoptotic cells was measured with the TUNEL method. Results from an experiment which illustrate the apoptotic population and cell cycle delays for different iso-dose heat treatments are shown in Figure 7.1. Small numbers of apoptotic cells are not shown in the dual-parameter histograms because the contour levels exclude them. It is apparent that the

Reproduced with permission of the copyright owner. Further reproduction prohibited without permission.

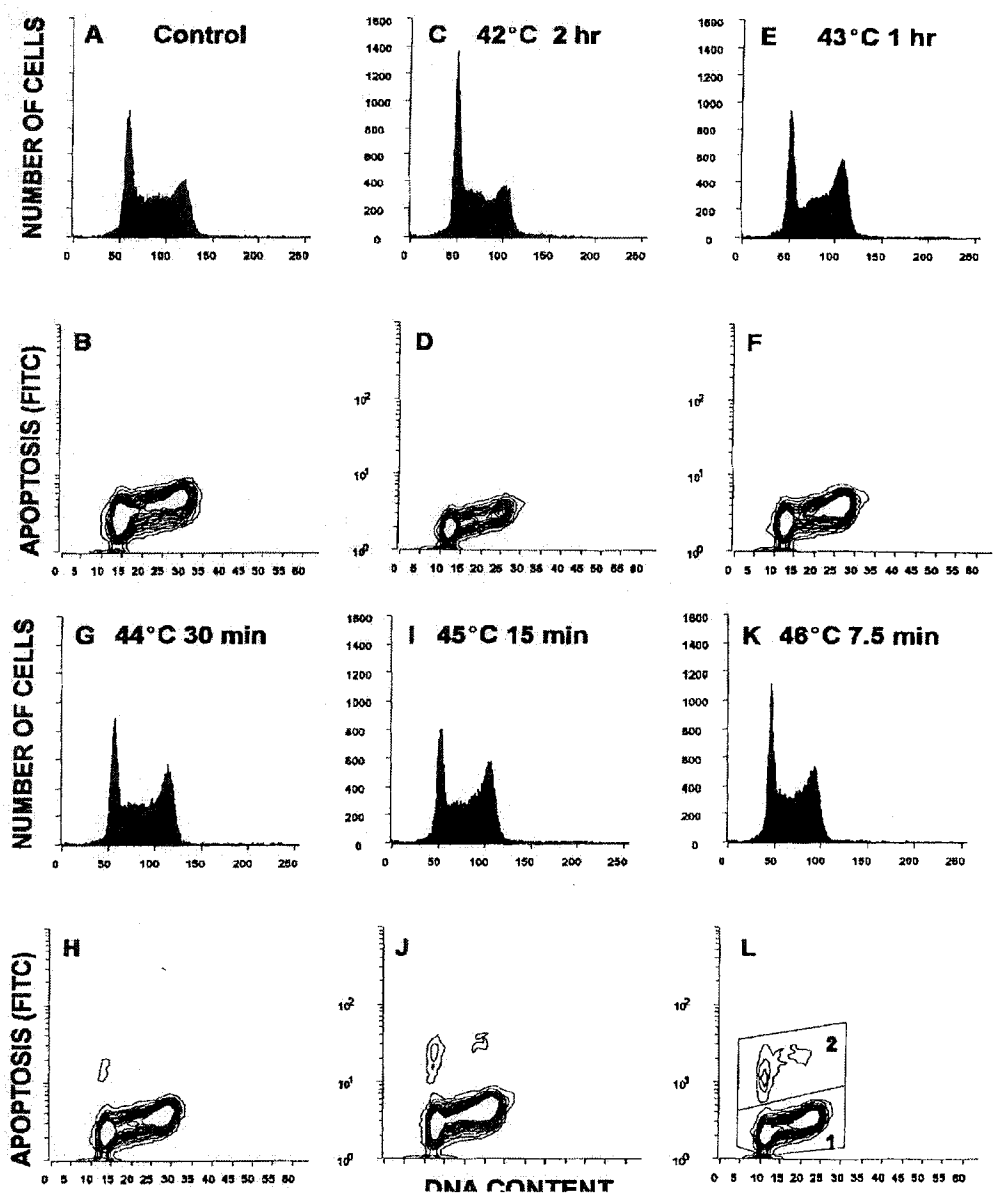

Figure 7.1 Cell cycle distributions and dual parameter histograms showing apoptosis (FITC) and DNA content (PI) for control and heated cells, (A and B) control cells (C and D) heated 2 hr at 42.0° C (E and F) heated 1 hr at 43.0° C (G and H) heated 30 min at 44.0° C (I and J) heated 15 min at 45.0° C (K and L) heated 7.5 min at 46.0° C. All samples were taken after 6 hr of incubation at 37° C.

Reproduced with permission of the copyright owner. Further reproduction prohibited without permission.

different heat treatments cause substantially different changes in the cell cycle distribution as well as in the apoptosis fraction.

The number of apoptotic cells in each sample were derived from the dual parameter histograms shown in Fig. 7.1. A region was drawn around the apoptotic population and the number of cells in the region was determined from the Cicero software (Region 2, Fig. 7.1L). The total number of cells for control and treated samples after treatment is shown in Fig. 7.2. All heat treatments inhibited cell growth though there was slight growth after 2 hr 42.0° C treatment.

The number of apoptotic cells were determined using the Cicero data acquisition and display system software installed in a Coulter EPICS V cell sorter as well as Multi-2D® and Multicycle® software. To quantitatively describe the percentage of cells in each phase of the cell cycle after the different heat treatments shown in Fig. 7.1, the DNA histograms were analyzed with Multicycle® software. Because the DNA histograms include the apoptotic population, however, they cannot be analyzed directly to determine the fraction of cells in each cell cycle phase for the non-apoptotic cells. To quantitatively describe the cell cycle distribution of the non-apoptotic cells, a gate was drawn around the non-apoptotic population using Multi-2D® and the data within the gate were saved as a single parameter DNA histogram which could then be analyzed by Multicycle®. This analysis then gave the cell cycle distributions of the surviving (non-apoptotic) cells.

The number of non-apoptotic cells in each phase of the cell cycle for each heating time-temperature combination is shown in Fig. 7.3. The number of cells in G_1 phase decreased up to 45.0° C and then increased. The number of cells in G_2/M phase

Reproduced with permission of the copyright owner. Further reproduction prohibited without permission.

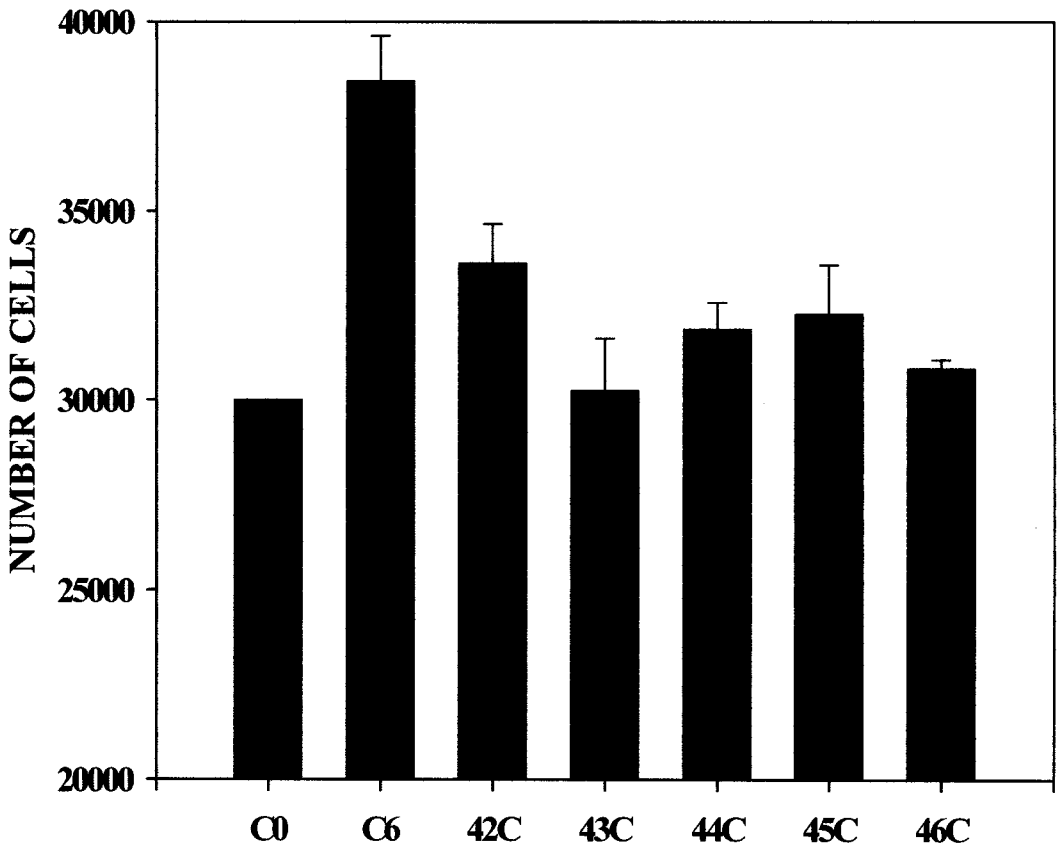

Figure 7.2 The change in cell number with different iso-dose heat shock treatments in HL-60 cells. Cells are counted at 6 hr after heat shock. The bars represent measured values with error bars representing ± one standard error. C0: Control cells at time 0 hr; C6: control cells after 6 hr; 42C: 42.0° C heat shock for 2 hrs; 43C: 43.0° C heat shock for 1 hr; 44C: 44.0° C heat shock for 30 min; 45C: 45.0° C heat shock for 15 min; 46C: 46.0° C heat shock for 7.5 min.

Reproduced with permission of the copyright owner. Further reproduction prohibited without permission.

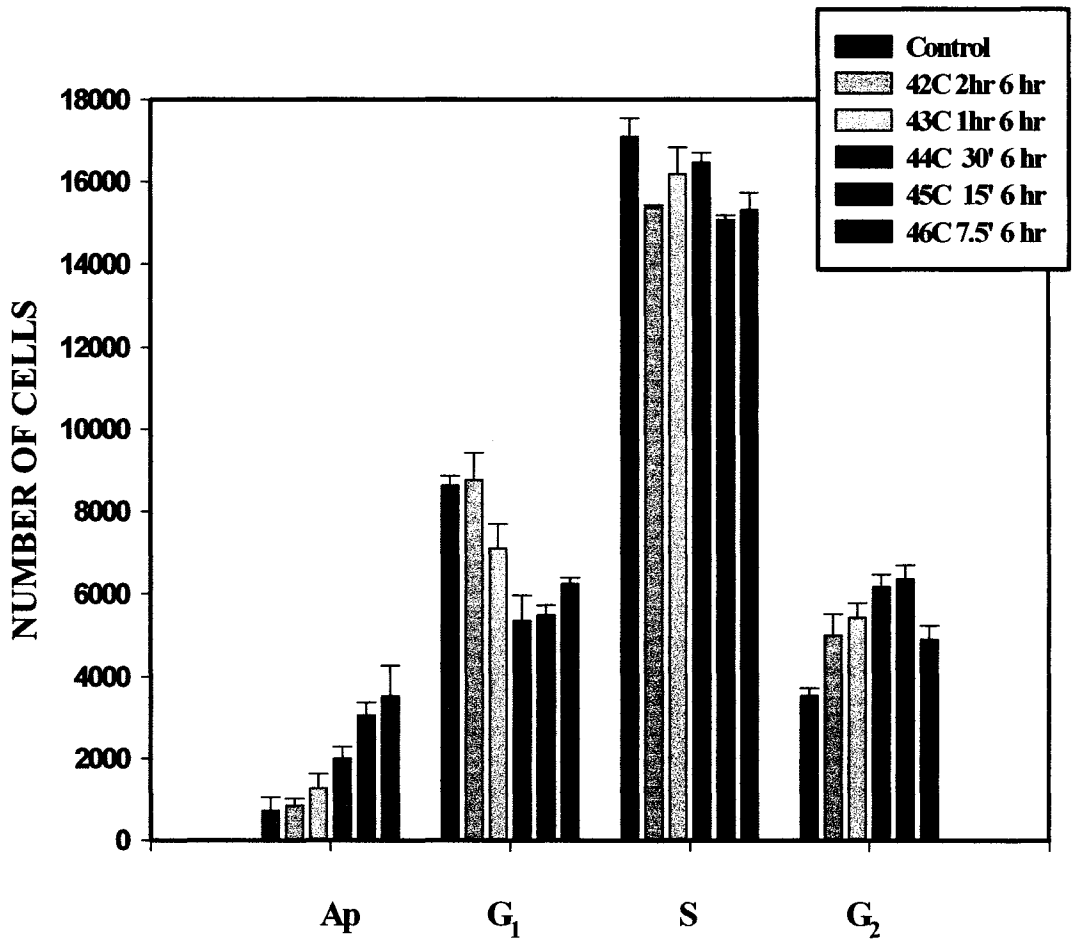

Figure 7.3 The number of non-apoptotic HL-60 cells in each cell cycle phase 6 hr after different heating time and temperature heat shocks. Control: untreated cells. The error bars represent standard error of the mean (SEM). These data are based on at least four independent experiments.

Reproduced with permission of the copyright owner. Further reproduction prohibited without permission.

increased up to 45.0° C and then decreased at 46.0° C. The number of cells in S phase decreased slightly after 43.0° and 44.0° C and decreased more after 42.0°, 45.0°, 46.0° C. From these results, it appears that apoptosis mainly occurs in G_1 cells at all temperatures and S phase at 45.0° and 46.0° C. This interpretation is complicated by the fact that there are also apparent cell cycle blocks. After all heat treatments, cells blocked in G_2/M phase.

The number of apoptotic cells from a sample heated with different time-temperature conditions is given in Fig. 7.4. A statistical comparison by t-test shows that there is no statistically significant difference in the number of apoptotic cells for heat treatments at 42.0° C for 2 hrs compared to control, but there is a significant difference between heating above 43.0° C for 1 hr. There is no statistically significant difference between 42.0° and 43.0° C, and between 45.0° and 46.0° C. Thus, in the apoptotic analysis of iso-dose heat shock, 44.0° C is a changing point. A multiple comparison method and pairwise analysis were used for the statistical difference between the treatments.

The results reported here do not support the initial hypothesis that HL60 cells would undergo apoptosis at temperatures of 43.0° C and below but undergo necrosis at temperatures above 43.0° C. Instead, the fraction of apoptotic cells continuously increased as the temperature increased to 46.0° C, though there was apparently a greater amount of necrosis and less apoptosis at 46.0° C. These results also show that HL-60 cells treated with all different combination of temperature/time are blocked in G_1 and G_2/M at 42.0° C, and G_2/M phase above 43.0° C. Previous studies have been done with fibroblast cells, thus it may not be surprising that our results differ from

Reproduced with permission of the copyright owner. Further reproduction prohibited without permission.

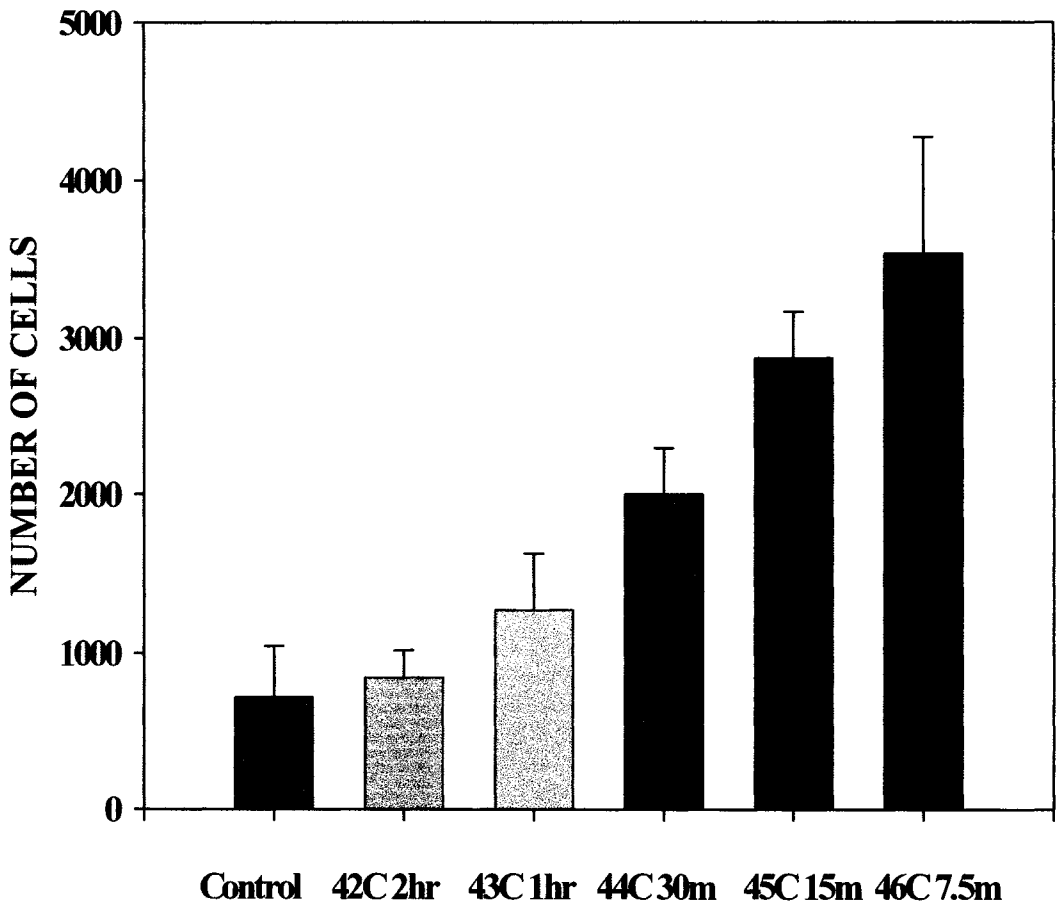

Figure 7.4 The number of apoptotic cells after various heating time-temperature combinations after 6 hr at 37° C. The results represent the mean and standard error of the mean (SEM) from at least 4 independent experiments. Control: untreated cells; 42C 2hr: 42° C heat shock for 2 hrs; 43C 1hr: 43° C heat shock for 1 hr; 44C 30m: 44° C heat shock for 30 min; 45C 15m: 45.0° C heat shock for 15 min; 46C 7.5m: 46° C heat shock for 7.5 min.

Reproduced with permission of the copyright owner. Further reproduction prohibited without permission.

those previously reported. These results also do not agree with the concept of isodose heat treatments based on Arrhenius plots. The times and temperatures chosen for these experiments were expected to give equivalent amounts of cell killing. While this was true for the iso-dose heat treatments with temperatures of 42.0 – 44.0° C, there was significantly greater cell killing at 45.0° C and 46.0° C. This indicates that there may be a different mechanism leading to apoptosis and necrosis at these higher temperatures.

7.4 Discussion

Arrhenius plots based on clonogenic survival data show the existence of a transition point in hyperthermia treatment. In iso-dose experiments reported here, a heat shock lower than 44.0° C (42.0° – 43.0° C) could cause repair process as a dominant phenomenon. The heat shock higher than 44.0° C (45.0° – 46.0° C) could cause apoptotic process as a dominant phenomenon. This idea could explain similar results from the first region of dose-dependent AI in Fig.6.5. Contrary to a transition point at 43.0° C for CHO cells (3), 44.0° C for 30 min is the changing point in HL-60 cells. Thus, because fibroblasts are more resistant to heat than cell lines of lymphoblast origin, HL-60 iso-dose time-temperature conditions have to be increased twice or more to get results similar to those obtained with fibroblasts (i.e., 44.0° C for 30 min to 44.0° C for 1 hr). The time-temperature conditions have to be chosen in the exponential region of the curve in Fig. 6.5. These data confirmed again the importance of proper time-temperature combinations for hyperthermia.

Reproduced with permission of the copyright owner. Further reproduction prohibited without permission.

Reference List

1. Allan DJ, Harmon BV: The morphologic categorization of cell death induced by mild hyperthermia and comparison with death induced by ionizing radiation and cytotoxic drugs. Scanning Electron Micosc Pt 3:1121-1133, 1986.

2. Barry MA, Behnke CA, Eastman A: Activation of programmed cell death (apoptosis) by cisplatin, other anticancer drugs, toxins, and hyperthermia. Biochem Pharmacol 40:2353-2362, 1990.

3. Dewey WC, Hopwood LE, Sapareto SA, Gerweck LE: Cellular responses to combinations of hyperthermia and radiation. Radiology 123:463-474, 1977.

4. Fairbairn JJ, Khan MW, Ward KJ, Loveridge BW, Fairbairn DW, O'Neill KL: Induction of apoptotic cell DNA fragmentation in human cells after treatment with hyperthermia. Cancer Lett 89:183-188, 1995.

5. Gorczyca W, Gong J, Ardelt B, Traganos F, Darzynkiewicz Z: The cell cycle related differences in susceptibility of HL-60 cells to apoptosis induced by various antitumor agents. Cancer Res 53:3186-3192, 1993.

6. Goto A, Shomori K, Ohkumo T, Tanaka F, Sato K, Ito H: Hyperthermia-induced apoptosis occurs both in a p53 gene-dependent and - independent manner in three human gastric carcinoma cell lines. Oncol Rep 6:335-339, 1999.

7. Hall EJ: Radiobiology for the Radiobiologist. 4th Edition. J.B. Lippencott Co., Philadelphia, PA, 1994.

8. Harmon BV, Corder AM, Collins RJ, Gobe GC, Allen J, Allan DJ, Kerr JFR: Cell death induced in a murine mastocytoma by 42-47° C heating in vitro: Evidence that the form of death changes from apoptosis to necrosis above a critical heat load. Int J Radiat Biol 58:845-858, 1990.

9. He L, Fox MH: Variation of heat shock protein 70 through the cell cycle in HL-60 cells and its relationship to apoptosis. Exp Cell Res 232:64-71, 1997.

10. Li WX, Chen CH, Ling CC, Li GC: Apoptosis in heat-induced cell killing: The protective role of hsp70 and the sensitization effect of the c-*myc* gene. Radiat Res 145:324-330, 1996.

11. Nakano H, Kurihara K, Okamoto M, Tone S, Shinohara K: Heat-induced apoptosis and p53 in cultured mammalian cells. Int J Radiat Biol 71:519-529, 1997.

12. Nishita M, Inoue S, Tsuda M, Tateda C, Miyashita T: Nuclear translocation and increased expression of Bax and disturbance in cell cycle progression without prominent apoptosis induced by hyperthermia. Exp Cell Res 244:357-366, 1998.

Reproduced with permission of the copyright owner. Further reproduction prohibited without permission.

13. Pantazis P, Han Z, Wyche J: Schedule-dependent efficiency of thermochemotherapy in vitro with etoposide and heating at 43 degrees C. Anticancer Res 19:995-998, 1999.

14. Roti Roti JL, Turkel N: Heat-shock-induced changes in nuclear protein and cell killing in thermotolerant HeLa cells. Radiat Res 138:286-290, 1994.

15. Sellins K, Cohen JJ: Hyperthermia induces apoptosis in thymocytes. Radiat Res 126:88-95, 1991.

16. Shchepotin IB, Soldatenkov V, Buras RR, Nauta RJ, Shabahang M, Evans SRT: Apoptosis of human primary and metastatic colon adenocarcinoma cell lines *in vitro* induced by 5-fluorouracil, verapamil, and hyperthermia. Anticancer Res 14:1027-1032, 1994.

17. Takasu T, Lyons JC, Park HJ, Song CW: Apoptosis and perturbation of cell cycle progression in an acidic environment after hyperthermia. Cancer Res 58:2504-2508, 1998.

18. VanderWaal R, Thampy G, Wright WD, Roti Roti JL: Heat-induced modifications in the association of specific proteins with the nuclear matrix. Radiat Res 145:746-753, 1996.

19. Westra A, Dewey WC: Variation in sensitivity to heat shock during the cell-cycle of chinese hamster ovary cells in vitro. Int J Radiat Biol 19:467-477, 1971.

20. Yonezawa M, Otsuka T, Kato T, Moriyama A, Kato KH, Asai K, Matsui N: Hyperthermic induction of apoptosis in malignant fibrous histiocytoma cells: possible involvement of a p53-independent pathway in the induction of bax gene. J Orthop Sci 7:117-122, 2002.

21. Zamai L, Falcieri E, Zauli G, Cataldi A, Vitale M: Optimal detection of apoptosis by flow cytometry depends on cell morphology. Cytometry 14:891-897, 1993.

Reproduced with permission of the copyright owner. Further reproduction prohibited without permission.

CHAPTER 8

Conclusions and Discussion

The development of assays to measure apoptosis has led to a great deal of research to understand its role in cancer therapy. Most approaches are limited to measuring the fraction of cells undergoing apoptosis at a given time, or the apoptotic index (AI). While the AI is valuable in assessing the outcome of therapy, since apoptosis is a kinetic event, this estimation of the fraction of apoptotic cells can be inaccurate and underestimated. Furthermore, each apoptotic assay can detect apoptotic cells only in specific time-window based on the specific detection method. The time window depends on the time of appearance of apoptotic cells after the inducing event and the length of time before apoptotic cells disintegrate in culture or are phagocytosed *in vivo*, or are no longer responsive to the specific assay. The cell type and apoptotic inducer also make the length of the time-window variable. Once the individual cells pass the specific time-window of the assay they are not counted as apoptotic cells. This underestimation of apoptosis is a critical disadvantage in interpreting apoptosis induction by therapeutic agents.

The estimation of the cumulative amount of apoptosis is much more valuable than apoptotic index for determining the effectiveness of therapy. A couple of methods

Reproduced with permission of the copyright owner. Further reproduction prohibited without permission.

have been used to acquire a more accurate estimation of the incidence of apoptosis. One is to halt the apoptotic disintegration process and the other is to calculate the disintegrated population. The purpose of both methods is to calculate the cumulative apoptotic index (CAI) (19,21). The fluorescent inhibitor of caspases (FLICA) FAM-VAD-FMK (2,20) was used to arrest cells in apoptosis, thereby preventing their disintegration or exit from the time-window of the assay (22). However, the FLICA assay has several disadvantages. First, the continuous existence of inhibitor can affect the kinetics of apoptosis induction, the cell cycle, and other cell signaling and metabolic activities. When cell cycle perturbations are analyzed along with apoptosis detection, the FLICA assay is not an appropriate method. Second, the FLICA assay is applicable only in the analysis of caspase-mediated apoptosis. Third, the existence of additional binding sites for FLICA could result in the overestimation of CAI. Fourth, this assay should be carefully tested for the proper concentration of FLICA to block the progression of apoptosis. In the second approach for CAI, a non-cycling cell line was used so there are no new cells resulting from cell division. Thus, the comparison of cell number before and after a treatment allows one to calculate the disintegrated cells and correct for them (19). This method is not good for cycling cells, though.

As the knowledge of genes involved in apoptosis grows, there is a need for new tools and models for evaluating therapy at the individual cell level with the change of status of multiple genes. Although DNA chip technology gives information on gene expression, the signal networking of these genes and overall cellular phenomena could not be analyzed with only chip technology. Moreover, a quantitative and mathematical analysis of the relationship between cell cycle specific apoptosis, CAI and cell cycle

Reproduced with permission of the copyright owner. Further reproduction prohibited without permission.

progression has not yet been developed. Such an analysis may be useful in studies exploring the cell cycle response to suppression of genes and therapeutic drugs. Cancer cells frequently abrogate cell cycle checkpoints while normal cells activate their checkpoints in response to DNA damaging agents. The differences between normal and cancer cells to a therapeutic treatment could be better understood with a new model. In the present study, I have developed three techniques; an 'apoptotic quotient calculation' to estimate the amount of apoptosis from each cell cycle phase, a 'CAI estimation model' to calculate the CAI using time course AI data, and a 'cell cycle progression model' to understand and evaluate apoptosis and its interaction with cell proliferation.

The apoptotic quotient calculation is for estimating how many apoptotic cells come from each cell cycle phase. This calculation is performed with Multi-2D® and Multicycle® software.

To overcome the disadvantages of FLICA and non-cycling cell assays for estimating the cumulative apoptotic index (CAI), as described above, I developed the CAI estimation model to estimate CAI by the kinetics of apoptosis. Based on measuring apoptotic index (AI) at multiple time points after a treatment, the kinetics of apoptosis can be explained as follows: First, the cells, which start apoptosis early, exit the time-window early (first in, first out). Second, the time-window (T_w) is a constant time in a given system. Third, the shape of the AI time-dependent graph is a guideline for how many phases of apoptosis exist. When the graph is symmetrical (the apoptotic induction rate (AIR_i) equals the exit rate from the time-window), apoptosis occurs in a uni-phasic manner. If not, it could bi- or multi-phasic. Fourth, the apoptotic induction rate (AIR_i) of each phase is calculated. Fifth, the length of each phase (T_i) is calculated.

Reproduced with permission of the copyright owner. Further reproduction prohibited without permission.

In order to obtain a comprehensive understanding of the effects of a treatment on apoptosis and cell cycle alterations, I developed a cell cycle progression model, which determined other important cell parameters. The number of cells counted at each time point, the amount of induced apoptotic cells at each time point by AI and CAI, and the change of cell number in each cell cycle phase between every time point were measured, analyzed, and calculated based on the explanation and equations in the Materials and Methods section (Chapter 2). A cell cycle progression model was used to calculate all constants and variables, including the number of apoptotic cells from each cell cycle phase, the existence of cell cycle blocks with cell cycle progression, and cell cycle-specific resistance or sensitivity to apoptosis. I defined several parameters for explaining the model, which are the *apoptotic quotient (ApQ)*, *apoptosis probability index (API)*, *efflux coefficient (EC)* and the degree of sensitivity. *ApQ* represents the amount of apoptosis for each cell cycle phase, *API* represents the number of apoptotic cells expected in each phase if the treatment is not cell cycle specific and *EC* represents the existence of blocks in cell cycle phases. When *EC* is negative, it represents a cell cycle block. The degree of sensitivity indicates whether specific cell cycle phases are sensitive or resistant to an apoptotic agent.

The results after a 6.25-μg/ml etoposide treatment for 3 hr reported in Chapter 3 support previous results that apoptotic HL-60 cells mainly came from S phase (77.9 % = S phase apoptosis/total apoptosis) (13). These results also show that HL-60 cells treated with 6.25-μg/ml etoposide for 3 hr are blocked in G_1 and G_2/M phases. G_1 arrest is greater than G_2/M arrest. G_2/M arrest is not large when compared to heat shock-induced G_2/M block, maybe due to the nature of S-phase specific topoisomerase-induced

Reproduced with permission of the copyright owner. Further reproduction prohibited without permission.

apoptosis. This cell cycle arrest may permit DNA repair prior to mitosis. It has been reported that a larger G_2 arrest results from a lower concentration of etoposide (6,10). Apoptosis could be induced following a G_2 block with prolonged drug-treatment time at relatively low drug-concentrations (6,10). DNA damage induced by higher doses of etoposide could trigger cell suicide through apoptosis directly, without cell progression to G_2. This phenomenon may be referred to as interphase cell death (23).

By comparing *ApQ* and *API*, G_1 and G_2/M phases in HL-60 cells are resistant to etoposide and the S phase cells are sensitive. This indicates that the major target of etoposide in the cell cycle is S phase. This observation is consistent with the increased sensitivity of S phase cells to etoposide reported in the literature (5,7,17).

Etoposide treatment of HCW-2 cells, an apoptotic resistant variant of HL-60 cells (14,15,16), gave an early S phase arrest, late G_1 phase arrest, continuous G_2/M phase block and increasing T_{pot}. After a 6.25-μg/ml, 3 hr etoposide treatment G_2/M arrest increased with time. Slow progression and large delays lead to a larger doubling time. The increased T_{pot} in etoposide-treated cells resulted from effects on cell cycle progression without apoptosis.

The major differences between the parental cell line (HL-60 cells) and mutant cell line (HCW-2 cells) after 6.25-μg/ml etoposide treatment for 3 hr are proliferation rate, fractions between cell cycle phases and cell progression. HL-60 cells showed more production of G_1 cells than HCW-2 cells when total number of cells is compared. Cell progression from S to G_2/M (β_2) and cell division (γ_2) in Table 3.3 showed big decreases with etoposide treatment when compared with control HCW-2 data in Table 3.2. HCW-2 cells, which did not produce apoptotic population, showed stronger G_2/M cell cycle arrest

Reproduced with permission of the copyright owner. Further reproduction prohibited without permission.

than HL-60 cells. Although HCW-2 cells do not undergo apoptosis because of their inability to release cytochrome C from mitochondria, HCW-2 cells would experience the same amount of DNA damage by etoposide as to HL-60 cells. Thus, HCW-2 cells have to repair the DNA damage to finish the cell cycle because HCW-2 cells are not able to get rid of these damaged cells by apoptosis. Severe DNA damage substantially delays exit from mitosis in many cell types. This arrest occurs during metaphase by spindle assembly checkpoint after the destruction of cyclin A, and it is independent of functional p53 pathway (18). Therefore, HCW-2 cells do need more time for repair and have a stronger G_2/M cell cycle arrest. Does this represent the gain of function for another cell cycle arrest relating gene, especially in the M phase checkpoint by etoposide treatment or the same cause with different results by nonfunctional apoptosis with the same cell cycle checkpoint gene functions?

A heat shock for 15 min at 45.0 °C produced 34.8 % cumulative apoptotic cells during 24 hr post-culture. Analysis by the model predicted four apoptotic phases: first, T_w equals 7, T_1 equals 3 and AIR_1 equals 4.5 % /hr; second, T_w equals 7, T_2 equals 3 and AIR_2 equals 2.8 % /hr; third, T_w equals 7, T_3 equals 3 and AIR_3 equals 2.4 % /hr; and fourth, T_w equals 7, T_4 equals 3 and AIR_4 equals 1.9 % /hr. Early apoptosis come from G_2/M phase. This apoptosis is caused by disruption of microtubular proteins (4). Second apoptosis from G_1 phase is caused by cells in division at the time of heating, which entered G_1 without completing division. Apoptotic population from early S phase has less time available for the repair of DNA damage before entering into the S phase without p53 (24), which leads to problems during replication and causes some kind of interphase

Reproduced with permission of the copyright owner. Further reproduction prohibited without permission.

death (25). Apoptosis from G_2/M phase after 20 hr comes from cell cycle block with damaged slow moving cells.

A heat shock for 30 min at 45.0° C produced 93.6 % cumulative apoptotic cells during 24 hr post-culture. The model predicted three apoptotic phases: first, T_w equals 10, T_1 equals 4 and AIR_1 equals 9.9 % /hr; second, T_w equals 10, T_2 equals 4 and AIR_2 equals 7.5 % /hr; and third, T_w equals 10, T_3 equals 4 and AIR_3 equals 6.0 % /hr. When heating time was increased from 15 min to 30 min, CAI increased 2.69 times (34.8 to 93.6 %), T_w increased from 7 hr to 10 hr and T_i increased from 3 hr to 4 hr. Early apoptosis come from S and G_2/M phase. This apoptosis is caused by direct damage of cellular proteins for DNA replication machinery and mitosis. Later apoptosis from all cell cycle phases is caused by undivided cells in G_1, S phase cells with unrepaired DNA damage (25), and disruption of microtubular proteins in G_2/M phase cells (4). Third apoptosis comes from G_1 and S phases. Cellular damage induced by higher doses of hyperthermia could trigger cell suicide through apoptosis directly, without cell cycle arrest at G_2/M phase (9). After the cells with heavy damage are removed the remaining cells appears to follow the 45.0°C for 15 min heat shock response. The degree of the block and sensitivity to apoptosis could be changed based on the doses of heat and culture time.

The CAI estimation model revealed important new information about the induction of apoptosis by hyperthermia. When the heat dose was increased from 15 to 30 min, CAI, T_w and T_i were also increased. The increase in CAI and T_i with a larger heat dose resulted in the production of more apoptotic cells and an increase in T_w, which means that the substrate for the assay existed longer for a greater heat shock.

Reproduced with permission of the copyright owner. Further reproduction prohibited without permission.

The analysis also demonstrated that apoptosis developed in several phases with different induction rates, and the AIR_i decreased as the phase number increased. Apoptotic cells in the first phase could be a subpopulation of cells sensitive to the specific treatment. For example, S phase cells are sensitive to topoisomerase inhibitors (e.g., camptothecin and etoposide) as well as hyperthermia (8). After the sensitive population underwent apoptosis, the next phase of apoptotic cells could be dependent on several factors, including when damaged cells passed a cell cycle checkpoint after a single treatment (e.g., irradiation with post-culture) or when healthy cells progressed into a sensitive cell cycle phase during continuous treatment (e.g., continuous culture with drugs). Thus, there is a gap between the phases, and the CAI curve increased step-wise instead of continuously. Both continuously increasing and step-wise increasing CAI curves have been reported with FLICA experiments (21).

The CAI estimation model has several advantages when it is applied to different systems and cell line for understanding the kinetics and responses to the treatment. First, it gives the cumulative information. Second, CAI could also estimate the kinetics of disintegration of apoptotic cells, but the starting point of disintegration could not be determined with our data. Previous approaches for calculating the disintegration of apoptotic cells were done in non-cycling cell population (19). Computerized video time-lapse microscopy can be used for determining the initiating point of disintegration (9,11,12). If one time-window is greater and includes the other time-window, that time-window could include part of the cumulative apoptosis from the other time-window. For example, the loss of membrane integrity is very late step (9,11,12) and could happen just before disintegration of apoptotic cells. Thus, the time-window for membrane integrity

Reproduced with permission of the copyright owner. Further reproduction prohibited without permission.

measured by dye exclusion is greater than the time-window for other assays such as TUNEL. Third, when CAI is compared with clonogenic survival, it should give a much better agreement than comparing AI with clonogenic survival. The existence of non-apoptotic death, or necrotic death by insult could be inferred by a disagreement of CAI and clonogenic survival. Fourth, this model could also be applied to different types of time-lapse data for calculation of cumulative results (i.e., cumulative protein expression and cumulative mutation frequency, etc). In detail, when a particular cyclin is measured with flow cytometry, the cumulative number of cells which express cyclin could be calculated. This calculation could provide information on the fraction of cycling cells in the population. Moreover, the model could analyze how long a specific protein is active or functional and the cumulative amount of protein expression. Finally, this model is not limited to certain cell lines and assays, does not need special treatment to culture, and does not affect the assays, which other assays could do.

The apoptotic population with dose-dependent heating at 45.0° C followed a sigmoid curve when the heating time increased. A mild heat shock (45.0° C, 5-20 min) caused the accumulation of cells in G_1 and G_2/M phases after 12 hr at 37° C whereas a severe heat shock (45.0° C, 20-60 min) reduced the number of non-apoptotic cells in all phases because apoptotic population are increased. The apoptotic population came from S phase cells after mild heat shock and from all cell cycle phases after severe heat shock. These results indicate that there are significant changes in the response of cells after 15-30 min at 45.0° C, and after 45 min at 45.0° C. Between 15 and 30 min of heating there was a transition from cell cycle blocks to apoptosis in G_1 and S phase and a maximum cell cycle block in G_2/M phase. Between 45 and 60 min of heating there were significant

Reproduced with permission of the copyright owner. Further reproduction prohibited without permission.

changes in all cell cycle phases, probably representing a change in cell killing from apoptosis to necrosis or some other mode of cell death.

In iso-dose experiment a statistical comparison by t-test shows that there was no statistically significant difference in the number of apoptotic cells for heat treatments at 42.0° C for 2 hrs and control, but there was a significant difference between heating above 43.0° C for 1 hr and control. There was no statistically significant difference between 42.0° and 43.0° C, and between 45.0° and 46° C. Thus, in the apoptotic analysis of iso-dose heat shock, 44° C is a changing point. Heat shock lower than 44.0° C (42.0° – 43.0° C) could cause repair as a dominant phenomenon. Heat shock higher than 44.0° C (45.0° – 46.0° C) could cause apoptosis as a dominant phenomenon. Contrary to changing point (43.0° C) of CHO cells (8), 44.0° C for 30 min is the changing point in HL-60 cells. This difference might come from different assay and different cell line. Because fibroblasts are more resistant to heat than lymphoblast cell lines, my iso-dose time-temperature conditions had to be increased twice or more to get similar results as for fibroblast (i.e., 44.0° C for 30 min to 44.0° C for 1 hr). If the time-temperature conditions are chosen in exponential area of the curve in Fig. 6.5, the results would show the different changing time-temperature combination. These data confirmed again the importance of proper time-temperature combinations for hyperthermia. Moreover, apoptosis also show the changing point of iso-dose hyperthermia.

Several advantages are suggested when *'cell cycle progression model'* is applied to different system and cell line for understanding the cell cycle and cell responses to the treatment. First, if any apoptotic-labeling assay could be used with bivariate histograms

Reproduced with permission of the copyright owner. Further reproduction prohibited without permission.

and paraformaldehyde fixation using flow cytometry, this model could provide much cell cycle information. For example, data from a fluorescent inhibitor of caspases (FLICA) FAM-VAD-FMK assay with paraformaldehyde fixation could be used with this model (21). Also, data from Bax labeling for translocation to mitochondria could be used (1). The sub-G_1 apoptotic assay is used for measuring apoptosis by univariate DNA histograms based on the loss of low molecular weight DNA during the apoptosis. However, this method has a problem for accurately measuring apoptosis. When the permeabilization step shows the sub-G_1 peak, the apoptotic cells shift to lower DNA content because of loss of DNA. If all cell cycle phases undergo apoptosis, the apoptotic population from G_2/M phase could overlap with G_1 peak, thus underestimating the apoptotic cell number. Thus, sub-G_1 method can be used only for detecting an apoptotic population qualitatively. Unlike univariate histograms, bivariate histograms could give more data (apoptotic and non-apoptotic populations) and no overlapping results. If the cells could be labeled with an apoptosis-specific antibody and produce bivariate data from flow cytometry, *'cell cycle progression model'* could be applied. Second, *'cell cycle progression model'* is unlike any other previous model using exponential growth population and mathematics because *'cell cycle progression model'* is calculated by actual flow cytometry data. By using 9 measured parameters (N_0, N_t, Ap, A_0, B_0, C_0, A_t, B_t *and* C_t), 15 parameters (*ApQ* (α_1, β_1 *and* γ_1), *API* (G_1, *S and* G_2), α_2, β_2, γ_2, α_3, β_3, γ_3, EC_{G1}, EC_S *and* $EC_{G2/M}$) could be calculated with all equations in Materials and Methods. The third advantage is the analysis of differences between the normal and cancer cells. A strategy designed to protect normal cells from cycle-dependent lethal agents by exploiting differences in cell cycles of normal and cancer cells is applied for cancer

Reproduced with permission of the copyright owner. Further reproduction prohibited without permission.

therapy. In the combination of pretreatment and post-treatment, such pretreatment prevents normal cells from entering S or M phase and thus protect them against S-phase- and M-phase-specific agents. For the selective protection of normal cells, several mechanism should be considered as follows; i) loss of p53-dependent checkpoints, ii) growth factor-activated pathways, iii) CDK inhibitors, and iv) drug resistance (3). Toxicity to normal cells is unavoidable if drugs do not have a highly specific cancer cell target. When the differences between normal and cancer cells are maximized with *'cell cycle progression model'*, the side effects are minimized and better tumor control could be achieved. The fourth advantage is that *'cell cycle progression model'* can be used as a searching tool for a new cell cycle regulating proteins. The data from cell cycle blocks and progression could be a good guide in searching for possible candidate by narrowing down the possibility and a good help for selecting genes when DNA array is designed. For example, if a G_1 cell cycle block was detected in a p53 mutant cell line, it indicates the probable existence of a G_1 related checkpoint protein other than p53 after treatment. Fifth, in the reverse way, the effect with gene-knockout or gene-interference by SiRNA treatment and inhibition of a group of cell cycle regulating member could be assayed and the changes in cell cycle arrest and progression could be calculated by *'cell cycle progression model'*. This study could be extended to an analysis of cell cycle progression and apoptosis changes in mutants, and could help to understand the molecular basis of cell cycle and apoptosis interactions by diverse mutations in genes regulating cell cycle and apoptosis. Although our model is not strong enough to explain all the questions for understanding cell cycle phenomena, *'cell cycle progression model'* could be a good

Reproduced with permission of the copyright owner. Further reproduction prohibited without permission.

system for explaining cell cycle progression, arrest and cell cycle-specific apoptosis, and mechanism-based therapeutics for better cancer treatment.

A possible problem could be suggested when *'cell cycle progression model'* is applied to different systems. Prolonged cultures could have an undetectable necrotic population. It indicates the probability of underestimation of cell death population. This problem could be solved with the help of necrotic cell detection methods, such as annexin-V assay and FLICA assay if cells undergo caspase-mediated apoptosis (21) and computerized video time-lapse microscopy (9,11,12).

Reproduced with permission of the copyright owner. Further reproduction prohibited without permission.

Reference List

1. Bedner E, Li X, Kunicki J, Darzynkiewicz Z: Translocation of Bax to mitochondria during apoptosis measured by laser scanning cytometry. Cytometry 41:83-88, 2000.

2. Bedner E, Smolewski P, Amstad P, Darzynkiewicz Z: Activation of caspases measured in situ by binding of fluorochrome- labeled inhibitors of caspases (FLICA): correlation with DNA fragmentation. Exp Cell Res 259:308-313, 2000.

3. Blagosklonny MV, Pardee AB: Exploiting cancer cell cycling for selective protection of normal cells. Cancer Res 61:4301-4305, 2001.

4. Coss RA, Dewey WC, Bamburg JR: Effects of hyperthermia on dividing Chinese hamster ovary cells and on microtubules in vitro. Cancer Res 42:1059-1071, 1982.

5. Del Bino G, Darzynkiewicz Z: Camptothecin, teniposide, or 4'-(9-acridinylamino)-3-methanesulfon-m- anisidide, but not mitoxantrone or doxorubicin, induces degradation of nuclear DNA in the S phase of HL-60 cells. Cancer Res 51:1165-1169, 1991.

6. Del Bino G, Skierski JS, Darzynkiewicz Z: The concentration-dependent diversity of effects of DNA topoisomerase I and II inhibitors on the cell cycle of HL-60 cells. Exp Cell Res 195:485-491, 1991.

7. Deptala A, Li X, Bedner E, Cheng W, Traganos F, Darzynkiewicz Z: Differences in induction of p53, p21WAF1 and apoptosis in relation to cell cycle phase of MCF-7 cells treated with camptothecin. Int J Oncol 15:861-871, 1999.

8. Dewey WC, Hopwood LE, Sapareto SA, Gerweck LE: Cellular responses to combinations of hyperthermia and radiation. Radiology 123:463-474, 1977.

9. Endlich B, Radford IR, Forrester HB, Dewey WC: Computerized video time-lapse microscopy studies of ionizing radiation- induced rapid-interphase and mitosis-related apoptosis in lymphoid cells. Radiat Res 153:36-48, 2000.

10. Facompre M, Wattez N, Kluza J, Lansiaux A, Bailly C: Relationship between cell cycle changes and variations of the mitochondrial membrane potential induced by etoposide. Mol Cell Biol Res Commun 4:37-42, 2000.

11. Forrester HB, Albright N, Dewey WC, Ling CC: Computerized video time-lapse analysis of apoptosis of REC:Myc cells X- irradiated in different phases of the cell cycle [In Process Citation]. Radiat Res 154:625-639, 2000.

12. Forrester HB, Vidair CA, Albright N, Ling CC, Dewey WC: Using computerized video time lapse for quantifying cell death of X- irradiated rat embryo cells transfected with c-myc or c-Ha-ras. Cancer Res 59:931-939, 1999.

Reproduced with permission of the copyright owner. Further reproduction prohibited without permission.

13. Frey T: Correlated flow cytometric analysis of terminal events in apoptosis reveals the absence of some changes in some model systems. Cytometry 28:253-263, 1997.

14. Han Z, Bhalla K, Pantazis P, Hendrickson EA, Wyche JH: Cif (Cytochrome c efflux-inducing factor) activity is regulated by Bcl- 2 and caspases and correlates with the activation of Bid. Mol Cell Biol 19:1381-1389, 1999.

15. Han Z, Chatterjee D, Early J, Pantazis P, Hendrickson EA, Wyche JH: Isolation and characterization of an apoptosis-resistant variant of human leukemia HL-60 cells that has switched expression from Bcl-2 to Bcl-xL. Cancer Res 56:1621-1628, 1996.

16. Han Z, Li G, Bremner TA, Lange TS, Zhang G, Jemmerson R, Wyche JH, Hendrickson EA: A cytosolic factor is required for mitochondrial cytochrome c efflux during apoptosis. Cell Death Differ 5:469-479, 1998.

17. Li X, Darzynkiewicz Z: The Schrodinger's cat quandary in cell biology: integration of live cell functional assays with measurements of fixed cells in analysis of apoptosis. Exp Cell Res 249:404-412, 1999.

18. Mikhailov A, Cole RW, Rieder CL: DNA damage during mitosis in human cells delays the metaphase/anaphase transition via the spindle-assembly checkpoint. Curr Biol 12:1797-1806, 2002.

19. Prieto A, Diaz D, Barcenilla H, Garcia-Suarez J, Reyes E, Monserrat J, San Antonio E, Melero D, De La HA, Orfao A, Alvarez-Mon M: Apoptotic rate: A new indicator for the quantification of the incidence of apoptosis in cell cultures. Cytometry 48:185-193, 2002.

20. Smolewski P, Bedner E, Du L, Hsieh TC, Wu JM, Phelps DJ, Darzynkiewicz Z: Detection of caspases activation by fluorochrome-labeled inhibitors: Multiparameter analysis by laser scanning cytometry. Cytometry 44:73-82, 2001.

21. Smolewski P, Grabarek J, Lee BW, Johnson GL, Darzynkiewicz Z: Kinetics of HL-60 cell entry to apoptosis during treatment with TNF- alpha or camptothecin assayed by the stathmo-apoptosis method. Cytometry 47:143-149, 2002.

22. Smolewski P, Grabarek J, Phelps DJ, Darzynkiewicz Z: Stathmo-apoptosis: arresting apoptosis by fluorochrome-labeled inhibitor of caspases. Int J Oncol 19:657-663, 2001.

23. Solary E, Bertrand R, Pommier Y: Apoptosis induced by DNA topoisomerase I and II inhibitors in human leukemic HL-60 cells. Leuk Lymphoma 15:21-32, 1994.

24. Wolf D, Rotter V: Major deletions in the gene encoding the p53 tumor antigen cause lack of p53 expression in HL-60 cells. Proc Natl Acad Sci U S A 82:790-794, 1985.

25. Zolzer F, Streffer C: Quiescence in S-phase and G1 arrest induced by irradiation and/or hyperthermia in six human tumour cell lines of different p53 status. Int J Radiat Biol 76:717-725, 2000.

Reproduced with permission of the copyright owner. Further reproduction prohibited without permission.